Bioengineering The Fracture Callus: Bone Repair Through Fracture Mimetics

By

Wollis Jude Vas

Thesis submitted in fulfilment of the requirements for the degree of Doctor of Philosophy in the Division of Surgery and Interventional Science at University College London.

November 2018

Acknowledgements

Firstly, I would like to thank Dr Scott Roberts for providing me with the opportunity to peruse my PhD. His extensive knowledge of bone biology and tissue engineering has helped guide and shape this project, without whom this project would not be possible. I would also like to thank ORUK for providing me with the funding that supported my PhD programme and made this work possible.

The members of the research group have also made massive contributions to the work being presented in this thesis, I would, especially, like to thank Dr Mittal Shah for supporting and guiding me through many of the challenges I faced. Dr Umber Cheema has also ensured that I experienced the full benefits of being the student at the division. Overall, I would like to extend my gratitude to the members of IOMS, who were there to show me the ropes as I started my journey as a PhD student. I would like to thank Prof Frank Luyten for his contribution of human periosteal stem cells, used extensively throughout my work. I would also like to thank Prof Duchen and Dr Blacker for lending me their support and expertise with the SHG/FLIM imaging.

I would like to thank again the Co-Authors Dr Mittal Shah, Rawiya Al Hosni, Dr Helen C Owen and Dr Scott Roberts who contributed to my published literature review which was the basis for the introduction to my thesis.

Ultimately, all this work would not be possible without the unconditional support I received from my family. They have joined me in celebrating my milestones while being ever present to support me during my troubles.

Abstract

Fracture non-union is estimated to occur in approximately 5-10% of bone fractures. Tissue engineering strategies that aim to replicate mature tissue may be unresponsive to the cues observed during the initiation of fracture repair, and as such have limited ability to integrate with the host tissues. As such, this thesis aims to develop an implant that mimics the cartilaginous callus, the initial reparative stage of the body's response to fracture; through the development of decellularised xenogeneic hyaline cartilage in combination with skeletal (stem) cells.

This thesis presents data on the optimisation of an osmotic shock based decellularisation methodology (Vac-OS) for costal cartilage. The resultant scaffolds (dcECM) were investigated for the removal of cellular content and maintenance of cartilage-specific proteins such as sulfated glycosaminoglycans. The Vac-OS methodology efficiently lowered DNA content to levels below *in vivo* immunological response thresholds, while eliminating the highly immunogenic and abundant alpha-gal epitope. Interestingly, immunogenic neutralisation was achieved while retaining over 80% of the sGAG content, surpassing published hyaline cartilage decellularisation methodologies. Extracellular matrix (ECM) integrity was using a novel methodology based on fluorescence lifetime imaging (FLIM) and further assessed using differential scanning calorimetry (DSC). Both FLIM and DSC indicated a lack of significant change in cartilage ECM integrity, post Vac-OS decellularisation. The bioactivity of the dcECM was subsequently assessed using various skeletal cell populations, indicating an inherent capacity to enhance chondrogenesis. Furthermore, post-implantation in immunocompetent mice, the dcECM promoted a regenerative response, in contrast with native costal cartilage. The dcECM was also fabricated into porous scaffolds capable of being upscale to meet clinical demands and gel coatings that enhance *in vitro* chondrogenesis. This thesis demonstrates the dcECM's potential as a fracture callus mimetic. The study, therefore, concludes that these constructs could potentially enhance bone repair in cases of atrophic non-union fracture, where the failure of callus formation is a defining event.

Impact Statement

Fracture non-union results in around 10% of all fractures. Currently, the gold-standard treatment for non-unions remains autologous bone grafts (ABG). The use if ABG, however, requires multiple operations and is often accompanied by reports of complication such as post-operative pain, and is ultimately limited by the amount of available donor tissue. Moreover, synthetic and natural bone grafts substitutes attempt to mimic the characteristics of autologous bone grafts are often unresponsive to the cues present at early stages of endochondral fracture healing, resulting in poor graft remodelling and integration into host tissue.

The novel research carried out during the duration of this project focused on developing a grafting material that mimicked the early phase of fracture repair; The fracture callus. This approach harnessed the recent evidence generated by the scientific community that has driven a gradual shift towards engineering a developmental or repair process to produce more biomimetic strategies for bone repair. In 2017, an article was published in Tissue Engineering: Part A, highlighting the creation of a chondroinductive, decellularised cartilage-derived scaffold (dcECM). The optimised vacuum assisted methodology (Vac-OS) effectively balanced the removal of immunogenic components with minimal disruption to the extracellular matrix (ECM). Therefore, the Vac-OS methodology shows excellent promise for deriving decellularised scaffolds from other dense avascular tissues, creating impact beyond skeletal regeneration

Further work was carried out to optimise a methodology for the formation of 3D porous scaffolds using freeze-dried and milled dcECM granules embedded in a collagen type I scaffold. It was determined that the porous scaffolds support both cell infiltration and enhanced chondrogenesis.

Moreover, the dcECM could further be digested to form a chondrogenic tissue culture coating. Both these key findings are novel, and it is proposed that upon publication these papers will form seminal contributions to the field. Additionally, the findings highlighted in this thesis provides the fundamental knowledge to develop cartilage mimetic constructs that can be used to further

investigate mechanisms of diseases in pathologies such as osteoporosis, opening opportunities for further funding, such as the foundation fellowship funding stream from Arthritis Research UK.

There is currently no cartilage-derived bone graft substitute on the market, and with the bone graft and substitutes market being valued at 2.4 billion USD in 2016 and a CAGR of 5.5% by 2025, there is excellent potential for a revolutionary approach such as described in this thesis to fill this gap the market. Moreover, key players such as Medtronic PLC, Nuvasive, Inc and Stryker Corp adopt strategies that include collaboration with academia for the innovation of novel bone regeneration strategies, opening further opportunities for funding and commercialisation.

Abbreviations

ABG - Autologous bone grafting

ACI - Autologous chondrocyte implantation

ANOVA - Analysis of variance

BCA - Bicinchoninic acid

bFGF - Basic fibroblast growth factor

BMP - Bone morphogenic proteins

CAM - Chorioallantoic membrane

CD - Cluster of differentiation

C-dcECM – Compressed dcECM

cDNA - Complementary DNA

ChM-I - Chondromodulin 1

CREB - Element-Binding Protein

CTECs - Cartilage tissue-engineered constructs

DAPI - 4′,6-diamidino-2-phenylindole

DNA – Deoxyribonucleic acid

DNase - Deoxyribonuclease

DSC – Differential scanning calorimetry

ECM - Extracellular matrix

EGF - Endothelial Growth Factor

EO - Endochondral ossification

Erk - Extracellular Signal-Regulated Kinase

ESC - embryonic stem cell

FAK - Focal adhesion kinase

FBS - Foetal bovine serum

FDA - Food and Drug Administration

FGF - Fibroblastic growth factor

FLIM - Fluorescence lifetime imaging microscopy

GAG – Glycosaminoglycan

GDF5 - Growth/Differentiation Factor 5

GF's – Growth Factors

H&E – Haematoxylin & Eosin

hESCs - Human embryonic stem cells

hPDSCs - Human periosteum-derived stem cells

HPLC - High Performance Liquid Chromatography

IFN-γ - Interferon- γ

IL - Interleukin

IM - Intramembranous

iPSCs - Induced pluripotent stem cells

ITS – Insulin transferrin selenium

LSCM - Laser-scanning confocal microscopy

MM – Micromass

MSCs - Mesenchymal stem cells

NBF – Neutral buffered formalin-saline

NIH - National institute of health

PCL – Polycaprolactone

P-dcECM - Porous dcECM

PDCs - Periosteum-derived cells

PDGF - Platelet-derived growth factor

PGA – Polyglycolide

PI3K - Phosphoinositide 3-kinase

PLA - Polylactic acid

PSU – Polysulfone

qRT-PCR - quantitative reverse transcription–Polymerase Chain Reaction

RIPA – Radioimmunoprecipitation

RNase – Ribonuclease

ROI - Regions of interest

SDC - Sodium deoxycholate

SDF1α - Stromal-derived factor 1 alpha

SDS - Sodium dodecyl sulfate

sGAG – Sulfated glycosaminoglycan

SHG - Second harmonic generation

TGFβ1 - Transforming growth factor beta-1

TNF-α - Tumour necrosis factor-α

TNF-β - Tumour necrosis factor-β

UV - Ultraviolet

Vac - Vacuum assistance

VEGF - Vascular endothelial growth factor

Wnt- Wingless-related factors

μCT - Microcomputed tomography

Contents

Table of Figures and Tables

1. Introduction

Bone is one of the few tissues that have the remarkable ability to regenerate without the formation of fibrous scar tissue, attributed to the underlying repair mechanisms that recapitulate bone development. There have been several advances in the understanding of fracture healing and the cues involved in the highly complex process. However, despite this incredible capacity for regeneration, both external and pathophysiological factors can affect this regenerative process, leading to slow healing times and in some cases non-unions[1,2]. There has, therefore, been an intense drive towards researching strategies to optimise the fracture healing process and reduce the incidence of its failure[3]. The following review is adapted from Val et al[4].

1.1 The fracture healing process

To better understand developments within the field of skeletal regeneration and fracture management, we need an understanding of the complex and carefully orchestrated process that underpins fracture healing. Fractures heal through two key pathways; Direct or intramembranous (IM) fracture healing occurs in less than 2% of fractures, requiring rigid fixation and a gap size of less than 0.01mm. Formation of cutting cones near the fracture ends creating longitudinal cavities initiates the process of IM. Subsequently, bone laid down by osteoblasts then bridge the gap and re-establish bone's lamellar structure without the formation of a cartilaginous callus[1].

Long bones, however, heal through the process of indirect fracture healing (Figure 1.1), driven primarily by the process of endochondral ossification (EO). EO has thus become a critical area of focus for the development of tissue engineering-based regenerative strategies [5–8]. Unlike direct fracture healing, the process of EO is enhanced by limited micromotion at the fracture site[1,2].

There are several key stages in the process of endochondral bone formation, as illustrated in Figure 1. EO recapitulates many aspects of skeletogenesis as

observed pre-natal bone development. The process of EO begins with the initial inflammatory response that leads to the formation of a haematoma; this lays down a template for callus formation. The repair process is initiated by the secretion of proinflammatory cytokines, triggered by the release of platelet-derived interleukin 1β [9,10], IL-6 [11,12], tumour necrosis factor-α (TNF-α) [13,14] and IL-17 [10,15,16]. These proinflammatory cytokines modulate immune and surrounding skeletal stem cell populations [14,15,17–20].

Additionally, hypoxic conditions within the haematoma lead to an increase in the expression of pro-angiogenic factors promoting vascularisation around the fracture site [19,21]. Several growth factors including transforming growth factor beta-1 (TGFβ1), fibroblastic growth factors (FGFs), bone morphogenic proteins (BMPs), platelet-derived growth factor (PDGF) and stromal-derived factor 1 alpha (SDF1α) play a key role in the activation and recruitment of skeletal progenitor cells from the surrounding periosteum and bone marrow space [20,22–25]. Several studies indicate that the hypoxic conditions present within the fracture site is a driver of skeletal stem cell differentiation towards a chondrogenic phenotype, subsequently producing an avascular cartilage callus [1,21,26]. The fracture callus provides some degree of stability while chondrocytes within the fracture callus eventually stop proliferating and become hypertrophic.

Chondrocyte apoptosis and matrix mineralisation result in the subsequent degradation/resorption of the cartilage matrix [1], through the actions of osteoclasts and osteoblasts, gradually replacing the mineralised callus with woven bone. The cortical shell surrounding the callus provides stability by bridging the bone ends; this allows for limited weight bearing. Eventually, woven bone is replaced with lamellar bone. Although the process of remodelling is initiated at 3-4 weeks, depending on the age of the patient the process can take years to complete[1].

The biological processes that drive fracture repair can be affected by several factors leading to the disruption of bone healing. These include the severity of the fracture and resulting damage to the surrounding soft tissue and vasculature, associated with high impact fractures [27]. However, the most

common factors are inherent to the host. These include metabolic diseases such as diabetes [28], lifestyle choices such as smoking [29]. Moreover, other underlying pathologies such as the age of the patient or osteoporosis can also affect bone quality [30]. One or several of these factors can result in the failure of the finely balanced bone repair process, resulting in a delayed or non-union [31].

A non-union as defined by the Food and Drug Administration (FDA) is incomplete fracture healing after nine months, alongside a lack of radiological characteristics associated with fracture healing observed during the first three months[32]. Around 10% of all the fractures seen in the UK result in non-unions annually. The estimated cost to the NHS can range from £7000 to £79000, with the higher costs being associated with failed surgical interventions and repeat surgeries. Overall, results in an annual burden of over £670 million which is predicted to rise[33].

Non-unions are classified as hypertrophic or atrophic, determined via the radiological examination of the fracture callus[34]. Hypertrophic non-unions are classified by the presence of a fracture callus that has taken a distinct horseshoe like morphology. Additionally, they have a good vascular supply and are, therefore, associated with poor fixation. In contrast, atrophic non-unions are identified by a lack of cartilage callus formation, instead replaced by the formation of fibrous tissue at the fracture ends. Atrophic non-unions are also commonly associated with poor vascularisation around the fracture site, often linked to underlying host factors such as smoking or diabetes or a significant loss of surrounding tissues, as seen in complex fractures[29,28].

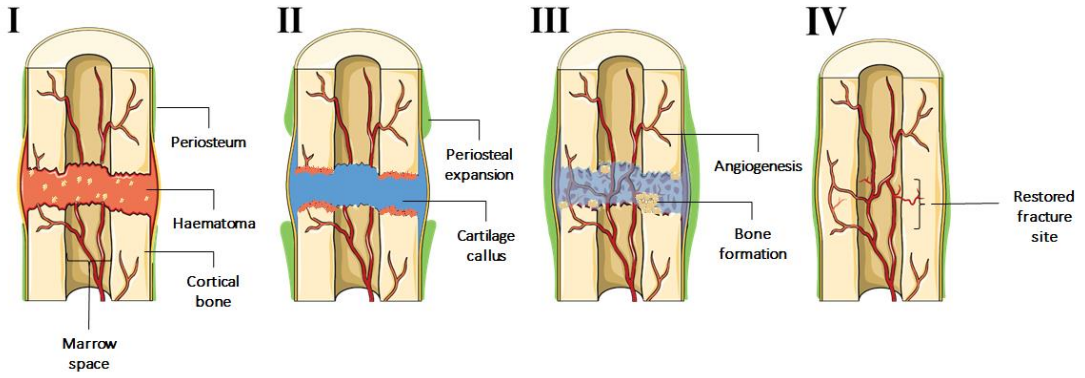

Figure 1.1: Stages of endochondral ossification during fracture repair. Stage I - Haematoma: Initial injury leads to the disruption of surrounding vasculature resulting in the formation of a platelet-rich fibrin clot. Secreted chemokines promote stem cell expansion and localisation to the fracture site; **Stage II - Soft Callus:** Hypoxic conditions and instability at the fracture fracture site favour chondrogenic differentiation of stem cells from the periosteum resulting in a cartilage callus; **Stage III - Hard Callus**: Chondrocytes within the stabilised callus undergo hypertrophy and eventually apoptosis permitting the invasion of blood vessels and woven bone formation; **Stage IV - Remodelling:** Woven bone is remodelled into lamellar bone through the synergistic action of osteoblasts and osteoclasts thus re-establishing native bone physiology. Figure generated using the Servier medical art database (http://www.servier.com/Powerpoint-image-bank) and adapted from Roberts et al.; 2014[35] and Vas et al., 2017[4].

1.2. Clinical approaches to non-union fracture management

In most cases fractures, especially non-union fractures, efficient bone regeneration and union cannot be achieved without external intervention. In a majority of hypertrophic non-union fractures, efficient stabilisation of the fracture site results in union. However, atrophic non-unions, especially open fractures or those accompanied by significant bone or soft tissue loss require further intervention to prevent infection and promote fracture healing[36–40]. The overall aim of treatment is to improve the mechanical and biological environment at the fracture site, thus making it conducive to bone regeneration. In brief, the treatment of atrophic non-unions involves a combination of rigid fixation and the use of grafting material. To date, autologous bone grafting (ABG) is considered to be the gold standard[41]. Below, we further discuss some of the clinical approaches used in combination with fixation to enhance bone regeneration.

1.2.1. Bone Grafts

Globally, around 2.2 million orthopaedic grafting procedures are carried out annualy[42]. The biological activity of bone grafts is often described in terms of their osteoconductivity, osteoinductivity and osteogenicity.

Osteoconductivity is the ability of a graft to direct resident skeletal cell migration into the scaffold, in turn producing new bone and directing the in-growth of new blood vessels. Osteoinductivity is a characteristic that is attributed primarily to the 3D structure of the graft and is, therefore, a passive process. Osteoinductivity is the ability of a graft to stimulate the deposition of new bone through the recruitment and differentiation of skeletal stem cells towards a chondrogenic or osteogenic lineage. This process is driven primarily by the presence of factors such as PDGF, (BMP) -2, -4 and -7 and interleukins [43,44]. In contrast, the osteogenicity of a graft is associated with the presence of bone-forming cells within the graft[45].

The ideal bone graft substitute would be osteoinductive, osteoconductive and osteogenic while carrying no inherent risk of infection or host rejection. Furthermore, a bone graft should undergo complete remodelling and integration. The characteristics above are present in autologous bone tissue (Figure 1.2). Therefore, autologous bone grafting has mostly remained the gold standard for the treatment of non-unions and other bone defects[46]. Therefore, the development of grafting materials has primarily focused on mimicking the properties of mature bone or the use of growth factors that drives bone formation (Table 1.2). Some of these approaches are further discussed below.

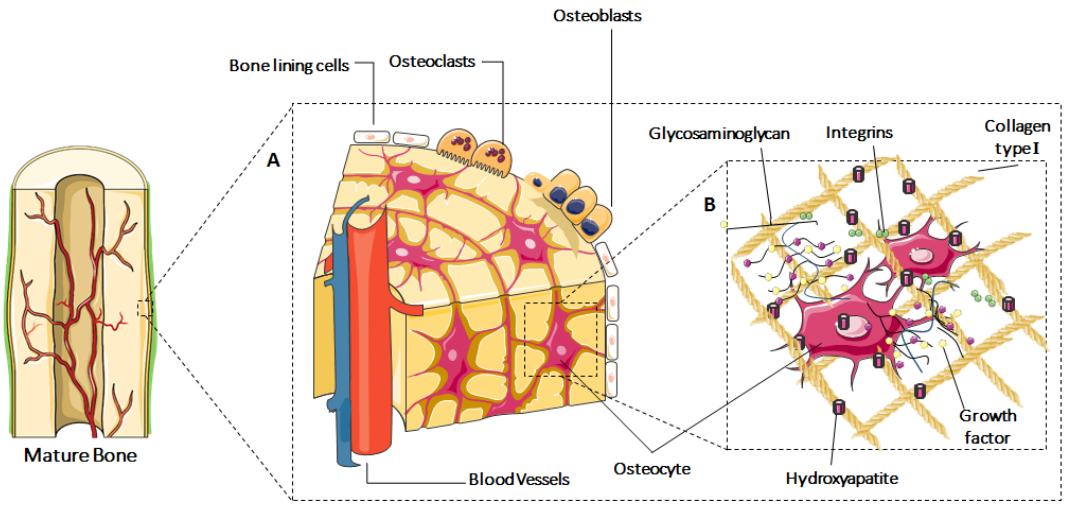

Figure 1.2: (A) Gross structural illustration of cortical bone: Haversian canals contain blood vessels that provide nutrient supply and waste removal to the osteocytes contained within each osteon. Osteoclasts are involved in bone resorption, whiles osteoblasts form new bone, both participating in the process of bone remodelling[47]. Bone lining cells envelop the bone surface and may be a source of mature osteoblasts during bone remodelling[48]. **(B) Potential cell-matrix interactions within the bone extracellular matrix**: Osteocytes within the bone extracellular matrix may be tethered to collagen type I through integrins[49]. Hydroxyapatite can also bind to collagen type I fibrils. Glycosaminoglycans that are bound to the collagen structure and sequester local growth factors within the ECM. Sequestered growth factors interact with resident osteocytes, modulating their interaction with progenitors in the bone marrow[50]. Figure created using the Servier medical art database (http://www.servier.com/Powerpoint-image-bank). The figure was adapted from Vas et al., 2017[4]

1.2.2. Autografts

Autografts make for an ideal choice due to properties that are osteoinductive, osteoconductive and osteogenic (Table 1.1). Furthermore, as they are obtained from the patient, they demonstrate good histocompatibility and healing rates[51,46,52]. Cancellous bone is often the preferred choice for autografts due to its higher osteogenic potential, associated with an abundant population of osteoblasts and osteocytes that direct bone formation and remodelling, required for the successful incorporation of the graft with the host bone. This process occurs primarily through the process of intramembranous ossification[53]. Despite these ideal characteristics, complication rates have been reported to range from 20% to 50%, with a significant drawback being donor site morbidity. Further complications have been associated with variations of bone graft quality, vitality, handling and processing [54,55,56], while the need for additional surgery increases the risk of infection[57,58]. Additionally,

the cost of harvesting itself can exceed the cost of commercially available bone graft substitutes, however, by far the most significant limiting factor is the inadequate supply of tissue for grafting[58,59]

1.2.3. Allografts

Allografts are a common alternative to ABG, as they can circumvent significant problems associated with ABG such as graft availability, donor site morbidity and long-term pain. Another derivative of allografts is demineralised bone matrix (DBM). DBM is produced through the removal of the mineral content of bone using acid extraction[60]. Allografts, however, demonstrate primarily osteoinductive properties, largely dependent on their maintenance of the bone 3D microenvironment that contains collagen type 1. Any osteoconductive properties are dependent on the variable amounts of present growth factors[61]. Their use, however, also carries significant risks that include bacterial or viral disease transmission, especially during procedures involving fresh implants[62]. In an attempt to mitigate the infection risk, some processing methodologies involve subjecting allografts to harsh gamma irradiation. Coupled with inadequate storage and handling, the resultant damage to the extracellular matrix and its components can cause variations in its biological properties varying clinical outcomes[63].

1.2.4. Synthetic bone graft substitutes

Synthetic bone graft substitutes are also a common alternative, due to their relatively cheap pricing and the absence of limiting factors faced by allografts; these include potential donor site morbidity and the risk of disease transmission. Additionally, synthetic bone graft substitutes can be manufactured in several forms, from powders to pellets, to a high compressive strength cement; this provides versatility during clinical application. Typical examples are calcium phosphates based bone graft substitutes that aims to mimic the mineral hydroxyapatite that comprises 70% of the dry weight of bone[64]. Furthermore, some substitutes can be mixed with antibiotics making

them effective for the treatment of infected orthopaedic defects. Research is also underway to combine synthetic bone graft substitutes with growth factors, some of which have received clinical approval such as, rhBMP-7 (INFUSE Bone Graft, Medtronic Spinal and Biologics)[65]; and stem cell populations to obtain a more osteogenic material. These attempts aim to mimic the desirable properties of autografts[66,62,67,68]. A significant drawback of using synthetic variants, however, is a slower resorption rate when compared to naturally occurring bone grafts; they have therefore been shown to remain at the fracture site several years post implantation[69].

1.2.5. Factors affecting graft incorporation

Several factors can impact the ability of a bone graft material to incorporate with host bone tissue. Vascularisation plays an essential role in the remodelling process. Therefore, the ability of the graft to allow for and promote angiogenesis has a significant impact on graft incorporation[70,71]. The initial immune response also has an impact on the graft remodelling and eventual incorporation. A dysregulated secretion of pro-inflammatory cytokines such as tumour necrosis factor-β (TNF-β), interferon- γ (IFN-γ) and interleukin-2 (IL-2), produced by Th1 lymphocytes can indicate host rejection that adversely impacts bone remodelling[72,73]. However, cytokines such as IL-10, IL-6, IL-5 and IL-4, secreted by Th2 cells are also involved in tissue remodelling and can be considered a positive indicator for tissue remodelling and repair[72,73].

1.2.6. Growth factors

The fracture healing process is reliant on the temporospatial secretion of growth factors. The growth factors (GF's) acting on the cellular component of a fracture site are either embedded within the bone extracellular matrix (ECM) or is secreted by various cellular populations at the fracture site[74]. GF's have therefore become the focus of research aimed at enhancing the fracture healing process[75]. A vital group of osteoinductive factors associated with autologous bone grafts are BMPs as first described by Urist and colleagues[76].

BMP-2 and 7 have been strongly implicated in bone regeneration and have therefore been implemented into long bone fracture non-union management approaches[77–81]. Despite the benefits, however, it has been suggested that supraphysiological levels of BMP's may lead to the formation of ectopic bone or stimulate cancer cell growth. There is, however, little evidence to established a definitive link between BMP's used orthopaedic applications and an increased risk of developing malignancies[82].

Manufacturer	Product Name	Composition/Use	Approved by
AlloSource	AlloFuse™	Heat sensitive copolymer with DBM in injectable gel and putty form/ Bone void filler	US FDA
Integra LifeSciences Holdings Corporation	Acell TBM®	DBM/ Bone void filler	US FDA
MTF	DBX	DBM in sodium hyaluronate carrier/ Bone void filler	US FDA
Tutogen Medicals	Tutoplast®	Allograft Bone/ Bone void filler	US FDA
IsoTis OrthoBiologics Inc.	OrthoBlast® II	DBM/ Bone void filler	US FDA and EU
Weyth Pharma	InductOS®	BMP-2 in bovine collagen sponge carrier/ Anterior lumbar spine fusion	US FDA and EU
Medtronic	Infuse® Bone Graft	BMP2 Absorbable collagen sponge/ Anterior lumbar spine fusion	US FDA
Stryker	OP-1™	BMP-7 in a collagen carrier/ Autograft alternative	US FDA and EU

Table 1.1: Commercially available osteoinductive bone substitutes. DBM = Demineralised Bone Matrix. BMP = Bone Morphogenic Protein. US FDA = United States Food and Drug Administration. EU = European Union. Adapted from Miron et al[83] and Lui et al[84].

1.3. Harnessing the fracture repair process as a strategy for non-union repair

The majority of long bone fractures heal primarily EO, which closely replicates the mechanisms of bone developmental. Lenas and colleagues defined the concept of "developmental engineering" as a modality for the creation of reparative implants that mimic tissue repair or development intermediates. The concept of developmental engineering states that tissue development progresses through several intermediates, which can be incorporated into an engineered regenerative strategy [85,86]. EO that occurs during fracture repair progresses through several stages (Figure 1). A critical intermediate stage of endochondral fracture healing includes the formation of a cartilage callus (soft callus) [87]. Therefore, understanding the fundamental components that make up its ECM of this tissue could be vital for the development of biomaterials capable of participating in the process of EO. Besides, factors that regulate cartilage callus formation should be carefully considered to mimic its ECM or in priming its progenitor cells.

The ECM is an elaborate 3D scaffolding structure particular to each tissue type [88,89]. The versatility of the ECM allows it to regulate the production, degradation and remodelling of its macromolecules, thus facilitating in the development, function and repair of tissues [88–90]. The cartilage ECM is largely composed of collagen type II, non-collagenous glycoproteins, hyaluronan and proteoglycans [90] (Figure 1.3). Collagen type II is formed by a self-assembly process that results in a crystalline D-periodic structure, *in vivo*, proteoglycans such as fibromodulin and decorin bind to the collagen type II fibrils to stabilise fibril bundles that are larger[91]. However, stability is maintained mainly via the crosslinking between collagen molecules, driven by the covalent bonding of lysine and hydroxylysine; this crosslinking is crucial to maintain collagen type II stability *in vivo*[92]. The ECM also acts as a reservoir for growth factors and cytokines that initiate and are involved in regulating cell activation and turnover

[90,93,94]. Mimicking the complex structure of the ECM may allow us to harness the natural processes that govern tissue, thus improving tissue regeneration strategies, by providing niches to drive the generation of tissue-specific cell populations.

The concepts involving the creation of these mimetic niches will be further discussed in the context of improvement made in synthetic polymer engineering, natural scaffolds and tissue intermediates composed of stem cells and cell-derived matrix.

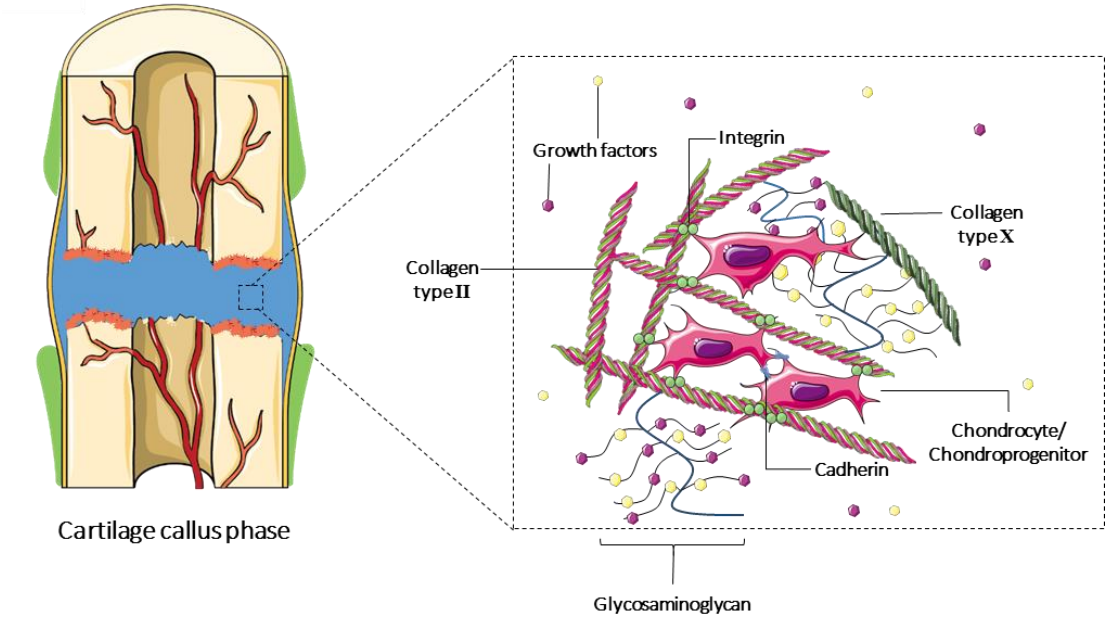

Figure 1.3: Potential cell-matrix interactions with the soft/hypertrophic callus. Chondrocytes and chondroprogenitor cells within the fracture cartilage callus extracellular matrix (ECM) may be tethered to collagen type II and X through integrins [90]. Cell to cell interactions occurs through cadherins. Glycosaminoglycans are bound to the collagen structure and sequester local growth factors within the ECM. Sequestered growth factors interact with chondroprogenitors, activating cell signalling pathways that promote chondrogenesis, which in turn promotes the expression of matrix remodelling factors [94]. Figure generated using the Servier medical art database (http://www.servier.com/Powerpoint-image-bank). Adapted from Vas et al[4].

1.3.1 Synthetic polymer engineering to mimic cell-matrix interactions

Scaffold design and fabrication have been significant areas of research in the field of tissue engineering and regenerative medicine [94–97]. Materials to create tissue-engineered constructs can be either synthetic or natural, and non-degradable or degradable depending on their application [97]. Some of the first biodegradable biomaterials used clinically were natural polymers [95]; their bioactivity was attributed to their ability to interact with cell populations. Natural polymers include proteins such as silk, gelatin, fibrinogen and collagen, and polysaccharides such as amylose, cellulose, chitin, dextran and glycosaminoglycans [97,98]. However, a significant limitation of most naturally derived polymers relates to manufacturability and functionalisation. Combined with inconsistent results, it means that synthetic polymers are not more widely investigated for tissue engineering purposes[97]. Much work is focussed on using fabricated polymer constructs to modulate the interaction of cells with the material in an attempt to replicate major cell niches. High throughput screen platforms have further driven the use of surface topography modulation for tissue engineering.

There are several synthetic polymers that have been used for bone and cartilage tissue engineering; these include polyglycolide (PGA), polylactic acid (PLA) and polysulfone (PSU) [99–102]. The applications of these polymers have been extensively reviewed [103,104] and cover their limitations which are primarily associated with their lack of bioactivity[105–107].

Surface modifications such as the use of heparin functional groups, growth factors such as basic fibroblast growth factor (bFGF) localised to the material surface have resulted in enhanced cell attachment and proliferation [108]. Moreover, modifying surface topography has also shown great promise in enhancing cell attachment and differentiation, with enhanced osteoblastic cell adhesion observed through the fabrication of specific nanoscale topographies [109–111]. Electrospun PLA/Polycaprolactone (PCL) hybrid scaffolds with controlled fiber alignment, demonstrate enhanced chondrogenic differentiation of septum-derived progenitors [112]. Similar studies have also reported success

in directing cells towards a chondrogenic fate through surface modifications [113–118]. Further modulation using methacrylates via the addition of functional groups such as phosphates and glycosaminoglycans, which are found in native bone and cartilage, induce hMSCs towards an osteogenic or chondrogenic lineage, respectively [119]. The approach of polymer modifications offers excellent promise as a tool for the development of novel biomaterials capable of regulating cellular function *in vivo*.

Polymer array technologies have employed varying physical properties or chemical concentrations allowing for the simultaneous screening of several polymer blends, reducing the time and resources needed to develop novel synthetic biomaterials. Polymer array technologies [120,121] (the emergence of polymer array technologies has been extensively reviewed elsewhere [122]). Recent developments in microfabrication using robotic liquid-dispensing technology has been used to examine various conditions and their impact on cell behavior, with research directed towards pluripotent stem cells [123,124], primary articular chondrocytes [125]. Moreover, polymer array technology has been utilised to identify specific material properties that can enhance the process of isolation, expansion, and differentiation of human skeletal progenitors [126,127]. There is a possibility that this technology could be leveraged to identify polymers that mimic specific cell-matrix interactions that are observed during the fracture repair process as a means to engineer the endochondral fracture healing response.

Technologies such as “TopoChip” have driven further automation of array screening; that uses unbiased algorithms to fabricate varying topographies on PLA. This approach resulted in the identification of specific patterns that demonstrate enhanced osteogenic differentiation [128,129]. The TopoChip was further optimised using a chip carrier has helped reduce variations within the culture system that may affect cell viability and adhesion [130]. Moreover, the emergence of additive fabrication techniques such as 3D printing allows for finer control of spacial arrangement, and more dynamic and rapid prototyping.

1.3.2. 3D printing of bone and cartilage tissues

The field of tissue engineering has strived to mimic the cellular and extracellular bone matrix as a means of restoring bone tissue and improving its functions *in vivo*. The tissue microenvironment, including bone and cartilage tissue, is a complex 3D structure that provides a template for cell adhesion and initiates bone repair *in vivo* [131,132]*.* It is essential to control the microenvironment to achieve efficient micronutrient transport and waste removal to and from the most innermost regions of the scaffold, this can be achieved either via controlling porosity or promoting vascularisation of the construct[132,133]. Traditional fabrication techniques such as particle/salt leaching [134], chemical/gas foaming [135] and thermally induced phase separation [136] only allow for gross control of the 3D structure and are thus limited in their ability to mimic the complex ECM micro-architecture. Therefore, the field has turned to additive manufacturing methods such as 3D printing. Izana and colleagues optimised a 3D printing process to obtain collagen and calcium phosphate-based scaffolds that demonstrated robust new bone formation when implanted into critically sized murine femoral defects in 9 weeks[137].

Developments such as biopolymer printing have resulted in the production of constructs aimed at cartilage and osteochondral tissue engineering [138–140]. Moreover, 3D printing offers a distinct advantage when it comes to cartilage tissue engineering due to due to the limited ability to incorporate cells into cartilage mimetic scaffolds. Additive manufacturing could be used to print and incorporate a cellular component into the scaffolds alongside key chondrogenic factors such as the TGF-β superfamily [141].

1.3.3. Biomimetics through the use of natural target-tissue ECM

The preliminary aim of tissue engineering was focused on developing materials that mimicked adult tissues, with the aim of incorporation into the host and subsequent remodelling, as defined by Langer and Vacanti in 1993 [142]. Initial attempts were made using biodegradable scaffolds in combination with adult cells. However, in the context of bone repair, this approach has to date provided no clinically approved therapies. Due to this, current research

towards improving the bioactive properties of regenerative implants through the use of naturally occurring target tissue ECM has emerged. Indeed, the process of xenogeneic tissue decellularisation and its use for tissue engineering strategies within the field of regenerative medicine has been intensively studied [143–146]. Xenografts overcome one of the key issues with transplantation; the lack of available tissue by providing a seemingly abundant source of material.

The process of decellularisation aims to remove all immunological components while leaving behind the ECM of the tissue and its associated growth factors, to maintain the ECM proteins complex spatial arrangement [147]. The ECM plays a crucial role in maintaining cell-matrix interactions that favour native tissue organisation and remodelling [88]. Importantly the structural and functional proteins in the ECM are well conserved within species. This high level of homology allows these matrices to be implanted in recipients of other species without rejection [148]. The past decade has driven research towards novel biomaterials through the process of organ and tissue decellularisation. Some of the many examples of positive clinical results include the use of FDA approved decellularised matrices such as porcine heart valves (Synergraft®; Cryolife) and acellular dermis (Alloderm®; LifeCell) [149].

The use of decellularised cartilage has drawn much attention due to its ability to harbour a large number of bioactive cues for tissue formation. The interaction of decellularised cartilage with resident cells, several chemotactic stimuli and activation of chondroinductive signalling pathways could result in continuous remodelling of the tissue. Decellularisation of cartilage, however, requires a vigorous protocol due to its dense nature, an approach known to reduce the glycosaminoglycan (GAG) content and elasticity of the matrix [147]. Despite this, the use of decellularised and lyophilised cartilage scaffolds have previously demonstrated bone formation in a rabbit model by Gawlitta and colleagues [150]. The study involved coupling pre-primed chondrogenic MSCs with decellularised cartilage scaffolds and demonstrated effective bone mineralisation when compared to the unseeded decellularised matrix. However, the contributing factors to the endochondral bone formation were unidentified but could include components within the decellularised

cartilaginous matrix, or factors produced by the cells as a result of the cell-matrix interaction [150]. The choice of articular cartilage-derived scaffolds used in the study by Gawlitta *et al.* do pose limitations due to both tissue physiology and *in vivo* function. Articular surfaces are formed during pre-natal skeletal development and are highly stable during adult life [151]. Indeed, factors such as chondromodulin 1 (ChM-I) have been implicated in the stability of articular cartilage by inhibiting EO in porcine models [152], and it has been further suggested that ChM-I functions as an inhibitor of angiogenesis, a process essential to endochondral remodelling [153,154].

Additionally, a plethora of Wnt and BMP signalling modulators have been implicated in articular cartilage stability. Therefore, there is a requirement for a source of chondrogenic ECM-derived scaffolds that is intrinsically primed for endochondral remodelling. Other cartilaginous regions such as costal cartilage provide a promising option, as it gradually undergoes EO well into adult development [155]. Furthermore, a study by Okihana & Shimomura (1992) indicated that when devitalised costal cartilage was implanted subcutaneously into rabbit and mouse models it underwent endochondral remodelling [156].

In summary, innovative decellularisation approaches may allow for the development of methodologies that minimise ECM damage and when combined with underexplored and more targeted tissue sources may be the key to developing viable grafts that can mimic a critical phase the endochondral repair process.

1.3.4 Mechanical Properties of a cartilage callus mimetic bone graft.

The mechanical properties of native tissue can be an indicator of its structural integrity, with several disease processes affecting the mechanical properties of both bone and cartilage. Several studies have therefore investigated the mechanical properties of bone and cartilage in both healthy and disease states[157–159].

Fracture stabilisation is, therefore, carefully considered during the treatment of fractures, especially non-unions[160,161]. Moreover, bone grafting materials, the mechanical properties of the graft must not only facilitate fracture stability but allow for graft placement without damage to surrounding tissues[162,163]. The most widely used method of autografting can utilise bone tissue from either cancellous regions or cortical regions, with the latter providing greater mechanical support, while the latter is more malleable and carried a reduced risk of intra-operative fractures during implantation.[164] Additionally, due to the limited mechanical stability provided by cancellous allografts, their use is limited to bone cavity defects[165].

There are several factors that may influence the mechanical properties of a bone graft substitute. For example, the porosity of a grafting material may be beneficial for cellular infiltration but may have a significant impact on the mechanical stability of the graft[166]. Assessment of these mechanical properties may therefore, provide important insight into the biological performance of a grafting material. Moreover, mechanical testing can be an important tool for the testing of decellularised tissues[167]. Properties such as flexural mechanical stiffness and Planar biaxial tensile strength can be assessed[168].

1.3.5. Stem cells for the creation of bone-forming tissue intermediates.

Many of the key developments within the field of tissue engineering centre on the ability of cells to interact positively with its carrier and mediate tissue formation and integration. It is therefore essential to investigate the interactions of key cell types in any regenerative approach to developing effective stem cell-based skeletal regenerative strategies.

Embryonic stem cells

The embryonic stem cell (ESC) is derived from an early mammalian embryo, and possesses a remarkable potential for differentiation into cell types from all three germ layers as demonstrated by Kaufman and colleagues using mouse

embryos, termed ES cells [169]. *In vitro,* culture protocols paved the way for isolation and culture of the first human ES cell in 1998 [170], where it was demonstrated that human ES cells could be kept in culture for up to 5 months followed by subsequent differentiation into all three embryonic germ layers. This facilitated further research into ES cell culture and differentiation programmes. Since then, ES cell research has generated promising results towards the treatment of diabetes [171], cardiovascular disease [172–174] and musculoskeletal regeneration [175]. *In vitro* differentiation of murine and human ES cells towards the osteogenic lineage has also been successfully achieved [176,177]. Although multiple studies have shown that ESCs seeded onto scaffolds and primed in osteogenic media do not produce bone *in vivo* [178,179], the formation of bone within teratomas aligned with hypertrophic cartilage regions has been observed, indicating the capacity of ES cells to form bone through the developmental process of EO. This potential to form endochondral bone was confirmed with murine ESCs which were seeded onto ceramic scaffolds and differentiated towards a chondrogenic lineage using TGF-β [178]. Furthermore, when implanted *in vivo* at an ectopic site into nude mice for 21 days, bone formation was observed on every one of the implanted cartilage tissue-engineered constructs (CTECs). Their capacity to form bone was further demonstrated when the CTECs were implanted orthotopically in rats with critical-size cranial defects. Similar results have also been obtained using human ESCs [180], thus highlighting the ability of ESCs to form bone via the endochondral pathway, hence mimicking both developmental skeletogenesis and fracture repair. Despite this vast potential of ESCs within tissue engineering and especially within the field of bone tissue engineering, their application is restricted by complex culture conditions, ethical constraints related to ESC isolation and their inherent tumour forming capacity [181,182].

Induced pluripotent stem cells

There was a renewed interest in pluripotent stem cells when Takahashi and Yamanaka broke new ground by re-establishing the principles of developmental biology, which state that somatic cell differentiation is an irreversible process. Transfecting murine and human fibroblasts with the embryonic factors Oct4, c-Myc, Sox2, and Klf4 caused the regression of cell

characteristics to a pluripotent, embryonic-like state, leading to them being named induced pluripotent stem cells (iPSCs) [183,184]. It was also demonstrated that like ES cells, iPSCs were able to form tissue from all three germ layers. However, iPSCs also had the inherent capacity to form teratomas (tumours) *in vivo*. Importantly, establishing a route for producing stem cell populations from a patient's cells overcomes many of the ethical issues faced by ES cell use.

In the context of bone repair, deriving progenitors with bone forming potential from iPSCs has been an intensively studied area. Recent work has described a xeno-free defined culture condition for the differentiation of iPSCs into iPSC-derived mesenchymal stem cells (iPS-MSCs), which were able to differentiate into chondrogenic, osteogenic and adipogenic lineages *in vitro* [185]. Furthermore, when these cells were osteogenically differentiated for 4 days and implanted into calvarial defects in immunocompromised mice, *de novo* bone formation originating from the implanted iPS-MSCs was observed [185]. A recent study by Shey and colleagues has also demonstrated the efficacy of iPSC-MSCs for the treatment of non-union defects in mice [186]. Furthermore, their chondrogenic differentiation capacity, and therefore their potential application towards endochondral tissue formation, has been demonstrated [187]. The ability to create iPSC-derived cartilage constructs was also demonstrated with optimised culture conditions utilising scaffold-free hyaline cartilage tissue that displayed good integration into surrounding cartilage tissue when implanted, while not forming tumour masses [188]. Although this study was targeted towards the treatment of cartilage defects, it is envisaged that the differential stimulation of these cartilage constructs may allow the generation of implants capable of bone repair. Indeed, iPSCs have been shown to undergo chondrocyte hypertrophy similarly to ESCs [180]. Furthermore, the possibility of direct cellular reprogramming towards chondroprogenitors, a process that takes many of the concepts used to derive iPSCs, has demonstrated the ability of engineered cells to undergo *in vitro* hypertrophic differentiation. Implants containing these cell populations can drive endochondral bone formation and remodelling post-implantation in nude mice [189].

Mesenchymal stem cells

One of the most desirable properties when choosing a cell type for bone tissue engineering is the ability to isolate tissue-specific regenerative cell populations. As previously discussed, ESCs provide a highly malleable cell source, and the development of iPSCs has further advanced the field of personalised medicine through the generation of pluripotent populations from somatic cell sources. However, despite these developments, the most popular cell type still employed for the development of skeletal regeneration strategies is the mesenchymal stem cell (MSC). MSCs are widely recognised for their ability to differentiate towards osteochondral lineages [190,191] and can be derived from several tissue sources. The most commonly used source of MSCs is the bone marrow, from which cells are isolated through the extraction of a bone marrow aspirate [192]. Another common source of MSCs is adipose tissue from which MSCs (pericytes) are isolated from digested fat tissue [193].

Caplan first coined the term MSC in 1991 [194]. It was, however, in the 1960s and 1970s that seminal studies by Friedenstein isolated mesenchymal stromal cells and revealed their osteogenic potential by heterotopic transplantation [195,196]. Since then, MSCs have been defined by the minimal criteria of positive expression of CD105, CD73, and CD90 and negativity for CD45, CD34, CD14, CD79α and HLA-DR [197]. MSCs have been extensively used and reviewed for their clinical applicability within the field of bone tissue engineering [198,199]. In relation to the treatment of bone fracture repair, it has been shown that the delivery of allogeneic BM-MSCs in combination with demineralised bone matrix enhances fracture healing in clinical models of diabetes mellitus in rats [200]. Similar results are also demonstrated by several other studies incorporating MSCs with scaffolding material for the treatment of fracture repair, particularly in their proposed use in non-union fractures [201–203].

Until now, the treatment of large bone defects has primarily relied on approaches that aim to harness the intramembranous pathway of bone regeneration. However, as discussed previously, recapitulating EO may be more efficacious. Martin and colleagues applied this approach by creating

cartilage constructs *in vitro* using human BM-MSC pellet cultures. Hypertrophy within these engineered constructs was induced through the withdrawal of TFG- β and the introduction of β-glycerophosphate with Thyroxin. The resulting constructs displayed increased collagen type X deposition, typical of hypertrophic cartilage. Upon implantation in immunocompromised mice, these engineered hypertrophic cartilage constructs formed bone around the periphery at four weeks, with extensive endochondral bone formation after eight weeks [5]. More recent work has also illustrated that the addition of anti-inflammatory/tissue repair macrophages may further enhance the cartilage forming capacity of BM-MSCs [204]. This highlights the potential role of inflammatory cells during the fracture repair process; however further orthotropic investigations are required to establish their clinical significance.

1.3.6 The periosteum – The master regulator of fracture repair

Despite the immense progress directed towards the design of fracture repair implants, the integration of all necessary tissue properties and functions into a single system remains a major research challenge. With this in mind, the ability to mimic cell-matrix interactions with novel biomaterials, developed using natural matrices or engineered through systematic screening of polymers and surface topography, is of course of key relevance. However, if these systems are to be combined with cells, these should also be carefully selected to represent those modulating the fracture repair process.

The periosteum is a highly vascularised connective tissue that envelops the bone surface of long bones [205]. It serves as a biophysical barrier to modulate the environmental conditions on the bone surface. The periosteum is composed of two distinct layers: an outer fibrous layer composed of fibroblastic cells in a collagen and elastin matrix and an inner cambium layer, which provides a niche for a range of cell types, including fibroblasts and stem/progenitor cells [205,206]. Recent prominent evidence has documented the regenerative potential of periosteal tissues and the functional capacity of periosteum-derived cells (PDCs) in the bone healing process [207,208]. The periosteum is predominantly responsible for 90% of cartilage and woven bone

formation in the early fracture callus, with its removal significantly attenuating bone repair [206,209]. In this respect, the periosteum has drawn considerable attention in pre-clinical bone tissue engineering approaches [35]. The regenerative potential of the cells contained within the periosteum has been further demonstrated *in vivo* where they play a role in direct bone formation as well as in chondrogenesis and EO [210].

Consequently, great efforts have made to target and isolate PDCs as a cell source for bone tissue engineering purposes. Previous work has shown that once these cells are inoculated into nude mice in scaffold [207] and scaffold-free systems [211], they give rise to bone and cartilage tissue. Indeed, murine PDCs expanded in the presence of FGF demonstrated an enhanced capacity for *in vivo* bone production mediated by BMP-2 via the endochondral pathway, a characteristic unique to PDCs. Although culture-expanded PDCs have increased our knowledge and understanding of the periosteum, *in vivo* targeting of these cells within their niche, or replication of this tissue and therefore mimicking the role of the periosteum are both attractive avenues for further investigation.

1.4. General Aim of the thesis

This thesis aims to investigate the potential of harnessing the process of endochondral ossification, developmental engineering and decellularisation to establish and validate a methodology to produce a hypertrophic cartilage-based fracture callus mimetic with the potential for clinical application (Figure 1.4).

Objective 1: Three distinct methodologies (Vac-Stx, Vac-OS and Vac-SDC) will be applied to porcine costal cartilage. Subsequently, the resultant scaffolds will be vigorously characterised for the elimination of immunogenic components, including key factors of graft rejection such as residual DNA and alpha-gal. Moreover, the matrix integrity of the resultant will initially be assessed using sulfated glycosaminoglycans (sGAGs) as an indicator. An optimal decellularisation methodology will be selected based on both efficient removal of immunogenthe ic components and the retention of sGAG content.

Objective 2: Scaffolds produced using the optimal decellularisation methodology (dcECM) will be subjected to further ECM analysis using highly sensitive, novel approaches such as fluorescence lifetime imaging microscopy (FLIM) and Raman spectroscopy that will aim to determine minute changes in the ECM post decellularisation.

Objective 3: The ability of the dcECM to promote or enhance chondrogenesis in skeletal articular chondrocytes and human periosteal stem cells (hPDSCs) will then be tested *in vitro*. Subsequently, the dcECM will be tested for it is *in vivo* biocompatibility via implantation into immunocompetent mice and assessed for the cellular immune response to the scaffolds.

Objective 4: The dcECM will be further processed to produce constructs that can be upscaled using a reproducible method. The upscaled scaffolds should have sufficient porosity to allow for cellular infiltration. Moreover, upscaled scaffolds should demonstrate chondroinductive properties when assessed using hPDSCs.

Objective 5: The dcECM will be digested and coated onto tissue culture plastic to give a chondroinductive tissue culture surface for the rapid differentiation of hPDSC's towards a chondrogenic phenotype. Moreover, the tissue culture coating will be sterilised using either an autoclaved solution or UV light.

Hypothesis

Through the development of an optimised decellularisation methodology porcine costal cartilage will be decellularised with minimal damage to the native extracellular matrix. Moreover, the decellularised cartilage matrix should be non-immunogenic and could be used to enhance chondrogenic differentiation in skeletal cell populations (Figure 1.4). Subsequently, the decellularised scaffolds will be used to generate upscalable constructs to meet clinical needs

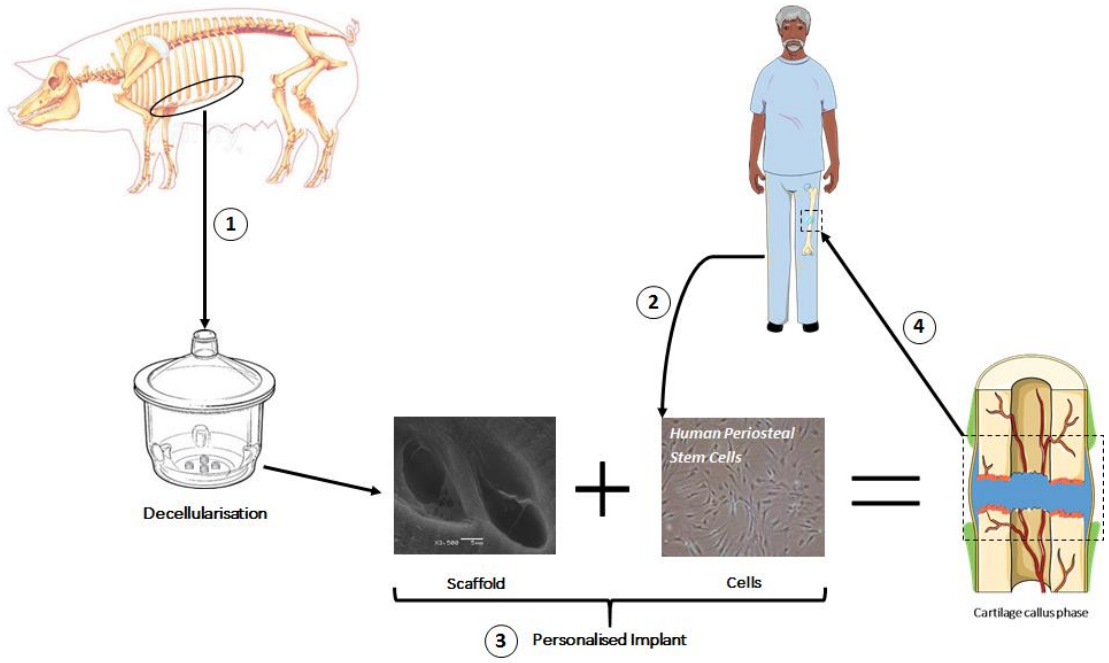

Figure 1.4: Illustration of the production process for a decellularised costal cartilage implant. (1) Fresh porcine costal cartilage will be obtained and subjected to an optimised decellularisation methodology and processed to form an implant of the required dimensions. (2) In tandem, autologous periosteum-derived cells will be obtained from the intended recipient and expanded. (3) Expanded patient cells will be seeded onto the scaffold and primed towards a chondrogenic phenotype. (4) Primed scaffolds will be implanted into the intended patient. Figure generated using the Servier medical art database (http://www.servier.com/Powerpoint-image-bank

2. Development of an optimised costal cartilage decellularisation methodology

2.1 Introduction

2.1.1 Overview of decellularisation

The concept of developing a bone graft substitute capable of mimicking the callus phase of endochondral fracture repair is based on the principle of developmental engineering, that suggests mimicking bone repair intermidiates of a repair process may be able to better participate in the early endochondroal fracture healing[8,19,212]. This approach may have an advantage over traditional bone grafts such as DBM, that mimic the bone microenvironment. Moreover, although massive strides have been made in the manufacture of synthetic scaffolds, through the use of innovative fabrication technique, they are unable to mimic the complex structure of the native ECM[213]. The use of natural tissue sources has, therefore, remained an area of interest since the establishment of the modern field of allografting, first pioneered during world war II[214]. The use of allogeneic tissues for transplantation eventually led to the exploration of the transplantation potential of xenogeneic tissues. Despite this, both allografting and xenotransplantation, are hapmpered by the host immune response they elicit in the recepient[215]. In the late 1970's more importance was given to the immunogenicity of orthopaedic allografts. Preliminary work demonstrated a reduction in immunogenicity when allografts were frozen and a further decrease when they were freeze-dried, whilst having minimal effect on functionality[216]. Since, it has been recognised that components of the ECM are conserved amongst species[217] and therefore well tolerated in xenogeneic transplants, while cellular components are largely responsible for the adverse immune response[218–220]. The processing of xenogeneic tissue for clinical application must, therefore, involve the removal of immunogenic cellular components[221], a process termed decellularisation.

The ideal outcome of decellularisation would be the complete removal of cellular components from a tissue or organ while retaining native ECM

structure and composition. To date, however, no decellularisation methodology has achieved complete removal of cellular components without some disruption to the extracellular matrix. A more realistic aim is, therefore, the reduction of immunogenic material to levels falling below the threshold required for an immune response, while causing minimal damage to the ECM. When considering the use of decellularised xenogeneic tissues, it becomes especially important to monitor levels of remnant cellular antigens such as alpha-gal and DNA, both key promoter of xenogeneic transplant rejection[222,223].

Optimal conditions for decellularisation can vary depending on the tissue being considered; this results from tissue specific differences in cell and matrix density. Several methods have been applied for the decellularisation of tissues and organs; these can be combined and modified for optimal efficiency. Cartilage due to its dense and avascular nature often requires more disruptive physical and chemical decellularisation approaches, as highlighted in Table 2.1 these include mechanical agitation and the use of ionic surfactants such as SDS and SDC. Generally, the methods most suitable for the decellularisation of dense tissues such as cartilage are also the most disruptive to the ECM.

Method	**Mechanism of Action**	**Impact on ECM**	**Tissues/ References**
Physical			
Mechanical Agitation	Can cause cell lysis, facilitate exposure to the decellularising agent and facilitate cellular removal	- Intense agitation can disrupt the ECM - Insufficient for the removal of DNA fragments	Heart Valves[224,225], Cartilage[226,227], Arteries[228] and Dermis[229–231]
Freeze-Thaw	Facilitates with cell lysis via formation of	- Has minimal impact on ECM	Cartilage[226,232], Tendon[233,234], Larynx[235]

	intracellular ice crystals	structure and protein content - Ineffective for DNA removal	
High hydrostatic pressure	Pressures greater than atmospheric pressure can be applied for cell lysis	- Denatures ECM Proteins	Blood Vessels[236,237]
Non-Ionic Detergents			
Triton X-100	Disrupts lipid-lipid interactions aiding in cell lysis	- Effectivity is highly dependent on the tissue. - Results in the disruption of GAG Content	Trachea[238], Tendon[239], Bone[240], Cartilage[241]
Tween20™	Disrupts lipid-lipid interactions and aids in the clearance of cell debris	- Ineffective unless it's combined with another decellularisation agent	Lung[242], Cartilage[243]
Ionic detergents			
Sodium dodecyl sulfate (SDS)	- Solubilise both cytoplasmic and nuclear membranes - Aids in clearing nuclear remnants and cytoplasmic proteins	- Can damage the collagen structure - Removes GAGs	Heart Valves[244], Dermis[245], Cartilage[150,226,246]

Sodium deoxycholate (SDC)	-Similar mechanisms to SDS	- More disruptive to ECM structure than SDS	Heart Valves[247], Trachea[238]
Enzymes			
Trypsin	Cleaves peptide bonds helping disassociate cell-matrix interactions[248]	- Can disrupt the ECM structure and facilitate GAG loss - Exposure to trypsin must be limited to prevent extensive damage	Heart Valves[225], Cartilage[249]
Deoxyribonuclease	Facilitates the hydrolysis of mid-fragment and terminal bonds of deoxyribonucleotide chains	May remain in decellularised ECM and elicit an immune response.	Whole hearts[250],Cartilage [246], Tendon-bone[251]
Ribonuclease	Facilitates the hydrolysis of mid-fragment and terminal bonds of ribonucleotide	Similar to Deoxyribonuclease	Annulus fibrosus[252], Cartilage[238]
Osmosis			
Hypotonic and hypertonic solutions	Cell lysis due to osmotic shock	May affect the mechanical properties of the ECM[253]	Cartilage[254,255], Dermis[231]

Table 2.1: Approaches for the declularisation of tissues and organs. Adapted from Yang et al[256] and Badylak et al[148]

2.1.2 The use of decellularised scaffolds in tissue engineering

Further justification for the use of decellularised scaffolds can be found in the abundance of decellularised ECM products that have been trialled for clinical use. Examples include but are not limited to porcine heart valves (Synergraft®; Cryolife) and Acellular dermis (Alloderm®; LifeCell). Furthermore, a pre-clinical study involving intestinal sub-mucosa has yielded positive results for the surgical repair of the rotator cuff [257] and Achilles tendon injuries[258]. Recent advances in tissue engineering have, however, shown that although biological scaffolds can be used at non-homogenous sites, tissue-specific scaffolds may yield better outcomes[259]. These findings stem from the fact that there is a huge variation in the ECM composition of various orthopaedic tissues such as cartilage, bone, tendon and ligaments[260]. Furthermore, the tissue-specific ECM composition allows seeded tissue-specific cells to follow intrinsic biological cues to produce the cell phenotypes required for maintenance of tissue or organ specific functions[89]. Current treatment approaches with xenografts have, however, yet to yield results that are comparable to the gold standard of autografting[261,262]. As previously suggested, a better approach to developing a bone graft for fracture healing may require the fabrication of an ECM derived scaffolds that mimics the cartilage callus phase of fracture repair, thus capable of undergoing endochondral ossification.

2.1.3 Decellularisation of dense avascular tissues

Due to its ability to gradually undergo endochondral ossification *in vivo* when subcutaneously implanted[156] and the physiological similarities between humans and pigs[263], porcine costal cartilage was an ideal source of tissue for the production of an endochondral scaffold primarily due to the ease of extraction and abundance of tissue. When compared to sources of articular cartilage, costal cartilage has the tendency to undergo gradual endochondral ossification throughout the life of the animal, while healthy articular cartilage is largely stable[264,265]. Since the aim of this study is to produce constructs that will be used as endochondral substrate, it is important to select a source that is pre-disposed to endochondral ossification. Moreover, articular cartilage in

porcine models on average are 1.5mm thick compared to costal cartilage that can range from 30-40mm in thickness depending on the age of the animal[266], this characteristic allowed us to investigate the effect of tissue thickness or volume on the decellularisation process. Costal cartilage, like other hyaline cartilage sources is sense and avascular in nature, hindering the delivery of decellularisation agents into tissues[267]. Overall, this characteristic can impede the process of decellularisation[148,268]. Studies such as that by Xu and colleagues attempt to overcome limited tissue permeability by utilising harsh ionic surfactants such as SDS in combination with hydrostatic pressure of up to 200 mmHg, [251]. Although this approach was successful in removing cellular content, significant loss of Glycosaminoglycans was reported. The principle behind the use of ionic surfactants and hydrostatic pressure for the decellularisation of dense avascular tissue, however, remains in its ability to disrupt the matrix allowing for better penetration of decellularisation agents and removal of cellular content. Unfortunately, the use of harsh ionic surfactants or physical methods results in the disruption of the structural and biological integrity of the native ECM. The use of ionic surfactants such as SDS and SDC can have a significant impact on the native sGAG content; this is evident with tissues such as hyaline cartilage[150,226,249,269]. Although, sGAGs that are present in various tissue types, they are especially abundant in cartilaginous ECM serving as both structural and functional components [267,270]. Additionally, besides their role in cartilage ECM homoeostasis [271], sGAGs have also been associated with their ability to promote chondrogenesis [272–274] and regulate endochondral ossification[275]. Therefore, it is essential to consider the maintenance of sGAG content, especially when developing a decellularised cartilage derived scaffold with a capacity for endochondral ossification. Gawlitta and colleagues faced similar challenges in the development of an articular cartilage derived endochondral substrate. The use of cryomilling and SDS during decellularisation resulted in morselised cartilage scaffold granules, there were further fabricated into scaffolds that that were incapable of driving orthotopic endochondral ossification without the addition of stem cell populations and extensive periods of chondrogenic priming[150]. Thus, in the pursuit of developing a cartilage callus mimetic, we faced the challenging task of developing a decellularisation methodology that effectively increases the

permeability of the dense costal cartilage ECM, allowing for enhanced cellular clearance, all while retaining substantial sGAG content.

Vacuum Assisted Decellularisation

Vacuum desiccators have been used extensively in the processing and storage of food items[276]. Additionally, freeze-drying under vacuum is routinely utilised for the removal of water content, thus facilitating long-term storage of clinically used, natural ECM derived tissue substitutes such as NuOss® and Acell TBM®. Since many clinically available decellularised tissues are stored in a freeze-dried state, time-consuming rehydration is required before use. Jun and colleagues incorporated the use of vacuum in a process they termed "vacuum pressure impregnation" to aid in speeding up the rehydration process. The study demonstrated that the use of vacuum assistance reduced rehydration times from 6 hours to just 30 minutes. These findings we attributed to the increased permeation of water into the freeze-dried tissues as a result of hydrating under a low-pressure environment. Lange and colleagues were the first to incorporate this principle into a decellularisation methodology for whole human and porcine trachea[238]. The principle of using vacuum assistance for decellularisation relies on the removal of air from the tissue, forcing water alongside any decellularising agent into the tissue, thus improving permeability (Figure 2.1). The results obtained by Lange and colleagues[238] demonstrated a distinct increase in decellularisation efficiency, especially when considering the hyaline cartilage tracheal rings. When vacuum was added to the protocol there was an 84% increase in the removal of residual DNA compared to an identical methodology lacking vacuum assistance. Overall, these results also suggested that the greater decellularisation efficiency would mean shorter decellularisation times when using vacuum assistance[277,278]. These findings were further confirmed in a study by Butler and colleagues[279] that utilised the same vacuum assisted decellularisation methodology for the production of human tracheal scaffolds for clinical implantation. Although both of the studies above have demonstrated a reduction in decellularisation times when combined with vacuum-assistance,

they report minimal differences in sGAG retention compared to non-vacuum assisted methodologies. These results may stem from the rapid removal of air from the tissues and replacement with the aqueous decellularisation solution, primarily due to the large water content forming an integral part of the cartilage ECM[280]. Moreover, both studies employ SDC as an ionic surfactant, known to cause extensive damage to the ECM[247]. Therefore, there is still the need for a decellularisation methodology that limits the used of ionic surfactants and enzymes that actively target the ECM.

It was therefore hypothesised that by incorporating vacuum assistance (Vac) alongside three previously established methodologies for the decellularisation of dense or cartilaginous tissues; would aid in the development of an optimal decellularisation methodology for porcine costal cartilage that minimises ECM disruption and sGAG loss.

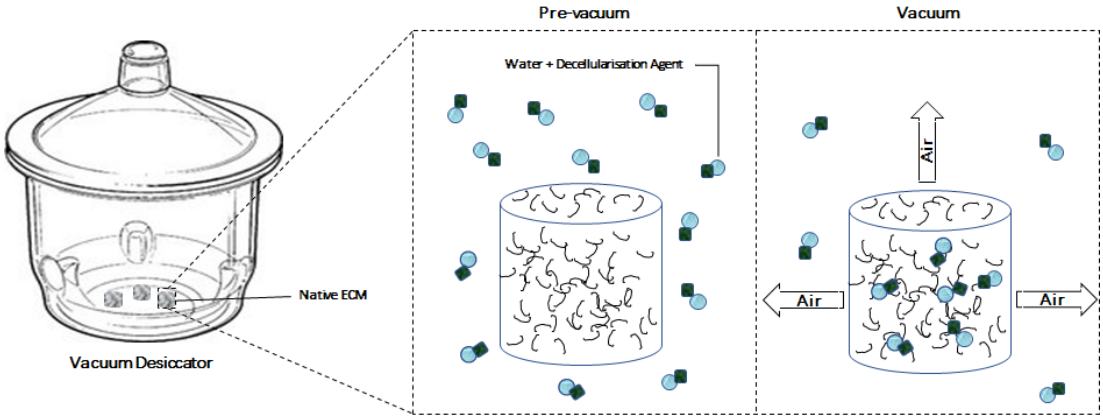

Figure 2.1: Schematic highlighting Mechanisms of forced tissue impregnation using vacuum assistance. Figure generated using the Servier medical art database (http://www.servier.com/Powerpoint-image-bank

2.2 Methods

2.2.1 Costal cartilage harvest

Fresh porcine costal cartilage was obtained from Large-White/Landrace crossbred pigs ranging from 40 to 70 Kgs (being terminated from unrelated studies at Northwick Park Institute for Medical Research; NPIMR, London, UK; approximately 8 ribs were harvested from each pig; n=5). Lateral thoracic

incisions were made and the soft tissue excised and cleared to expose the costal regions of the rib cage. Costal cartilage directly adjacent to the bone tissue was isolated from the rib cage. Any remaining adherent soft tissue was removed using a sterile scalpel and the harvested costal cartilage placed in sterile plastic bags and stored immediately at -20°C.

2.2.2 Development of decellularisation methodology

Frozen costal cartilage samples were defrosted at room temperature (18-21°C). The cartilage tissue was dissected into discs measuring 10 mm in diameter and 1 mm in height, with a volume of 78.5 mm^3. These discs were allotted into three groups each containing five discs. These groups were subjected to three independent decellularisation methodologies (Table 2.2). Post freeze-thaw, the subsequent steps in all the methodologies were carried out under negative pressure at 2000 µmHg (267 Pa) (Figure 2.2), using a vacuum desiccator (Sigma-Aldrich, Dorset, UK). All decellularisation methods utilised 250 mL of solution per step. All methodologies also included a nuclease digestion step to eliminate nucleic acids. The DNAse/RNAse buffers contained 10 mM $CaCl_2$ and 60 mM $MgCl_2$, required for the activity of nucleases. This step was carried out at 37°C under agitation using an orbital shaker (ThermoFisher, Bedford, UK). All non-enzymatic steps were carried out at 4-8ºC. Hypertonic solution contained 1M NACL, 50mM of Tris HCL and 10mM of EDTA. Hypotonic solution contained 10mM of Tris HCL and 5 mM of EDTA.

Vac-OS	Vac-STx	Vac-SDS
Freeze/Thaw Duration: 24 Hours	**Freeze/Thaw** Duration: 24 Hours	**Freeze/Thaw** Duration: 24 Hours
Distilled Water Duration: 6 Hours	**0.25% Triton X + 0.25% SOC** Duration: 24 Hours	**1% SDS** Duration: 4 Hours
Hypertonic Solution* Duration: 12 Hours	**HBSS** Duration: 24 Hours	**PBS** Duration: 12 Hours
Wash Buffer Duration: 12 Hours	**DNAse/RNAse** Duration: 24 Hours	**Hypertonic Sol** Duration: 10 Hours
Hypotonic Solution* Duration: 12 Hours	**HBSS** Duration: 24 Hours	**PBS** Duration: 12 Hours
Wash Buffer Duration: 12 Hours	Sterilisation	**Hypotonic Sol** Duration: 10 Hours
DNAse/RNAse Duration: 24 Hours		**DNAse/RNAse** Duration: 12 Hours
Wash Buffer Duration: 12 Hours		**PBS** Duration: 24 Hours
PBS Duration: 12 Hours		Sterilisation
Sterilisation		

Table 2.2: Decellularisation methodologies, highlighting each step along with the length of time. Methodologies were adapted from Greco, et al[231] and Lange, et al[238]. *****Hypertonic solution contained 1M NACL, 50mM of Tris HCL and 10mM of EDTA. Hypotonic solution contained 10mM of Tris HCL and 5 mM of EDTA. Vacuum was applied to all the described methodologies post freeze-thaw.

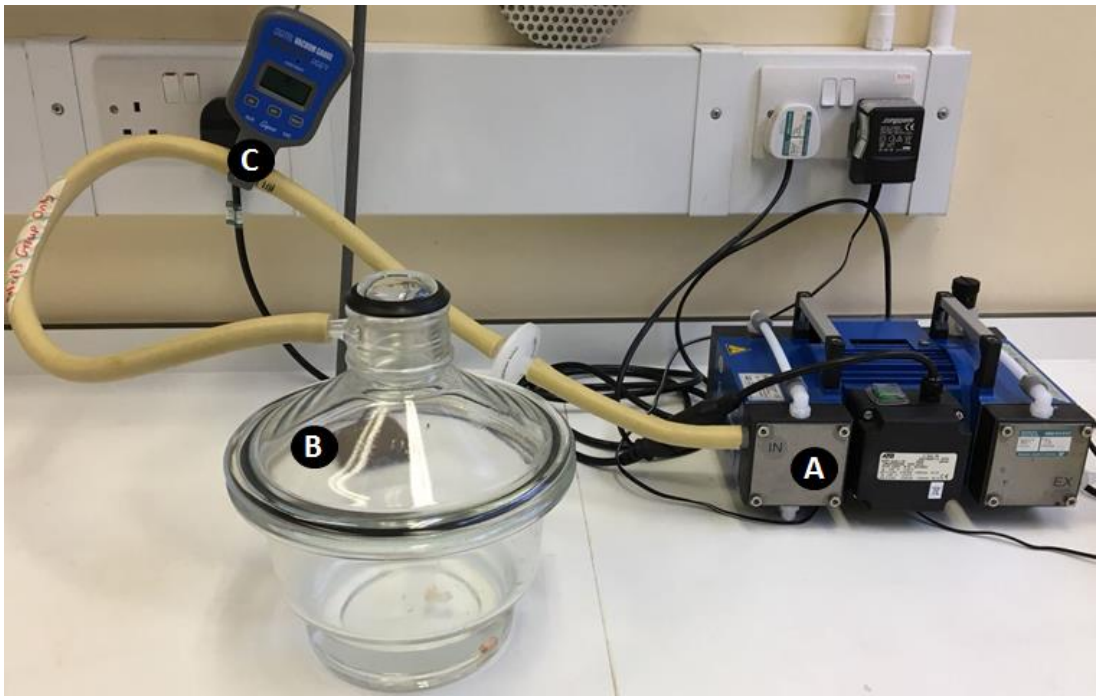

Figure 2.2: Vacuum assisted decellularisation setup. (A) Vacuum pump, (B) Vacuum desiccator, (C) Digital vacuum gauge.

Vac-OS methodology adapted from Greco and colleagues [231] utilised a freeze/thaw cycle to initiate cell disruption, followed by the use of hyper- and hypotonic steps in order to facilitate cell lysis. Washing with wash buffer containing 0.2% wt/vol Tween-20 (Sigma-Aldrich, Dorset, UK) was incorporated between each step to aid the removal fragmented cellular components.

Vac-STx methodology adapted from Lange and colleagues [238] utilised a freeze/thaw cycle to initiate cell disruption, followed by a combination of sodium deoxycholate (SDC) (Sigma-Aldrich, Dorset, UK) and Triton-X100 (Sigma-Aldrich, Dorset, UK) in order to facilitate cell lysis and the removal of cellular components, respectively.

Vac-SDS methodology utilised sodium dodecyl sulphate (SDS), a zwitterionic detergent that solubilises cell membranes and dissociates DNA from proteins along with hyper- and hypotonic solutions to further aid with cellular component fragmentation and removal.

2.2.3. Histological analysis

Histological examination was used to assess cellular clearance and gross tissue morphology. Briefly, samples from each of the methodologies, along with a control sample, were fixed in 10% NBF for 24 hours at room temperature (18-21°C). The samples were processed for paraffin wax embedding using routine histological techniques. Subsequently, 5 µM thickness paraffin sections were cut using a rotary microtome (ThermoFisher, Bedford, UK). The sections were mounted onto poly-lysine coated histology slides (ThermoFisher, Bedford, UK) and stained with haematoxylin & eosin. The dcECM was further stained for picrosirius red and toluidine blue, according to routine procedures. Additional sections were stained with 4′, 6-diamidino-2-fenylindool (DAPI) and visualised using inverted Axio fluorescence imager (Zeiss, UK). Nuclei were quantified using ImageJ (NIH). Based on histological examination the Vac-SDS was eliminated at this stage from further analysis.

2.2.4. DNA quantification

To assess the quantity of DNA present, cartilage samples were cryomilled using a SPEXSamplePrep 6775 freezer mill (SPEX, London, UK) into a homogenous paste. 25 mg of the resultant paste was transferred to DNase/RNase free microcentrifuge tubes. The total DNA of the samples was isolated using the GenElute mammalian genomic DNA miniprep kit (Sigma-Aldrich, Dorset, UK) in accordance with the manufacturer's instructions and eluted in 50 µL nuclease-free water. The eluted DNA was quantified using the NanoDrop ND1000 spectrophotometer by absorbance (ThermoFisher, Bedford, UK) and normalised to the wet mass of each sample. Based on DNA and GAG quantification the Vac-STX condition was eliminated from further analysis and the Vac-OS methodology selected as the optimal methodology.

2.2.5. Protein extraction and Western blotting for alpha-Gal content.

Western blot analysis was utilised to determine the presence of the Alpha-Gal epitope. Briefly, Control cartilage, muscle and Vac-OS decellularised cartilage (dcECM) were cryomilled using a SPEXSamplePrep 6775 freezer mill (SPEX, London, UK) to form a paste. To further solubilise, 200 mg of the sample paste was combined with 1 mL of RIPA buffer (Sigma-Aldrich, Dorset, UK) and frozen at -80^{o}C until analysed. The total protein content of the lysate was quantified using a BCA protein assay kit (ThermoFisher, Bedford, UK) in accordance with the manufacturer's instructions. 10 µg of the protein was combined with 2 x Laemmli sample buffer in a 1:1 ratio containing β-mercaptoethanol (Sigma-Aldrich, Dorset, UK) and size fractionated using SDS-PAGE, run on Mini-PROTEAN® TGX™ Precast Gels (Biorad, Herts, UK) followed by electrotransfer using the Trans-Blot® Turbo™ Mini PVDF Transfer Packs (Biorad, Herts, UK). The transferred proteins were stained using 1% Ponceau S (Sigma-Aldrich, Dorset, UK) for 1 hour. The blots were then blocked using 3% filtered bovine serum albumin (Sigma-Aldrich, Poole, UK), and incubated overnight at 4°C with an antibody against Alpha-Gal (EnzoLifeSciences, Exeter, UK) at 1:500 dilution. A secondary anti-mouse HRP conjugated antibody (VectorLabs, Cambs, UK) was then added to the blot at the concentration of 1:1000 and incubated for 1 hour at room temperature (18-21°C). Detected proteins were visualised using Clarity™ Western ECL Blotting Substrate (Biorad, Herts, UK) and images were obtained using ChemiDocXRS+ (Biorad, Herts, UK).

2.2.6. Sulphate glycosaminoglycan (sGAG) Quantification.

The sGAG content in both control cartilage samples and decellularised samples were measured using the Blyscan s-GAG assay kit (Biocolor, Ireland). Briefly, each sample was cryomilled using a SPEXSamplePrep 6775 freezer mill (SPEX, London, UK) and 50mg of the sample was placed in 1.0 mL papain digestion buffer containing 400 mg sodium acetate, 200 mg EDTA disodium salt, 40 mg cysteine HCL and 0.1mg papain for 12 hours at 65°C

with occasional mixing. The digests were centrifuged at 13,000 rpm for 10 minutes. 50 µL of each digest supernatant was mixed with 1.0 mL Blyscan dye reagent. The samples were mixed for 30 minutes using an orbital shaker (IKA, Staufen, Germany), followed by centrifugation at 13,000 rpm for 10 minutes to obtain a pellet containing insoluble sGAG-dye complex. 0.5 mL of dissociation reagent was added to each tube and centrifuged at 13,000 rpm for 5 minutes. A standard curve was generated with 50 µL serial dilutions ranging from 0.0-5.0µg/mL of chondroitin sulphate in distilled water. The standards and samples were mixed with 1.0 mL Blyscan dye reagent and 200 µL of each transferred into clear flat bottom 96-micro well plates in triplicate. The absorbance was measured using a Tecan Infinite M200pro microtiter plate reader (Tecan, Männedorf, Switzerland) at 656 nm. Absolute sGAG content in µg/mL was determined and samples normalised to the wet mass of each sample.

2.2.7. Statistical analysis

Data are expressed as the mean ± standard deviation (SD). Statistical significance was determined using one-way analysis of variance (ANOVA) with Bonferroni's posthoc corrections applied. Statistical significance is indicated on all graphs as follows: *$p<0.05$, ***$p<0.001$ ($n=3$). All statistical analysis was performed using GraphPad Prism version 6.0 for windows (GraphPad Prism Software, La Jolla California USA, www.graphpad.com).

2.3 Results

2.3.1. An optimised Vac-OS decellularised methodology results in the efficient removal of cellular components.

Macroscopic examination of the dcECM shows a pearlescent white scaffold, distinctive of decellularised tissues when cellular content has been eliminated (Figure 2.3A&B). Light microscopy of H&E stained sections revealed that all methodologies resulted in some level of cellular clearance, with the Vac-OS and Vac-STx methodologies resulting in the highest clearance. Some

morphological changes in lacunae structure can also be observed (Figure 2.3 ;C-F). Cellular clearance was further validated through nuclear staining with DAPI (Figure 2.4;A) and subsequent quantification (Figure 2.4;B). The Vac-SDS based methodology resulted in an 89.5% ($p<0.001$) reduction in DAPI positive nuclei while the Vac-STx and Vac-OS methodologies were the most effective at clearing cellular and nuclear content from the cartilage samples, as evidenced by a 100% ($p<0.001$) reduction in visible DAPI positive nuclei. These two methodologies were ,therefore, chosen for further characterisation and assessment.

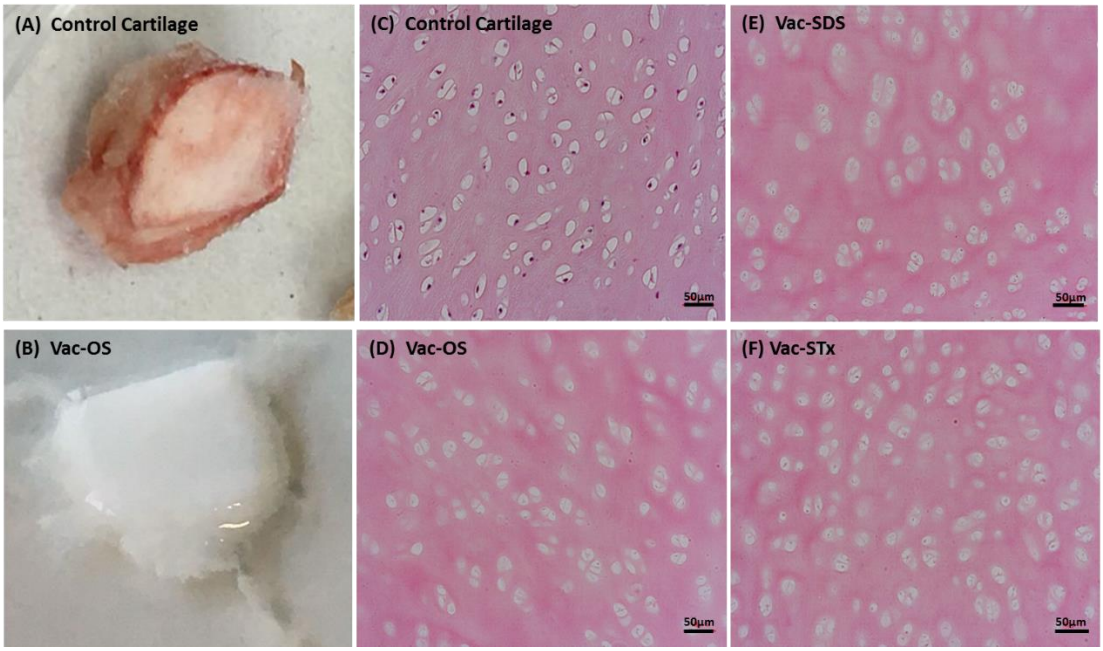

Figure 2.3: Macroscopic and histological examination of decellularised costal cartilage. Representative macroscopic image of control (A) and Vac-OS (B) decellularised costal cartilage. (C-F) Representative histological of H&E stained sections (n=3) for the analysis of cellular clearance from hyaline cartilage. There is a visible reduction in cellular content with all three methodologies (scale bar = 50 µm).

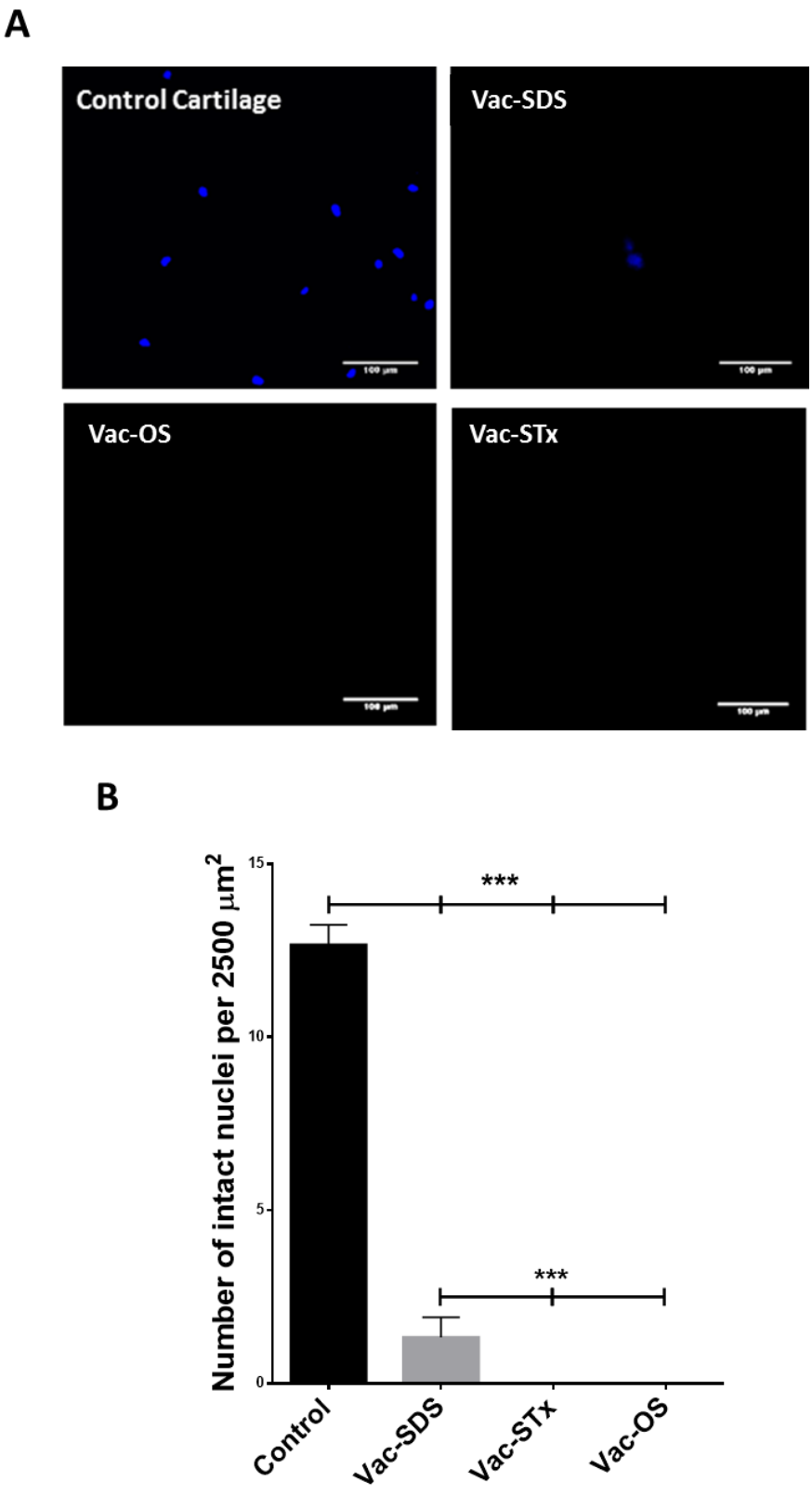

Figure 2.4: Nuclei staining and qualification of decellularised tissues (A) DAPI stained sections demonstrate an absence of intact nuclei in the Vac-OS and Vac-STx methodology. (B) Image-based quantification of intact nuclei using ImageJ presented as mean ±SD (n=3 **p<0.01, ***p<0.001). Statistical analysis performed using a one-way ANOVA using Bonferroni's posthoc correction.

2.3.2. Vac-OS decellularisation results in effective DNA content removal and superior sGAG retention

To validate the efficient removal of cellular and nuclear content from the decellularised cartilage samples the DNA content of the resultant scaffolds was analysed. Initially, total DNA content post Vac-OS and Vac-STx decellularisation was quantified in 78.5 mm^3 (small) tissue volumes. Sample voloume was upscale by a factor ten and DNA removal was assessed in the tissue samples with an increased volume of 785 mm^3 (large). Values were normalised to tissue wet weight and compared to the control native costal cartilage samples. There was no significant difference in DNA content between the small and large samples with either of the methodologies employed.

Furthermore, DNA content in both Vac-OS and Vac-STx decellularisation methodologies (Figure 2.5; A&B) fell below the clinically acceptable level of 50 ng/mg of tissue ($p<0.0001$) [147] for both tissue sizes. Despite the similarity in DNA content, distinct differences in sGAG retention (Figure 2.5; C&D) between the two methodologies and tissue volumes were observed. Tissue subjected to the Vac-OS methodology retained 85.79% ($p<0.05$) and 28.2% ($p<0.001$) sGAG for the large and small volumes, respectively; when compared to control cartilage tissue. Tissue subjected to the Vac-STx methodology, however, retained 57.64% ($p<0.001$) and 16.64% ($p<0.001$) for the large and small volumes, respectively. The results indicated that the Vac-OS decellularisation methodology resulted in 28.15% ($p<0.001$) higher sGAG content retention compared to the Vac-STx methodology, when considering the larger volumes. This difference in sGAG retention was not observed between the two methodologies in the smaller tissue volume. The Vac-OS decellularisation with larger tissue volumes was thus selected as the optimal methodology for costal cartilage and subjected to further analysis, and the resultant scaffolds were termed dcECM.

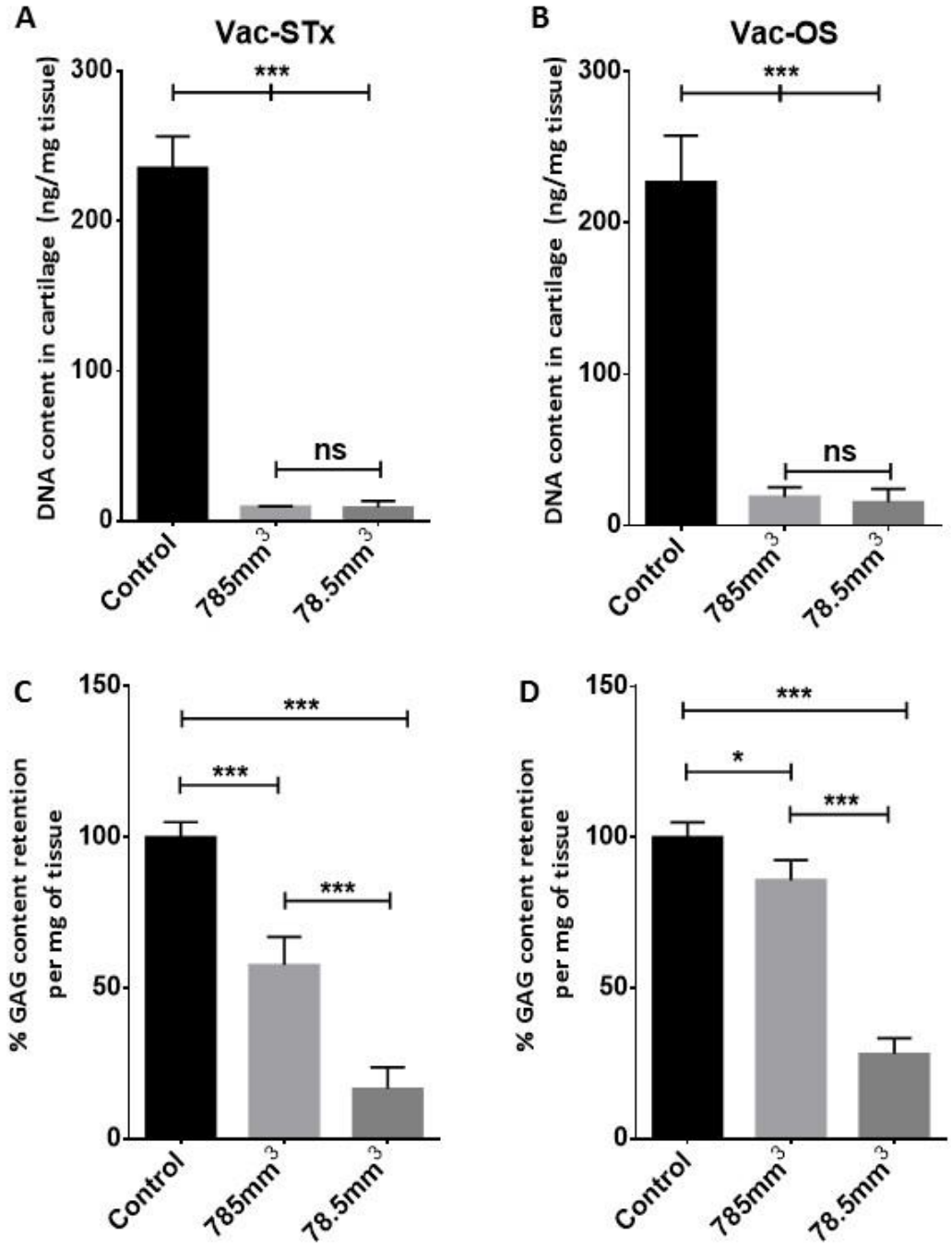

Figure 2.5: DNA and sGAG content analysis of decellularised tissues. DNA content in cartilage subjected to (A) Vac-STx (n=3) and (B) Vac-OS (n=5) based methodologies. Data presented as mean ng/mg wet mass of tissue ±SD. Both scaffold volume DNA contents fell below the threshold of 50 ng/mg for the Vac-STx and Vac-OS treated samples. Percentage sGAG content per mg wet mass tissue ±SD, subjected to (C) Vac-STx (n=3) and (D) Vac-STx (n=5) methodologies, normalised to native cartilage sGAG content. Statistical analysis was performed using a one-way ANOVA, using Bonferonni's posthoc correction. The figure has been reproduced from Val et al[281] with permission from Mary Ann Liebert, Inc., New Rochelle, NY

2.3.3. Vac-OS decellularisation results in effective removal of the highly immunogenic alpha-gal epitope.

The alpha-Gal epitope is an abundant immunogenic component found on the cell surface of all non-primate species, it has, therefore, been repeatedly implicated in an acute and adverse host immune response, facilitating tissue rejection[222]. Therefore, alpha-gal content post Vac-OS was investigated using immunoblotting. Protein loading was confirmed using ponceau S (Figure 2.6; A) as other markers that are cell or ECM-associated would be affected by the decellularisation process, the ponceau bands post Vac-OS are faint, potentially, due to the removal of a number of cell and matric-associated proteins during the Vac-OS decellularisation methodology. Control levels of alpha-gal were established using porcine costal cartilage and muscle tissue with distinct bands visible at 56 kDa (Figure 2.6 B; Lanes 1-4). The band indicative of alpha-gal is, however, absent in the Vac-Os decellularised costal cartilage tissue.

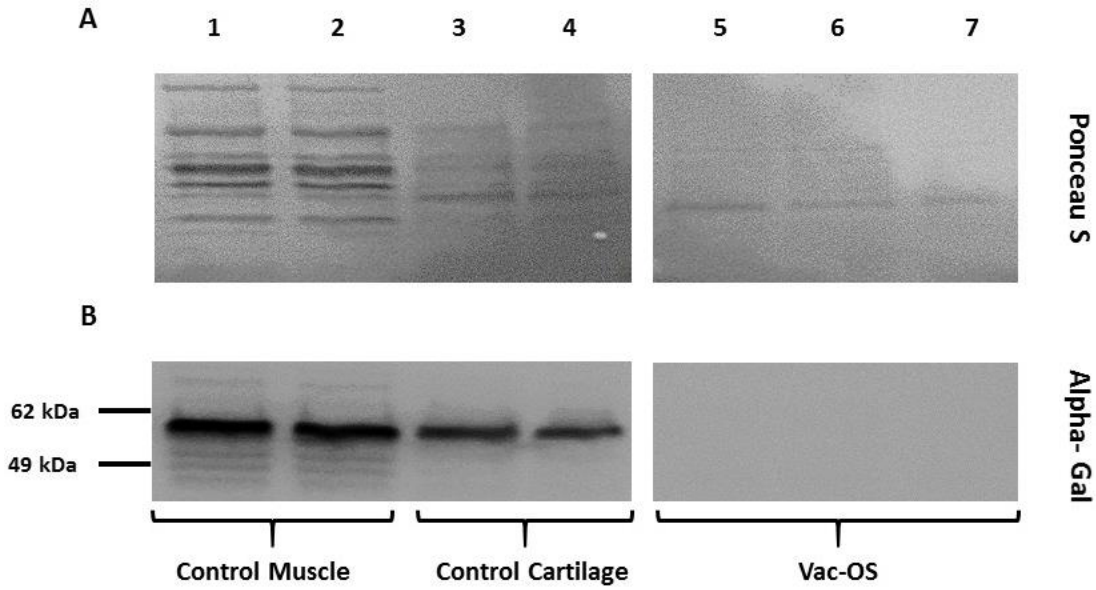

Figure 2.6: Western blot analysis of Alpha-Gal epitope residues. Vac-OS decellularisation eliminates highly immunogenic alpha-Gal epitopes. (A) Representative images of Ponceau S staining of transferred proteins indicating traces of protein bands in each lane. (B) Representative Immunoblot image illustrating the presence of the Alpha-Gal epitope at 56 kDa in both the control muscle (lanes 1&2), control cartilage samples (lanes 3 &4) and absence in Vac-OS decellularised cartilage (lanes 5, 6 &7) (n=3). The figure has been reproduced from Val et al[281] with permission from Mary Ann Liebert, Inc., New Rochelle, NY.

2.3.4. The dcECM demonstrates even collagen content maintenance and sGAG distribution.

To assess the impact of the Vac-OS decellularisation methodology on sGAG content distribution and collagen content, sections were stained using Alcian blue and picrosirius red (Figure 2.7). Analysis of the stained sections revealed almost identical structural morphology with minimal changes to the size and shape of the lacunae. The collagenous structure of the dcECM remained largely unchanged, with only a small observable change in staining intensity, consistent between the outer regions (Figure 2.7; A1&B1) and the inner regions (Figure 2.7; A2&B2).

Alcian blue staining (Figure 2.8) revealed a slight decrease in the amount of staining for indicative of a reduction in sGAG content; this corresponds in with the sGAG quantification values. However, a surprising observation is that despite the volume of the dcECM, sGAG content distribution remained identical between the outer margins and the inner regions of the dcECM. This is despite the inner regions of the native tissue having visibly higher sGAG content.

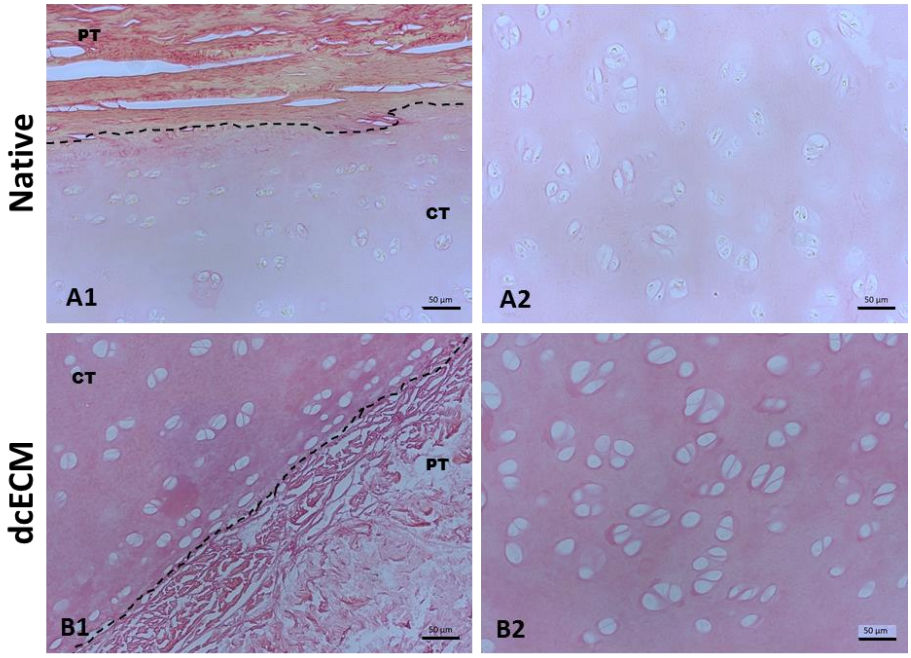

Figure 2.7: Picrosirius red stained dcECM. Representative brightfield images of (A) native costal cartilage tissue and the (B) dcECM. Picrosirius red was performed to visualise the collagenous content of the ECM. (1) Images were taken at the outer edge of the cartilage tissue (CT) with perichondrial tissue (PT) visible. (2) Images were taken at the centre of the sectioned tissue (Scale bar = 50 µm).

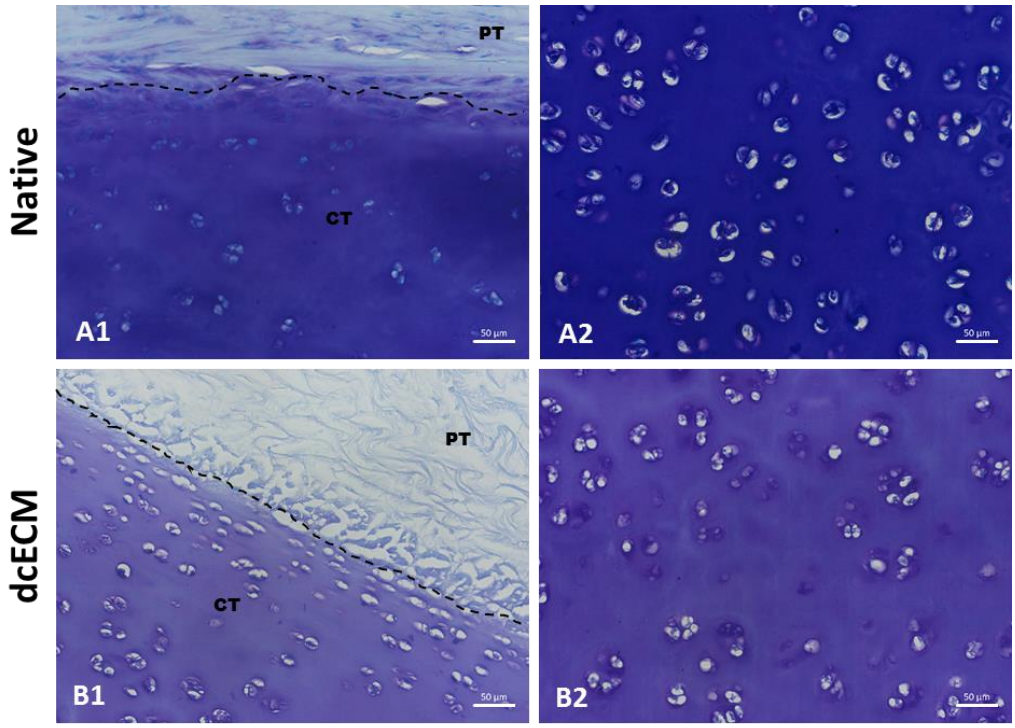

Figure 2.8: Alcian blue stained dcECM. Representative brightfield images of (A) native costal cartilage tissue and the (B) dcECM cartilaginous constructs. Alcian blue was performed to visualise the sGAG content of the ECM. (1) Images were taken at the outer edge of the cartilage tissue (CT) with perichondrial tissue (PT) visible. (2) Images were taken at the centre of the sectioned tissue. (A1& B1) There is visibly lower intensity of Alcian blue staining near the periphery of the Native tissue, this is not visible with the dcECM. Scale bars = 50 µm.

2.4 Discussion

There is currently an unmet need for a methodology capable of efficiently decellularising dense hyaline cartilage tissues with minimal disruption to the ECM. Herein, we describe the development of an optimised decellularisation methodology for porcine costal cartilage, capable of effectively removing cellular and immunogenic content while maintaining sGAG content levels far surpassing published methods.

The Vac-OS methodology was developed to efficiently decellularise hayline costal cartilage tissue without interfering with the integrity of the resultant ECM scaffold, thus, overcoming challenges in decellularising dense avascular tissues[148,150,268,282]. Recent studies applying vacuum-assisted decellularisation demonstrate increased decellularisation efficiency, especially concerning complex organs that include dense tissues, i.e. trachea and larynx [238,279]. The

enhanced cellular clearance reduces the need for harsh physical or enzymatic treatments that may contribute to the loss of bioactive molecules from the ECM [238,279]. Similarly, osmotic shock has also been applied towards the efficient decellularisation of dense tissues with minimal ECM disruption[231,255]. Both these approaches were, therefore, combined with vacuum assistance to formulate the optimised Vac-OS methodology used in this study.

Vac-OS was also compared to previously used vacuum-assisted decellularisation (Vac-STx) that incorporated the detergents triton-x and sodium deoxycholate (SDC) [238]. Interestingly, despite the Vac-OS methodology lacking any ionic surfactants, the resultant scaffolds (dcECM) exhibited DNA content falling below levels that are known to be immunogenic *in vivo* [147]. Additionally, enhanced sGAG retention was also observed with the Vac-OS methodology compared to both the Vac-STx and to the best of our knowledge, other published methodologies aimed at decellularising hyaline cartilage tissues. Often, to improve the efficiency of cellular content removal, studies have milled cartilage tissues, resulting in more effective removal of cellular content but also a significantly higher removal of sGAG's during the decellularisation process, highlighting the impact on tissue volume on decellularisation efficacy and sGAG retention[150,226]. To optimise the Vac-OS methodology for better sGAG retention larger tissue volumes were used. Results indicated that upscaling tissue size by a factor of 10 did not have a significant impact on the clearance of DNA content (Figure 2.5; A&B). This can be attributed this to the use of vacuum assistance, which has previously been used to enhance cellular clearance in dense whole organs such as the trachea and larynx[238,279]. Moreover, although not investigated in this study, the structure of costal cartilage may be more naturally permeable when compared to other sources of hyaline cartilage such as the articular regions as the costal regions are unstable and gradually undergoing endochondral ossification[155], potentially, resulting in the infiltration of blood vessels near the hypertrophic regions of costal cartilage. Although not explicitly investigated in this study, we hypothesised that the Vac-SDS approach that incorporated SDS a potent ionic surfactant would also cause a significant loss of sGAG's due to previous decellularisation approaches reporting similar results[147,256,283]. Moreover, DAPI

assessment revealed that the Vac-SDS was unable to effectively eliminate intact nuclei even with the addition of 1% SDS. Therefore, we eliminated the Vac-SDS methodology early during the optimisation process.

As previously emphasised, sGAGs are especially abundant in cartilaginous ECM and play a key role as facilitators of chondrogenesis and endochondral ossification by binding to and enhancing the functionality of chondrogenic growth factors such as TGF-β [267,270,272–275]. Therefore, the maintenance of sGAG content was a key factor when developing the optimised Vac-OS methodology. Indeed, Vac-OS allowed for the retention of up to 85% of the native sGAG content, which was observed specifically when tissue volume was upscaled by a factor of ten (Figure 2.5; C&D). Additionally, despite the larger tissue's volumes, Alcian blue staining of the dcECM reveals homogenously distributed sGAG content (Figure 2.8). Interestingly, alcian blue staining of native costal cartilage (Figure 2,8; A1&A2) reveals a lower intensity of sGAG content near the periphery of the costal cartilage flanking the perichondrium, these findings may highlight that the core of the costal cartilage should be isolated and used for the production of the dcECM due to their higher native sGAG content.

Homogeneity of sGAG content may be a factor in complete endochondral remodelling and integration of the dcECM. The enhanced retention of sGAG's alongside the removal of cellular material highlights the synergy between the use osmotic shock and vacuum assistance, evident when compared to the more disruptive Vac-STx methodology. These results further bolster previous findings that suggested the proteolytic nature of ionic surfactants such as SDC may be critical facilitators of sGAG loss[150,226,269,284]. More accurate methods could be used in future studies to measure sGAG content. Moreover, techniques such as HPLC could be used to determine how the sGAG profile changes post-decellularisation.

The enhanced maintenance of sGAG content demonstrated by the Vac-OS methodology may also be indicative of the overall preservation of the ECM ultrastructure, a desirable characteristic since the ECM structure and 3D spatial arrangement of macromolecules also both play a vital role in cellular

adhesion, stem cell fate determination and *in vivo* tissue remodelling [88,285,286]. The histological techniques employed so far, however, provide a limited view of the dcECM's ultrastructure. Therefore, more sensitive methodologies are needed to assess the full extent of any changes.

The dcECM was further characterised for remnant alpha-gal content. Its removal was essential due to the highly immunogenic nature of alpha-gal, making it a key barrier to clinical translation[222]. Moreover, failure to assess alpha-gal content in commercially available grafts has previously resulted in negative long-term clinical outcomes[223,287,288]. The Vac-OS methodology has overcome this key barrier to clinical translation by successfully eliminating alpha-gal from the native costal cartilage matrix as highlighted by immunoblotting (Figure 2.6B; lanes 5-7). The western blot methodology used for the assessment of residual Alpha-gal content may not have a limit of detection comparable to more sensitive approaches such as HPLC[289], this definitive establishment of a scaffold free of alpha-gal would be a crucial part of developing implant for human use. Although not investigated in this study, the waste decellularisation solution could be assessed for some of the key immunogenic and biological components that were assessed such as DNA, alpha-gal and sGAG content. This would aid in assessing the efficacy of each of the decellularisation steps in each methodology.

Conclusion

This study that has further optimised and build upon existing vacuum assisted methodologies, resulting in the Vac-OS methodology that is capable of efficiently removing cellular and immunogenic components from hyaline costal cartilage, maintaining 85% of its sGAG content and overcoming long-standing challenges associated with decellularising dense hyaline cartilage tissue, often requiring harsh physical or chemical approaching, resulting in a significant loss of structure and sGAG content. As the resultant dcECM retains the majority of its sGAG content there is great promise of retained matrix integrity and chondroinductive properties. The dcECM is, therefore, a promising construct for further investigations into its matrix integrity and its capability to drive

chondrogenesis. Moreover, due to the removal of highly immunogenic components such as DNA and Alpha-Gal, the dcECM is an ideal candidate for further investigations in vivo, both for its biocompatibility and potential to undergo endochondral ossification at an orthotopic site.

3. Characterising dcECM Matrix integrity

3.1. Introduction

The extracellular matrix (ECM) is a highly dynamic assembly of structural and functional proteins, present in all tissue types. The ECM is subjected to frequent yet highly regulated remodelling[89]. Moreover, every organ has a unique ECM composition that is established during the early stages of embryonic development[290]. Embryonic lethality commonly occur as a result of mutations in genes coding for ECM components[290–292]. Very early investigations into the ECM suggested that it fulfilled the role of a passive structural component, merely filling the space between cells. It was not, however, until the mid-1980's that through the discovery of key proteins such as integrins, the role of the ECM in tissue homeostasis, development and disease was fully appreciated[293] (Figure 3.1). Subsequent investigations have further elucidated underlying mechanisms that support the ECM's role as a mediator of tissue repair and regeneration[88,294–296]. The modulation of the ECM biochemical environment to influence stem cell behaviour has, therefore, emerged as a concept in regenerative medicine[297].

Cellular proteins such as integrin modulate Cell-ECM interaction by binding to cellular receptors and activating pathways such as phosphoinositide 3-kinase (PI3K) and focal adhesion kinase (FAK); involved in regulating cell renewal and proliferation[298–300]. In addition, the ECM can control cell behaviour through the binding and presentation of growth factors, a process that also allows for the creation of local growth factor gradients[301]. These gradients within the ECM allows for the differential regulation of resident and migratory cell populations; establishing various zones within the same tissue, as present in articular cartilage[267]. Examples of ECM-growth factor binding occurs with growth factors such as FGF and TGF-β that bind to the collagenous and proteoglycan component of the ECM, this enhanced its signalling potential and facilitates controlled release during ECM breakdown by enzymes such as matrix metalloproteinases[301,302].

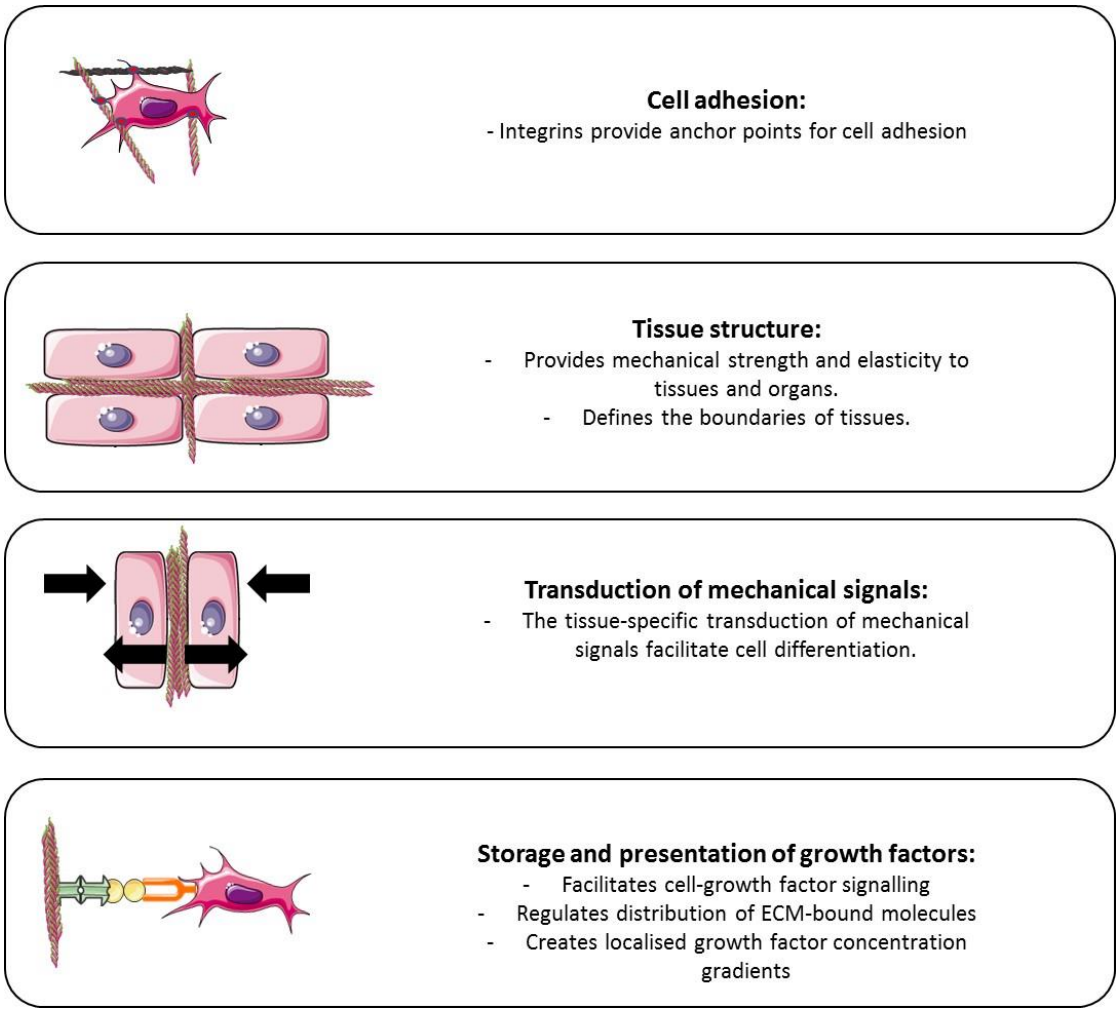

Figure 3.1: Cell-ECM interactions. A schematic summarising the functions of the ECM during tissue formation and homeostasis. Schematic was adapted from Rozario et al[290] &Frantz at al[213]. Figure generated using the Servier medical art database (http://www.servier.com/Powerpoint-image-bank

3.1.1. Key components of hyaline cartilage ECM

The ECM's composition and spatial arrangement are crucial to its functionality. In mammalian species, around 300 ECM-associated proteins have been identified; these are known as the core matrisome[213,303]. Included in the core matrisome are proteoglycans, collagens, and glycoproteins[213,303]. The differential expression of these proteins determines tissue type during development[213,290,303]. The aim of this thesis is the development of costal cartilage based endochondral bone graft. Therefore, the cartilage ECM will be the point of focus for discussion.

Human hyaline costal and articular cartilage have similar compositions[304]. However, the information we have on hyaline cartilage is obtained primarily from studies that focus on articular cartilage. A significant component of hyaline cartilage is water, representing about 65 to 80% of its total weight, while the dry weight of hyaline cartilage is composed mainly of collagens and proteoglycans[267]. Around 30% of the water content is associated with the collagenous structure, with approximately 70% of the overall water content residing in intracellular and pore spaces. The water component of hyaline cartilage plays a key role in the diffusion of nutrients and ions through the avascular ECM of hyaline cartilage[305,306]. Additionally, a majority of the unbound water in hyaline cartilage is present in the form of a gel with high frictional resistance, contributing to the compressive strength of hyaline cartilage, by reducing tissue permeability [307,308].

At around 60%, collagen type II is a significant contributor to the overall dry weight of hyaline cartilage[267] and it the major collagen type. Other collagen sub-types are present in small proportions; these include collagen type I, IV, V, VI, IX and X. Although not as abundant, the minor collagen types do play an essential role in stabilising the collagen type II structure[308]. Studies have, for example, found several sites within collagen type X that facilitate it's crosslinking it to either collagen type II or other type X molecules[309–311]. When considering articular cartilage, collagen type II expression is drastically reduced, post-skeletal maturation, however, the expression is upregulated post-injury[312].

Proteoglycans are the second largest group of macromolecules in hyaline cartilage[267]. These glycosylated protein monomers account for around 15% of the wet weight of hyaline cartilage. Aggrecan is the most abundant proteoglycan, with each monomer containing more than 100 keratin sulfate and chondroitin sulfate chains[267]. A fundamental characteristic of aggrecan is its ability to bind to hyaluronan, forming proteoglycan aggregates that occupy the interfibrillar space within hyaline, resulting in the typically observed osmotic properties and load-bearing capacity of cartilage[313]. Additionally, glycosaminoglycan chains that are associated with the proteoglycan core have

been implicated in sequestering and presenting growth factors, adding to the regulatory mechanism for cell-ECM signalling[314].

3.1.2. Assessment of extracellular matrix components

Due to the importance of the ECM in disease and regeneration, research has continually focused on establishing novel techniques for the evaluation of its structure and composition. Many of the standard established methods for the assessment of the ECM are destructive. These include histological techniques such as H&E's, picrosirius red and alcian blue[315]. Furthermore, these only yield qualitative data on gross morphology, collagen composition and sGAG distribution. Further assays are often required to obtain quantifiable outputs for each of the components above[316]. Additionally, these approaches ignore more subtle changes in collagen structure, while assay's that do target collagen quality through the monitoring of structural components such as hydroxyproline[317,318] are inherently limited, as they ignore other collagen interactions that contribute to overall ECM integrity. Despite their limitations, the assessment of decellularised tissues has remained largely dependent on these standardised techniques. All decellularisation approaches have an impact on native extracellular matrix integrity, there is, therefore, a need for the development of standardised, rapid and non-destructive methods, capable of robustly assessing decellularised tissue matrix integrity.

Palmer and colleagues utilised contrast-enhanced microcomputed tomography (μCT) to image proteoglycans in soft tissues and cartilage[319]. A concept that was further developed by Xie and colleagues to also allow for the identification of healthy and degraded cartilage by using sGAG distribution patterns [320]. This approach is, however, limited in its ability to monitor changes in other prominent ECM components. Additionally, the use of ionising radiation and a contrast agent limit its use in monitoring live cellular constructs.

Gessner and colleagues' utilised ultrasound to monitor ECM integrity non-destructively, eliminating the need for disruptive sample preparation or damaging ionising radiation[321]. The methodology was optimised for imaging cellular liver scaffolds and was especially effective at assessing blood vessel

formation. However, when ultrasound has been used to investigate dense cartilaginous tissues[322], it has demonstrated limited resolution, limiting its use to evaluating the gross morphological structure.

An alternative but less utilised approach to determining the biochemical makeup of biological tissues is Raman spectroscopy. The technique of Raman spectroscopy relies on quantifying changes in a photon's energy state after its collision with a target molecule; in a phenomenon known as Raman scattering[323]. The Raman spectra of a target sample are obtained via illumination with a monochromatic laser beam and the quantification subsequent loss or gain in photon energy that is recorded as a shift in wave numbers (cm^{-1}). The observed change in photon energy is unique to specific molecular interactions[323]. The resultant peaks, therefore, provide a molecular fingerprint of the sample, that can be obtained non-destructively[324]. Raman spectroscopy primarily serves as a powerful tool in law enforcement for the identification of illegal substances[325]. There have, however, been some reported studies that employ Raman spectroscopy for the assessment of biological tissues such as Bone[326], cartilage[327] and the cornea[328], while studies have also utilised Raman spectroscopy as an innovative tool for clinical diagnosis[329,330]. Recently, Raman spectroscopy has been applied to monitor the biochemical composition of decellularised tissue scaffolds, post decellularisation and subsequent recellularisation[331]. The need for highly specialised equipment and expertise has, however, limited the use of Raman spectroscopy in medical research.

Fluorescent probes have been used extensively for imaging components of the extracellular matrix, both in live and fixed tissues[332,333]. Fluorescence microscopy can enhance the inherent contrast of biological tissues, improving image resolution and allowing for the examination of more minute structural or morphological changes[334]. Furthermore, fluorescence microscopy allows for the imaging of specific protein targets[334]. The development of Imaging technologies such as laser-scanning confocal microscopy (LSCM) further improves fluorescence imaging approaches by allowing for the elimination of out of focus light, via the use of a pinhole aperture. The relevant software can use multiple confocal images to piece together a 3D image sequentially[335]. A

fundamental limitation of standard fluorescent microscopy, however, is its inability to track subtle biochemical changes in the target protein, especially in live cultures.

Fluorescence lifetime imaging microscopy (FLIM) can create a spatially resolved image of fluorescence decay; a characteristic that is independent of variables such as concentration[336]. Collagen forms a major component of the cartilage extracellular matrix of which around 90% is collagen type 2[337]. Collagen is also inherently autofluorescent when excited with single or two-photon excitation at around 730nm. Therefore, the lifetimes of the collagen have been harnessed to monitor collagen biochemical environment[338]. Additionally, collagen can also generate strong second harmonic signals that have been leveraged by techniques such as second harmonic generation (SHG) to identify collagen fibril arrangement and collagen crosslinking[339,340]. A study by Ranjit and colleagues demonstrated that a combination of FLIM and SHG could be applied to isolate and identify specific to various collagen subtypes[338]. Therefore, FLIM could have potential applications in monitoring biochemical changes in the ECM post decellularisation.

In this chapter, we address the need for more comprehensive methods for the assessment of the extracellular matrix, especially, post VacOS decellularisation. The dcECM was, therefore, subjected to in-depth matrix analysis using Raman spectroscopy, differential scanning calorimetry and the novel approach of using fluorescence lifetime imaging microscopy. These in combination provided an overall image of matrix integrity and would further confirm the results observed during initial histological and sGAG composition analysis.

3.2. Methods

3.2.1. Raman Spectroscopy

The dcECM and native costal cartilage samples (dimension ~5 mm height × 10 mm in diameter) were analysed without further processing. The spectra were acquired directly from the surface of the flat surface of the samples using

an InVia Raman microspectrometer (Renishaw). This was equipped with an 830-nm laser, producing 300 mW at source. Calibration was performed before every run using silicon which has a known Raman band (520.5 cm^{-1}), and on polystyrene to measure bands in the same range as that of cartilage (wave numbers between 1000 cm^{-1} and 1030 cm^{-1}). The spectra were acquired at a laser power of 2 mW for 1 second with 4 accumulations. 3 different spectra were acquired from each end of the flat ends of the cylindrical samples. The spatial resolution (at 50× objective) was 2 µm × 2 µm. No thermal heating or degradation of the samples was observed at the laser powers utilised. Data was analysed used Matlab 7 (Mathworks, UK), and peaks were identified using previously published literature (Table 3.1).

Raman shift (cm^{-1})	Assignment	ECM Component
822-875	C-C	Hydroxyproline (Collagen)
900-950	C-C, α helix	Proline (Collagen)
1001	H-O	Phenylalanine (Collagen)
1063	OSO3−, symmetric stretch	Chondroitin sulfate (sGAGs)
1230-1280	Amide III	Collagen
1620-1690	C==O, Amide I	Collagen

Table 3.1: Raman spectroscopy band assignments. Based on previous literature investigating collagen, glycosaminoglycans and amino acids[341–344].

3.2.2. Differential scanning calorimetry (DSC)

DSC was used to measure collagen denaturation temperatures as an indicator of the structural integrity of the matrix[345]. This has previously been applied to cartilaginous tissues[346]. Control native costal cartilage samples were compared to dcECM samples. Briefly, samples were cut into cubes weighing 10 mg each. Each 10mg sample was placed into 40 µL aluminium crucibles, that were unperforated to prevent background noise because of water

evaporation. Native samples did not undergo any prior processing. The dcECM, however, was washed overnight to remove any excess salts that have accumulated due to decellularisation process, as unwashed samples demonstrated inconsistent results. The calorimetric experiments were performed using Mettler Toledo DSC-1 calorimeter (Mettler Toledo, Greenfield, UK). All experiments were performed between 25 °C and 95 °C at a heating rate of 3 °C/min. Data analysis was carried out using the STARe Thermal Analysis Software (Mettler Toledo, Greenfield, UK). The obtained readings were normalised to an empty unperforated reference crucible.

3.2.3. Multiphoton imaging

SHG and FLIM were used to measure changes in the collagen biochemical environment as a measure of matrix integrity, this work was carried out in collaboration with the Duchen Lab (Department of cell and developmental biology, UCL). Without any prior processing Native costal cartilage and dcECM (dimension ~5 mm height × 10 mm in diameter) were placed in PBS in preparation for imaging. Laser scanning microscopy with multiphoton excitation was carried out using a Zeiss LSM 510 microscope (Zeiss, Oberkochen, Germany) with a 10x 0.3 N.A water-dipping objective and the 80 MHz pulsed output of a Chameleon (Coherent, Santa Clara, USA) Ti:sapphire laser. Second harmonic generation and autofluorescence were observed using 920 nm and 720 nm illumination wavelengths respectively. In both imaging modalities, a 650 nm dichroic filter separated the two-photon excitation from the shorter wavelength emission, collected with a 460(±25) nm band-pass filter before detection by a high-speed hybrid detector (HPM-100), (Becker & Hickl, Berlin, Germany). Single photon emission events were recorded by a commercial time-correlated single photon counting SPC-830 electronics module (Becker & Hickl, Berlin, Germany) in a desktop computer. Fluorescence lifetimes were extracted from the measured time-resolved emission data by least-squares fitting of a monoexponential decay in SPCImage (Becker & Hickl, Berlin, Germany).

3.2.4. Statistical analysis

Data are expressed as the mean ± standard deviation (SD). Statistical significance was determined as described in Chapter 2.2. All statistical analysis was performed using GraphPad Prism version 6.0f for windows (GraphPad Prism Software, La Jolla California USA, www.graphpad.com).

3.3 Results

3.3.1. Raman spectroscopy indicated the retention of key ECM-associated molecular bonds, post Vac-OS.

Raman spectroscopy utilises monochromatic light to harness the phenomena of inelastic scattering providing a qualitative view of the biochemical composition of a samples can be observed[347]. Raman spectroscopy was therefore utilised to monitor changes in the dcECM's composition. Raman spectra were obtained from both native costal cartilage and the dcECM. Key molecular interactions were identified and associated with hyaline cartilage ECM macromolecules using previous literature (Figure 3.2). The identified peaks included Hydroxyproline (850 cm^{-1}), Proline (920 cm^{-1}), Phenylalanine (1001 cm^{-1}), sulfated glycosaminoglycans (1063 cm^{-1}), Amide III (1230-1280 cm^{-1}) and Amide I (1630-1690 cm^{-1}) (Table 3.1).

Spectral analysis indicated that all bands present in the native costal cartilage tissue are retained post Vac-OS decellularisation. Qualitative analysis suggests there was a significant change in the intensity at band assignment 1063 cm^{-1}, indicative of sGAG associated chondroitin sulfate[342].

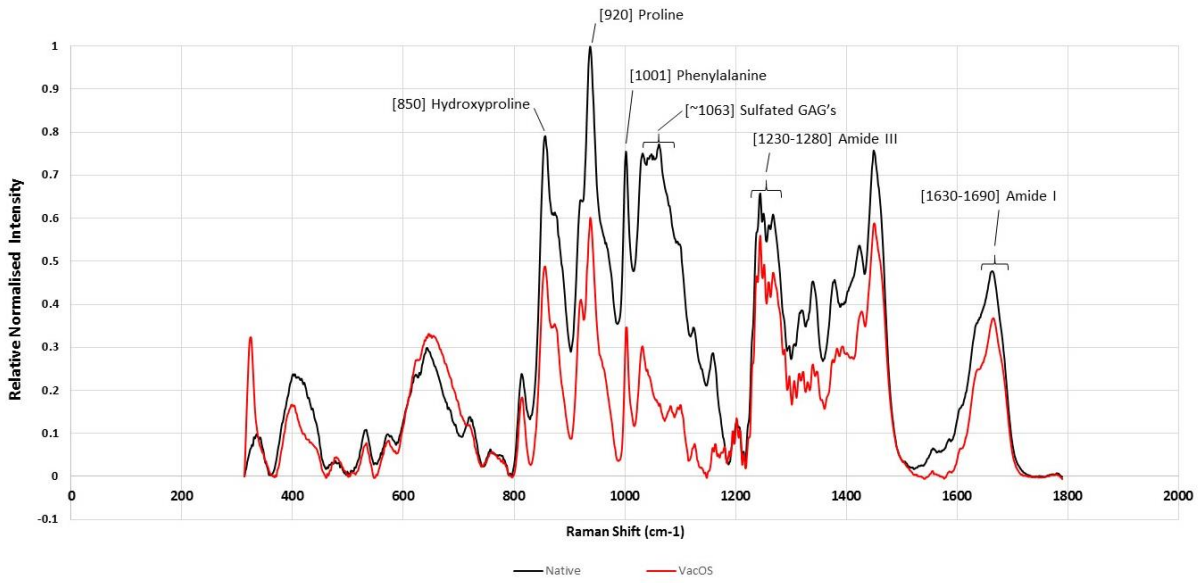

Figure 3.2: Raman spectroscopy comparing native costal cartilage and the dcECM. Average intensity of the obtained Raman spectra (Raman shift 750-1800 cm^{-1}) from native control costal cartilage (Black line) and VacOS treated costal cartilage samples (Red line).

3.3.2. Thermal analysis of the dcECM indicated minimal ECM damage post Vac-OS decellularisation.

Thermal denaturation of collagen is indicative of collagen crosslinking[345] and has been used to determine cartilage matrix integrity[346]. Therefore, DSC was used to compare collagen denaturation temperatures in the dcECM vs native costal cartilage. The STARe Thermal Analysis Software (Mettler Toledo, Greenfield, UK) was used to evaluate and analyse the obtained changes in enthalpy to determine peak denaturation temperatures (Figure 3.3; A). Thermal analysis indicated significant changes in the denaturation temperatures between the dcECM and native costal cartilage (Fig 3.3; A&B). However, a large amount of variation observed in the denaturation temperatures of the dcECM, with some readings lacking the presence of collagen denaturation curve. Further investigation was carried out to determine the cause of this variation.

These findings highlighted that the changes were observed were only in the Vac-OS decellularised samples. The VacOS methodology is based around the use of high salt concentrations, and although wash steps were incorporated in the methodology, it was hypothesised that salt residues present in the dcECM

might be interfering in the thermal analysis process[348]. Both native and decellularised cartilage samples were, therefore, washed in deionised water for 16 hours at 4 ºC. While there were no changes in the Native cartilage denaturation temperatures, there was a significant decrease in the variation of collagen denaturation temperatures when considering the dcECM. However, the observed decrease was still insignificant when compared to native costal cartilage (Figure 3.3B).

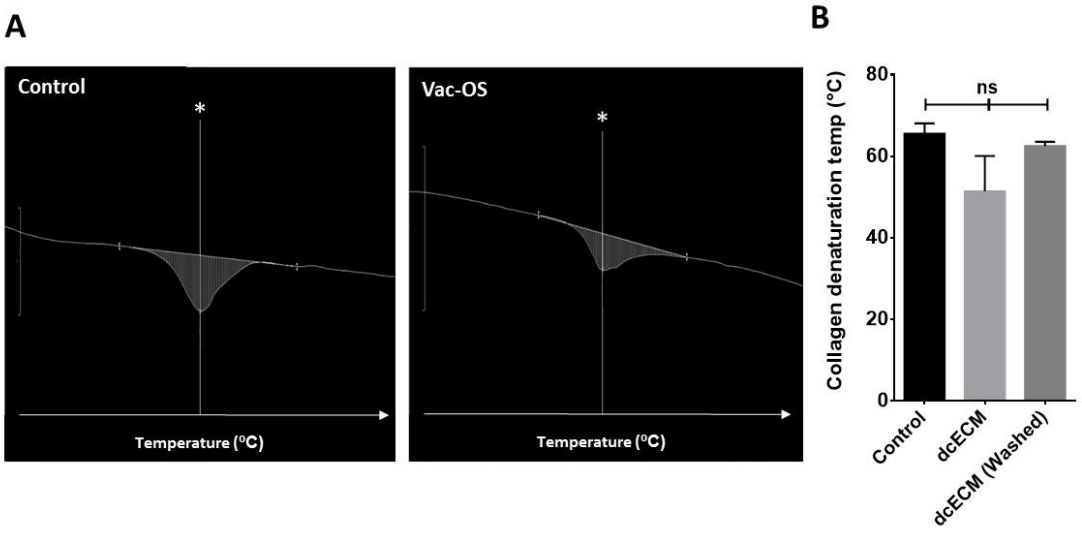

Figure 3.3: Thermal denaturation of the dcECM. (A) Representative differential scanning calorimetry thermal analysis curves and (B) quantification of average denaturation temperatures comparing control cartilage vs dcECM vs dcECM (Washed), (*Peak denaturation temperature). Data is expressed as mean ±SD (n= 4, ns = non-significant). Statistical analysis performed using a one-way ANOVA using Bonferroni's posthoc correction.

3.3.3. Optimised multiphoton imaging and analysis indicates minimal disruption to the Vac-OS decellularised matrix.

In order to non-destructively assess the matrix integrity of the dcECM multiphoton imaging and analysis techniques were applied (Figure 3.4 A-E). The highly non-centrosymmetric structure of fibrillar collagen gives rise to intense second harmonic generation when exposed to a high-intensity coherent light source [349]. This allows collagen structures to be imaged using laser scanning microscopy by observing light emitted from a sample at half the

wavelength of the incident illumination. Collagen also possesses intrinsic fluorescence properties due to the presence of a range of spectrally-overlapping endogenous fluorophores [350]. Changes in the local nanoscale environment of these fluorophores are reflected by alterations in their fluorescence lifetime[351], the average time taken for emission to occur following excitation. Combining second harmonic and fluorescence lifetime imaging would allow the assessment of morphological changes within the extracellular matrix. Initial assessment of the obtained FLIM images involved selecting nine random regions of interest (ROI) (Figure 3.4;D). Initial results indicate a significant shift in lifetimes when comparing control costal cartilage and the dcECM.

Closer examination of the SHG images, however, reveals subtle changes in lacunae size, post Vac-OS decellularisation when comparing native costal cartilage to the dcECM (Figure 3.4; A1&2). The lacunae being empty do not have an ECM associated lifetime reading. Therefore, variations in size could affect the total fluorescent signal-producing region of an image. In addition, as the methodology for ROI selection was random, it did not account for non-ECM specific signals or out of focus regions that did not have sufficient signal. SHG signals are produced due to the inherent fibrillar arrangement of collagen and therefore, was specific to the ECM. Considering this characteristic, Image J was used to select SHG signals above a given threshold, thus selecting a collagen-specific signal specifically from the ECM (Figure 3.5; A). The SHG generated ROI was subsequently applied to the corresponding FLIM image, isolating autofluorescence lifetime signals that were specific to the ECM (Figure 3.5; B). The optimised methodology demonstrated that there was no significant change in fluorescence lifetimes when comparing control costal cartilage and the dcECM (Figure 3.5; C).

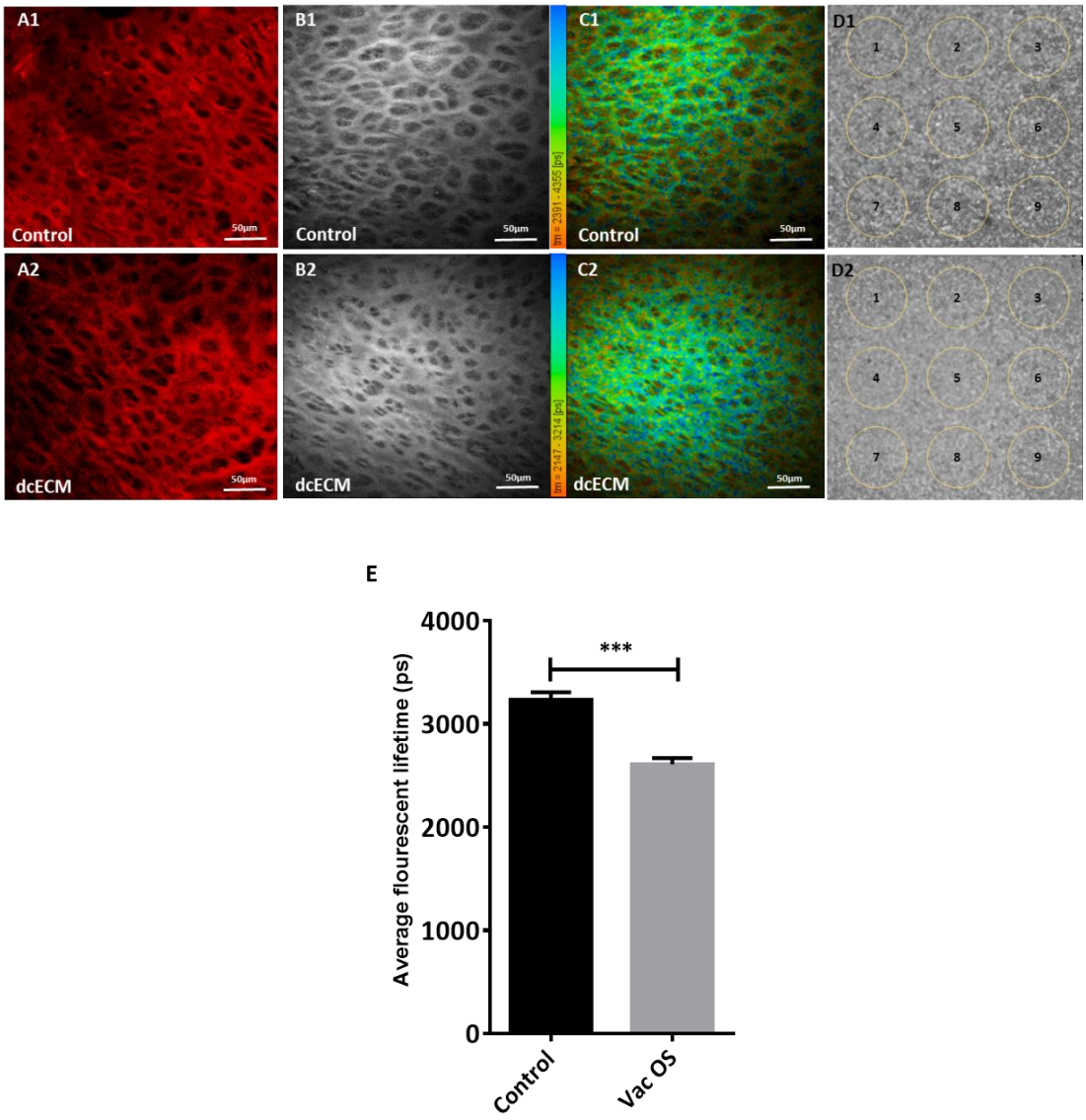

Figure 3.4: Pre-optimised FLIM and SHG imaging. (A) Second harmonic generation (SHG) microscopy image. The decellularised sample retains its architecture with minimal disruption to the collagen component of the extracellular matrix (B)Two-photon autoflouresence image at 720nm excitation. Cells are observed within the lacunae of the control sample while being absent within the osmotic shock treated sample. (C) False coloured fluorescence lifetime Imaging microscopy (FLIM) image indicative of the distribution of the fluorescence lifetimes within the samples (D) Relative FLIM intensity images with 9 regions within the sample quantified using imageJ (The displayed images are representative of four independent experiments; scale bar = 50µm). (A1-D1) Control costal cartilage samples, (A2-D2) VacOS decellularised costal cartilage samples (dcECM).(E) ImgeJ quantification of the ROI's indicate there is an overall decrease in the average fluorescence lifetimes due to the osmotic treatment. Representative quantification data are represented as mean ± SD (n=4; ***p<0.001).. Statistical analysis performed using an unpaired t-test with Welch's posthoc correction.

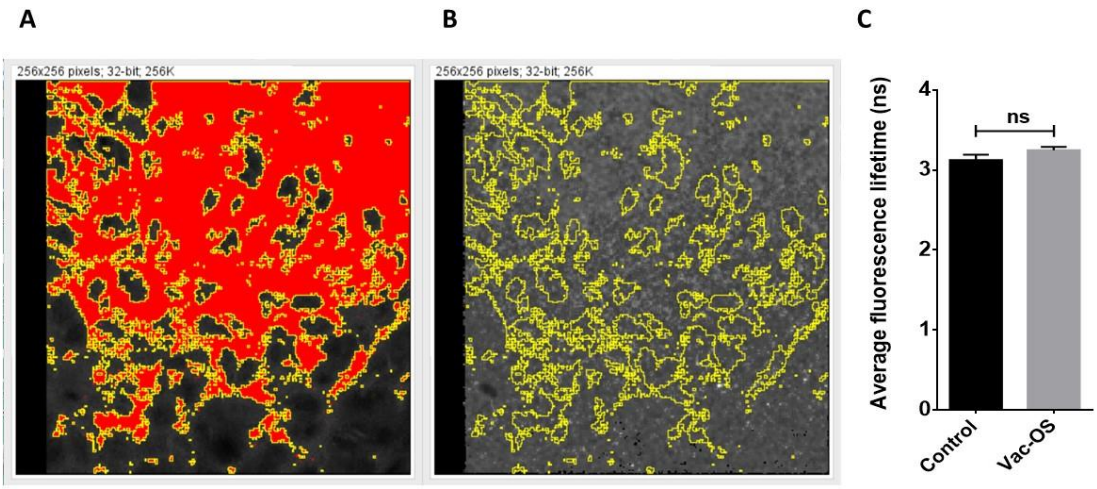

Figure 3.5: Optimisation of FLIM and SHG imaging. (A) Representative second harmonic generation (SHG). The ROI is selected using an intensity threshold, thus negating non-ECM regions. (B) Representative FLIM intensity image with the superimposed ROI obtained from the SHG image, used to quantify fluorescence lifetime. (The displayed images are representative of four independent experiments). (C) ImageJ quantification of the ROI's, measuring the average fluorescence lifetimes (n=4). Quantification data are represented as mean ± SD. Statistical analysis performed using an unpaired t-test with Welch's posthoc correction.

3.3.4. Thermal analysis and optimised multiphoton imaging are capable of detecting changes in cartilage ECM structure.

DSC and FLIM have both been applied to determine disease-associated changes in articular cartilage[346,352]. However, while DSC has been applied for the analysis of decellularised tissues[353,354], there are no identifiable studies that utilise FLIM. Moreover, it was essential that the ability of both DSC and FLIM to assess matrix integrity was verified. Therefore, the dcECM was further denatured using collagenase to induce matrix damage.

Auto fluorescence images demonstrate a clear disruption of the collagenase treated dcECM when compared to both the control cartilage and undigested dcECM (Figure 3.6; A-C). Changes in morphology are accompanied by a decrease in collagen denaturation temperatures when comparing the collagenase treated dcECM compared to both the untreated dcECM and control costal cartilage ($p<0.05$)(Figure 3.6; D). Collagenase digestion of the dcECM also has a significant impact on the autofluorescence lifetimes (Figure 3.6;E). However, more interestingly, the shift in lifetimes was more significant than the shift in denaturation temperatures($p<0.001$).

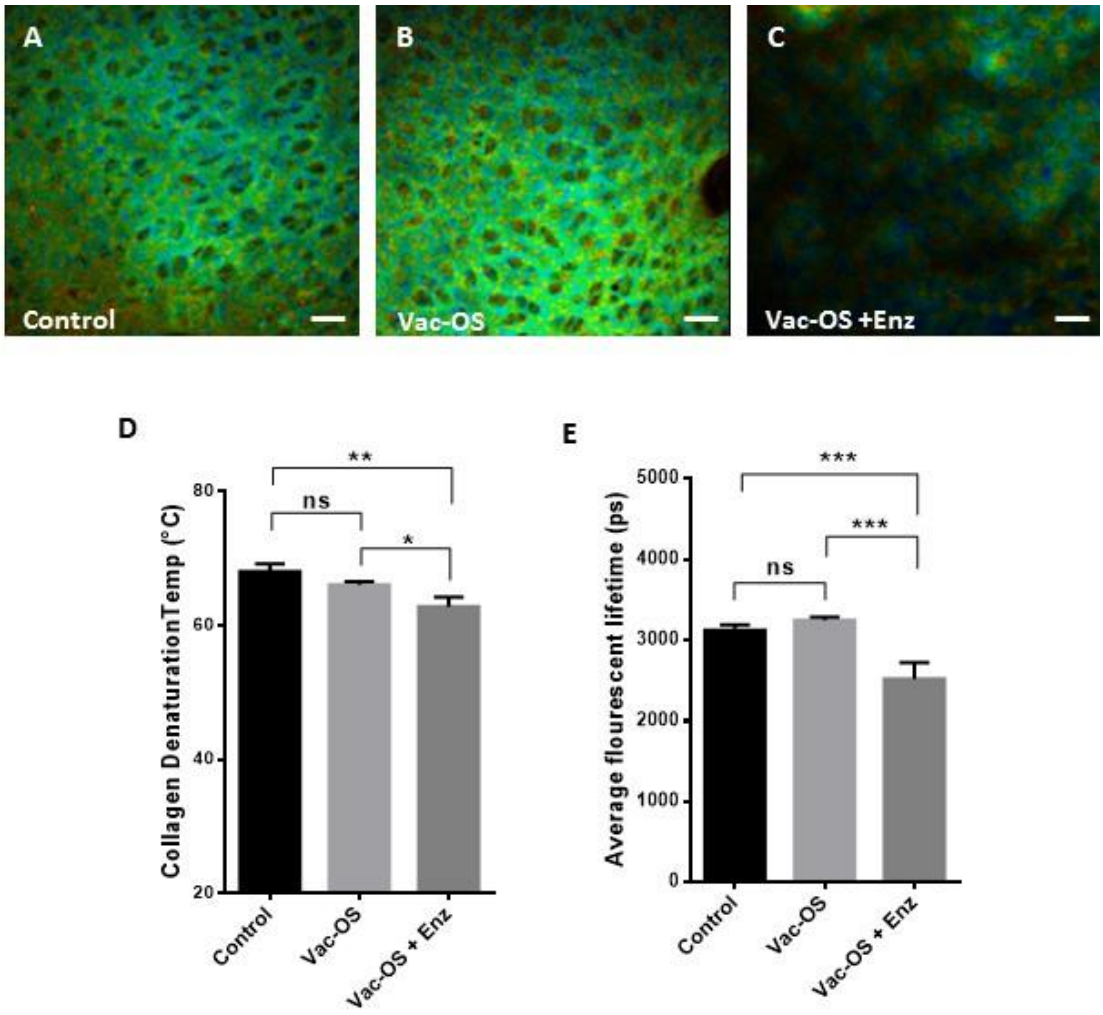

Figure 3.6: Quantitative FLIM analysis of the dcECM. Further disruption of the Vac-OS decellularised scaffold using collagenase. (A-C) False coloured fluorescence lifetime imaging microscopy (FLIM) images indicative of the distribution of the fluorescence lifetimes within the samples (scale bar= 50µm). (D) Quantification of average denaturation temperatures comparing control cartilage vs dcECM vs collagenase treated Vac-OS samples. (E) ImageJ quantification of the ROI's, measuring the average fluorescence lifetimes (n=4 *p<0.05, **p<0.01, ***p<0.001, ns= non-significant). Representative quantification data is expressed as mean ±SD. Statistical analysis performed using a one-way ANOVA using Bonferroni's posthoc correction.

3.4 Discussion

ECM structure, composition and 3D spatial arrangement of macromolecules play a vital role in cellular adhesion, stem cell fate determination and *in vivo* tissue remodelling [88,285,286]. Additionally, cartilage matrix components such as collagen type II and sGAGs play a crucial role in promoting chondrogenesis and endochondral ossification [272–275,355]. Maintenance of ECM structure was, therefore, thoroughly considered when developing the Vac-OS

decellularisation methodology. Most studies utilise standard histological techniques for the assessment of decellularised cartilaginous matrices, which only allow for the gross examination of matrix architecture [356,357]. This chapter considers the need for more in-depth ECM analysis that is rapid, sensitive and non-destructive and attempts to meet it.

Raman spectroscopy has been utilised for the assessment of biological tissues due to its molecular-level resolution, allowing for the monitoring of minute changes in matrix integrity[358] that may be otherwise missed by other gross assessment techniques. Raman spectroscopy was, therefore, utilised for qualitative analysis of the dcECM's molecular composition (Figure 3.2). Results indicate there were minimal changes in crucial collagen associated peaks such as hydroxyproline, proline, phenylalanine and amides. Proline and hydroxyproline levels have previously been used as an indicator of collagen systhesis[318], in combination with amides these key components have been heavily implicated in the unique structural organisation of collagen type II and it's stability[359]. Overall, the maintenance of these molecular interactions suggest the conservation of vital cartilage-associated proteins and, therefore, minimal damage to the cartilage matrix ultrastructure[341–344].

The only distinct difference highlighted by the Raman spectra was in the sGAG associated chondroitin sulfate peak at 1063 cm^{-1}, demonstrating a reduction relative peak intensity. The previous chapter reported a minimal 15% loss in sGAG content, post VacOS decellularisation. The two results, however, cannot be directly corroborated as the Raman spectra obtained only analysed chondroitin associated interactions and were not truly quantitative. Additionally, Raman spectroscopy gives a highly localised view of surface molecular composition and sGAG content, this leaves using Raman spectroscopy for quantitative analysis prone to inaccuracies. Destructive assays that quantify overall sGAG content may, therefore, supersede Raman in terms of overall quantification accuracy. The presence of a sGAG associated peak, however, is promising, due to the crucial role played by sGAG's in cartilage homeostasis[271], mechanical strength[360] and their ability to promote both chondrogenesis[272–274] and endochondral ossification[275].

There are a number of Raman spectroscopy methodologies that are available for the assessment of biological tissues; each specialised for detecting specific molecular interactions[347]. Therefore, the accurate quantification of molecular interactions using Raman spectroscopy requires highly specialised equipment, in-depth expertise and extensive optimisation. Furthermore, the presence of other organic compounds or matrix damage induced by the extended exposure to a laser may interfere with data quality[361]. Raman spectroscopy is a powerful non-destructive analytical tool for qualitative analysis. However, when applied for quantitative analysis, its accuracy is highly dependent instrument response, and levels of interference thus reducing its reliability[347]. This is further amplified when used with biological tissues as they contain a plethora of molecular interactions.

The underlying mechanisms of collagen crosslinking and its role in collagen structural integrity was first established in the late 1960's[362–366]. Furthermore, collagen crosslinking pathways are also activated during the repair of hyaline articular cartilage[367]. Methodologies such HPLC[367] and chromotography[368] have been applied for the in-depth analysis of collagen crosslinking in cartilage. While these approaches provide a comprehensive view of collagen crosslinking, they require extensive sample preparation making them both time consuming and labour intensive.

DSC is based on the principle of thermal analysis via the monitoring of changes in enthalpy that are associated with changes specific to the molecular composition of the desired substrate[369]. This approach has been applied to measure key ECM structural components such as proteins[370–372] and lipids[373]. Interestingly, it has also been reported that alterations in articular cartilage matrix integrity between healthy and osteoarthritic cartilage are reflected by variations in the collagen denaturation temperatures[374], that are affected by the extent of collagen crosslinking[375]. Therefore, determining collagen denaturation temperatures in native costal cartilage and the dcECM using DSC provides a reflective measure of collagen ultrastructure damage post Vac-OS decellularisation. The obtained results demonstrated a lack of change in collagen denaturation temperatures when comparing the dcECM to native costal cartilage. These results highlights the effective maintenance of collagen

crosslinking, indicative of minimal damage to the collagen ultrastructure post VacOS decellularisation.

In order to assess the efficacy of using DSC to monitor changes to the hyaline cartilage matrix, dcECM samples were digested using collagenase to induce matrix damage. The collagenase digested samples demonstrated a significant reduction in denaturation temperatures, verifying the capability of DSC to monitor matrix damage. DSC is, however, not immune to interference from other components such as salt content, this was demonstrated in the highly variable results that were obtained from the dcECM, with some runs' failing to demonstrate a visible collagen denaturation peak. It was only by washing the dcECM in deionised water that residual salt content could be removed providing more reliable results. Additionally, changes in enthalpy can also result from the evaporation of water[376], and while this study used sealed crucibles to prevent loss of water through evaporation, the prevention of evaporation could not be guaranteed, especially as the samples were subjected to near boiling point temperatures. This susceptibility to various factors associated with the environment and used has been highlighted by Deangelis and Papariello[377]. Furthermore, other analytical techniques such as FLIM allows for the non-destructive analysis of collagen crosslinking, while also monitoring other subtle change in collagen biochemical environment[378].

FLIM is based on the principle of measuring the lifetime of a fluorophore to determine its molecular interactions and thus its biochemical environment[379–381]. Recently, FLIM has been utilised as an alternative approach to monitor subtle changes in the ECM[382]. It is widely accepted that site-specific modifications in collagen cross-linking can be identified through imaging techniques that quantify the lifetimes of collagen auto-fluorescence[378]. Additionally, second harmonic generation (SHG) microscopy was developed as a method for the assessment collagenous structures[339] and when combined with FLIM has been efficiently applied for the identification and separation of collagens sub-types[338]. SHG and FLIM were, therefore, combined for both the gross morphological assessment of the collagenous architecture and the biochemical environment of the collagen, respectively.

The SHG images reveal a subtle change in lacunae size post decellularisation. The difference in lacunae size could result from the low atmospheric pressures that the costal cartilage is subjected to during VacOS decellularisation (Figure 3.4) causing ECM deformation. Initially, ROI's for FLIM analysis of each image were chosen as nine random regions of the same area using ImageJ. The results demonstrated a significant change in lifetimes when comparing native costal cartilage and dcECM samples. Upon closer examination of the raw data, it was apparent that the random selection of ROI's for each FLIM image was resulting in the selection of regions that were void of an autofluorescent signal, either as a result of a lack of focus or empty lacunae. This was also a disadvantage that was highlighted by Becker[336]. Attention was, therefore, drawn back to the changes in lacunae size, as they could impact the amount of non-ECM specific fluorescence, affecting the overall lifetime readout of each image. Since SHG relies on the non-centrosymmetric structure of collagen, an ECM-specific region can be obtained. Therefore, SHG images were used to choose threshold based ROI's, eliminating non-ECM specific areas (Figure 3.5). This approach ensured that each image had an ROI that was unaffected by changes in lacunae size or image focus. The optimised FLIM analysis approach demonstrated minimal changes in the lifetime when comparing native costal cartilage to the dcECM; this was also now in agreement with the DSC data.

An investigation into the efficacy of using FLIM for the monitoring of changes in collagen biochemical environment and ultrastructure was required. The dcECM was again subjected to matrix damage using collagenase. The enzyme-treated dcECM constructs demonstrated an evident shift in lifetimes, indicating the inherent capacity of the optimised FLIM analysis to detect and quantify changes in matrix integrity. Interestingly, the results also highlighted a more significant difference in lifetimes, between the digested dcECM and native costal cartilage, when compared to parallel results obtained from the thermal analysis. These findings suggest that the FLIM approach surpasses the DSC regarding sensitivity to changes in matrix integrity. Despite the advantage of non-destructively monitoring matrix integrity, the use of FLIM cannot identify specific changes in collagen when they do occur. Therefore,

further optimisation is required before FLIM can be utilised as an in-depth methodology for the molecular analysis of biological tissues. This study harnesses FLIM to assess matrix integrity of decellularised ECM and with sufficient optimisation could be widely applied in the non-destructive monitoring of tissue during the optimisation of decellularisation methodologies or fabrication of clinically applied decellularised substrates.

Investigations into the matrix integrity of the dcECM have yielded valuable information into the ultrastructure maintenance post-VacOS decellularisation. There are, however, approached such as biodegradation assay's that may provide an indirect measure of matrix integrity. This, in combination with the retention of crucial cartilage matrix components such as sGAG's highlights the dcECM's potential to drive chondrogenesis and promote endochondral ossification *in vitro*. There are, however, two essential steps for the development of a fracture callus mimetic; the production of a matrix and the use of an appropriate cellular component. The promising results obtained from the investigation of the dcECM now provides sufficient impetus for the further *in vitro* and *in vivo* investigations of the dcECM to analyse its bioactivity and non-immunogenic nature.

4. Biological characterisation of the dcECM

4.1. Introduction

Cellular interactions during fracture repair are an indispensable part of the healing process. Therefore, it is crucial to assess the *in vitro* and *in vivo* interactions of the dcECM with the relevant cellular population. Chapter 3 has highlighted that the dcECM retains its native structural integrity post Vac-OS decellularisation. Structural and functional components of the ECM such as the collagen type 2 fibrillar structure and GAG content could play a crucial role in promoting or enhancing chondrogenesis in relevant cell populations such as human-derived chondrocytes and hPDSC's. However, the bioactivity of the dcECM can only be determined via assessment of its interaction with relevant cellular populations, both *in vitro* and *in vivo*.

4.1.1 Monitoring cell-matrix interactions.

For the creation of a cartilage fracture callus mimetic, the dcECM needs to interact favourably with cell populations that are involved during the endochondral fracture healing. Therefore, the choice of cell type and culture conditions need to be carefully considered.

During the initial inflammatory phase of fracture healing, factors such as TNF-α, act as secondary inflammatory signals attracting surrounding stem cells from the bone marrow and periosteal niche via chemotaxis[383]. The stem cell population resident in the periosteal niche has been identified as a key regulator of fracture healing[384]. There has, therefore, been a drive to isolate PDCs as a cell source for bone tissue engineering purposes. Indeed, it has previously been shown that human periosteum-derived stem cells (hPDSC's) seeded onto a decellularised/devitalised bone matrix can undergo endochondral bone formation with the resulting bone containing a hematopoietic compartment [207], a process that is driven by early PKC, BMP

and Wnt signalling [385]. These promising characteristics of hPDSC's make them an ideal cell type for combination with the dcECM derived cartilage callus mimetic.

Underlying all biological processes is the multilayered, gene expression control mechanism that regulates protein expression and is, indeed, a critical factor in determining cell phenotype and function[386]. Gene expression analysis targets the principal component of the protein synthesis pathway, by quantifying intracellular mRNA levels. The gene expression profiles of skeletal stem cells undergoing chondrogenesis and maturation have been extensively studied, both *in vitro*[387,388] and *in vivo*[389,390]. SRY-related high-mobility-group box 9 (SOX9) has been recognised as the master regulator of chondrogenesis, as its role in enhancing the expression of cartilage matrix associated proteins such as aggrecan and collagen type II have been well established[391,392]. It is, therefore, widely accepted that the upregulation of *SOX9* expression is an early indicator of chondrogenesis in MSC's[393–395]. An upregulation of *COL2A1* swiftly follows upregulation of *SOX9* and its continued co-upregulation during the early stages of chondrogenesis[396,397]. Aggrecan accumulation as a result of *SOX9* promotion is also common during chondrogenesis and cartilage tissue formation[398], however, there is some doubt in using aggrecan gene expression as a reliable indicator for identifying early chondrogenesis, as studies have highlighted that aggrecan expression may be an *in vivo* phenomenon that is not replicated i*n vitro*[399]. SOX5 and SOX6 are transcription factors with closely related DNA binding regions to SOX9 and are upregulated during the later stages of chondrogenesis, forming the SOX-trimer super enhancer, further driving late chondrogenesis[400].

4.1.2 Factors that drive endochondral fracture healing

Recruited stem cell populations must undergo a tightly regulated process of cellular differentiation to generate the fracture callus; a crucial phase of endochondral fracture healing[2]. The process is primarily driven by the chondrogenic differentiation of stem cells, that largely originate from the periosteum niche[35].

Several biological and mechanical factors influence the chondrogenic differentiation cascade that results in the formation of the bridging cartilaginous callus, and its subsequent hypertrophy and ossification. The traumatic nature of bone fracture can also damage the surrounding soft tissues and vasculature resulting in localised hypoxia[31]. Research has suggested that the resultant hypoxia is a crucial environmental cue that promotes chondrogenesis of recruited stem cells as cells with a chondrocytic phenotype are more adapted to survive low nutrient and oxygen conditions[401]. However, prolonged hypoxia due to lack of angiogenesis can have a detrimental effect on endochondral ossification, resulting in delayed or non-union fracture healing[402,403]. Therefore, an inadequate blood supply has been identified as a principal underlying cause of atrophic non-unions[404]; a subtype commonly associated with prolonged treatment times and poor patient outcomes[405]. In response to the hypoxic environment, growth factors such as VEGF are secreted in a controlled manner, promoting neo-angiogenesis due to its ability to mobilise endothelial progenitor populations, influence their proliferation and promote cell differentation[406,407]. *VEGF* expression generally peaks during early fracture and later during chondrocyte hypertrophy[408].

In addition to environmental factors, several growth factors are also associated with the chondrogenesis and hypertrophy of mesenchymal and periosteum-derived stem cell populations. TGF-β is a common component in chondrogenic differentiation media due to the well-established role in driving the chondrogenesis via the binding of TGF-β to type II receptors, that further interact with type I receptors, the signal is then transduced via the phosphorylation of the R-SMAD signalling pathway, eventually promoting the transcription of chondrogenic genes[409]. TGF-β, therefore, regulates the expression of crucial chondrogenic transcription factors such as SOX9, subsequently upregulating the expression of cartilage matrix-associated proteins, especially *COL2A1*[410–412]. Bone morphogenic proteins (BMP's) are the largest group from the TGF-β superfamily, playing an important role in cartilage and bone formation[413,414]. Mutations in the DNA regions coding for BMP can cause severe impairment in endochondral bone formation; thus, dysregulating skeletal development[415]. The addition of BMP2 can initiate

chondrogenic lineage development in MSC's, including cell populations derived from the periosteal niche, where BMP also plays a crucial role in osteogenesis during endochondral bone formation[416–418].

4.1.3 Monitoring immunogenicity and biocompatibility of biological scaffolds.

ECM derived scaffolds, such as the dcECM, may be an ideal target for tissue engineering of the fracture callus due to its structural and biochemical homology with the target tissue. However, the host immune response to xenogeneic tissues remains a significant barrier to the clinical translation of xenogenic tissue-derived grafts[419]. The optimised Vas-OS decellularisation methodology was effective at reducing levels of immunogenic components such as DNA and Alpha-Gal below levels required for an adverse host inflammatory response. These findings do not, however, suffice as the sole predictor of *in vivo* immunogenicity thus requiring further *in vivo* biocompatibility.

The role of macrophages in the biological response to foreign antigens, including those presented by implanted biomaterials is well documented[420–422]. Macrophages primarily facilitate with the removal of residual cellular and fibrous debris via phagocytosis[423]. Moreover, they also secrete a plethora of chemotactic and inflammatory factors that initiate cellular recruitment required for tissue remodelling[423,424]. Macrophages activated by the cytokine release from damaged tissues or local immune cells, migrate to the source and acquire several transient polarisation states to fulfil their function[425]. These include pro-inflammatory M1 and pro-regenerative M2 populations, identified by their presentation of markers such as CD86 and CD163, respectively [426–428].

C57BL/6 and BALB/c mice are the most commonly used strains used in biomedical research [429,430]. Subcutaneous implantation of scaffolds into BALB/c mice has previously been employed to investigate the host response to the constructs in the context of musculoskeletal applications including large bone defect healing[431,432]. Overall these studies have illustrated that BALB/c mice are capable of eliciting a host rejection response towards xenogeneic

grafts while also being capable of driving tissue integration and remodelling. Considering this evidence, BALB/c mice would be an ideal choice to assess the acute immune reaction to the dcECM while also gauging its potential for subsequent tissue remodelling and integration[432].

This chapter addresses the need to assess the bioactivity of the dcECM and elucidate the underlying mechanism and conditions that drive the cellular differentiation of relevant skeletal and *in vitro* and immunogenicity *in vivo*.

4.2. Methods

4.2.1 Human articular chondrocyte isolation.

Human cartilage was harvested from the articular surfaces of the knee and hip from patients undergoing joint replacement surgeries. Articular chondrocytes were extracted from cartilage using a methodology that was adapted from previous studies [207,411,433,434]. Briefly, two grams of cartilage were finely minced and placed into a collagenase type IV (consisting of 4400 enzyme activity units) digestion buffer containing growth medium (GM) comprising of high-glucose Dulbecco's Modified medium supplemented with 10% foetal bovine serum (FBS) (Invitrogen, Paisley, UK), 1 mM sodium pyruvate (Invitrogen, Paisley, UK) and antibiotic-antimycotic solution (100 units/mL penicillin, 100 µg/mL streptomycin and 0.25 µg/mL amphotericin B; Invitrogen, Paisley, UK) for 16 hours. The digest was passed through a 70µM cell strainer and centrifuged at 1300 rpm for 10 minutes. The resultant chondrocyte pellet was resuspended in growth medium and expanded in monolayer until passage 2 and cryopreserved. Informed consent was obtained preoperatively from each patient in accordance with the approval from the Ethical Committee of the Royal National Orthopaedic Hospital in compliance with the United Kingdom Human Tissues Act 2004.

4.2.2 Chondrocyte seeding and micromass culture

Chondrocytes are the primary cell population in hyaline cartilage[435]. It was, therefore, essential to assess the interaction of chondrocytes with the dcECM. Human primary articular chondrocytes were thawed, sub-cultured and upon confluence at passage 3. Cells were counted using a Neubauer hemocytometer containing 0.4% trypan blue and culture media at a ratio of 1:2. Subsequently, cells were seeded in micromass cultures directly onto the plastic surface or onto dcECM at a density of $5x10^5$ per 100 µL of growth media into the centre of a well. Micromass culture is extensively used in chondrogenic differentiation protocols as it effectively mimics cell aggregation and allows an intra-aggregate environment to be acquired that is permissive for differentiation[436]. These events mimic those that occur *in vivo* during limb development. Briefly, dcECM was cut into 6 mm diameter and 1 mm thick sections using a biopsy punch (ThermoFisher, Bedford, UK). $5x10^5$ chondrocytes in 10 µL of growth media were seeded onto the surface of the dcECM, whereby the low seeding volume aided localisation of the cells on the surface of the dcECM until attachment. Cells were seeded in micromasses and onto the dcECM surface at the same density. The cells were left for 3 hours to attach, following which 2 mL of growth media supplemented with 5% FBS was added, micromasses were cultured in these conditions for 7 days (n=3 per group). The media in each well was replaced daily with fresh growth media.

4.2.3. Human periosteal stem cell culture and expansion (hPDSCs).

hPDSC's are a key cell skeletal cell population, playing a major role in both bone homeostasis and fracture repair[35] and were, therefore, a key cell type for investigating the *in vitro* bioactivity of the dcECM. hPDSCs were isolated as previously described [207] (obtained from Prof Frank Luyten, KU Leuven, Belgium). Subsequently, hPDSCs from a pool of six different donors were expanded to passage 5**.** All experiments described herein were performed in pooled hPDSCs at passage 6. All cell counting was carried out by combining

0.4% trypan blue and culture media at a ratio of 1:2, that was manually counted using a Neubauer hemocytometer (Sigma, UK).

4.2.4 Optimisation of scaffold seeding

It was observed during initial seeding with chondrocytes that cellular content does not remain localised on the surface of the dcECM, even when small seeding volumes were utilised, this was primarily due to the dcECM surface not being completely flat and due to the dcECM being used while wet. Therefore, alternative methodologies that facilitated better cell localisation were required, before further investigations. Moreover, two prominent RNA isolation methodologies were investigated by employing the RNeasy Mini Kit (Qiagen, UK) and the Direct-zol RNA MiniPrep kit (Zymo, Cambridge Biosciences, Cambs, UK).

Sterile dcECM was cut into 6 mm diameter and 1 mm thick sections (n=3) using a biopsy punch matching the diameter of Nunc 96-well tissue culture plate (Thermo Fisher Scientific, UK). It was proposed that a majority of the seeded volume would remain on the dcECM surface (Figure 4.1; B) due to a large proportion of the volume being localised on the dcECM surface. An additional group of plates (n=3) were filled with sterile 2% agarose. The agarose was poured into each well and allowed to cool to 40°C at which point a cut out dcECM constructs was pushed down into the agarose, ensuring that the surface of the dcECM was not covered. It was hypothesised that that agarose would cover any gaps between the dcECM and the walls of the well, limiting localisation of the cells to the surface of the dcECM, as the cells and media used would not flow into the gaps between the dcECM and well plate. (Figure 4.1; A). All wells were seeded with hPDSCs (passage 6) at a cell density of $1x10^6$ per 100 µL of growth media (10%FBS) into 96-well plates. Control micromasses of the same density (n=3) were seeded onto the surface of the 96 well plates as a comparator. After 24 hours each well was lysed in accordance with manufacturers instructions for each kit. Briefly, in accordance to the Zymo kit guidelines, all dcECM constructs and micromasses were washed in sterile PBS, sterile forceps were used to move the dcECM

constructs into 1.5 mL micro-centrifuge tubes (Star Labs, UK) containing 350 µL of Trizol (Sigma-Aldrich, UK). For micromasses 350 µL of Trizol was added into each well and rigorously scraped, the lysate was transferred into 1.5 mL micro-centrifuge tubes (Star Labs, UK). For extraction using the Qiagen Mini-prep kit, the previously described process was repeated and Trizol was replaced with 350 µL of the provided Qiagen RLT lysis buffer. For the rest of the extraction, the manufacturers' instructions for each kit were followed. Total RNA isolated was quantified using the Nanodrop 1000 spectrophotometer (ThermoFisher, Bedford, UK).

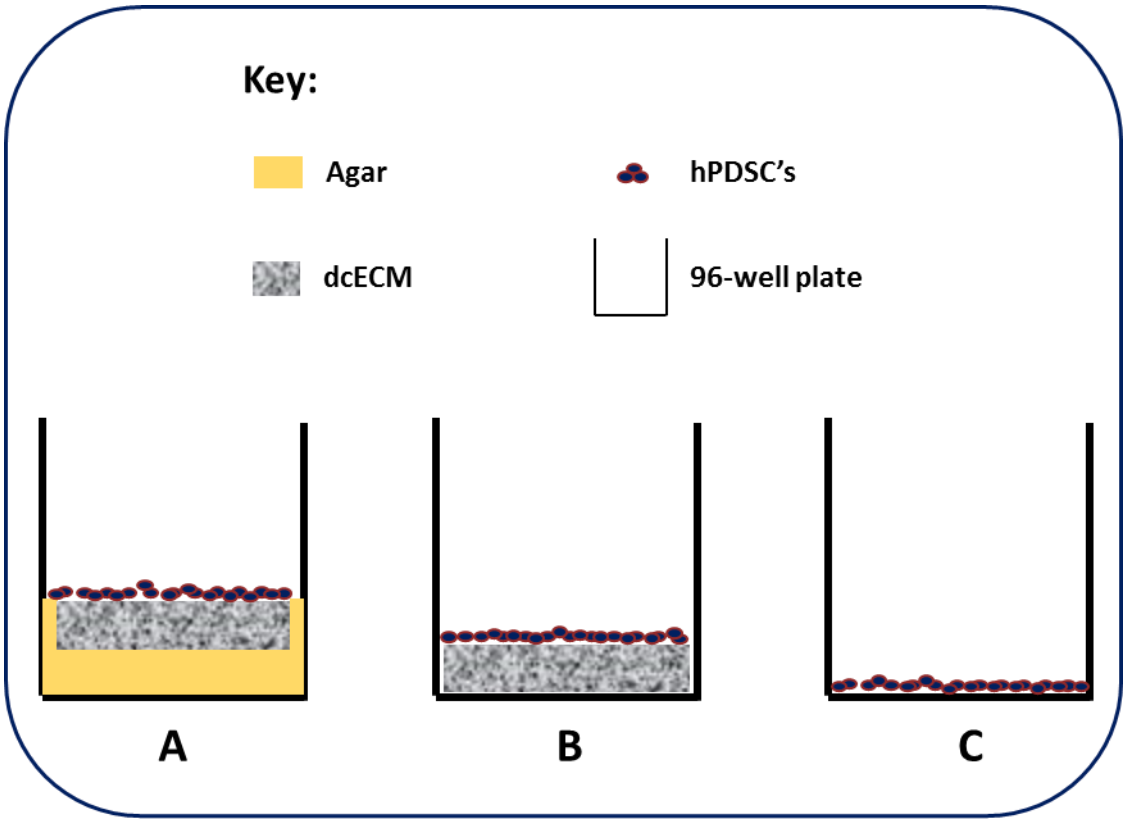

Figure 4.1: hPDSC seeding optimisation. Schematic illustrating the experimental layout for establishing an optimal seeding and RNA extraction methodology for maximum yield.

4.2.5. hPDSC seeding and micromass culture.

It was determined that the dcECM seeded in a 96-well was the optimum condition for total RNA extraction and this was, therefore, used as the optimal seeding conditions for further cell seeding experiments.

Micromass cultures (MM) were seeded as previously described. Briefly, hPDSCs (passage 6) were seeded at a cell density of $1x10^6$ per 100 µL of growth media into 96-well plates. Cells were seeded at this density onto the dcECM as previously described and allowed to attach for 3 hours before being treated with various chondrogenic media. The cells seeded in micromasses and on the dcECM were segregated into three media condition groups (n=3 per group). The control group was treated with low glucose DMEM (Invitrogen, Paisley, UK) supplemented with 2% FBS, (Invitrogen, Paisley, UK) and antibiotic-antimycotic solution (100 units/mL penicillin, 100 µg/mL streptomycin and 0.25 µg/mL amphotericin B; Invitrogen, Paisley, UK). The second group consisted of basal chondrogenic group or C(-) group consisting of low-glucose DMEM (Gibco, UK) supplemented with 100µM ascorbate-2-phosphate (Sigma-Aldrich, Dorset, UK), 100nM dexamethasone (Sigma-Aldrich, Dorset, UK), 40 mg/mL proline (Sigma-Aldrich, Dorset, UK), ITS+premix universal culture supplement (BD Biosciences, Bedford, MA) and 10 µM of Y27632 (Axon Medchem, Groningen, Netherlands). The final group consisted of chondrogenic or C(+) group containing basal chondrogenic media supplemented with 10 ng/mL of TGF-β.

4.2.6. Total RNA extraction and quantitative reverse transcription–Polymerase Chain Reaction (qRT-PCR) analysis

Previous investigations revealed that the Zymo Direct-zol RNA MiniPrep kit was the most effective for RNA isolation from seeded constructs and was therefore used for all further RNA isolation. Briefly, seeded dcECM constructs were washed with PBS, placed in 350 µL of Trizol (Invitrogen, Paisley, UK) and homogenised. Total RNA was isolated from each of the micromasses and dcECM using the Direct-zol RNA MiniPrep (Cambridge Biosciences, Cambs, UK) according to the manufacturers' instructions. Total RNA isolated was quantified using the Nanodrop 1000 spectrophotometer (ThermoFisher, Bedford, UK). Complementary DNA (cDNA) was synthesised by reverse transcription of 200ng of total RNA using the high capacity cDNA reverse transcription kit (Applied Biosciences, ThermoFisher, Bedford, UK). To detect

messenger RNA (mRNA) transcripts, primers (exon spanning, designed using Primer3 Plus, NCBI or obtained from published sources) were premixed with iTaq universal SYBR green supermix (Biorad, Herts, UK) and 10 µL aliquots were applied to Hard-Shell® 96-Well PCR Plates (Biorad, Herts, UK). Thermal cycling conditions were as follows: 10 min at 95°C, with 40 cycles of 15 seconds at 95°C, 30 s at 60°C, and 20s at 72°C, on a Bio-Rad CFX1000 Real-Time System (Biorad, Herts, UK). Target gene quantification was achieved using the $2^{-\Delta\Delta CT}$ method described by Livak *et al.* [437] relative to *hPRT1* as the housekeeper gene. Primers were designed for this study using the Primer-Blast tool (NCBI, USA). All primers were exon spanning with a product size of 100-150 base pairs and primer sizes between 18-20 base pairs. Primer melting temperatures were between 60-63ºC with a GC content ranging from 50-55%. Primers used in this study are listed in Supp Table 1.

4.2.7 Optimisation of chondrogenic media components.

Standard chondrogenic media C+ consisting of low-glucose DMEM (Gibco, UK) supplemented with 100µM ascorbate-2-phosphate (Sigma-Aldrich, Dorset, UK), 100nM dexamethasone (Sigma-Aldrich, Dorset, UK), 40 mg/mL proline (Sigma-Aldrich, Dorset, UK), ITS+premix universal culture supplement (BD Biosciences, Bedford, MA) and 10 µM of Y27632 (Axon Medchem, Groningen, Netherlands) and 10 ng/mL of TGF-β was compared to other published chondrogenic conditions that contained the same basal media from the C+ but an optimised growth factor combination. The study by L.Mendes and colleagues [411] illustrated the role of bone morphogenetic proteins as drivers of chondrogenic differentiation. This study incorporated the use of factorial design to ascertain various combinations of TGFβ1, FGF2, BMP2, BMP6 and GDF5, that promoted chondrogenesis and thence mineralisation. The results of this study indicate that the various combinations of growth factors have a different impact on chondrogenesis and hypertrophy. The overall conclusion of the study was that BMP2 and BMP6 enhanced chondrogenesis, while GDF5 promoted chondrocyte hypertrophy. Other studies investigating BMP2 and BMP6 have also confirmed their role in

chondrogenesis [438,439,440]. The study by Mendes and colleagues concluded on two conditions that either promoted potent, stable chondrogenesis (C4) or chondrocyte hypertrophy (C8). The C4 condition contained the previously defined standard basal chondrogenic media formulation [C(-)] with the addition of addition to 0.1 ng/mL of TGF-β (Peprotech, UK), 0.2 ng/mL of FGF-2 (Thermofisher Scientific, UK), 100ng/mL of BMP-2 (Peprotech, UK), 100 ng/mL of BMP-6 (Peprotech, UK) and 1 ng/mL of GDF5 (Peprotech, UK). The C8 contained standard basal chondrogenic media [C(-)] with the addition of 10 ng/mL of TGF-β (Peprotech, UK), 0.2 ng/mL of FGF-2 (Thermofisher Scientific, UK), 100ng/mL of BMP-2 (Peprotech, UK), 1.0 ng/mL of BMP-6 (Peprotech, UK), and 100ng/mL GDF-5 (Peprotech, UK). Other than the media conditions seeding of the dcECM was the same as described in section 4.2.5. Both C4 and C8 were investigated with hPDSC's seeded onto the dcECM, using the standard seeding methodology described in section 4.2.5.

4.2.7 Chorioallantoic membrane (CAM) assay

Angiogenesis is a crucial process that occurs during endochondral fracture healing[2]. It has been suggested that costal cartilage undergoes gradual endochondral ossification postnatally. Bahrami and colleagues have suggested that costal cartilage contains trace amounts of the hypertrophy-associated protein collagen X[155]. It was, therefore, hypothesised that residual VEGF content might be present within native costal cartilage, potentially promoting angiogenesis *in vivo*. Therefore, the capacity of native costal cartilage and the dcECM to drive angiogenesis was investigated using a CAM assay.

All animal procedures were carried out in accordance with the guidelines and regulations laid down in the Animals Scientific Procedures Act 1986. Eggs for the study were obtained from Medeggs (Henry Stewart & Co, UK). (Figure 4.2) Eggs were incubated horizontally at 37 °C and 60% humidity for 4 days. After the 4-day incubation period, the eggs were monitored using candling to verify the position of the embryo, a square incision area of 0.6cm^2 was marked on the shell accordingly and covered using Scotch tape (Scotch, UK) to reduce

egg shell fragmentation during cutting. Fine scissors were used to make the 0.6cm^2 incision in sterile conditions three edges were cut leaving one edge intact so that the window could be covered again. The egg fragment held by the tape was lifted to expose the CAM. Sterile native cartilage and dcECM cylinders were individually placed on the CAM of each egg (n=10 per group). Scotch tape was used to re-seal the window, and the eggs were re-incubated. Candling was used to examine the eggs daily, and non-viable embryos or infected eggs were removed. After 6 days, the windows on each egg were opened and visualised. CAM integration and interaction with vasculature was visualised using the Stemi 305 compact stereomicroscope (Zeiss, UK). Photographs were captured using the paired Axiocam 506 colour camera (Zeiss, UK). Forceps were used to retrieve both native and dcECM samples from each egg. Samples were lysed for RNA extraction and gene expression analysis.

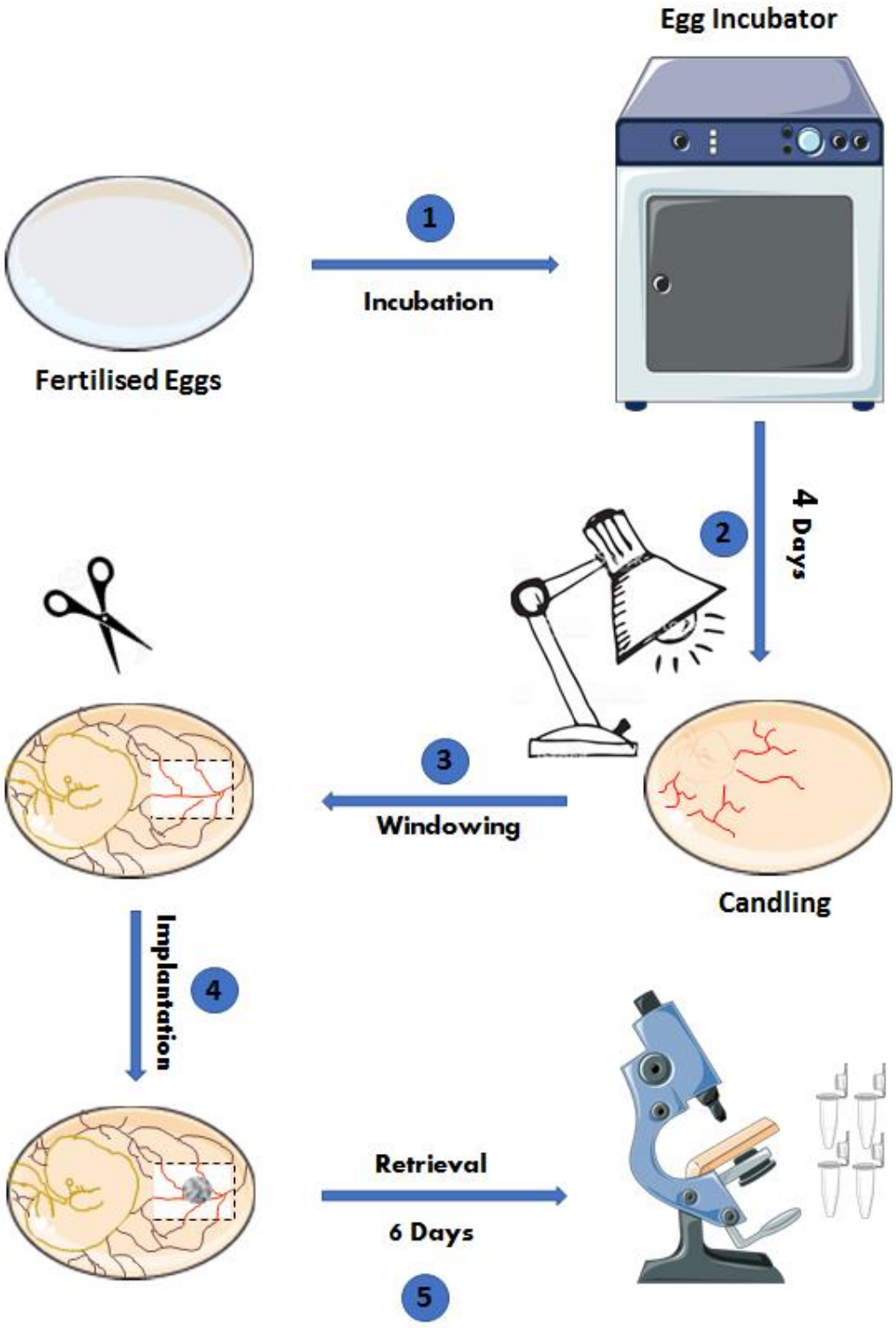

Figure 19: Schematic representation of the experimental procedures carried out during the CAM assay assessment of the dcECM and native costal cartilage. (1) Fertilised clinical eggs are obtained and incubated at 37 ºC for 4 days. (2) Candling is utilised to locate the embryo and eggs without an embryo will be discarded. (3) A window ~0.6 mm^2 is cut out to reveal the CAM below. (4) The dcECM and native costal cartilage samples are cut into cylinders (D= 6 mm, H= 1 mm) and placed on top of the CAM. Samples were incubated for another 6 days. (4) Samples were retrieved from the CAM and subjected to histological and molecular analysis. Figure was created using the Servier medical art database (http://www.servier.com/Powerpoint-image-bank

4.2.9. *In vivo* biocompatibility

A controlled inflammatory response is an essential underlying process in fracture healing, uncontrolled or pro-inflammatory responses associated with graft rejection could have a significant impact on the clinical translatability of the dcECM[441]. After successfully *in vitro* demonstration of the removal of immunogenic components the immunogenicity of the dcECM was further investigated *in vivo* (Figure 4.3). The *in vivo* biocompatibility study was carried out by Dr Wenhui Song (UCL, United Kingdom), Dr Gui Teoh (UCL, United Kingdom), and Shudong Zhao (UCL, United Kingdom) at the Biology Unit, Royal Free and University College London Medical School, London, UK

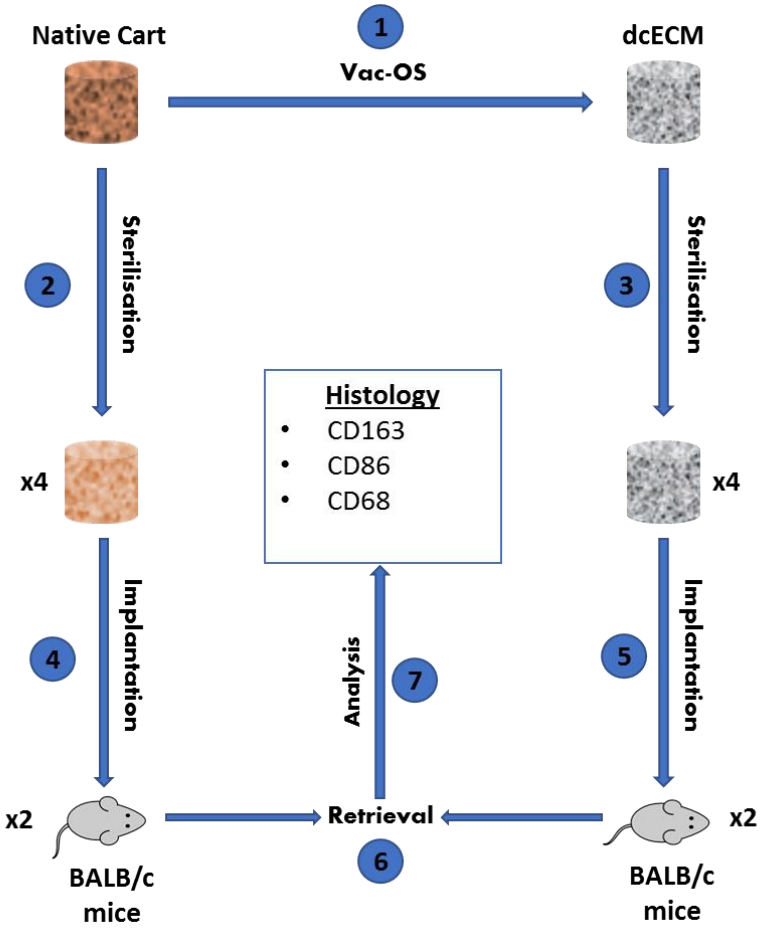

Figure 4.3: *In vivo* biocompatibility experimental layout. Schematic representation of the in vivo biocompatibility study. (1) Native costal cartilage was subjected to Vac-OS decellularisation. (2&3) Both native costal cartilage and the dcECM were sterilisation. (4&5) Sterile dcECM and native costal cartilage samples were implanted subcutaneously; 2 of each group were implanted into each mouse. (6) Samples were retrieved, fixed and processed for histology. (7) Samples were assessed using IHC for the immune cell markers DC86 (M1-macrophage marker), CD163 (M2-macrophage marker) and CD68 (Pan-macrophage marker). Figure was created using the Servier medical art database (http://www.servier.com/Powerpoint-image-bank.

6-week old BALB/C mice were purchased from Charles River, UK and were housed in polypropylene cages at 21°C (±2°C), subjected to 12-hour light and dark cycles, and were acclimatised for one week before use. Mice were fed a standard RM1 maintenance diet *ad libitum* (Rat and Mouse No.1; Special Diet Services). All procedures were conducted in accordance with the United Kingdom Animal Scientific Procedures Act, 1986 and were approved by the Ethics and Welfare Committee of the Comparative Biology Unit, Royal Free and University College London Medical School, London.

Mice were anesthetised (3–5% isoflurane, O_2 flow rate of 1.0 mL/min) and two 8 mm dorsal incisions created per mouse. The subcutaneous pockets on each mouse were filled with either two dcECM constructs or two native cartilage constructs (6 mm in diameter and 1 mm thick). The incisions were then sutured with Vicryl Rapide sutures (Ethicon, UK). After 2 and 8 weeks of implantation (Figure 19), mice were sacrificed by CO_2 inhalation. The dorsal skin was carefully resected and implants retrieved. The dcECM and native cartilage tissue were fixed in 10% neutral buffered formalin (pH 7.4) (VWR, UK) for 24 hours at room temperature (18-21°C).

The 10% NBF fixed tissues ((n=4) dcECM; (n=4) native costal cartilage), 2 and 8 weeks respectively) were dehydrated in graded alcohol, embedded in paraffin, and sectioned at 5 µm. Immunohistochemical analysis of CD68 (Pan-macrophage marker; Abcam, Cambridge, UK), CD86 (M1 macrophage marker; Abcam, Cambridge, UK), and CD163 (M2 macrophage marker; Abcam, Cambridge, UK) was performed following deparaffinization and rehydration of the tissue sections. All sections were blocked in 2.5% horse serum (VectorLabs, Cambs, UK) and 3% H_2O_2 (Sigma-Aldrich, Dorset, UK). For CD68 and CD163 detection, antigen retrieval was performed by incubation with Tris-EDTA buffer (10 mM Tris base, 1 mM EDTA solution, 0.05% Tween 20, pH 9.0) at 60°C overnight. Antigen retrieval for CD86 was performed by incubation with proteinase K (Proteinase K ready to use solution (Dako, UK) for 2 minutes at room temperature (18-21°C). Sections were then incubated with primary anti-CD68 (1:500 rabbit polyclonal anti-mouse; VectorLabs, Cambs, UK), anti-CD86 (1:500 mouse monoclonal anti-mouse; VectorLabs, Cambs, UK) and anti-CD163 (1:500 rabbit polyclonal anti-mouse; VectorLabs,

Cambs, UK) at 4°C overnight. Subsequently, CD86 and CD163 sections were incubated with HRP-conjugated anti-rabbit secondary antibody solution (VectorLabs, Cambs, UK), CD86 sections were incubated with HRP-conjugated anti-mouse secondary antibody solution (VectorLabs, Cambs, UK) for 1 hour at room temperature (18-21°C). All targets were visualised by incubation with the substrate 3,3′-diaminobenzidine (VectorLabs, Cambs, UK) for 1 minute. Tissue sections were counterstained with Haematoxylin solution (Sigma-Aldrich, Dorset, UK) and visualised using the Zeiss Apotome.2 microscope under bright field settings (Zeiss, UK).

4.2.10. Statistical analysis

Data are expressed as the mean ± standard deviation (SD) or mean ± standard error mean (SEM). Statistical analysis was carried out as described in Chapter 2. All statistical analysis was performed using GraphPad Prism version 6.0f for windows (GraphPad Prism Software, La Jolla California USA, www.graphpad.com).

4.3 Results

4.3.1. The dcECM is capable of re-establishing the chondrogenic phenotype in dedifferentiated human articular cartilage-derived chondrocytes.

To assess the capacity for cellular differentiation towards a chondrogenic phenotype, de-differentiated human chondrocytes, the predominant cell population in hyaline articular cartilage[308], were seeded onto the dcECM (Figure 4.4).

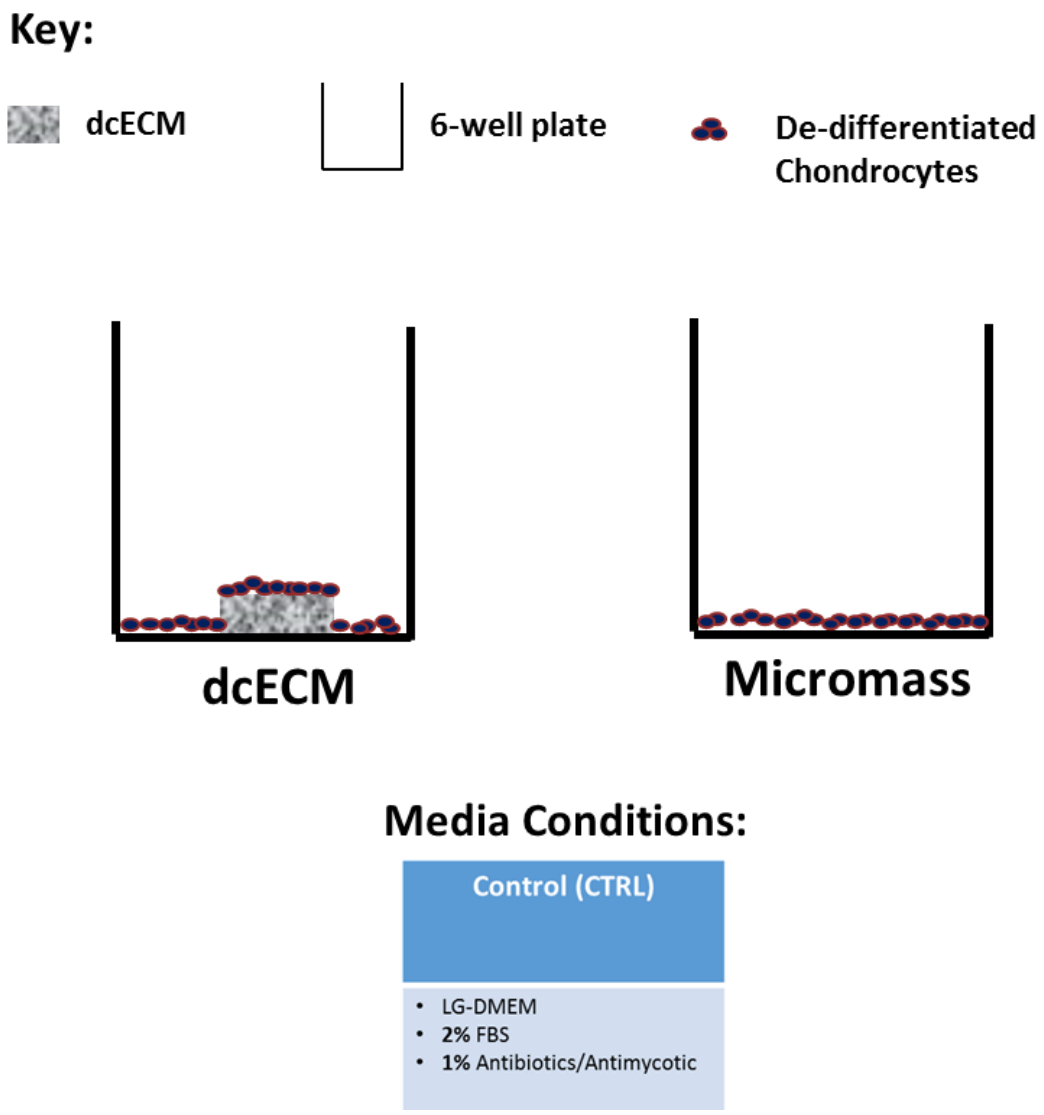

Figure 4.4: Chondrocyte seeding experimental layout. Schematic representation highlighting the seeding and media conditions for seeding dedifferentiated Human articular cartilage-derived chondrocytes.

Brightfield microscopy revealed that cells near the dcECM had a distinct cobblestone morphology (Figure 4.5; A&B), this also suggested that several cells did not localise on the dcECM surface. Nuclear and cytoskeletal staining using DAPI and Phalloidin illustrated cell attachment onto the dcECM (Figure 4.5; C&D). Moreover, the attached cells established themselves in the vacant chondrocyte lacunae. The re-establishment of a chondrogenic phenotype of seeded cells was confirmed by a significant 4-fold ($p<0.01$) increase in *COL2A1* mRNA expression associated with cartilage matrix maintenance

(Figure 4.6). There was, however, no significant difference in the expression of the chondrogenic commitment marker *SOX9*.

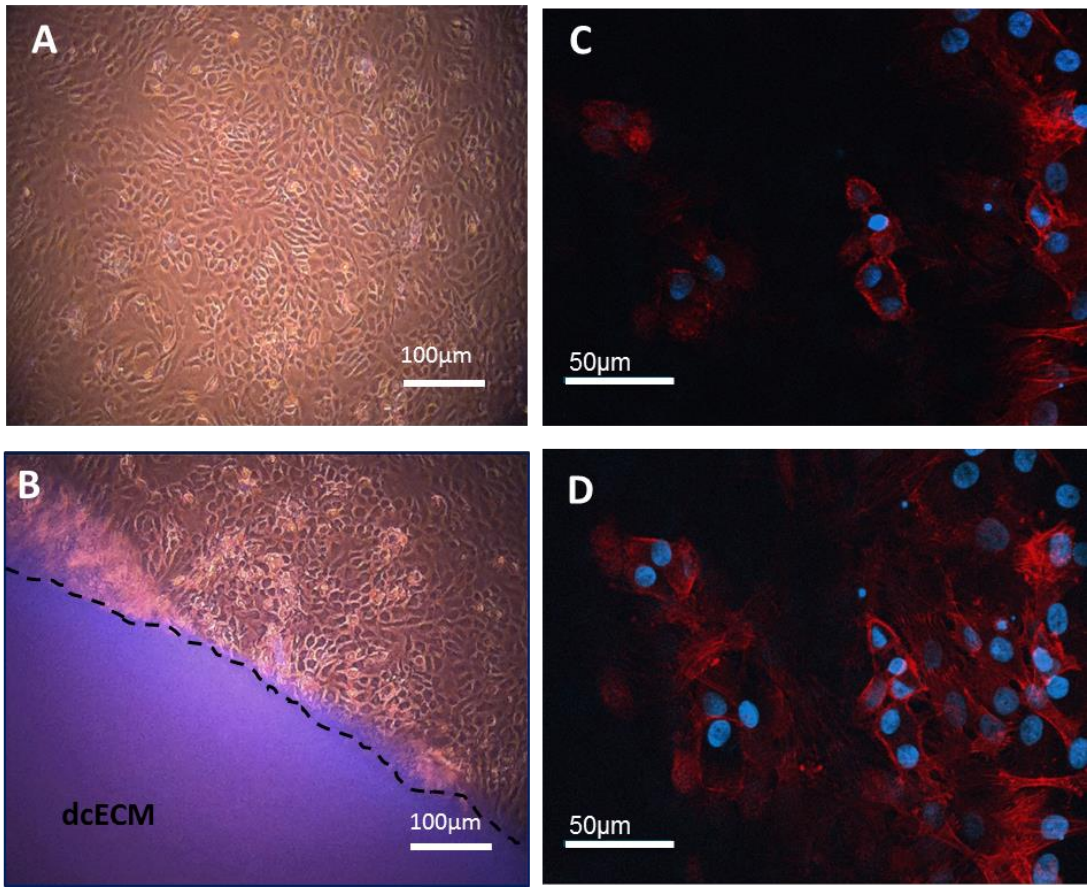

Figure 4.5: Histological analysis of chondrocyte seeded dcECM(A) Brightfield microscopy image of a micromass seeded in a six-well plate. (B) Brightfield microscopy image of the seeded dcECM surrounded by dedifferentiated chondrocytes on tissue culture plastic. (C&D) Structured illumination microscopy images of dedifferentiated chondrocytes seeded on dcECM and stained with DAPI/phalloidin indicating cells residing within the lacunae. The figure has been reproduced from Val et al[281] with permission from Mary Ann Liebert, Inc., New Rochelle, NY

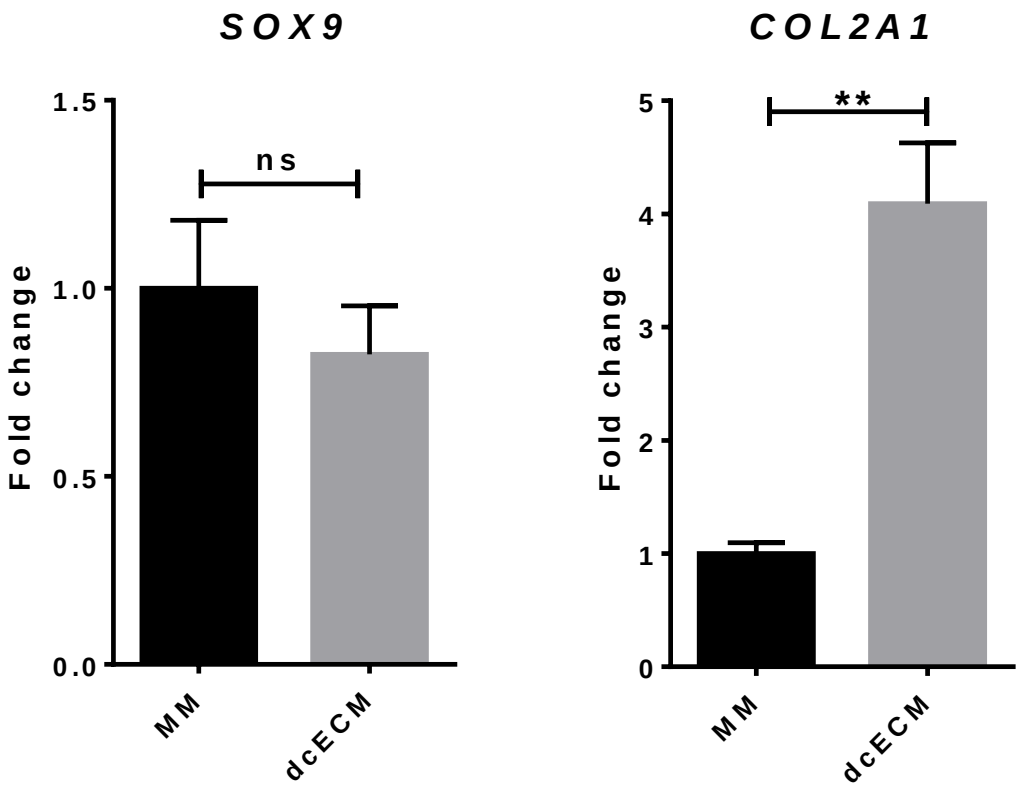

Figure 4.6: Gene expression of dcECM seeded chondrocytes. Gene expression analysis of dedifferentiated chondrocytes both in micromass and seeded onto the surface of the dcECM(ns = non-significant, $p<0.05$, **).(Fold changes normalised to micromasses. Statistical analysis performed using an unpaired t-test with Welch's posthoc correction., error bars = SEM).

4.3.2. Optimisation of scaffold seeding methodology for optimal RNA yield.

Initial seeding experiments in 6-well plates revealed that some cells did not localise precisely on the scaffold as cells were visible on the tissue culture plastic. It was hypothesised that the lack of cell localisation on the dcECM surface had an impact on mRNA retrieval. This required optimisation of the seeding conditions by seeding cells onto the dcECM in a 96-well plate, with or without agar (Figure 4.1). Furthermore, two RNA extraction kits were also utilised, each containing a proprietary mix of chaotropic salts, affecting nucleic acid isolation and binding to the silica column. There was a significant 600 and 700 ng increase in RNA yield when using the Zymo Kit ($p<0.05$) when comparing micromass and dcECM samples extracted using the Qiagen vs

Zymo kits respectively (Figure 4.7). There was also a trend towards a higher RNA yield with the Zymo kit when considering dcECM(Agar) samples. Additionally, while there was no significant difference in total RNA retrieval between dcECM and dcECM(Agar) for each extraction technique, the addition of agar increased variation in total RNA content when using the Zymo kit.

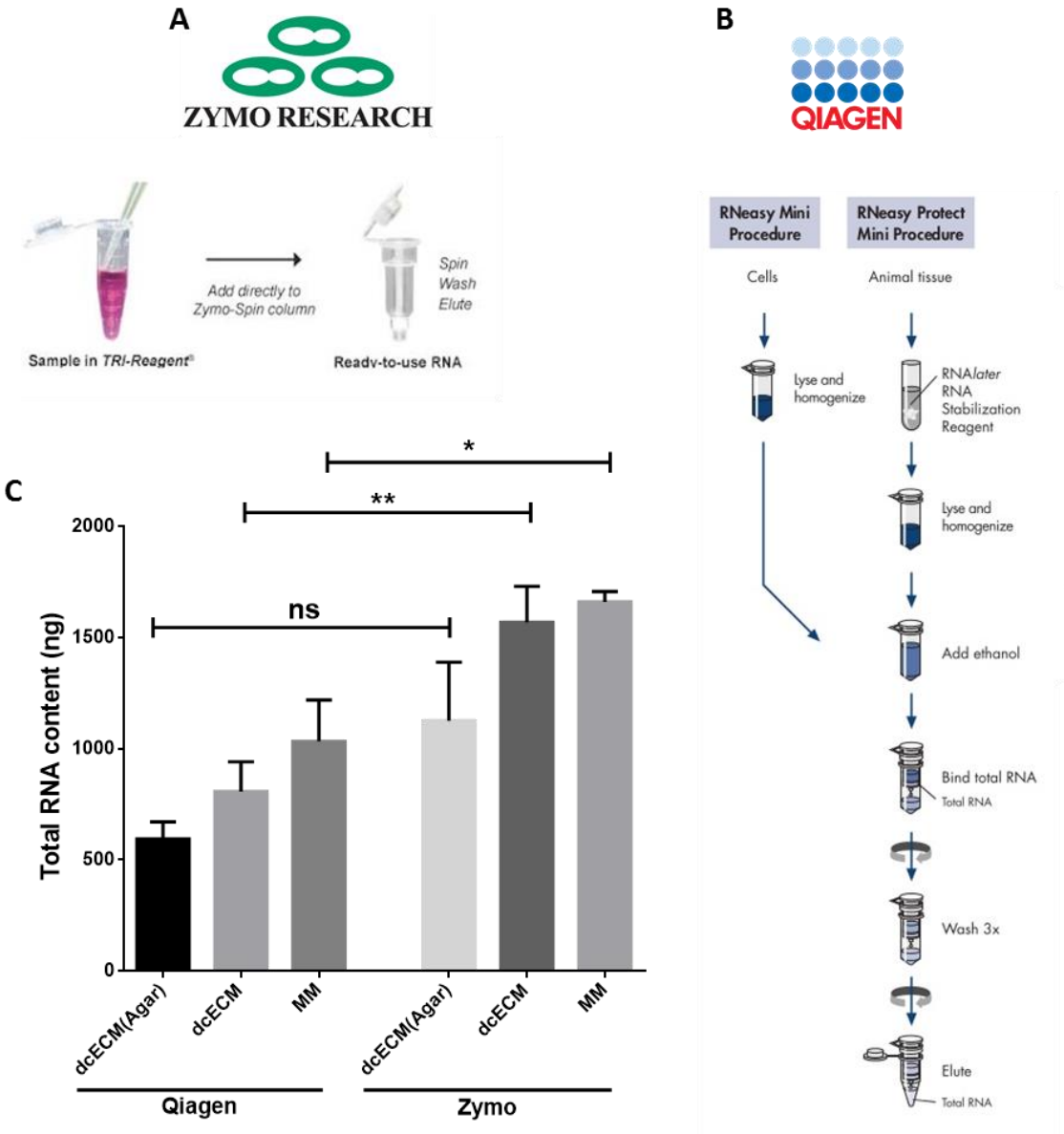

Figure 4.7: Total RNA content for RNA seeding optimisation (A) Simplified schematic protocol for the purification of RNA using the Zymo DirectZol kit. (B) Simplified schematic protocol for the Qiagen RNA extraction kit. (C) Total RNA content comparing values obtained using Qiagen and Zymo RNA extraction kits. (Statistical analysis performed using a one-way ANOVA, corrected for multiple comparisons using Tukey's post hoc multiple comparisons test, error bars = SEM; *p<0.05, ** p<0.001).

4.3.3. The dcECM enhances chondrogenic differentiation in hPDSC's in the presence of ROCKi.

To further examine the chondrogenic potential of the scaffolds, hPDSCs were seeded onto the dcECM and as control micromasses cultures. Chondrogenic conditions [C(+)] were compared to control conditions (CTRL). Additionally, TGFβ and ROCKi are commonly incorporated into chondrogenic media formulations due to their ability to drive and enhance chondrogenesis. ROCK is a downstream effector of the Rho kinase family of GTPases that are involved in regulating chondrogenic gene expression by regulating actin cytoskeleton rearrangement[442,443]. Therefore, ROCKi was eliminated from comparator culture conditions. (Figure 4.8).

Brightfield microscopy images revealed distinct curling of the micromasses when ROCKi was eliminated from the culture(Figure 4.9). Gene expression, however, revealed molecular changes associated with chondrogenic differentiation. dcECM in combination with the C(+) condition enhanced chondrogenic gene expression(Figure 4.10 & 4.11) , highlighted by the significant upregulation of the *SOX*-trimer; *SOX9*; *SOX5* and *SOX6* with a 3-, 5- and 3.6-fold ($p<0.05$) respectively, compared to micromasses in the same condition. Furthermore, under chondrogenic C(+) conditions an 8- and 4-fold ($p<0.05$, $p<0.01$) upregulation in cartilage matrix specific markers *ACAN* and *COL2A1* were observed. This was also accompanied by an upregulation of markers associated with chondrocyte hypertrophy with a 2-, 2.9- and 5-fold ($p<0.05$, $p<0.01$, $p<0.01$) increase in *RUNX2*, *COL10A1* and *VEGFA* expression respectively. When ROCKi was eliminated from the basic chondrogenic media (-R), there was a trend towards a decrease in *SOX*-trimer and a significant 9-fold decrease in *COL2A1* ($p<0.01$) with micromasses in C(+) conditions. There was, however, a trend towards an increase in the hypertrophic markers *RUNX2* and *VEGFA* but a decrease in *COL10A1*. The dcECM cultured in C(+) conditions without ROCKi, resulted in significant 1.5-, 1- and 2-fold decrease in SOX9, 5 and 6 ($p<0.01$, $p<0.05$, $p<0.01$) respectively, Alongside a 3-fold decrease in *COL2A1* ($p<0.01$). In contrast, there was a 5-fold increase in *VEGFA* ($p<0.001$).

The elimination of TGFβ in the C(-) conditions had a significant impact on the expression of chondrogenic markers with *SOX9*, *SOX5*, *ACAN* and *COL2A1* not being expressed above the basal levels (CTRL) when compared to micromass cultures.

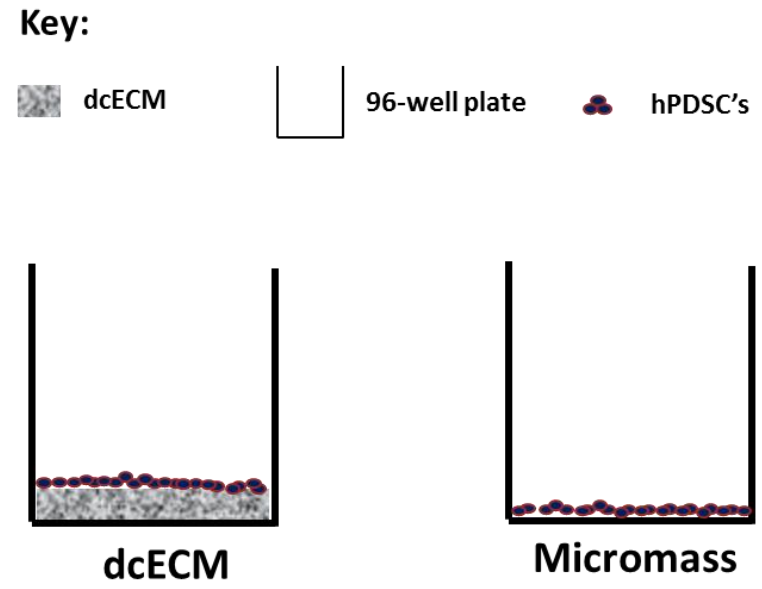

Media Conditions:

CTRL	C(-)	C(+)
• LG-DMEM • **2%** FBS • **1%** Antibiotics/Antimycotic	• LG-DMEM (Gibco, UK) • **1×** insulin-transferrin-selenium • **100 nM** dexamethasone • **100 µM** ascorbate-2-phosphate • **40 µg/ml** proline • **1%** Antibiotics/Antimycotic • **20 µM** Y27632	• LG-DMEM (Gibco, UK) • **1×** insulin-transferrin-selenium • **100 nM** dexamethasone • **100 µM** ascorbate-2-phosphate • **40 µg/ml** proline • **1%** Antibiotics/Antimycotic • **20 µM** Y27632 • **10 ng/ml** TGF-β1

C(-) (-R)	C(+)(-R)
• LG-DMEM (Gibco, UK) • **1×** insulin-transferrin-selenium • **100 nM** dexamethasone • **100 µM** ascorbate-2-phosphate • **40 µg/ml** proline • **1%** Antibiotics/Antimycotic • ~~**20 µM** Y27632~~	• LG-DMEM (Gibco, UK) • **1×** insulin-transferrin-selenium • **100 nM** dexamethasone • **100 µM** ascorbate-2-phosphate • **40 µg/ml** proline • **1%** Antibiotics/Antimycotic • ~~**20 µM** Y27632~~ • **10 ng/ml** TGF-β1

Figure 4.8: Requirement of ROCKi for chondrogenesis. Schematic representation highlighting the seeding and various media conditions for the assessment of the dcECM using hPDSC's.

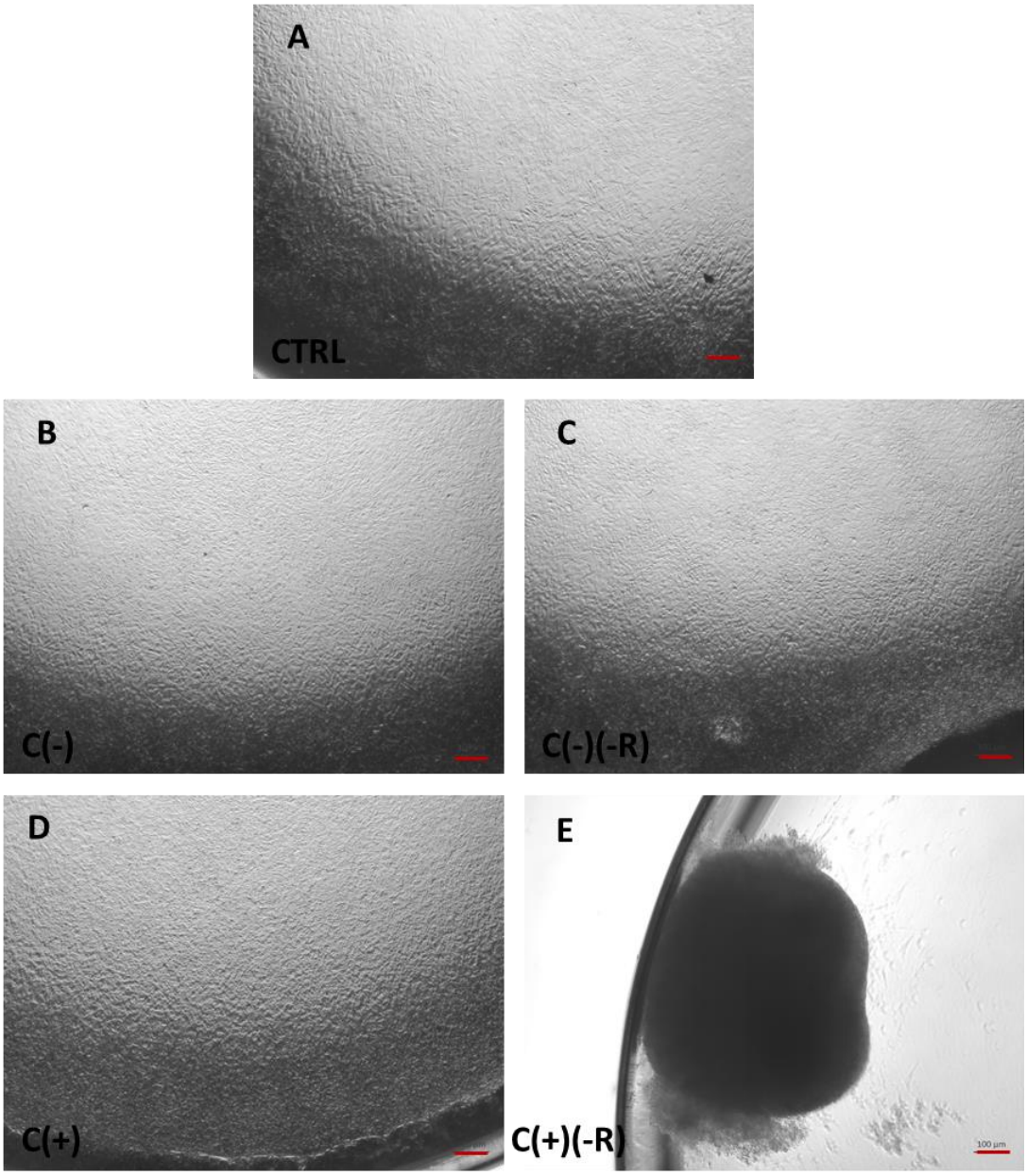

Figure 4.9: Investigation of removing ROCK on micromass morphology Representative brightfield images of micromass cultures at a seeding density of 300,000/cm^2 in CTRL[A] , C(-)[B], C(+)[D] conditions. C(+) and C(-) conditions also had ROCKi eliminated from the culture (-R)[C&E]. (E) C+ conditions without ROCKi resulting in the curling of the micromass, while there were no distinct changes observed in the rest of the cultures. Images were obtained 7 days post culture. Scale bar = 100µm.

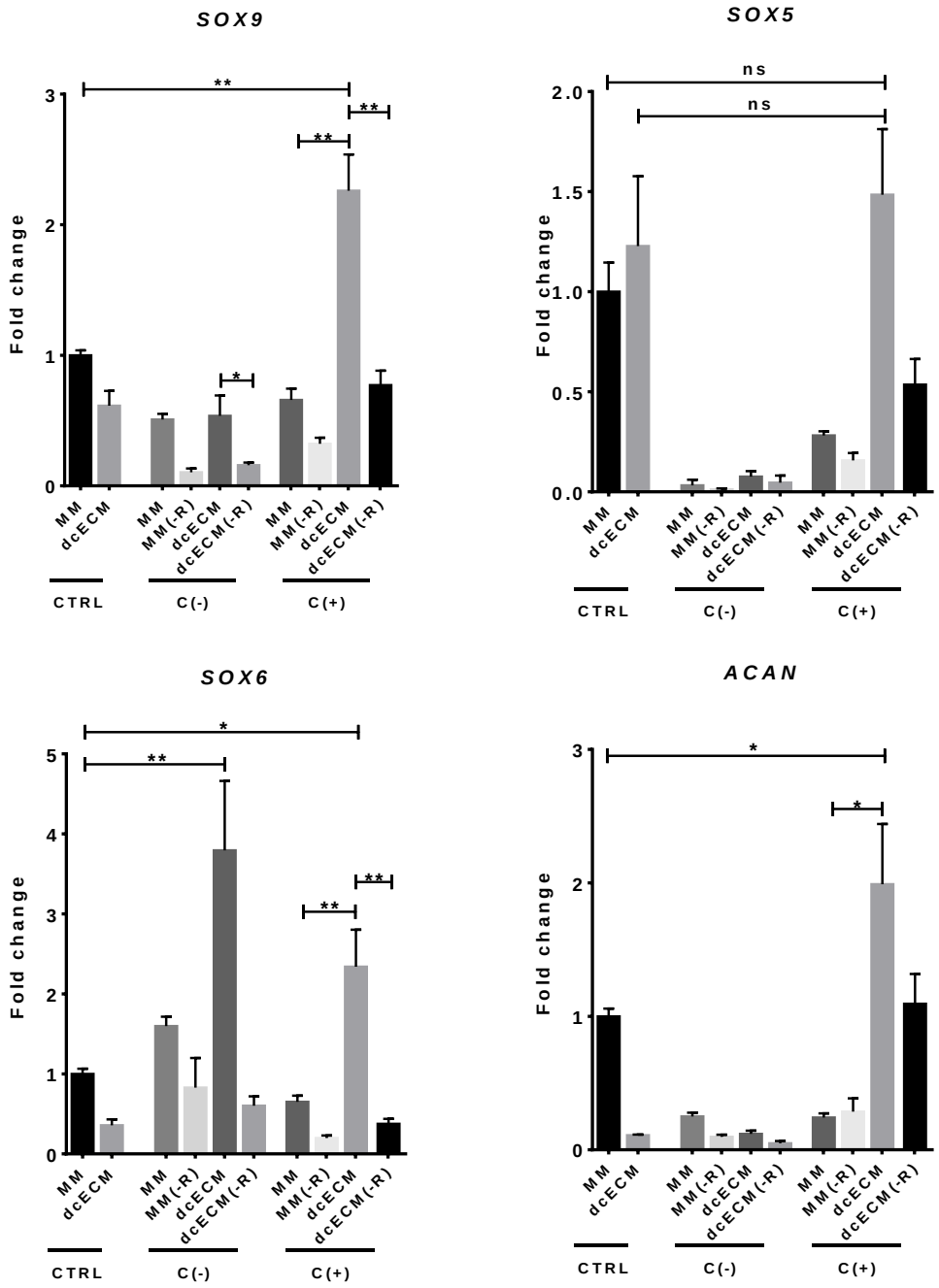

Figure 4.10: Removal of ROCKi and its impact on chondrogenic gene expression. Chondrogenic gene expression (SOX9,5,6 and ACAN) of hPDSCs seeded in MM and dcECM under control conditions (CTRL), chondrogenic conditions (C+) and chondrogenic media without TGF-β (C-). C(+) and C(-) conditions were also had ROCKi eliminated from their formulations (-R). n=3 *p<0.05, **p<0.01, ***p<0.001)(Fold changes normalised to micromasses in CTRL conditions). Statistical analysis was performed using one-way ANOVA corrected for multiple comparisons using Bonferroni's posthoc analysis.

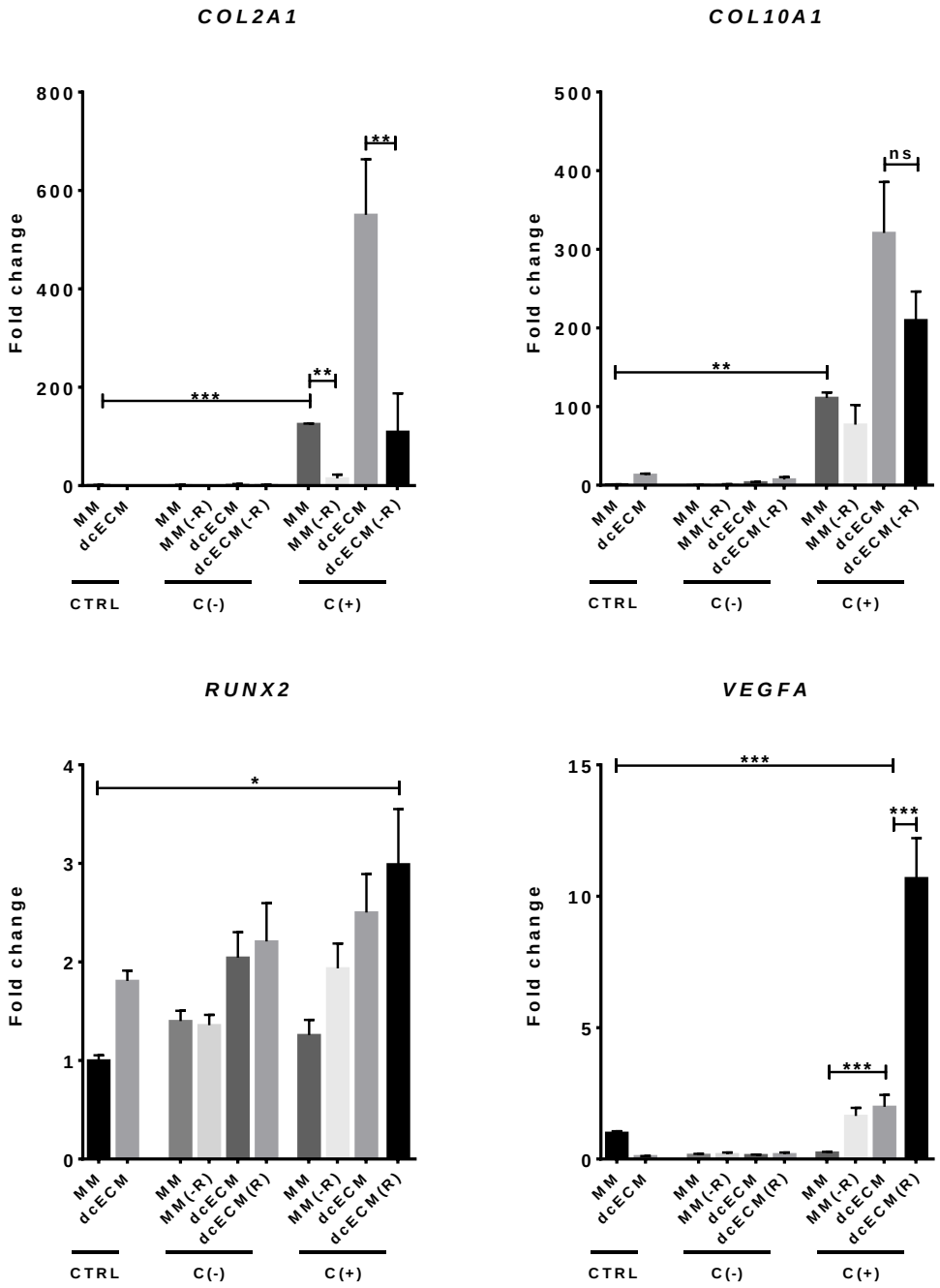

Figure 4.11: Chondrogenic and chondrocyte hypertrophy gene expression (COL2A1, COL10A1, RUNX2 & VEGFA) of hPDSCs seeded in MM and dcECM under control conditions (CTRL), chondrogenic conditions (C+) and chondrogenic media without TGF-β (C-). C(+) and C(-) conditions were also had ROCKi eliminated from their formulations (-R). n=3 *p<0.05, **p<0.01, ***p<0.001) (Fold changes normalised to micromasses in CTRL conditions). Statistical analysis was performed using one-way ANOVA corrected for multiple comparisons using Bonferroni's posthoc analysis.

4.3.4. Hypoxia has limited effect on chondrogenesis in hPDSC seeded onto the dcECM in tested conditions.

During fracture repair, oxygen tension can play a crucial role in stem cell chondrogenesis[444]. The role of hypoxia in contributing to the bioactivity of the dcECM was, therefore, investigated by culturing cells in 5% O_2. Gene expression was measured 3 and 7 days post culture (Figure 4.11).

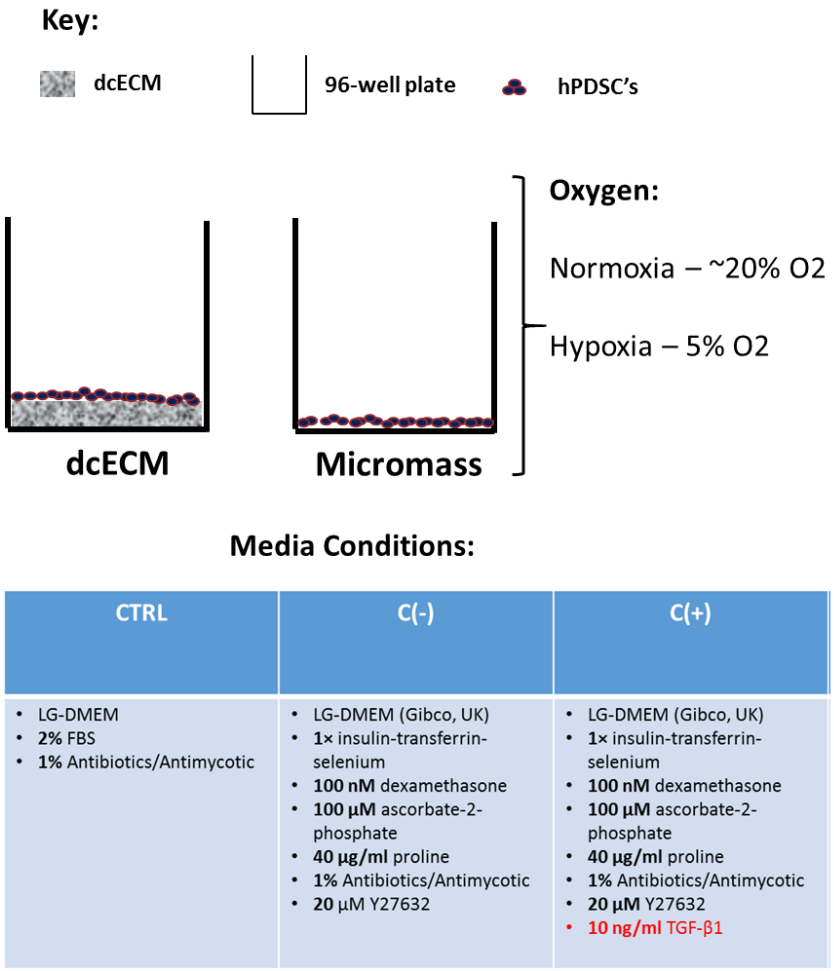

Figure 4.12: Experimental layout to investigate the chondrogenic potential of hypoxia in hPDSC seeded dcECM. Schematic representation highlighting the seeding and various media conditions for the assessment of the dcECM using hPDSC's in low-oxygen conditions.

No differences in gene expression were observed in C(-) conditions both at 3 and 7 days(Figure 4.13 & 4.14). Hypoxia had a positive impact on chondrogenesis and hypertrophy only in micromass conditions with a 2.5- and a 2-fold increase in the relative expression of chondrogenic markers *SOX6* ($p<0.05$) and hypertrophic marker *COL10A1* ($p<0.05$), this trend present at day 3 was repeated at day 7. An interesting observation, however, was that

hypoxia did not facilitate chondrogenesis in 3D cultures containing at dcECM. In normoxia, however, the dcECM demonstrated an enhanced 2-, 3.2-fold upregulation of the chondrogenic markers *SOX9* ($p<0.05$), and *COL2A1* ($p<0.05$) at day 7 in chondrogenic conditions.

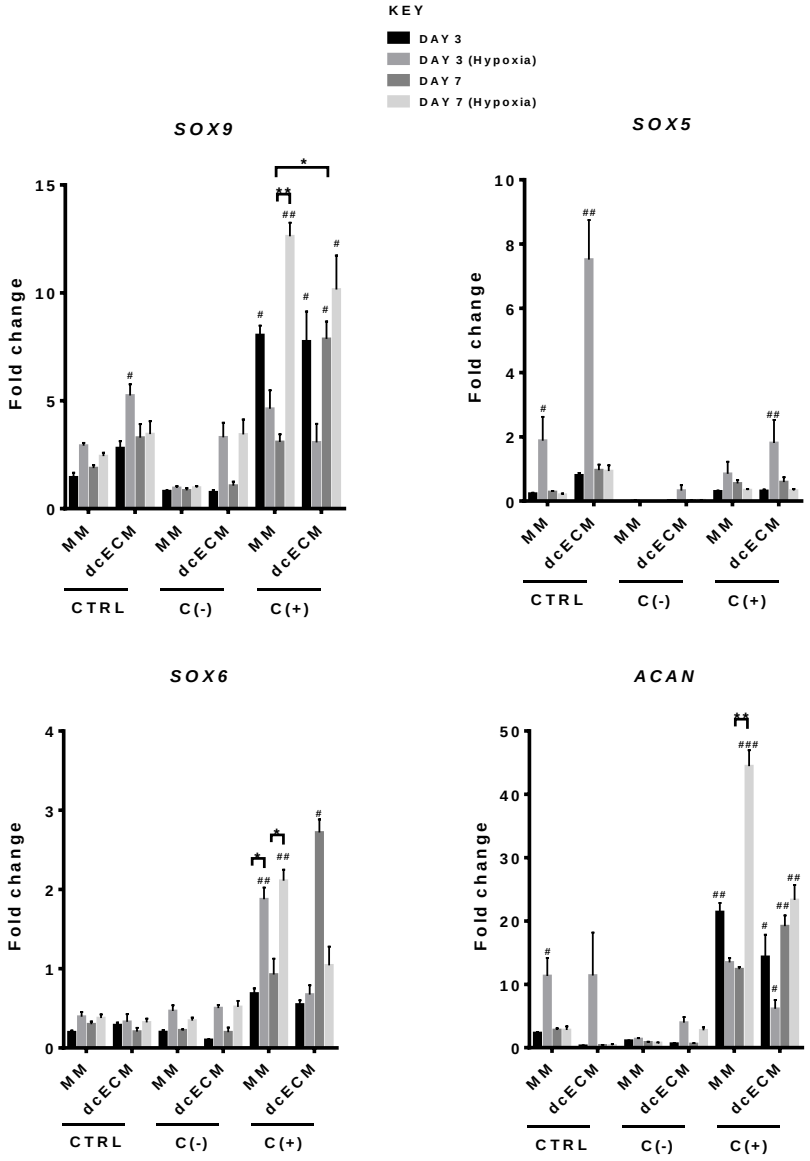

Figure 4.13: **Hypoxia investigation gene expression data**. Chondrogenic gene expression (*SOX9,5,6* & *ACAN*) of hPDSCs seeded in MM and dcECM under control conditions (CTRL), chondrogenic conditions (C+) and chondrogenic media without TGF-β (C-) at day 3 and 7. Each group was also subjected to hypoxia (5% O2). One set of the stared conditions was subjected to hypoxia. Fold changes normalised to micromasses cultures in control (MM-CTRL) conditions at day 3 . Significance in relation with control micromasses is indicated by # (# $p<0.05$,## $p<0.01$, ### $p<0.001$) Significance between experimental groups is indicated by * (* $p<0.05$, ** $p<0.01$ and *** $p<0.001$) . Statistical analysis was performed using one-way ANOVA corrected for multiple comparisons using Bonferroni's posthoc analysis.

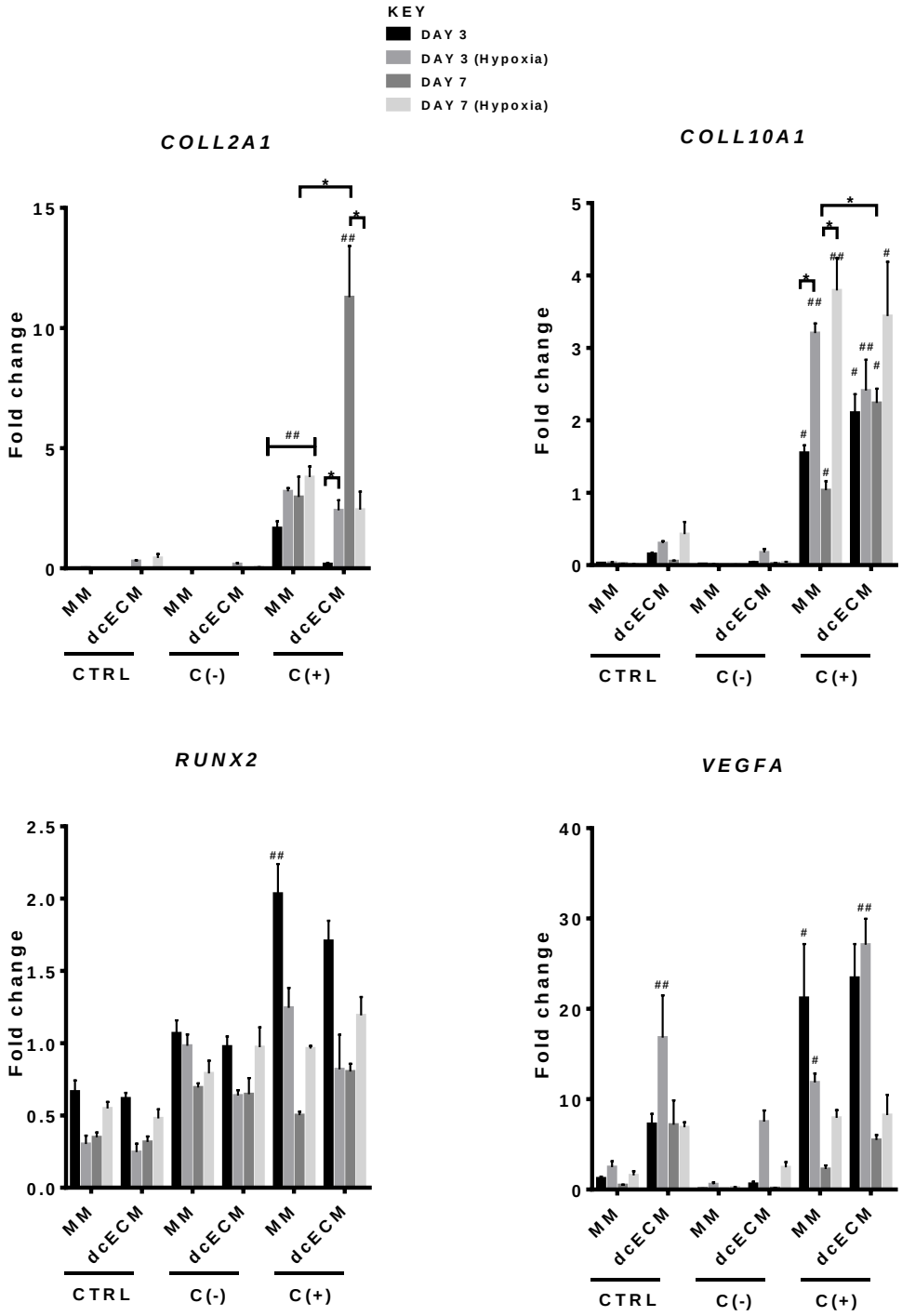

Figure 4.14: Chondrogenic gene expression (*COL2A1, COL10A1, RUNX2* and *VEGFA*) of hPDSCs seeded in MM and dcECM under control conditions (CTRL), chondrogenic conditions (C+) and chondrogenic media without TGF-β (C-) at day 3 and 7. Each group was also subjected to hypoxia (5% O2). One set of the stared conditions was subjected to hypoxia. Fold changes normalised to micromasses cultures in control (MM-CTRL) conditions at day 3 . Significance in relation with control micromasses is indicated by # (# p<0.05,## p<0.01, ### p<0.001) Significance between experimental groups is indicated by * (* p<0.05, ** p<0.01 and *** p<0.001) . Statistical analysis was performed using one-way ANOVA corrected for multiple comparisons using Bonferroni's posthoc analysis.

4.3.5. Conditions containing BMP2 and GDF5 enhances the expression of chondrogenic and hypertrophic genes in hPDSC's.

Previous work carried out by Mendes and colleagues[411] demonstrated that the inclusion of differential concentrations of TGFβ, FGF2, BMP2, BMP6 and GDF5 could enhance chondrogenic differentiation of hPDSC's. Condition C4 and C8, as previously defined, enhanced stable chondrogenesis and hypertrophy respectively. These conditions and their growth factor concentration profile were, therefore, selected for investigation with the dcECM (Figure 4.15).

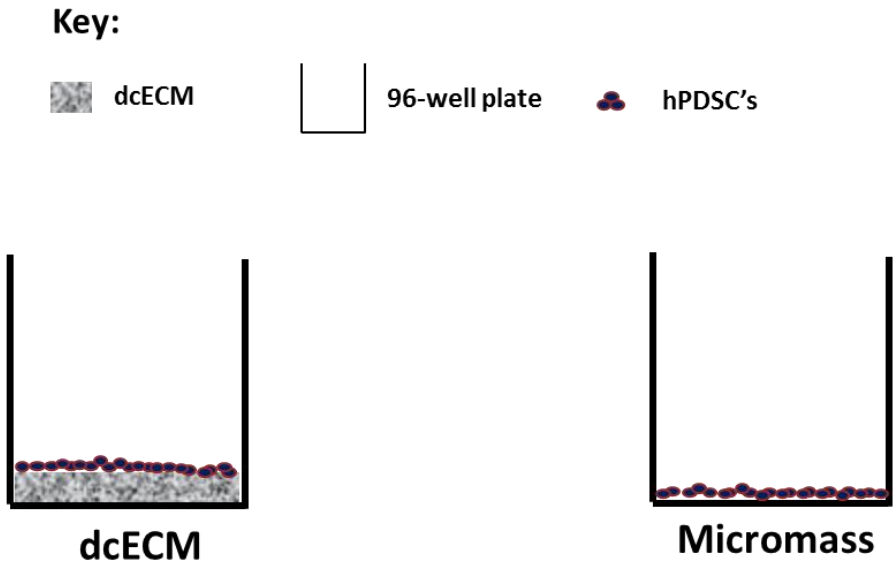

Media Conditions:

CTRL	C(+)	C(4)	C(8)
• LG-DMEM • **2%** FBS • **1%** Antibiotics/Antimycotic	• LG-DMEM (Gibco, UK) • **1×** insulin-transferrin-selenium • **100 nM** dexamethasone • **100 µM** ascorbate-2-phosphate • **40 µg/ml** proline • **1%** Antibiotics/Antimycotic • **20 µM** Y27632 • **10 ng/ml** TGF-β1	• LG-DMEM (Gibco, UK) • **1×** insulin-transferrin-selenium • **100 nM** dexamethasone • **100 µM** ascorbate-2-phosphate • **40 µg/ml** proline • **1%** Antibiotics/Antimycotic • **20 µM** Y27632 • **0.1 ng/ml** TGF-β1 • **0.2 ng/ml** FGF2 • **100 ng/ml** BMP2 • **100 ng/ml** BMP6 • **1.0 ng/ml** GDF5	• LG-DMEM (Gibco, UK) • **1×** insulin-transferrin-selenium • **100 nM** dexamethasone • **100 µM** ascorbate-2-phosphate • **40 µg/ml** proline • **1%** Antibiotics/Antimycotic • **20 µM** Y27632 • **10 ng/ml** TGF-β1 • **0.2 ng/ml** FGF2 • **100 ng/ml** BMP2 • **1.0 ng/ml** BMP6 • **100 ng/ml** GDF5

Figure 4.15: Growth factor optimisation experimental layout. Schematic representation highlighting the assessment of various growth factor combinations on hPDSC's seeded onto the dcECM. Conditions C(4) and C(8) were adapted from Mendes and colleagues[411].

Brightfield microscopy images revealed some curling of micromasses cultured in C(+) conditions and visible differences in morphology in micromasses that were cultured in C(8) conditions (Figure 4.16). To evaluate the chondrogenic capacity under the C(+) and C(8) conditions, chondrogenic markers were evaluated (Figure 4.17 & 4.18). C8 conditions potently upregulated chondrogenic markers with a 3.5, 6.5, 3 and 120 fold upregulation of *SOX5, SOX6, ACAN* and *COL2A1 respectively,* when compared to C(+) conditions. Moreover, similar results were observed when comparing hPDSC's in C(8) micromasses cultures to C(8) conditions containing the dcECM. However, the dcECM in C(+) conditions demonstrated a trend towards higher *COL10A1* expression.

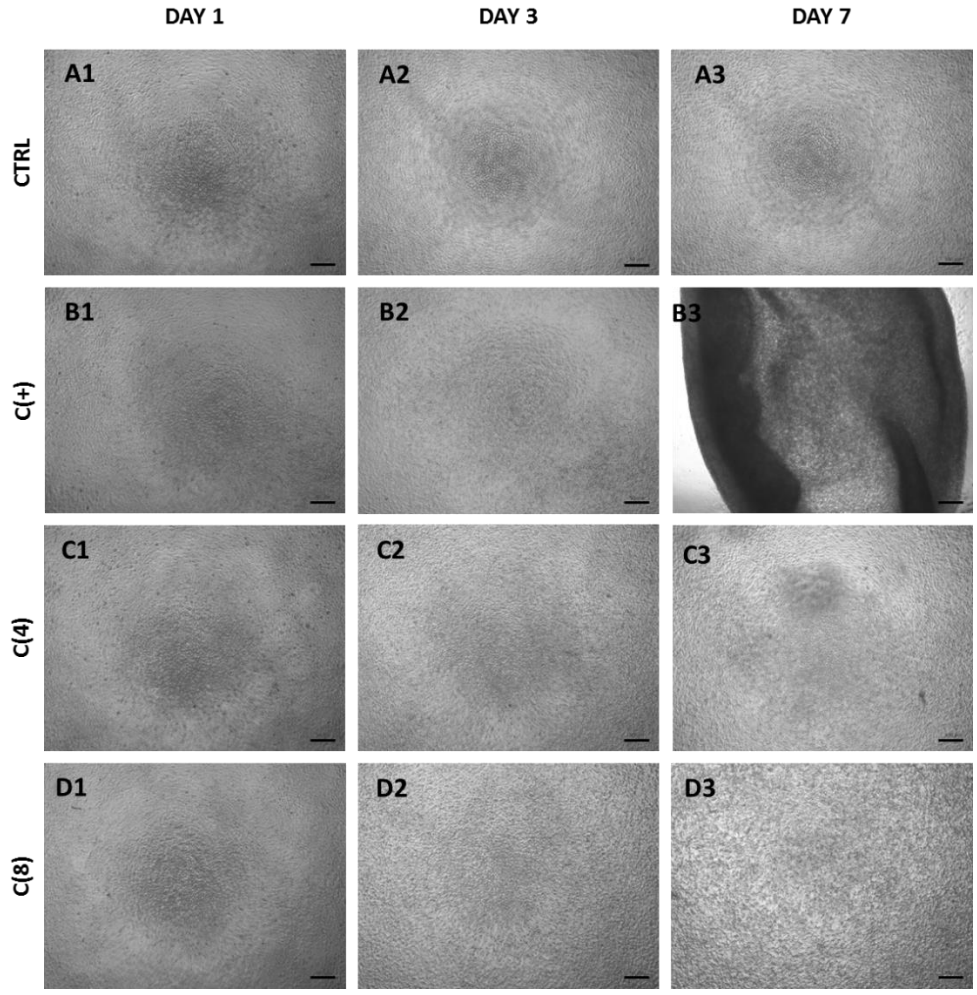

Figure 4.16: Growth factor optimisation brightfield images. (A-D) Representative brightfield images of hPDSC micromass cultures at a seeding density of 300,000/cm^2. hPDSC's were cultured in CTRL[A], C(+)[B], C(4)[C] and C(8)[D] conditions at day 1,3 and 7 (scale bar = 100 µm).

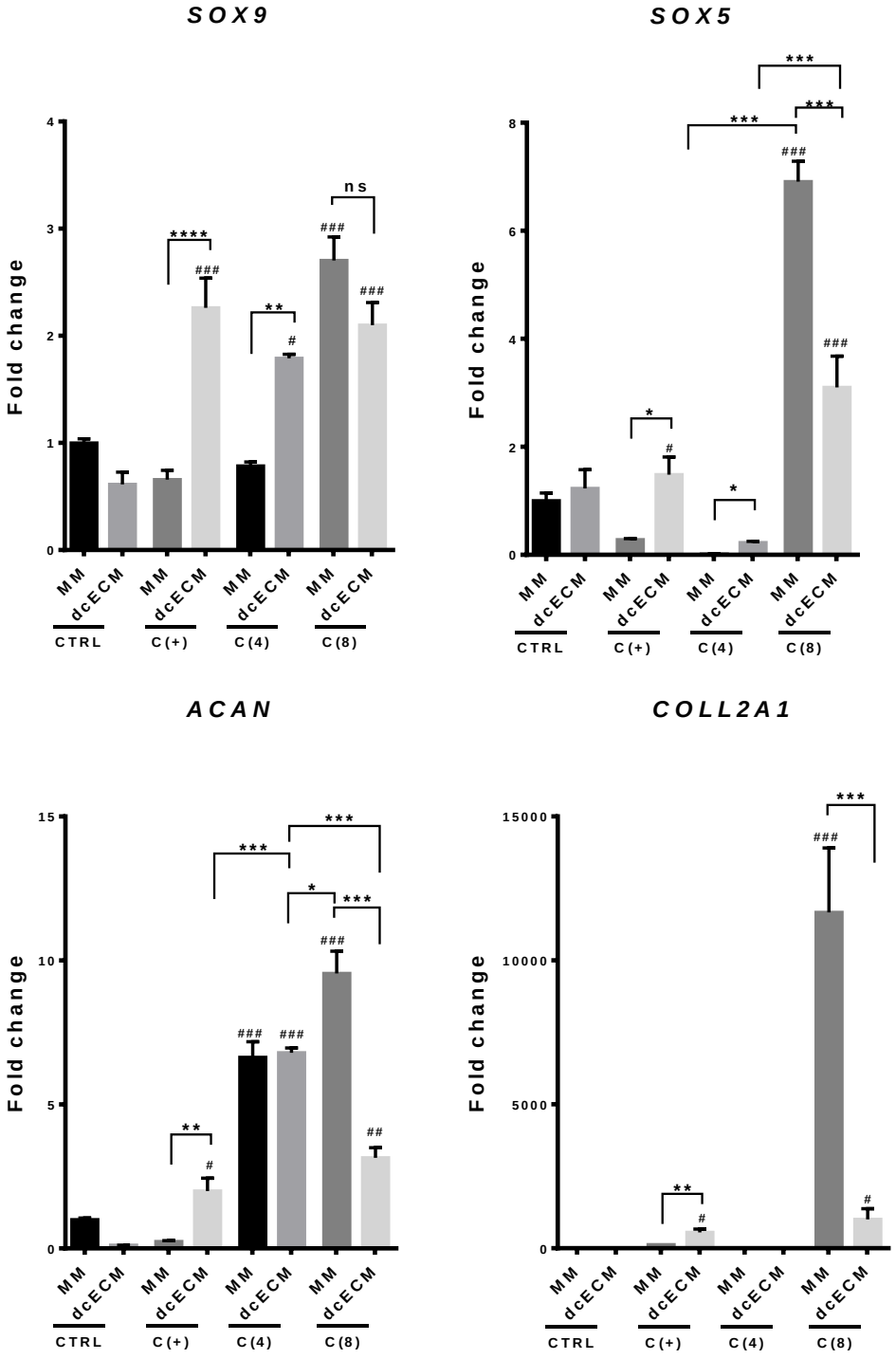

Figure 4.17: Growth factor optimisation gene expression data. qPCR based gene expression analysis for the chondrogenic marker genes *SOX9*, *SOX5*, *ACAN* and *COLL2A1*. Fold changes normalised to micromasses cultures in control (MM-CTRL) conditions significance in relation with control micromasses indicated by # (# p<0.05,## p<0.01, ### p<0.001). Significance between experimental groups is indicated by * (* p<0.05, ** p<0.01, ***).(Statistical analysis performed using a one-way ANOVA, corrected for multiple comparisons using Tukey's post-hoc multiple comparisons test, error bars = SEM).

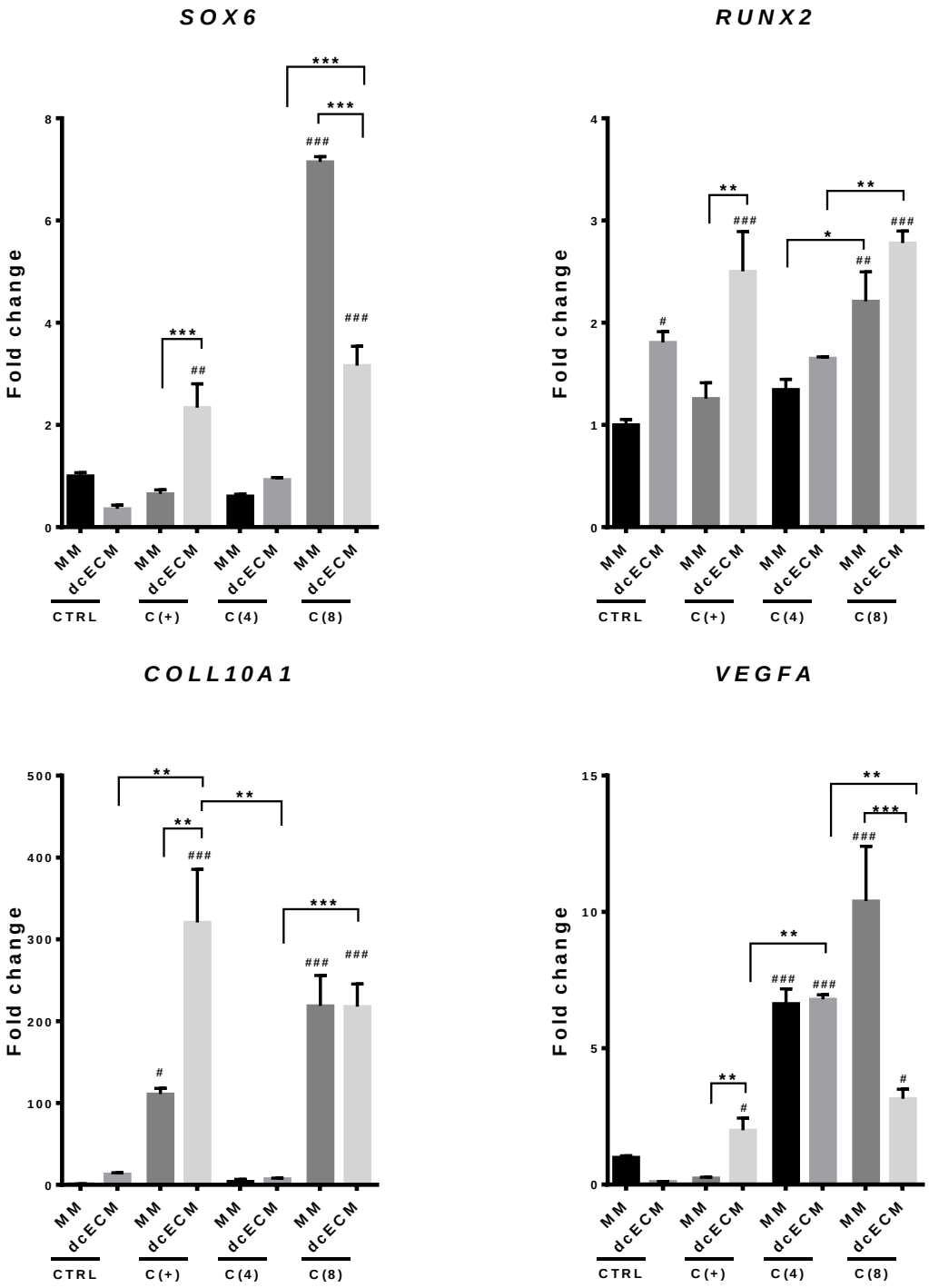

Figure 4.18: Growth factor optimisation gene expression data. qPCR based gene expression analysis for the chondrogenic marker genes *SOX6*, *RUNX2*, *COL10A1* and *RUNX2*. Fold changes normalised to micromasses cultures in control (MM-CTRL) conditions significance in relation with control micromasses indicated by # (# p<0.05,## p<0.01, ### p<0.001). Significance between experimental groups is indicated by * (* p<0.05, ** p<0.01, ***).(Statistical analysis performed using a one-way ANOVA, corrected for multiple comparisons using Tukey's post-hoc multiple comparisons test, error bars = SEM).

4.3.6. CAM assays demonstrate that the dcECM retains some inherent ability to promote angiogenesis.

The inherent capacity of the native costal cartilage and the dcECM to promote angiogenesis were investigated using a CAM assay. Images obtained using a brightfield stereomicroscope demonstrated blood vessel attraction towards both the native costal cartilage and the dcECM when placed on the CAM (Figure 4.19; A-B1&2). Explanted native and dcECM constructs also demonstrated blood vessel infiltration into the constructs (Figure 4.19; A3&B3). Gene expression data for *cd31* indicated that the native costal cartilage caused a 10-fold higher expression when compared to dcECM constructs ($p<0.001$) (Figure 4.20).

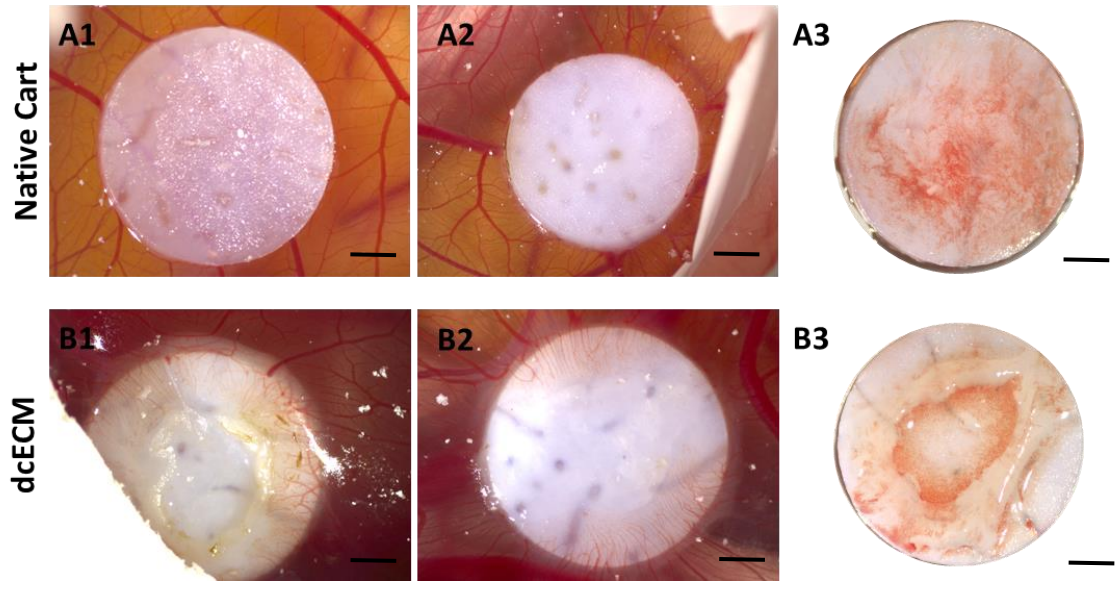

Figure 4.19: dcECM CAM assay Images. (A-B, 1-2) Representative images of the native costal cartilage and the dcECM placed onto the CAM of a 4 day old chick embryo and imaged after 6 days of *in ovo* culture. (A3&B3) Native costal cartilage and dcECM samples explanted after 6 days of culture *in ovo*. Scale Bar = 1 mm

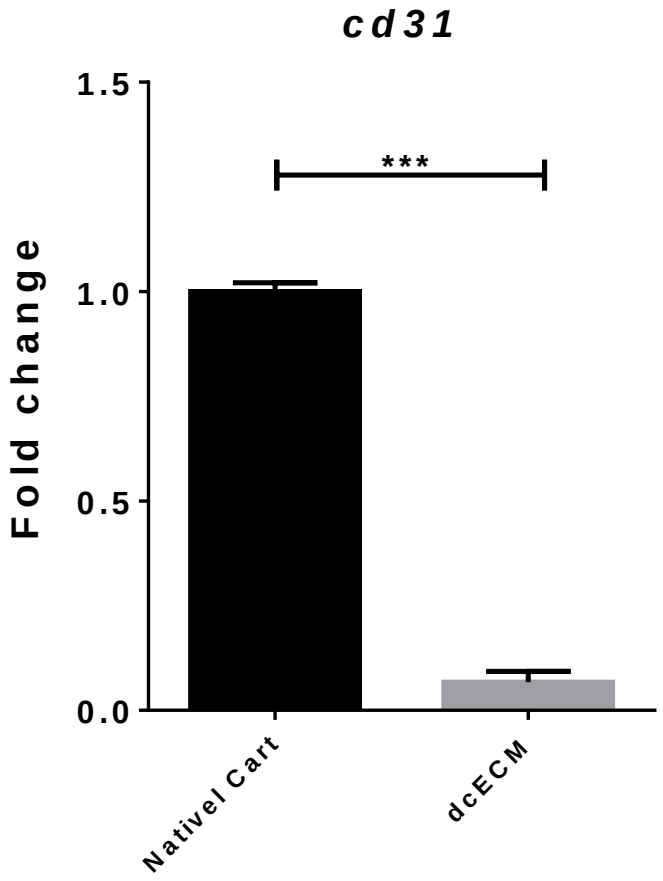

Figure 4.20: dcECM CAM assay gene expression. Gene expression analysis of chicken cd31. (*** p<0.001). Fold changes normalised to native costal cartilage. Statistical analysis performed using an unpaired t-test with Welch's posthoc correction., (error bars = SEM).

4.3.7. Subcutaneously implanted dcECM elicits a predominantly M2 macrophage-mediated anti-inflammatory, regenerative response

The dcECM was subcutaneously implanted into mice to assess the *in vivo* immune response in comparison to native costal cartilage tissue. Explanted samples were subjected to immunohistochemical (IHC) analysis for CD68 (Pan-macrophage marker), CD86 (M1-macrophage marker) and CD163 (M2-macrophage marker) (Figure 4.3). Qualitative analysis (Figure 4.21) of the stained sections revealed a similar CD68 positive immune cell presence within the fibrous tissue (FT) that bordered the implant, between both the native costal cartilage and the dcECM at 2 and 8 weeks. After 8 weeks, however, there was an observed decrease in CD86 staining with the dcECM compared

to the 2-week samples and native samples at this time point. Another distinct observation was the presence of CD163 positive cells in the FT surrounding the dcECM both at the 2 and 8-week time points, compared to the native cartilage samples. This indicated a predominantly M2 macrophage-mediated immune response towards the dcECM.

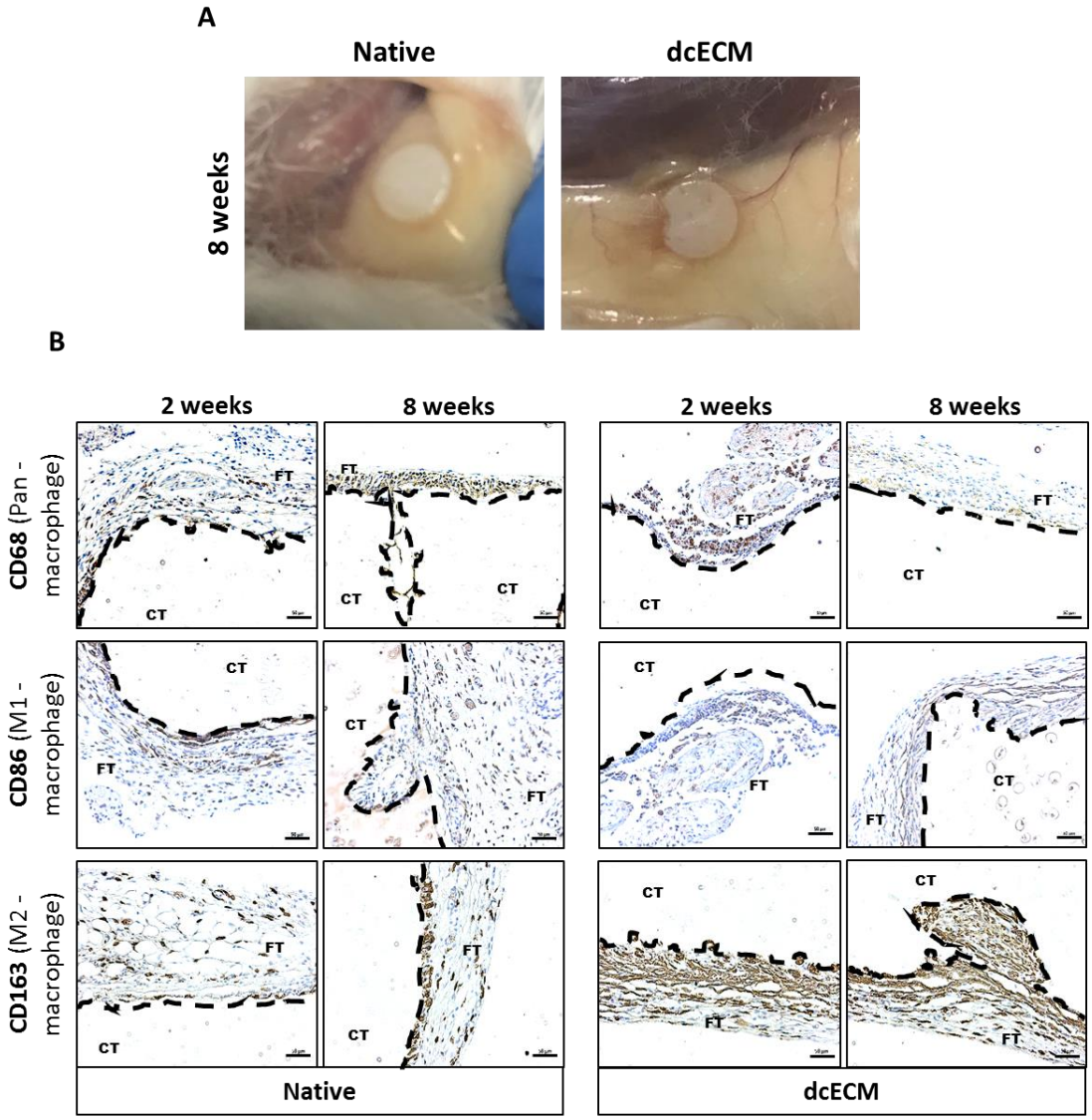

Figure 4.21: In vivo biocompatibility IHC analysis. (A) Representative in vivo photographs of subcutaneously implanted native costal cartilage and the dcECM 8 weeks post-implantation (B) Representative brightfield images of subcutaneously implanted native and dcECM cartilaginous constructs (CT) and host cellular infiltrate (FT). IHC was performed to visualise CD68 (Pan-macrophage marker), CD86 (M1-macrophage marker) and CD163 (M2-macrophage marker). Scale bars = 50 µm. The figure has been reproduced from Val et al[281] with permission from Mary Ann Liebert, Inc., New Rochelle, NY

4.4 Discussion

The successful clinical application of a tissue-engineered implant depends on its ability to attract and direct tissue-specific remodelling via its interaction with relevant stem cell populations[445]. The work carried out within this chapter, therefore, focuses on investigating the ability of the dcECM to interact favourably with skeletal cell populations and drive chondrogenic differentiation processes and are crucial for endochondral fracture healing.

Chondrocytes are the predominant cell type in hyaline cartilage and a key modulator of cartilage homoeostasis [435], they are, however, known to rapidly lose their chondrocytic phenotype following culture in monolayer, in a process that has been termed dedifferentiation[446,447]. Interestingly, dcECM promoted the re-establishment of a chondrogenic phenotype from culture expanded (dedifferentiated) chondrocytes, indicated by a significant upregulation of *COL2A1* expression (Figure 4.6). These results could potentially be the result of the retention of sufficient sGAG content [94,270,448], an undisrupted ECM ultrastructure[449] and, although not investigated in this thesis, the presence of remnant growth factors such as TGF-β [450], BMP2 [451], FGF-2 and FGF-18[452]. Investigations using de-differentiated chondrocytes also highlighted an inefficient localisation of cellular content on the surface of the dcECM, potentially, due to the dcECM surface not being perfectly flat, this could result in a lower and more inconsistent cell density on the surface of the dcECM. It was essential to obtain more consistent seeding as work by Bornes, and colleagues highlight the impact of varying cell densities on the chondrogenesis of MSC's seeded onto 3D collagen scaffolds[453]. The seeding methodology was, therefore, modified by seeding into a 96-well that closely matched the 6 mm diameter of the dcECM construct, thus improving localisation and maintaining a consistent seeding density.

hPDSC's were used to further investigate the bioactivity of the dcECM due to extensive published results and work within the group, highlighting the role of hPDSC's in fracture repair and bone tissue engineering [209,384,454,455]. Overall, gene expression data (Figure 4.10 & 4.11) highlighted that in chondrogenic conditions the dcECM significantly upregulated the expression of the SOX-

timer (*SOX9,5&6*). Lui and Lefebvre, suggest that the cooperative action of the SOX-trimer forms a super-enhancer complex that drives potent chondrogenesis[400], further highlighting the chondroinductive potency of the dcECM. Chung and colleagues do, however, note that the individual transcription factors within the SOX-trimer are upregulated during different stages of chondrogenesis[456]. Therefore, to further elucidate the underlying process of chondrogenic differentiation, several earlier time points may be required. An interesting observation was that the upregulation of chondrogenic markers was limited to seeded dcECM constructs, cultured in conditions containing TGF-β; these findings helped formulate two conclusions. Firstly, the dcECM may lack the endogenous growth factors necessary for chondrogenic differentiation of hPDSCs. Secondly, the dcECM may still be capable of enhancing the chondrogenic properties of exogenously added TGF-β due to the retention of the sGAGs content within the dcECM, capable of sequestering exogenously added TGF-β, and thus enhancing its chondrogenic potential. Previous work has extensively highlighted the role of sGAG's in facilitating and enhancing chondrogenesis [94,270,448].

Additionally, dcECM conditions containing TGF-β also demonstrated upregulation of hypertrophic markers such as *COL10A1* and *VEGFA*. Zeng and colleagues suggest that the expression of the *COL10A1* gene is critical for chondrocyte hypertrophic differentiation[457]. However, Mwale and colleagues suggest that *COL10A1* may be an unreliable marker for hypertrophy due to its upregulation during early chondrogenesis[399]. Pelttari and colleagues suggest that the early induction of *COL10A1* expression during chondrogenesis in vitro correlates with *in vivo* calcification and vascular invasion when MSC's derived cartilage constructs were ectopically implanted into SCID mice[458]. *VEGFA* was also upregulated in dcECM conditions and plays and is involved in facilitating cartilage hypertrophy and the blood vessel infiltration that eventually leads to new bone formation during endochondral ossification[459]. Overall, these findings suggest the dcECM may have the potential to undergo endochondral ossification *in vivo*.

Previously studies have demonstrated that culturing differentiated chondrocyte cell populations on tissue culture plastic often results in stress fibre formation

mediated via the ROCK pathway, subsequently, leading to their dedifferentiation[460]. This finding highlighted a potential mechanism for inhibition to enhance chondrogenesis[461,462]. Therefore, the inhibition of the ROCK pathway using a ROCK inhibitor (ROCKi) has become more prominent in chondrogenic media formulations[411,463] as it limits stress fibre formation and enhances chondrogenesis[464]. It was hypothesised that the 3D surface of the cartilage ECM derived dcECM constructs would not induce stress fibre formation when seeded with hPDSC's, therefore did not require the addition of ROCKi. Interestingly, the removal of ROCKi from the C(+) media formulations resulted in suppressed chondrogenic differentiation both in micromass and 3D cultures (Figure 4.10 & 4.11) Moreover, the removal of ROCKi, caused the micromass cultures to curl, potentially, due to the production of stress fibres.

Moreover, there is still an upregulation of chondrogenic markers (ACAN & COL2A1) with chondrogenic conditions that contain the dcECM, but no ROCKi compared to MM's in the same conditions. These findings are in agreement with Woods and colleagues who suggest that ROCKi may regulate *SOX9* expression independently of the seeding surface[461]. Moreover, Xu and colleagues suggested a synergistic mechanism for ROCKi with TGF-β, via their interaction with the SMAD signalling pathway[465]. Therefore, conditions for the chondrogenic and hypertrophic priming of hPDSC's even when seeded onto a 3D cartilaginous scaffold may require the inclusion of ROCKi. Alternatively, Kim and colleagues suggest that inhibition of the RhoA and not the ROCK pathway enhances chondrogenesis in chick limb MSC's[466]. Future optimisation of seeding conditions could, therefore, include both ROCKi and RhoA inhibitors, however, since RhoA, B and C are all implicated in stress fibre formation inhibiting ROCKi may be a more effective approach[467]. Overall, the potent ability of the dcECM to upregulate both chondrogenic and hypertrophic marker expression within just 7 days may demonstrate the importance of preventing the loss of crucial structural and biological cues in the dcECM.

Hypoxia was also considered for investigation due to its pivotal role in facilitating early chondrogenesis during fracture repair[401]. hPDSC's in micromass cultures demonstrated enhanced chondrogenesis in hypoxia, agreeing with similar findings in MSC's as highlighted by Lee and

colleagues[468]. Interestingly, when hypoxia was coupled with the dcECM, chondrogenesis was suppressed at day 7, however, upon examination of the results obtained 3-days post culture, there was an upregulation of *COL2A1* suggesting that hypoxia could drive earlier chondrogenesis that could have been suppressed by day 7 (Figure 4.13 & 4.14). There currently are no studies that precisely measure oxygen levels at the fracture site in humans, and more importantly oxygen levels at fracture sites with reduced viable vascular tissue. Therefore, the hypoxic conditions used in the study may not be representative of *in vivo* conditions. Moreover, although both MSC's and hPDSC's reside in highly vascularised native environments, there may be subtle differences in oxygen concentrations[384,469]. The role of hypoxia should, therefore, be further investigated with a broader array of oxygen concentrations and other skeletal cell populations in tandem with hPDSC's.

Several factors in addition to TGF-β that can promote chondrogenesis and hypertrophy in mesenchymal cell populations[470,471]. A study by Mendes and colleagues[411] is, however, the only study that investigates the effect of several of these factors on chondrogenesis specifically in hPDSC's. The study was, however, limited to micromass cultures. Therefore, the experiments carried out in this chapter were aimed at further investigating chondrogenesis using two of the optimal conditions (C4 & C8) when combined with a the dcECM. In line with previous results within this chapter, the dcECM demonstrated a robust upregulation of both chondrogenic and hypertrophic markers in standard chondrogenic conditions (Figure 4.17 & 4.16). Moreover, the findings in this chapter are in agreement with Mendes and colleagues as they demonstrated a potent upregulation of the hypertrophic markers *COL10A1* and *VEGFA* in the C8 but not C4, suggesting that C4 may drive the establishment of a more stable chondrocyte phenotype. More interestingly, although the dcECM enhanced chondrogenesis in C4 and C(+) conditions, compared to micromasses in the same comditions, rthe micromasses outperformed the dcECM in C8 conditions and the greatest upregulation overall. As Coleman and colleagues suggest, although factors such as GDF5, present in high levels can promote chondrocyte hypertrophy[472], their interaction with components of the dcECM such as heparin sulfate may alter their functionality, as also

proposed in a study by Ayerst and colleagues[473]. Moreover, these results further highlight the importance of TGF-β in promoting chondrogenesis[474–476], as C4 containing low TGF-β levels do not promote chondrogenic gene expression as potently as C8 that contained higher levels of TGF-β. Moreover, as suggested bt Shen and colleagues BMP2 enhances TGF-β3 mediated chondrogenesis, potentially demonstrated in the synergistic interaction of TGF-β and BMP2 in C8[477]. The underlying mechanism for this synergy could rely on the fact that both BMP2 and TGF-β bind to specific type II receptors and utilise the Smad pather for signal transduction (Figure 4.22). However, while TGF-β signalling is transduced through Smad2 and 3, BMP signalling relies on Smad 1, 5 and 8[478]. Overall, the evidence presented strongly suggests that conditions optimised in micromass cultures cannot always be directly translated into conditions containing a 3D bioactive scaffold. It further highlights the need for tuning the ideal growth factor cocktail with the dcECM, a crucial factor when considering priming tissue engineered scaffolds for *in vivo* implantation. A key factor to consider for a future study would be the potential disparity between gene expression and protein expression due to layers of post-transcriptional regulation[479,480]. The use of protein expression may, therefore, be more definitive.

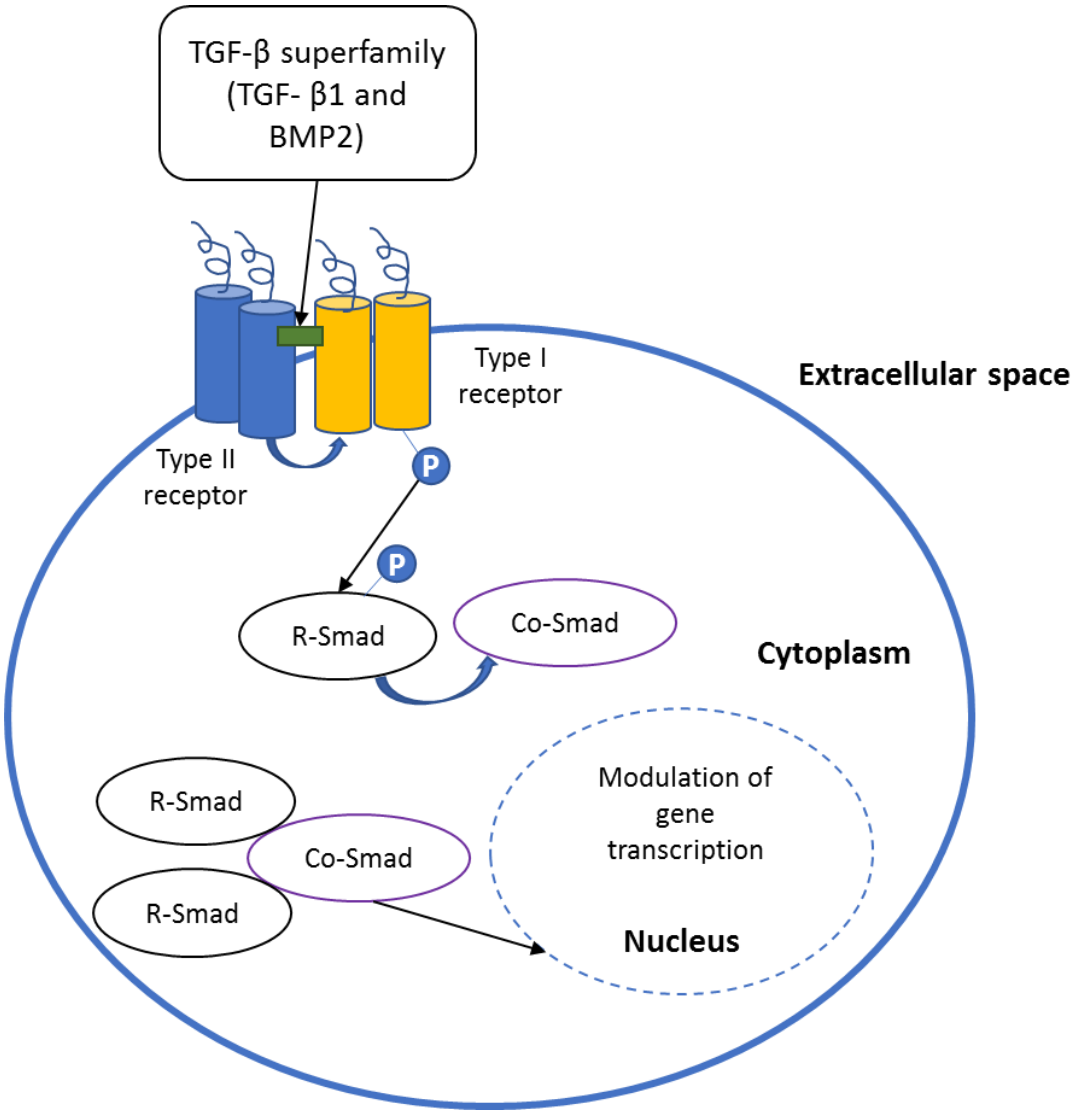

Figure 4.22: TGF-β superfamily signalling pathway. Schematic representation of the SMAD signalling pathway utilised by the TGF-β superfamily. Schematic was adapted from Danisovic and colleagues[470].

Angiogenesis plays a key role during fracture repair, facilitating cellular migration during the early stages of repair and driving callus ossification during the latter stages[481]. We, therefore, investigated the dcECM's capacity to facilitate angiogenesis using a *in ovo* CAM assay. Overall, the dcECM constructs did not remained localised under the window, this was a major issue when for obtainig sufficient visualisation of the surrounding vasculature, required to draw any difinitive conclusions. Gene expression data obtained form the cellular content localised on the implanted native costal cartilage constructs, 6 days post *in ovo* culture, indicated an upregulation of CD31, a

marker associated with endothelial cell populations[482]. These findings potentially suggest some degree of angiogenic potency in native costal cartilage tissue or a lack of angiogenic inhibitors. However, the gene expression seems to highlight that this ability to attract angiogenic cells is lost post Vac-OS decellularisation. The CAM assay was not conclusive. However, future work can consider alternative approaches such as the use of *ex ovo* CAM assays[483], providing a much larger and more even area for the localisation and visualisation of the constructs. Moreover, the 1 mm thick constructs could be breaking through the CAM and failing to localise on the surface; future work should use smaller and lighter dcECM fragments.

In vitro testing provided valuable data on the bioactivity of the dcECM; however, these conditions fail to mimic the more dynamic and multicellular *in vivo* environment. Successful translation of a tissue engineered constructs is dependent on its ability to elicit a favourable immune response upon implantation, predictive of clinical response to the engineered constructs. The dcECM was, therefore, implanted into immunocompetent BALB/c mice for the assessment of biocompatibility. There was a distinct lack of granular tissue formation around both native costal cartilage constructs and the dcECM when observed macroscopically(Figure 4.20; A), It has been suggested that whole hyaline cartilage may have some degree of immune privilege due to its dense avascular structure[484]. Upon microscopic examination (Figure 4.20; B), however, more distinct differences were observed. The dcECM demonstrated a predominantly M2 macrophage response at 2 and 8 weeks, which was indicative of favourable long-term outcomes and tissue-specific remodelling [485]. This was in contrast with the native costal cartilage comparator that demonstrated a predominantly M1 macrophage response, linked to the initiation of inflammation[425], further supporting the *in vitro* analysis in chapter 3 that demonstrated the effective removal of immunogenic factors. Due to the dense nature of hyaline costal cartilage, cellular infiltration into the cartilage is limited, which could be a limiting factor in eliciting a more aggressive cellular response. Almeida and colleagues also observed that Macrophages with higher metabolic activity were pro-inflammatory[486]. Future work could take advantage of live cell metabolism imaging techniques such as FLIM[487] for the

assessment of the immune cell metabolic profile. Moreover, there are a plethora of other markers associated with cell populations that are involved in foreign body mediated immune response; These include CD44 (helper T-Lymphocytes) and CD8 (Cytotoxic T-Lymphocytes)[488]. The biocompatibility study was carried out in non-primate species and, therefore, cannot be used as a model to confirm the presence of Alpha-Gal a key limitation of this study. Non-primate species lack circulating Anti alpha-gal antibodies and are, therefore, non-reactive to the alpha-gal epitope, otherwise highly immunogenic in humans[222].

In conclusion, the dcECM demonstrated an inherent capacity to enhance chondrogenesis and chondrocyte hypertrophy, surpassing similar published studies employing decellularised cartilage derived scaffolds such as those employed by Gawlitta et al[150] and Cunniffe and et al. [431]. Moreover, the use of a bioactive scaffolding material can overcome the limited tissue volume available from the cell only approaches such as those applied by Cunniffe et als[431]. Additionally, the predominantly regenerative response elicited by the dcECM makes it an ideal candidate for clinical application. It has to be noted, however, that the size of the dcECM used in this study would be too small to be implanted into critical-sized clinical non-union defects. Further work is, therefore, required to explore alternative and optimised methods to transform the dcECM into a suitable format for clinical delivery, while not compromising the chondroinductive properties of the dcECM. As the preliminary *in vivo* work has yielded promising results, it warrants further development of more tailored tools for seeding, chondrogenic priming, and investigating cellular behaviour.

5. Preparation of an upscaled dcECM scaffold for clinical application

5.1. Introduction

Bone tissue engineering has yielded a diverse range of implants that aim to address skeletal pathologies such as fractures and large bone defects, arising from injury and metabolic bone diseases. During the development of these solutions, careful consideration of the clinical scenario and current treatment approachs is required. Currently, depending on the severity and location of the fracture, effective reparative options can range from mechanical support to vascularised bone grafts that are capable of rapidly remodelling and integrating with surrounding bone tissues[489,490], tissues engineered alternatives have to, therefore, demonstrate similar or improved efficacy to the current approaches.

5.1.1 Clinical developments in the management of bone disease pathologies.

With between 3.6 to 6 million bone fractures occurring in the united states and around 850,000 occurring in the UK bone is the second most transplanted tissue, after blood, driving research into novel approaches to address the demand[33,491]. Over a decade ago Medtronic® and Stryker® developed a caged putty-based BMP delivery system derived from demineralised bone. The osteoinductive capacity of these collagenous constructs effectively drove endochondral bone regeneration and was harnessed for non-union fracture intervention and spinal fusion[492,493]. They also offered a key advantage when used clinically due to their adaptability. Investigations into the use of BMP's for bone regeneration, however, raised some speculation with regards to the treatment of open tibial fractures[494]. Moreover, there have also been reports of adverse side effects when using supraphysiological levels of BMP-2[495], resulting in complications such as heterotrophic ossification or osteolysis, and possibly their association with promoting the pathogenesis of some cancer

sub-types[496–498]. Therefore, the use of stem cell populations with an osteogenic potential was as an alternative approach to fracture management[190]. In an attempt to find an alternative approach, fresh bone marrow aspirate was combined with ceramic bone grafts, which has shown efficacy for spinal fusion procedures[499,500]. A study by Damron and colleagues has, however, demonstrated that for the treatment of large bone defects, the addition of bone marrow aspirates provides no advantage[501]. There is however, growing evidence for the use of skeletal stem cells for the treatment of non-union fractures, with a consensus that highlights the advantages of using a scaffolding material in conjunction with the relevant stem cell populations, as this allows for the localisation of therapeutic stem cells and a better ability to treat large bone defects[502,503].

The majority of clinically available bone grafts and tissue engineering approaches focus on mimicking the characteristics of the clinically accepted gold standard; Autologous bone grafts. However, chapter 1 highlights a shift towards developing grafts that mimic tissue intermediates involved in the fracture healing process, such as the cartilaginous callus. Engineering the cartilage niche, however, presents a unique set of challenges, especially with regards to creating cell-laden constructs.

5.1.2 Engineering the cartilage niche.

Native hyaline cartilage is an avascular, dense tissue, which limits cellular infiltration if seeded, which restricts the use of whole cartilage ECM-derived constructs without further processing. Huey and colleagues have extensively reviewed and discussed these challenges[504]. Currently, the gold standard methodology for creating cell-laden cartilage construct relies on the developmental process of stem cell condensation and chondrogenesis. Several stem cell populations have been studied for their ability to undergo chondrogenesis, and are extensively reviewed in chapter 1. The general principle for chondrogenic differentiation involves seeding relevant cells into high-density cultures in conjunction with the addition of exogenous chondroinductive growth factors[505–509]. As demonstrated by Detzel and

colleagues this process of condensation *in vitro* can be further enhanced using centrifugal force[510]. Obtaining cell-derived cartilage constructs requires a large vast number of cells and extensive culture times, thus limiting its scalability. Moreover, the mechanical properties of the cell-generated cartilage ECM is dependent on the cell type used, with chondrocytes producing more robust cartilage-ECM compared to bone marrow-derived(BM) MSC's[511–513]. Overall, these findings provide further evidence for coupling stem cell populations with a cartilage-mimetic construct.

Several factors must be considered when engineering a cartilage mimetic construct; these include ECM biochemical composition, structure, and ability to achieve efficient cellular distribution when seeded. Additionally, as these factors are paramount for the clinical translatability, novel fabrication and seeding approaches have been developed. Nasiri and colleagues have achieved this by generating chemically cross-linked chitosan-ECM constructs, which allow for the control of pore size and, therefore, cellular infiltration[514]. Moreover, methodologies such as freeze-drying have been applied by Amadari and colleagues for the generation of highly porous cartilage mimetic constructs, the principle of which relies on the extraction of water from a hydrated gel-like construct, leaving behind a porous material[515]. Yang and colleagues have further incorporated decellularised cartilage ECM-derived granules into a cross-linked gel suspension that was freeze-dried to give porous constructs[516]. When implanted into nude mice in combination with bone BM-MSC's, cartilage ECM deposition was observed. The poor seeding efficiency and homogeneity of cartilage mimetic constructs have been addressed in a study by Chen and colleagues buy incorporation a hydrostatic pressure bioreactor system to better mimic the native microenvironment present during cartilage development *in vivo* [517].

The previous chapters highlighted the development of the dcECM; a chondroinductive cartilage mimetic scaffold that retains its native biochemical composition post-decellularisation. This chapter builds upon these previous findings to further investigates a proof of concept methodology for processing the dcECM to create scalable chondrogenic constructs with the potential for clinical translation.

5.2. Methods

5.2.1 Preparation of compressed dcECM derived constructs.

Sterile dcECM was placed into a T-75 tissue culture flask with a 0.2 micron vented cap (Corning, UK), the vented cap allowed for gas exchange while maintaining the sterility of the samples. Samples were frozen at -80 ºC for 8 hours prior to initiating the freeze-drying process The T-75 flask containing the dcECM were freeze-dried (Christ, UK) for 24 hours at -55 ºC. Freeze-dried dcECM samples were subsequently removed from the T-75 flask and placed into sterile cyromill tubes (Spex sample prep, UK). The freeze-dried dcECM was then freeze-milled in a liquid nitrogen cooled mill (Spex sample prep, UK) at a rate of 15 cycles per second (cps) for 10 mins. The milling process was repeated 3 times per sample after which the milled contents were transferred into a 50 mL falcon tube (Corning, UK) and stored at room temperature (18-21°C). To maintain sterility, the transfer of the dcECM was carried out in a sterile environment.

For the fabrication of the compressed dcECM constructs either 5mg, 10mg or 15mg of the freeze-dried dcECM was added into 1 mL C-DMEM containing 10% FBS (Invitrogen, Paisley, UK) and antibiotic-antimycotic solution (100 units/mL penicillin, 100 µg/mL streptomycin and 0.25 µg/mL amphotericin B; Invitrogen, Paisley, UK). 100 µL of the mixture was added into a well of a 96-well plate. A 96-well absorber (Lonza, UK) was used to remove the media resulting in the compression of the freeze-dried dcECM granules into a circular construct (Figure 5.1). The compression process occurred from the removal of the water and soluble content from the mixture. The varying weight of the absorber also provided the additional force required for compression, this however varied throughtout the compression process due to the absorbtion of water from the mixture. The resultant compressed dcECM derived constructs (C-dcECM) were subsequently seeded and assessed for cellular infiltration.

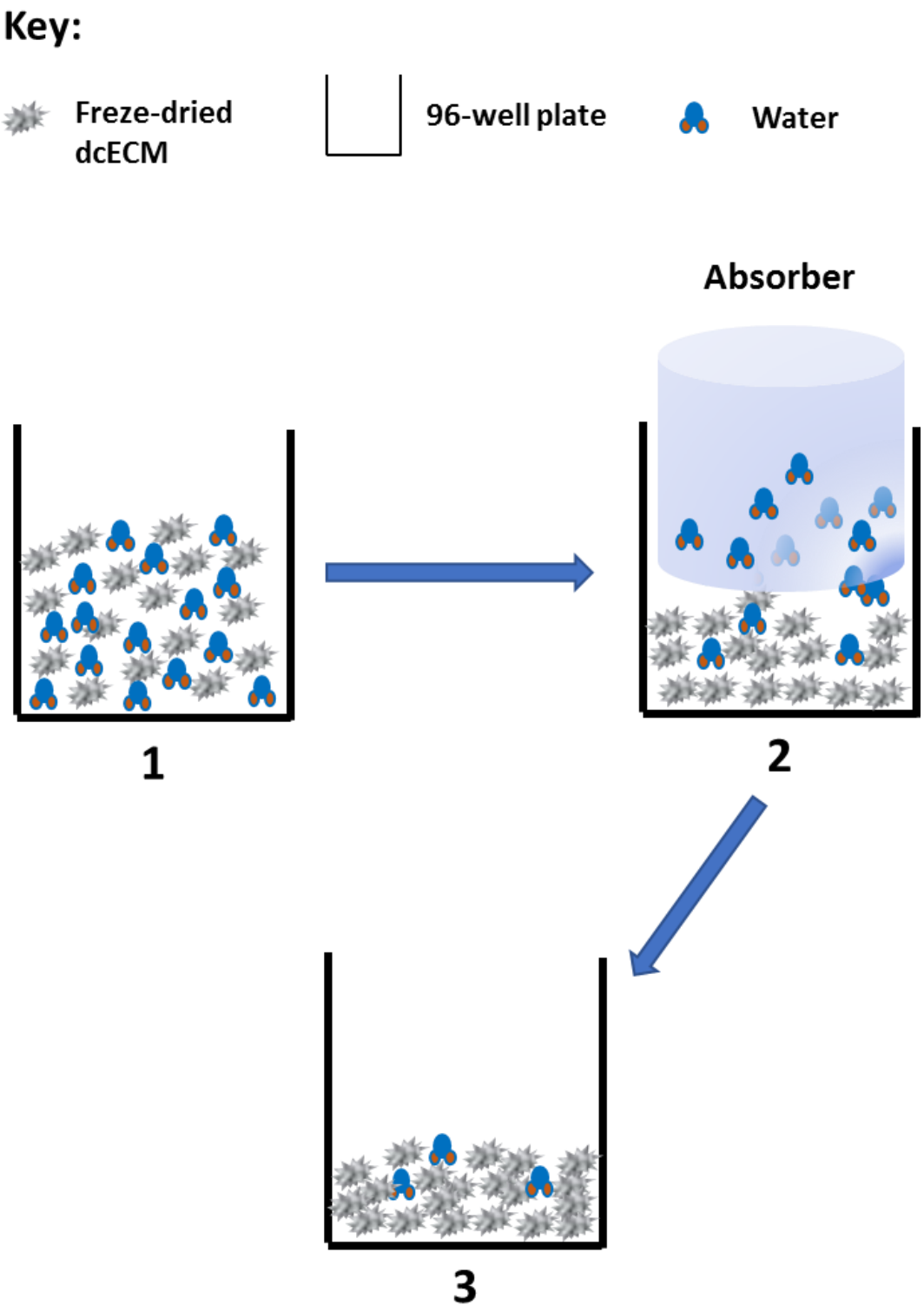

Figure 5.1: Schematic representation of the fabrication of compressed dcECM-derived constructs. (1) freeze-dried dcECM granules are mixed with C-DMEM containing 10% FBS and antibiotic-antimycotic solution. (2) The mixture of dcECM granules and C-DMEM is compressed using an absorber, removing a portion of the water content and soluble components. (3) The absorber is removed leaving behind a compressed dcECM derived construct.

5.2.2. Human periosteal stem cells (hPDSCs).

hPDSCs were isolated as previously described in Chapter 4.2 (obtained from Prof Frank Luyten, KU Leuven, Belgium).

5.2.3. hPDSC expansion and micromass culture.

hPDSC's were expanded and seeded into micromass cultures as described in Chapter 4.2

5.2.4 Fabrication of porous dcECM-collagen type 1 hybrid constructs.

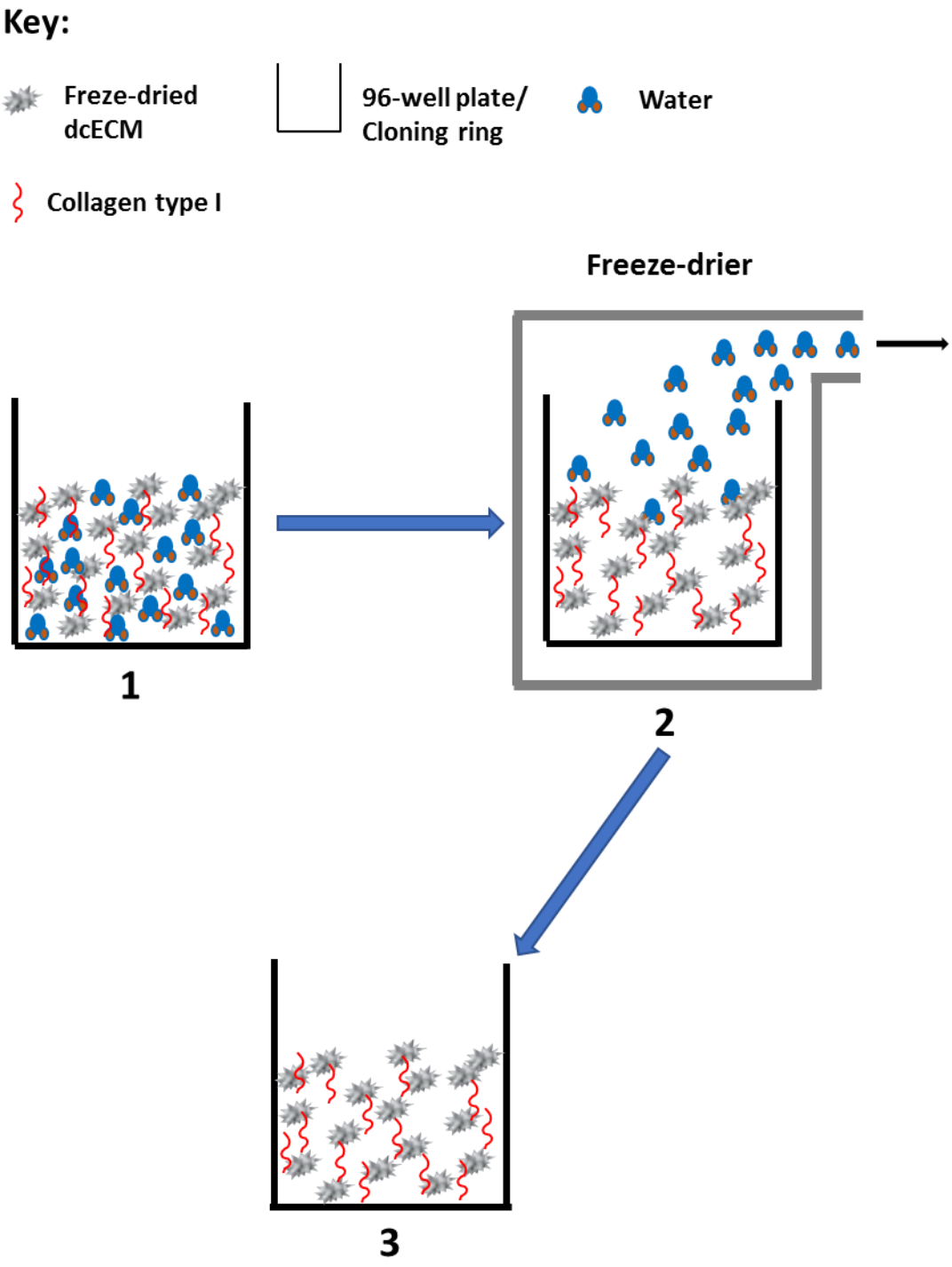

Figure 5.2: Schematic representation of the creation of porous dcECM derived constructs. (1) A gel mix is created by adding freeze-dried dcECM to neutralised rat tail collagen type I. The gel mix is placed into a freeze-drier for 24 hours, removing water content from the mix. (3) Post freeze-drying, a porous dcECM derived construct is left behind.

To fabricate porous dcECM derived constructs, rat tail collagen type I (First-link, UK) was neutralised using a neutralising agent (Lonza, UK), amount of neutralising agents vary depending on the amount being neutralised, this is provided as part of the standard protocol included in the RAFT 3D cell culture kit (Lonza, UK). Freeze-dried and milled dcECM was added into the gel mixture at a concentration of 16 mg/mL. 150 µL of the gel mixture was added into 6 mm cloning rings or 96 well plates and incubated at 37ºC to gelate (Figure 5.2). The 96-well plates were placed in the freeze drier while, the cloning rings containing the gelated mix were transferred into T75 flask before being freeze-dried, as previously described. The process of freeze drying was used to remove the water content from within the gelated constructs, thus creating air pockets within the construct, and subsequently creating a porous dcECM-derived construct (P-dcECM) (Figure 5.2).

5.2.5 Differential scanning calorimetry (DSC) analysis of the P-dcECM

DSC was used to measure collagen denaturation temperatures of the P-dcECM as an indicator of the structural integrity of the matrix as previously described in Chapter 3.2.

5.2.6 Multiphoton Imaging of P-dcECM samples

Second harmonic generation and fluorescence-lifetime imaging microscopy (FLIM) were used to measure changes in the collagen biochemical environment as a measure of matrix integrity. Without any prior processing native costal cartilage (dimension ~5 mm height × 10 mm in diameter) and P-dcECM (dimensions ~9 mm height x 3 mm in diameter) were placed in PBS in preparation for imaging. Laser scanning microscopy with multiphoton excitation was carried out as described in Chapter 3.2.

5.2.7 Seeding P-dcECM constructs.

Porous dcECM derived constructs formed using cloning rings (P-dcECM) were selected for further *in vitro* analysis using hPDSC's (Figure 5.3). Sterile P-dcECM constructs were placed into 15 mL falcon tubes (Corning, UK). hPDSC's were seeded onto the surface of each of the P-dcECM constructs at a density of $3x10^5$ cells in 10 µL of C-DMEM supplemented with 10% FBS, (Invitrogen, Paisley, UK) and antibiotic-antimycotic solution (100 units/mL penicillin, 100 µg/mL streptomycin and 0.25 µg/mL amphotericin B; Invitrogen, Paisley, UK). The constructs were left for 2 hours at 37ºC and 5% CO_2. In parallel cells were seeded into pellet cultures of equivalent density. Briefly, hPDSC's were pipetted into 15 mL falcon tubes at a density of $3x10^5$ in 5 mL of C-DMEM. Subsequently, the samples were centrifuged (Fisher scientific, UK) at 1500 RPM for 10 minutes to form pellets, that were also incubated for 2 hours at 37ºC and 5% CO_2. After two hours the media was switched to control (CTRL) and chondrogenic C(+) conditions, these conditions are previously defined in Chapter 4.4. Cells were cultured for 7 days.

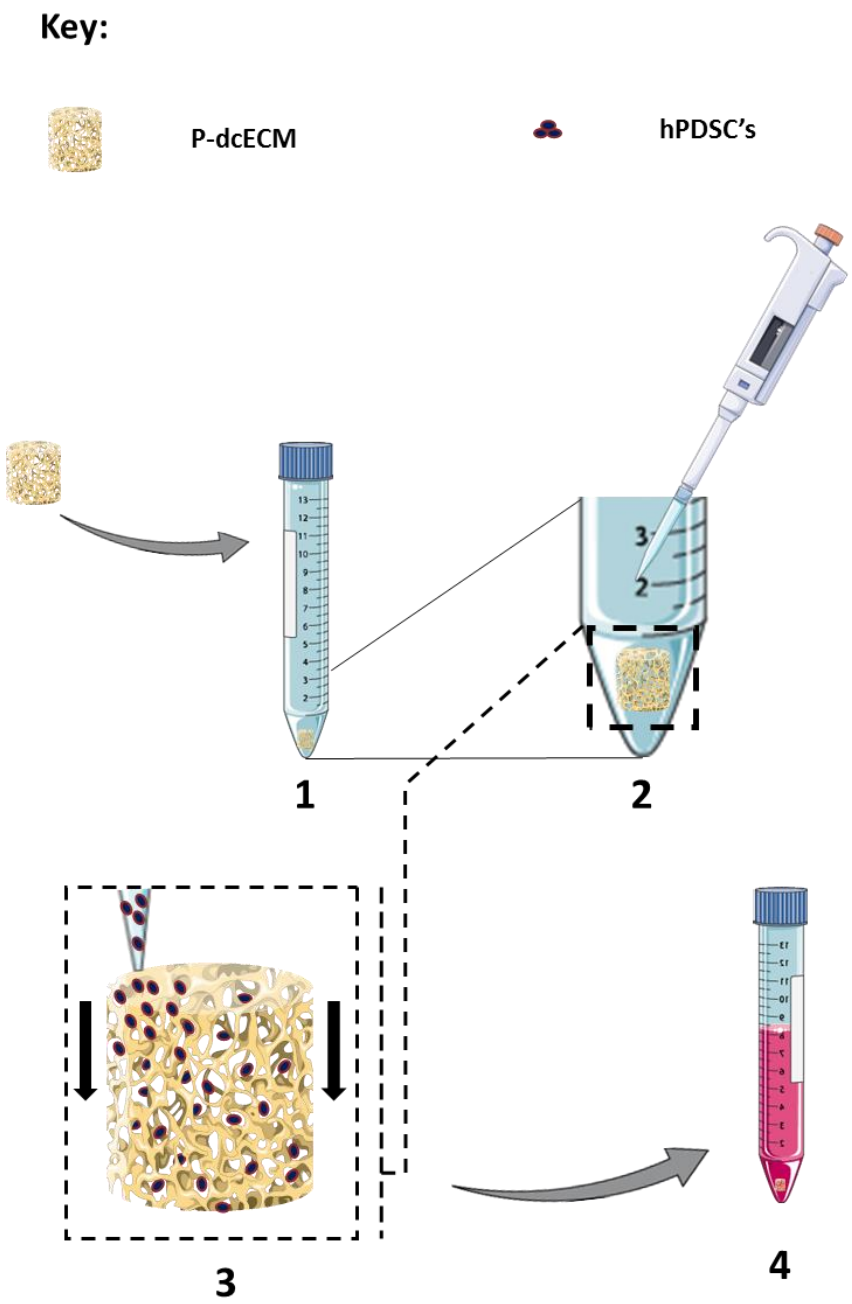

Figure 5.3: Schematic representation of the methodology for seeding the P-dcECM. (1) The P-dcECM is placed into a 15 mL falcon tube. (2) 300,000 hPDSC's are dispensed onto the surface of the P-dcECM in 10 µL cell suspension. (3) Seeded P-dcECM constructs are incubated for 30 mins to allow the cell suspension and cells to impregnate the whole construct. (4) culture DMEM is added into the tube containing the seeded construct. Figure generated using the Servier medical art database (http://www.servier.com/Powerpoint-image-bank

5.2.8. Total RNA extraction and quantitative reverse transcription–Polymerase Chain Reaction (qRT-PCR) analysis

Gene expression analysis was used as an indicator of cellular differentiation. Briefly, all seeded constructs were washed with PBS, before being transferred into new 1.5 mL micro centrifuge tubes (Star Labs, UK), placed in 350 µL of Trizol (Invitrogen, Paisley, UK) and homogenised. Total RNA was isolated from each of the micromasses, pellets, compressed dcECM and P-dcECM using the Direct-zol RNA MiniPrep (Cambridge Biosciences, Cambs, UK) according to the manufacturers' instructions. mRNA isolation and qRT-PCR was carried out as described in Chapter 4.2. Primers used in this study are listed in Supp Table 1.

5.2.9. Statistical analysis

Statistical analysis was carried out as described in Chapter 2.2. All statistical analysis was performed using GraphPad Prism version 6.0f for windows (GraphPad Prism Software, La Jolla California USA, www.graphpad.com).

5.3 Results

5.3.1 Compressed dcECM derived constructs do not allow for cellular infiltration when seeded.

Brightfield microscopy images of H&E stained sections reveal that constructs formed with a dcECM granule concentration of 15 mg/mL had sparse distribution of dcECM granules and were unable to form a scaffold, unlike constructs fabricated with 10 or 15 mg/mL of dcECM granules. (Figure 5.4; D&E). At all concentrations variation in dcECM granule size can be observed (Figure 5.4; A&B).

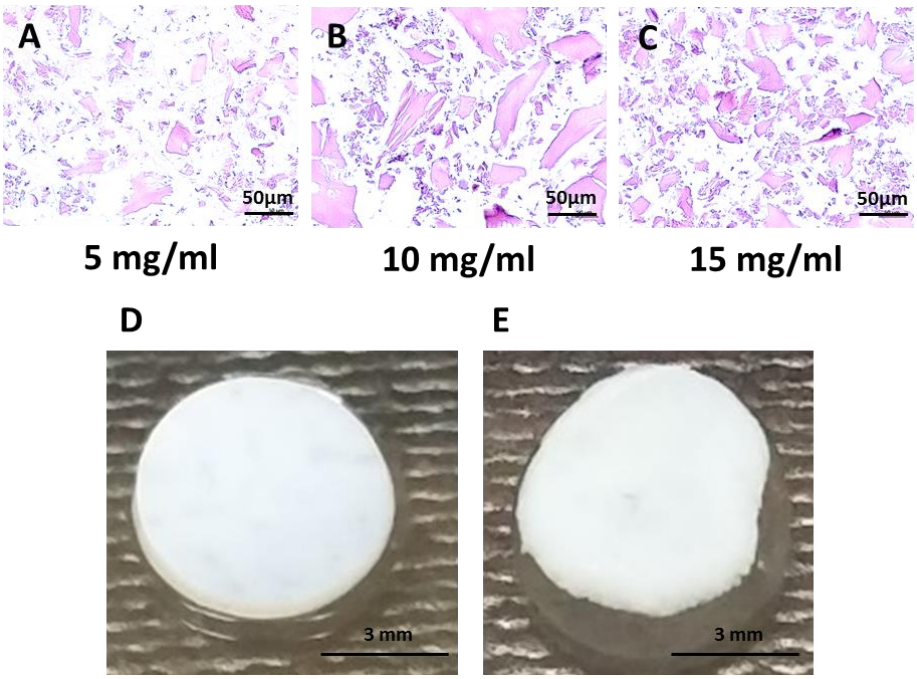

Figure 5.4: Histological examination of compressed dcECM-derived constructs (A-C) Representative brightfield microscopy images of compressed dcECM derived constructs containing 5,10 and 15 mg of freeze-dried dcECM, sections (scale bar = 50 µm). (A&B) Representative stereomicroscopy images of dcECM derived constructs containing 10 mg/mL of freeze-dried dcECM (scale bar = 3 mm).

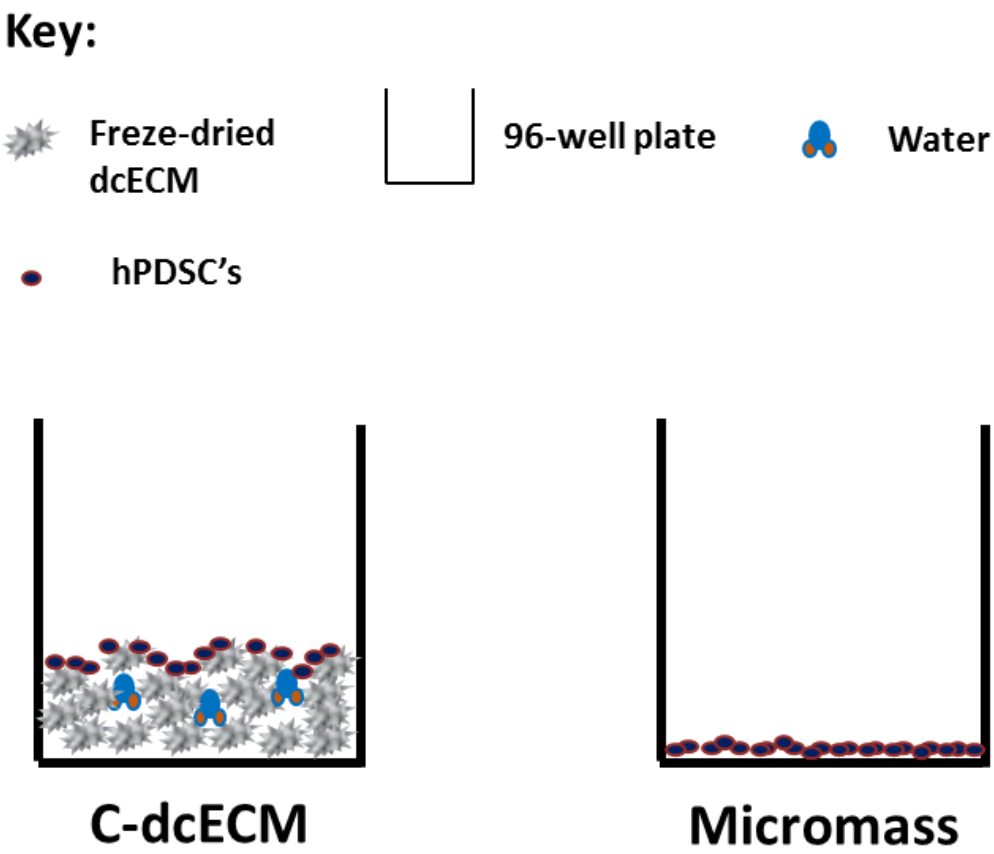

Media Conditions:

CTRL	C(+)
• LG-DMEM • **2%** FBS • **1%** Antibiotics/Antimycotic	• LG-DMEM (Gibco, UK) • **1×** insulin-transferrin-selenium • **100 nM** dexamethasone • **100 µM** ascorbate-2-phosphate • **40 µg/ml** proline • **1%** Antibiotics/Antimycotic • **20 µM** Y27632 • **10 ng/ml** TGF-β1

Figure 5.5: Seeding schematic highlighting the seeding and media conditions used for the investigation of compressed dcECM derived constructs (C-dcECM) using hPDSC's.

The compressed scaffold containing a dcECM granule concentration of 10 mg/mL were seeded using hPDSC's to assess cell attachment and infiltration (Figure 5.5). DAPI stained images of the scaffold surface indicates the presence of cells attached to the surface of the scaffold, both in CTRL and chondrogenic conditions (Figure 5.6; A&B). However, H&E stained cross-sections reveal that a majority of the cellular population is localised on the surface of the scaffold, with little migration into the deeper regions (Figure 5.6; C&D). Closer examination also revealed a dense matrix that potentially limited cellular migration.

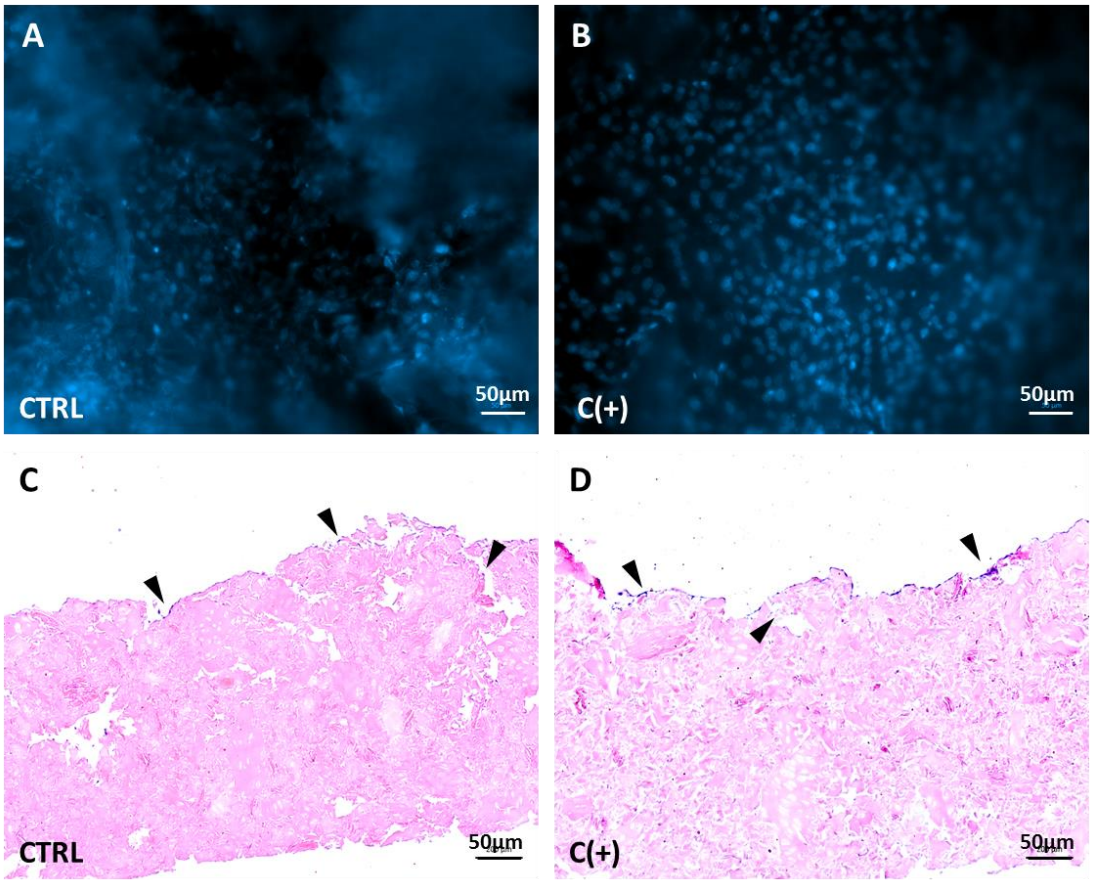

Figure 5.6: Histological analysis of seeded compressed dcECM-derived constructs. (A&B) Structured illumination microscopy images of hPDSC's seeded onto the on the surface of compressed dcECM derived constructs in CTRL and C (+) conditions and stained with DAPI. (C&D) Brightfeild images of the seeded dcECM derived constructs with hPDSC's localised on the surface (black arrow) stained using H&E. (scale bar = 50µm)

5.3.2 The dcECM can be combined with collagen type I to give porous freeze-dried constructs.

Histological examination of the compressed dcECM derived constructs indicated a lack of porosity, as a result, seeded hPDSC's although attached, remained primarily localised on the seeding surface. Therefore, a methodology to obtain a more porous scaffold (P-dcECM) was developed.

Macroscopic examination of the P-dcECM constructs revealed visiably porous cylindrical structure when fabricated with either cloning rings or 96-well plates (Figure 5.7; A-D). Upon qualitative histological inspection of the P-dcECM constructs using H&E stained sections, the cloning ring fabrication approach produced a more porous scaffold with pore size ranging from ~70-200µm. Additionally, both methods resulted in P-dcECM constructs with a homogenous distribution of the dcECM (Figure 5.7; E&F). Due to its porosity, the cloning ring based approach was selected for further analysis.

One of the key findings highlighted in this thesis was the minimal damage inflicted to the native costal cartilage ECM post Vac-OS decellularisation, potentially resulting in a more chondroinductive scaffold. It was, therefore, crucial that the biochemical structure of the P-dcECM is assessed.

DSC analysis of the P-dcECM revealed a significant decrease in collagen denaturation temperatures ($p<0.01$) compared to both the native costal cartilage samples and the dcECM (Figure 5.8; A). Similarly, there was also a significant difference in flourescence lifeitime images(Figure 5.8; B). Overall these results highlight changes in the matrix structure of the P-dcECM.

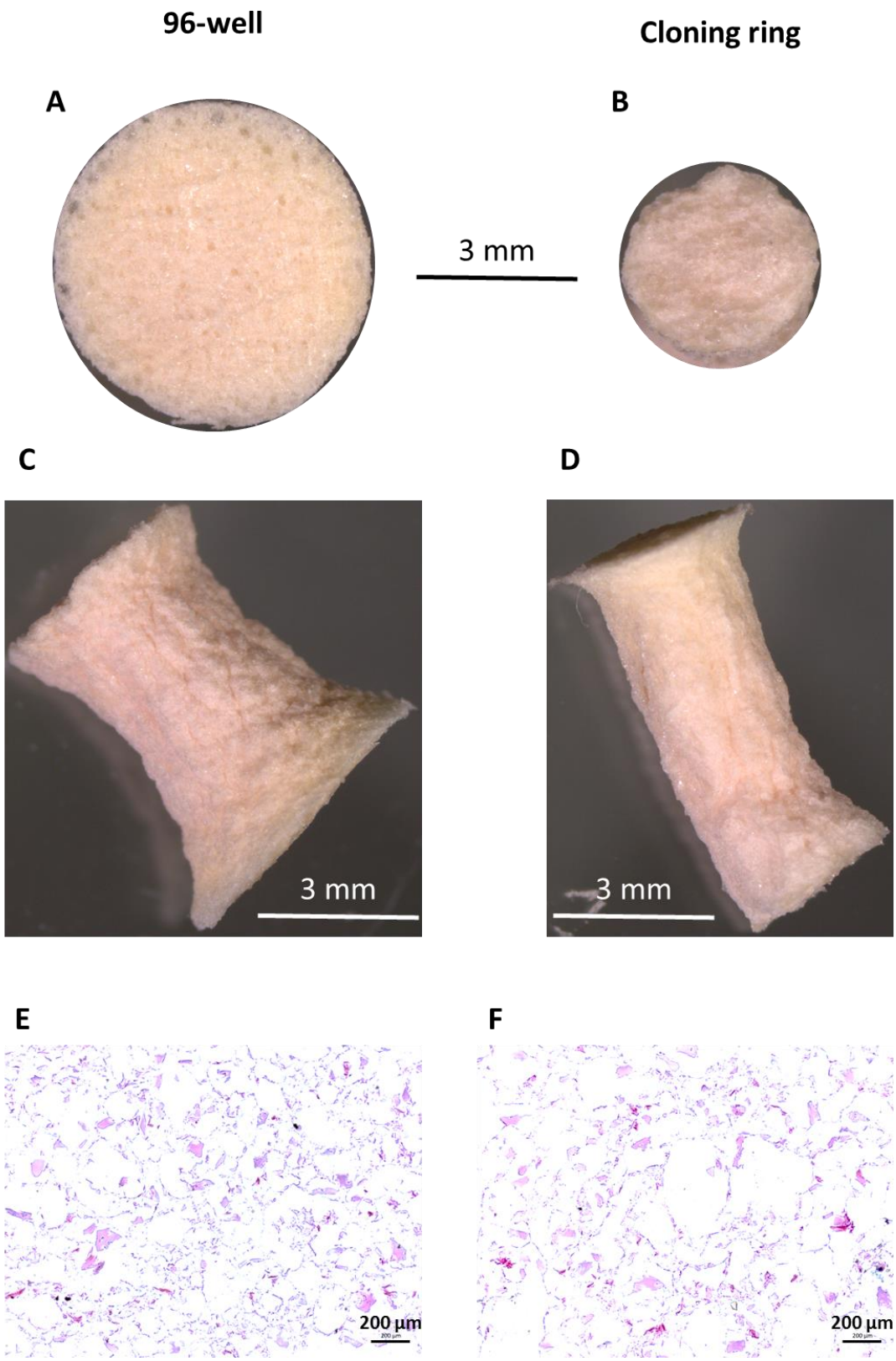

Figure 5.7: Histological analysis of the P-dcECM. (A-D) Stereomicroscopy images of porous dcECM derived scaffolds formed using 96-well plates and 6 mm cloning rings. (E&F) Brightfield microscopy images of dcECM derived porous scaffold sections stained using H&E.

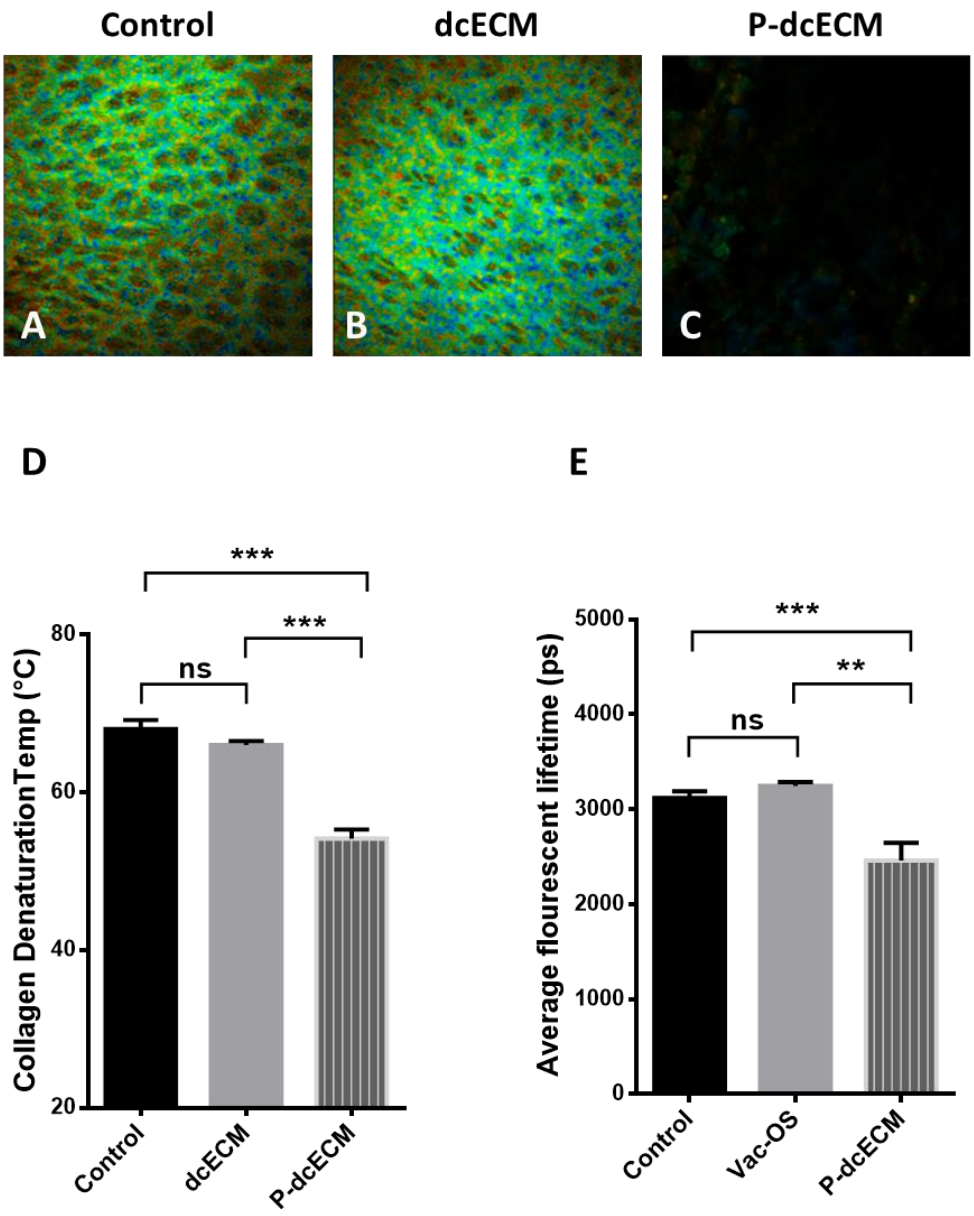

Figure 5.8: Quantitative FLIM analysis of the P-dcECM. (A-C) False colour images of FLIM readouts of Control, dcECM and P-dcECM. Quantification of average denaturation temperatures comparing control cartilage vs dcECM vs P-dcECM samples. (D-E) ImageJ quantification of the ROI's, measuring the average fluorescence lifetimes (n=4 *p<0.05, **p<0.01, ***p<0.001). Representative quantification data is represented as mean ± SD. Statistical analysis performed using an unpaired t-test with Welch's post-hoc correction.

5.3.3 The P-dcECM supports cellular infiltration and chondrogenic differentiation.

One of the key requirements for developing the P-dcECM was its potential to allow for cellular migration into scaffold, unlike the dcECM or the compressed dcECM derived scaffolds previously investigated. Moreover, it was essential the P-dcECM maintain the chondroinductive properties observed with the dcECM. hPDSC's were, therefore, seeded onto the P-dcECM and cultured for 7 days before being assessed (Figure 5.9).

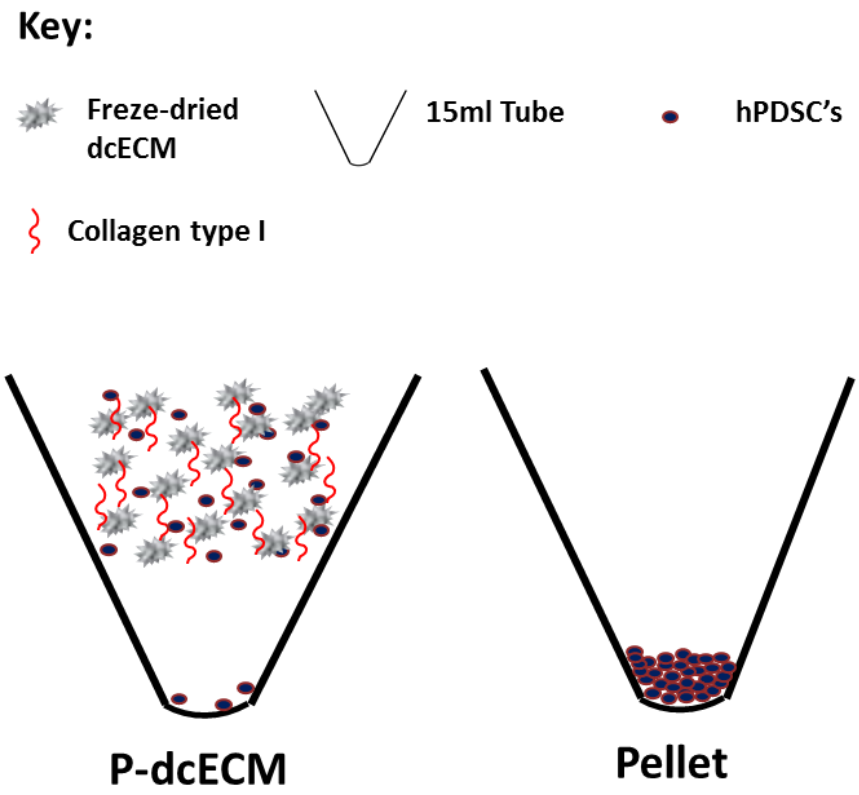

Media Conditions:

CTRL	C(+)
• LG-DMEM • **2%** FBS • **1%** Antibiotics/Antimycotic	• LG-DMEM (Gibco, UK) • **1×** insulin-transferrin-selenium • **100 nM** dexamethasone • **100 µM** ascorbate-2-phosphate • **40 µg/ml** proline • **1%** Antibiotics/Antimycotic • **20 µM** Y27632 • **10 ng/ml** TGF-β1

Figure 5.9: Schematic representation highlighting the seeding and media conditions used for the investigation of porous dcECM derived constructs (P-dcECM) using hPDSC's

Histological examination of H&E stained cross-sections of the seeded P-dcECM reveals the migration of seeded hPDSC's into the centre of the scaffold. This occurred in both control and chondrogenic conditions (Figure

5.10; A&B). Closer examination of the sections reveals that hPDSC's have primarily localised around the centre of the P-dcECM and potentially attached to dcECM fragments present. Overall, the cells are non-uniformly distributed.

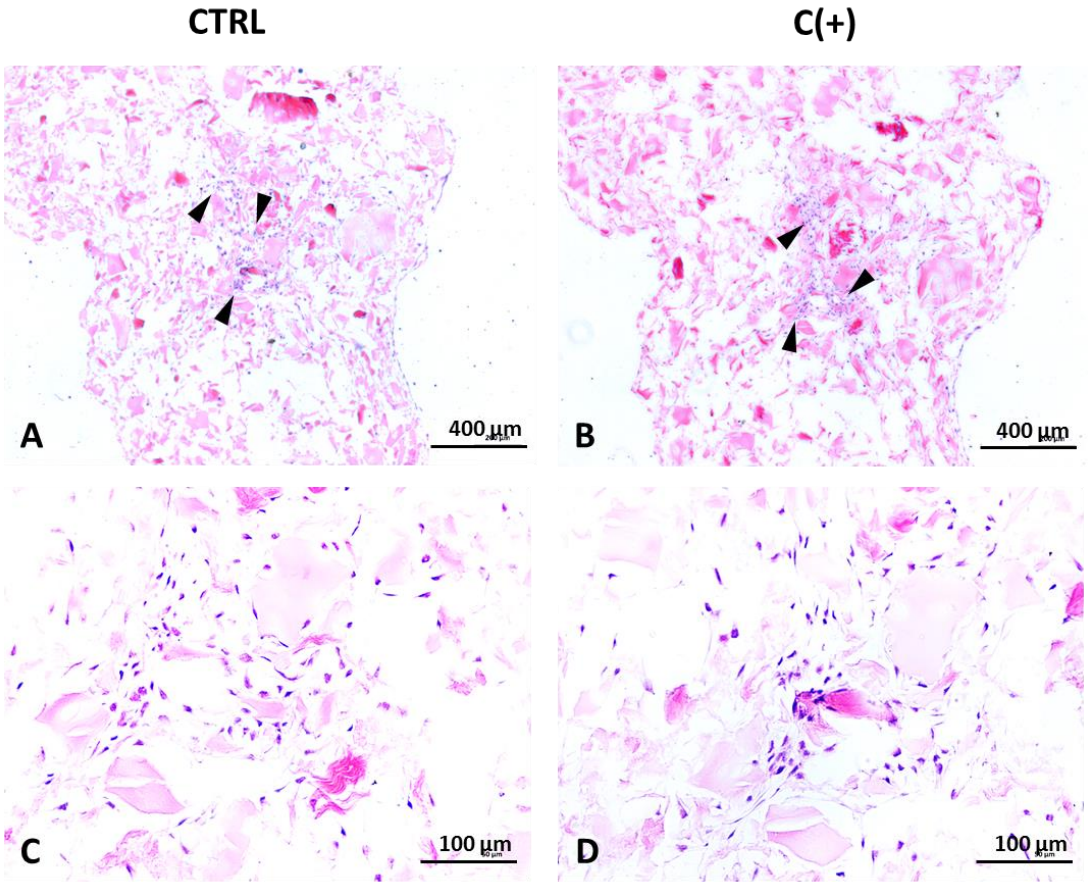

Figure 5.10: Histological analysis of P-dcECM. (A-D) Representative H&E stained histological sections of the P-dcECM seeded with hPDSC and cultured for 7 days. (Cells are indicated by black arrows) Scale bar = 400 µm (A&B) and 100 µm (C&D) respectively.

When examined for gene expression on day 7, it was evident that hPDSC's seeded into the P-dcECM in chondrogenic conditions demonstrated a significant 20-, -9, 10-, 45 and 5- fold increase in the chondrogenic markers *SOX9*, *SOX5*, *SOX6*, *ACAN* and *COL2A1,* respectively when compared to control chondrogenic pellet conditions (Figure 5.11&5.12). Moreover, there is also a significant 5-fold upregulation in the hypertrophic marker *COL10A1*.

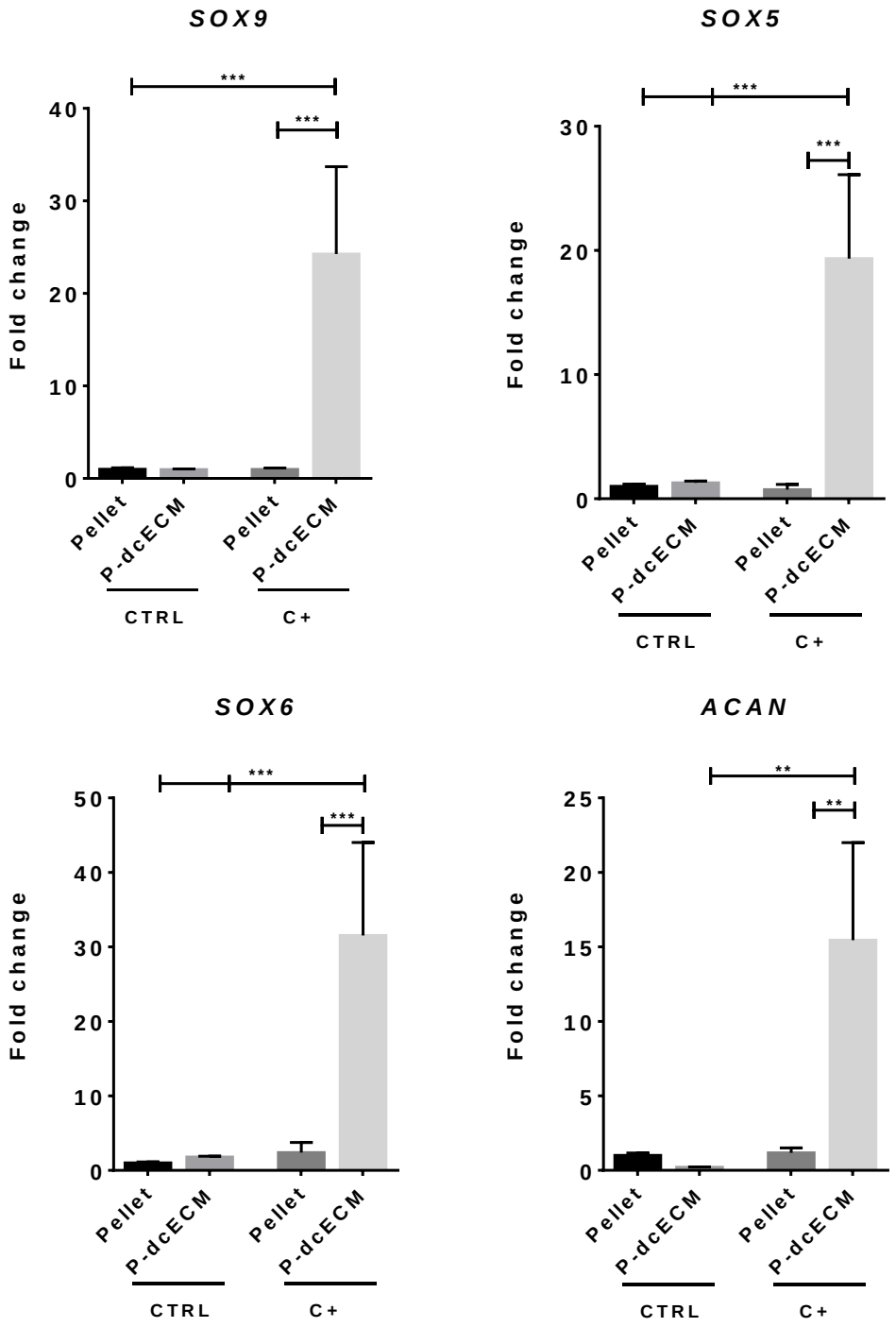

Figure 5.11: Chondrogenic and chondrocyte hypertrophy gene expression (*SOX9*, *SOX5*, *SOX6* & *ACAN*) of hPDSCs seeded in MM and dcECM under control conditions (CTRL) and chondrogenic conditions (C+). (n=3 *p<0.05, **p<0.01, ***p<0.001). (Fold changes normalised to pellet cultures in CTRL conditions). The culture period was 7 days. Statistical analysis was performed using one-way ANOVA corrected for multiple comparisons using Bonferroni's posthoc analysis.

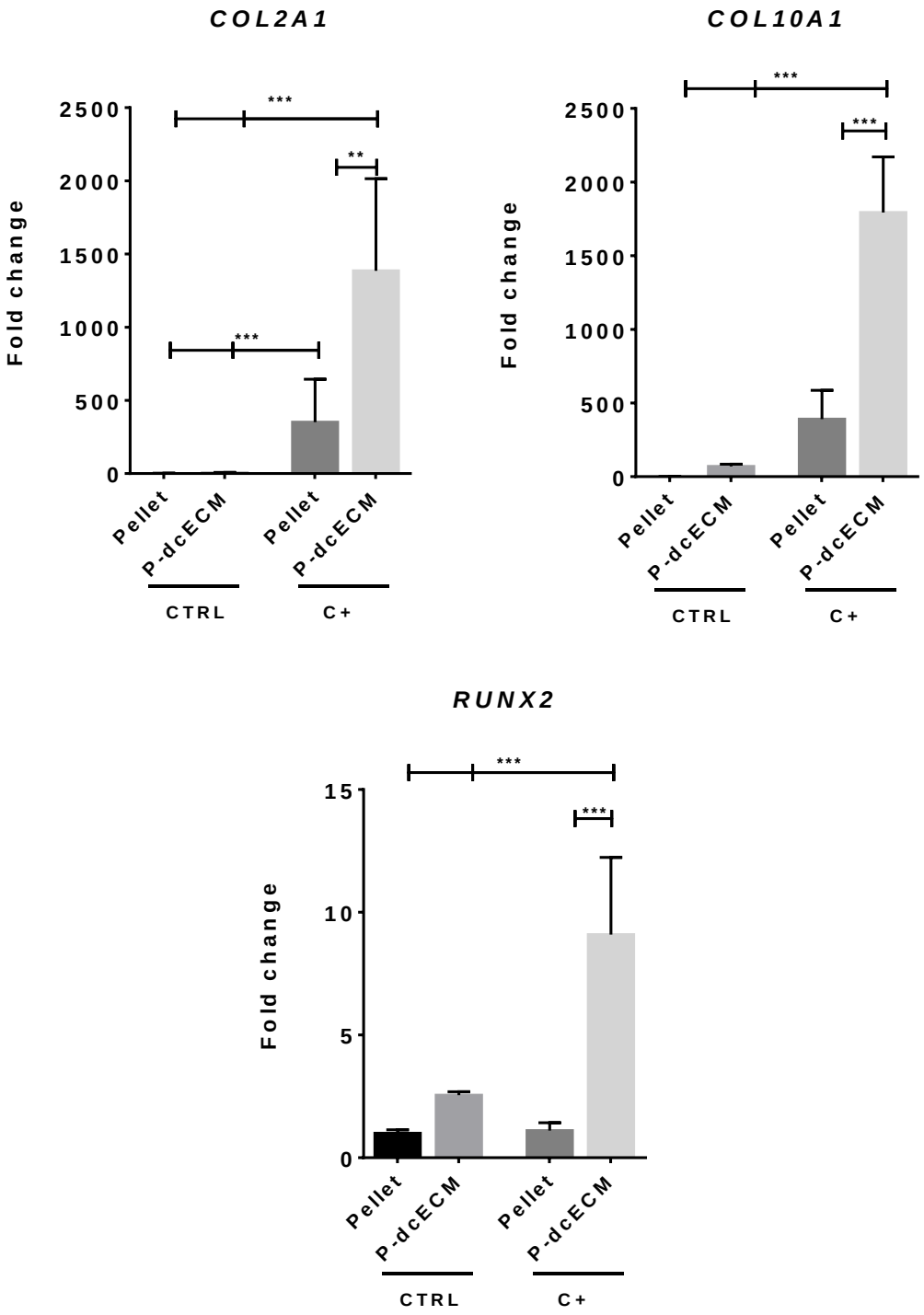

Figure 5.12: Chondrogenic and chondrocyte hypertrophy gene expression (*COL2A1*, *COL10A1* & *RUNX2*) of hPDSCs seeded in MM and dcECM under control conditions (CTRL) and chondrogenic conditions (C+). The culture period was 7 days (n=3 *p<0.05, **p<0.01, ***p<0.001). (Fold changes normalised to pellet cultures in CTRL conditions). Statistical analysis was performed using one-way ANOVA corrected for multiple comparisons using Bonferroni's posthoc analysis.

5.4 Discussion

One of the key aims of the thesis was the development of a chondrogenic construct capable of mimicking the cartilage callus phase of fracture repair. The previous chapters and published findings have demonstrated that the Vac-OS decellularisation methodology was capable of producing a non-immunogenic, potently chondroinductive construct[281]. However, the dcECM in its native form was not of sufficient size for clinical application. Moreover, due to the dense avascular nature of the native source costal cartilage tissue, the dcECM did not allow for homogenous seeding throughout the entire scaffold. Therefore, this chapter focused on developing a proof of concept methodology for the development of a an upscalable and cell-permeable construct.

There have been several studies utilising cartilage ECM derived granules for the fabrication of constructs that aimed to mimic the cartilage niche[514,518,519]. Intial attempts highlighted in this chapter were, therefore, focused on compressing freeze-milled dcECM into a mouldable construct. Qualitative histological examination of the resultant constructs revealed a pore size between 30-70 µm (Figure 5.4). It was evident that the C-dcECM was too dense for cellular infiltration limiting cellular localisation at the seeding surface (Figure 5.6). Work by Griffon and colleagues suggested that a pore size between 70-120µm is required for cell infiltration and cartilage matrix deposition when creating chitosan-based cartilage constructs [520]. Nasiri and colleagues have further expanded on this approach by combining decellularised cartilage granules with chitosan to fabricate constructs that had sufficient porosity, allowing for the homogenous distribution of the decellularised cartilage derived granules[514]. Collectively, both these studies highlight the need for a supporting structure within which cartilage granules can be homogenously distributed, providing a porous scaffold that supports cellular infiltration.

Based on this principle, the fabrication methodology was further modified by adding freeze-dried dcECM granules into a collagen type I gel. Collagen type I was chosen due to its excellent gelation properties and its ability to bind to collagen type 2, a major component of the dcECM[521]. Once fabricated the constructs were freeze-dried to remove water content from the construct

resulting in the P-dcECM a pore size of approximately 70-200μm (Figure 5.7). This pore size was ladger than most skeletal cell populations, allowing for infiltration. In addition to producing porous constructs, the freeze-drying process was also a useful approach for creating a scaffold permissive for long-term storage and transport; key factors when creating an off the shelf solution. The effecacy of using freeze dried, ECM-derived grafts has been demonstrated by their widespread clinical use [522,523]. The process of freeze-drying isnt, however, without its limitations. A report by Draenert and colleague suggested that the process of freeze-drying form ice crystals thus damaging cartilage-derived tissues[524]. DSC and FLIM were previously used to investigate the ECM structural integrity of the dcECM[281] and were, therefore, applied to study the degree of biochemical changes in the P-dcECM. Both the DSC and FLIM investigations reveal a significant shift in denaturation temperatures and lifetimes (Figure 5.8), suggesting there were substantial differences in collagen crosslinking and biochemical composition. These changes could have resulted from the removal of one of the most abundant components of native cartilage ECM; water, or through the addition of collagen type I. It was, therefore, essential to assess if these changes had an impact the capacity of the P-dcECM to enhance chondrogenesis as effectively as the dcECM alone. Therefore, the P-dcECM was seeded with hPSC's. Qualitative histological examination of the seeded P-dcECM revealed efficient cellular infiltration, aided by the larger pore size compared to the C-dcECM. However, the cellular distribution appreared to be primarily at the center of the P-dcECM, this may be indicative of the overall structural heterogeneity of the scaffold, that may vary between the periphery and center of the scaffold. The histological method used to determine pore size does not give the 3D porosity across the scaffold, a technique such as μCT may provide a more comprehensive view of the scaffold allowing for determination of pore size and distribution, as utilised by previous studies[525–527].

Gene expression analysis (Figure 5.11 & 5.12) revealed that in standard chondrogenic conditions the P-dcECM potently upregulated the *SOX*-trimer (*SOX9*, *SOX5* and *SOX6*) as well as cartilage matrix-specific markers *COL2A1* and *ACAN*. Additionally, there was also an upregulation in the hypertrophic

marker *COL10A1*. These findings suggest that the P-dcECM retained its chondorinductive properties despite significant changes to its biochemical structure that resulted from the fabrication methodology.

The methodology for seeding the P-dcECM could be further improved to provide a better approach for priming. Work by Leijten and colleagues suggests harnessing a crucial process in cartilage development; cell agregation[528]. A patterned silicon wafer was used to produce hPDSC derived micro-aggregates of homogenous density. This approach could potentially be applied to seeding the P-dcECM, thus further enhancing chondrogenesis and cartilage matrix deposition via both cell-matrix and cell-cell interactions. Furthermore, this could be combined with a bioreactor system that aims to mimic native cartilage developmental environment while incorporating novel external chondroinductive stimuli such as ultrasound[529] or mechanical stimulation[530] or electrical stimulation[531]. Moreover, the concentration of dcECM granules within the P-dcECM could also be investigated as work by Rowland and colleagues suggest that the overall concentration of the decellullarised cartilage-ECM within a porous construct impacts chondrogenesis and cartilage matrix deposition[518], as previously hilighted the approach by Nasiri and colleagues[514] of using chitosan as a supporting gel for dcECM granules may alternatively be combined with the dcECM. Several studies have hilighted the potential of chitosan to support the chondrogenesis of mesenchymal stem cells[532–534], making it a more effective choice than collagen type I. Moreover, future studies should include control conditions that contain only the supporting scaffold such as collagen type I, without the presence of the dcECM to determine the degree of impact the dcECM actually has on the chondrogenesis of skeletal cell populations.

The work in this chapter has provided preliminary data that suggests a promising approach for the fabrication of porous chondroinductive scaffolds for clinical traslation towards fracture repair. However, further developments in seeding and chondrogenic priming are needed to improve the applicability of the P-dcECM in clinical scenarios.

6. Development of a chondrogenic cell culture coating for stem cell priming

6.1. Introduction

Standard methodologies for the expansion of adult cell population that involve the use of tissue culture plastic are an extremely different from the native *in vivo* cell microenvironment as they lack a majority of structural and functional moieties present in ECM[89], these include cartilage specific factors such as aggrecan, collagen type 2 and Glycosaminoglycans[313,535]. Often, this disparity between physiological and *in vitro* conditions cause phenotypic changes that can result in loss of native function[536], altering cellular response to exogenously added growth factors or drugs[537,538] and affecting their capacity for differentiation[539,540]. An example of this occurs when chondrocytes cultured on tissue culture plastic. Over as little as two passages they rapidly lose their phenotype, a process that is known as dedifferentiation[446]. This limited capacity for in vitro expansion restricts their usage to procedures dealing with small cartilage defects, applied in approaches such as autologous chondrocyte implantation (ACI)[541–543]. Several studies have, therefore, suggested the use of chondroprogenitors as an alternative for cartilage tissue engineering[544–546]. This approach, however, requires consideration of optimal conditions for their chondrogenic differentiation.

6.1.1. ECM-derived cell culture coating.

The ECM's role in regulating cell survival, attachment, proliferation and differentiation are well established[547–550]. However, a majority of studies generally investigate coating single ECM associated proteins and defining their influence on cell behaviour[551,552]. Some strategies attempt to mimic the more complex native microenvironment using a combination of ECM-derived components such as fibronectin, collagen and laminin[553,554] It has long been known that the adsorbtion of components such as fibronectin to the cell culcute surface facilitates cell attachment and survival, in most standard cell culture

mediums, FBS is used to derive a number of proteins that adsorb to the culture plastic surface[555], these tissue culture treated surfaces when combined with FBS drastically improve cell survivability compared to non-treated culture surfaces[556]. The use of cartilage-ECM derived components to induce chondrogenesis *in vitro* has been studied, which highlighted their advantages over synthetic biomaterials[281,557,558]. Recent work by Cheng and colleagues suggest that Recombinant human fibrillin-1 and fibronectin fragments we capable of driving chondrogenesis of human embryonic stem cells (hESCs)[559]. There is also further evidence to suggest enhanced chondrogenesis in cultures that employ collagen type 2[560,561] and GAG's[507], both key component of hyaline cartilage ECM. Lei and colleagues further validate this finding by demonstrating enhanced chondrogenesis in cultures that include heparin sulfate[562]. The addition of individual ECM-associated components, however, does not mimic the complex tissue-specific combinations, or ratios present in the ECM. In response, studies have explored the use of cell-derived ECM coatings; these include fibroblast treated plates[563–565]. This approach has also been harnessed to produce commercially available gel coatings such as Matrigel[566]. The inclusion of these cell-derived cell culture coatings has been shown to enhance cell attachment, and survivability[567], they do not, however, mimic tissue-specific ECM such as hyaline cartilage[568–570]. Moreover, extended culture periods are required for the generation of these coatings[571], followed by the removal of the cellular component using trypsin before they are used as a substrate for seeding, making the process inefficient. Therefore, it could be advantageous to develop a gel coating that is tissue ECM derived, an approach that was employed by by DeQuach and colleagues[572]. Furthermore, Shawn and colleagues demonstrated the efficacy of enhancing chondrogenesis using zonal cartilage derived ECM gels that contained key components such as collagen type II and hyaluronan[573]. Despite this overwhelming evidence there are no known studies that are aimed at developing a chondroinductive cartilage ECM derived tissue culture coating.

6.1.2. Nano-topography and control of cellular differentiation.

A study by Wu and colleagues investigated the modulation of nano-topographical design using thermal nano-imprinting on polycaprolactone surface to generate various nano-patterns. These were assessed for their effect on cell phenotype and differentiation[574]. The investigation revealed that changes in the surface nanotopography directly affected cellular cytoskeleton arrangement, resulting in morphological changes. Moreover, they also found that specific patterns resulted in enhanced chondrogenesis and cartilage-specific ECM deposition when compared to a non-patterned surface. This is supported by previous studies that establish the link between a more rounded spherical shape and chondrocytic phenotype.[461,575,576].

The previous chapters have investigated the efficacy of using the dcECM to enhance chondrogenesis in hPDSC's and created porous scaffolds that could be upscaled for clinical use. There is, however, much room for optimising culture conditions to support the chondrogenic priming of hPDSC's and expansion of chondrocytes. The chondroinductive potency of the dcECM was, therefore, harnessed to create ECM-derived coatings with the potential of enhancing chondrogenesis or maintain a chondrocytic phenotype.

6.2. Methods

6.2.1 Creation of dcECM derived digests.

Sterile dcECM was digested for the creation of coatings (Figure 6.1). The methodology was adapted from Sawkins and colleagues[577]. Briefly, the digestion solution was prepared by first adding 50 µL of a 10M HCL solution to deionised water and mixed gently. 50mg of Pepsin (Singma-Aldrich, UK) was then added to the solution giving a final pepsin concentration of 1 mg/mL in 0.01M HCL. Sterile freeze-milled dcECM granules were added into the digestion solution at a concentration of 10 mg/mL and mixed thoroughly to ensure no clumps were present. The digestion mix was left to digest for 96 hours at 21 ºC. Digests were stored at 4ºC and subsequently sterilised prior to being used to coat tissue culture plastic.

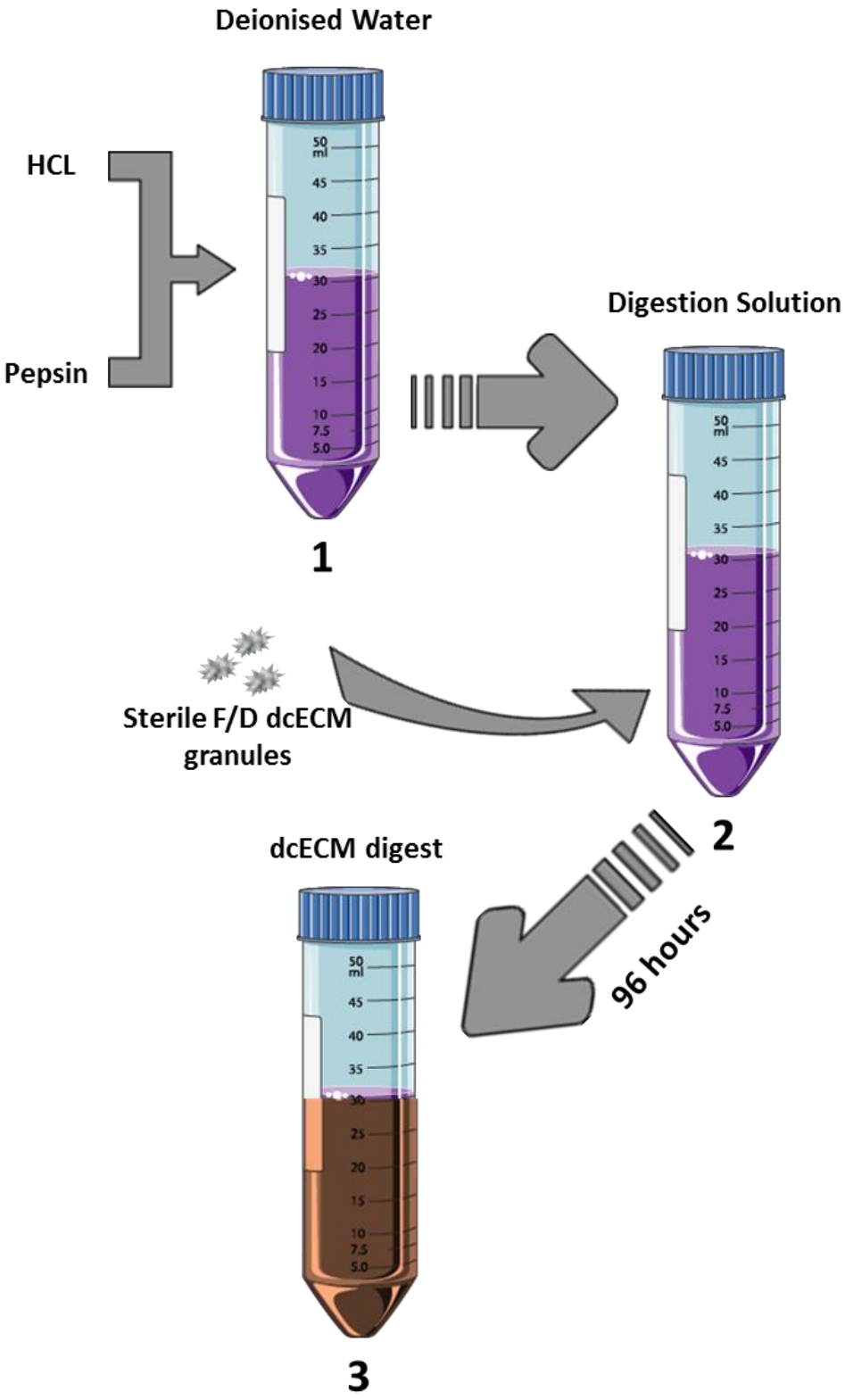

Figure 6.1: The creation of dcECM derived digests. (1) The digestion solution was created by mixing HCL and pepsin into deionised water giving a final pepsin concentration of 1 mg/mL in 0.01M HCL. (2) sterile freeze-dried dcECM granules are added into the digestion solution at a concentration of 10 mg/mL. (3) Solution is left to digest at 21ºC for 96 hours. Figure generated using the Servier medical art database (http://www.servier.com/Powerpoint-image-bank

6.2.2 Sterilisation and coating of dcECM derived digests.

The dcECM derived digest was sterilised using either UV light or heat-mediated autoclave sterilisation (Figure 6.2).

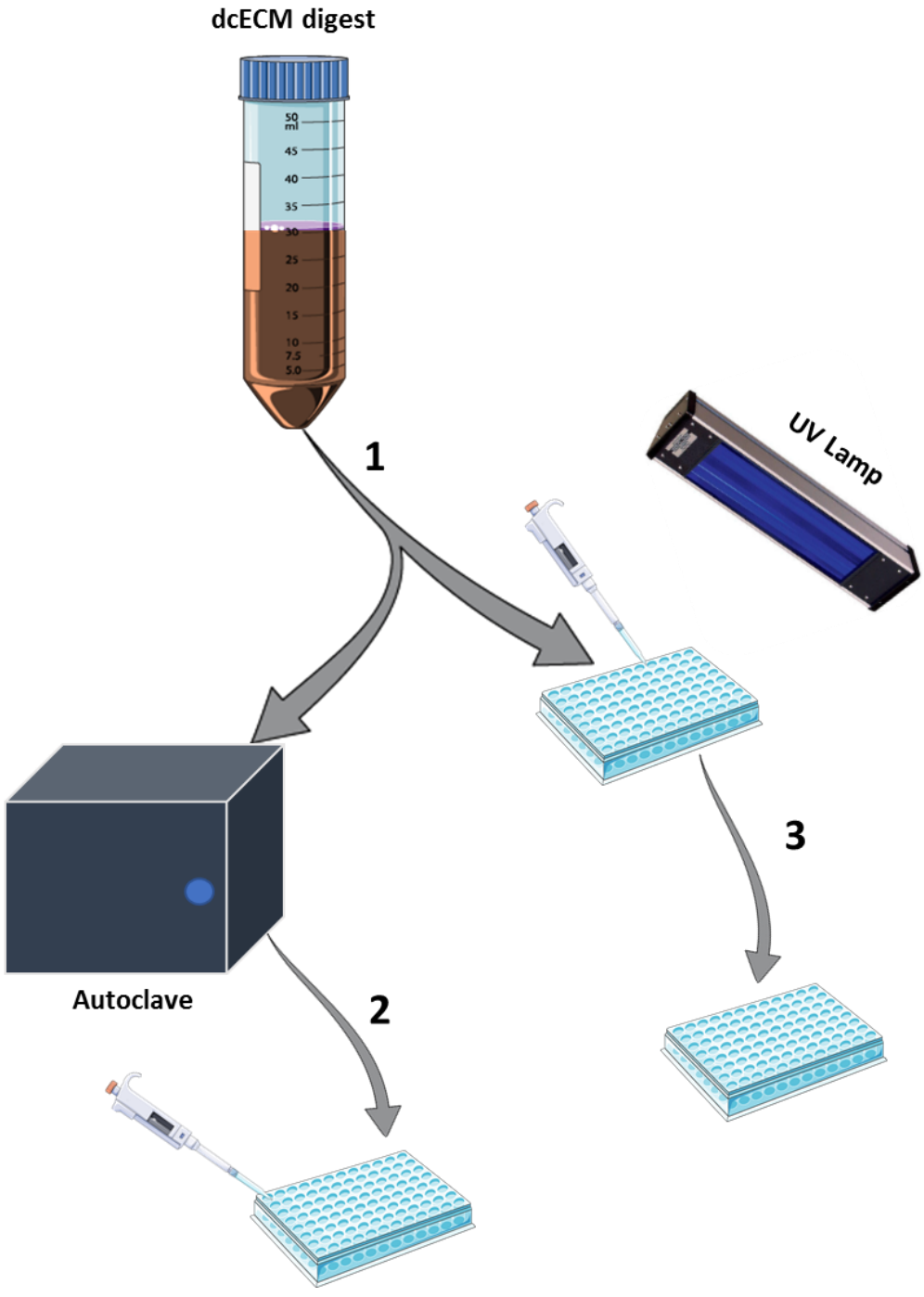

Figure 6.2: Sterilisation and coating of dcECM derived digests. (1) The dcECM digest was sterilised using one of the two methods, UV sterilisation and autoclaving. For autoclave sterilisation dcECM digest was transferred into autoclave before running it on a standard autoclave cycle, Alternatively, the sample was placed into a 96-well plate and left under UV light for 12 hours. (2) Autoclaved digest was pipetted into a 96-well plate and left to dry for 72 hours. (3) UV sterilised digests were left to dry for a further 60 hours. Figure generated using the Servier medical art database (http://www.servier.com/Powerpoint-image-bank

For UV sterilisation, 30 µL of the dcECM digest was pipetted onto each well of a 96-well plate. Samples were left under UV light in a tissue culture flow hood (Thermofisher, UK) for 12 hours at room temperature(18-21°C); the digest coating was further dried without UV exposure for 60 hours. Autoclave sterilisation was carried out by pipetting 4 mL of the dcECM digest into glass autoclave tubes (Corning, UK). Samples were, subsequently, autoclaved (Invitrogen, UK) using the standard media sterilisation cycle. 30 µL of the solution was pipetted onto 96-well plates and left to dry in a sterile dry incubator (Thermofisher, UK) for 72 hours after which cells were seeded onto the surface. As a control, dcECM-derived digest was coated as previously described, without any sterilisation steps, referred to as non-sterile (NS) coatings.

6.2.3. Human periosteal stem cells (hPDSCs).

hPDSCs were isolated as previously described in Chapter 4.2 (obtained from Prof Frank Luyten, KU Leuven, Belgium).

6.2.4. hPDSC seeding and micromass culture.

hPDSC's were seeded onto the surface of the dcECM derived digest coated wells to assess cell attachment and differentiation. All wells were seeded with hPDSCs (passage 6) at a cell density of $1x10^6$ per cm^2 in 100 µL of growth media (10%FBS) into 96-well plates. Control micromasses of the same density (n=3) were seeded onto the surface of the 96 well plate as a control. Cells were left to attach for 3 hours before the media was changed to CTRL and C(+) conditions as previously described in Chapter 4.2.

6.2.5. Total RNA extraction and quantitative reverse transcription–Polymerase Chain Reaction (qRT-PCR) analysis of dc-ECM digest coated samples.

Gene expression analysis was used as an indicator of cellular differentiation. Briefly, both Coated and non-coated wells were washed with 300 µL of PBS. Samples were lysed and processed for qRT-PCR using the method described in Chapter 4.2.

6.2.6. Statistical analysis

Statistical analysis was carried out as described in Chapter 2.2. All statistical analysis was performed using GraphPad Prism version 6.0f for windows (GraphPad Prism Software, La Jolla California USA, www.graphpad.com).

6.3 Results

6.3.1 dcECM can be used to form a sterile chondroinductive coating for tissue culture plastic.

dcECM derived coatings were created, sterilised and tested for their ability to enhance chondrogenesis. Brightfield images taken at Day 7 highlighted distinct morphological changes in hPDSC's that were seeded onto the autoclaved dcECM derived (Auto) coating, reminiscent of a cobblestone pattern. Moreover, the differences observed in the Auto coated well were limited to chondrogenic conditions; no other seeded group demonstrated any distinct morphological changes (Figure 6.3). Qualitative analysis of the live-dead staining (Figure 6.4) revealed a visibly higher number of dead cells in the chondrogenic condition containing the auto dcECM-derived coating, not observed in any other condition.

The gene expression at day 7 highlighted that only the Auto coating resulted in a significant 2- and 1.7 fold upregulation in *SOX9* and *ACAN* respectively, when compared to non-coated micromasses in chondrogenic conditions (Figure 6.5& 6.6). Interestingly, the non-sterile coating did not upregulate any chondrogenic genes. Moreover, to determine if the coatings were driving cells down an osteogenic lineage, ALP expression was quantified as it has been

identified as an early marker of osteogenesis[578]. However, there was no significant upregulation in ALP with any of the coated or non-coated chondrogenic conditions. The Auto coating was chosen as the optimal coating methods, due to its ability to potently enhance chondrogenesis and was subject to further optimisation and analysis.

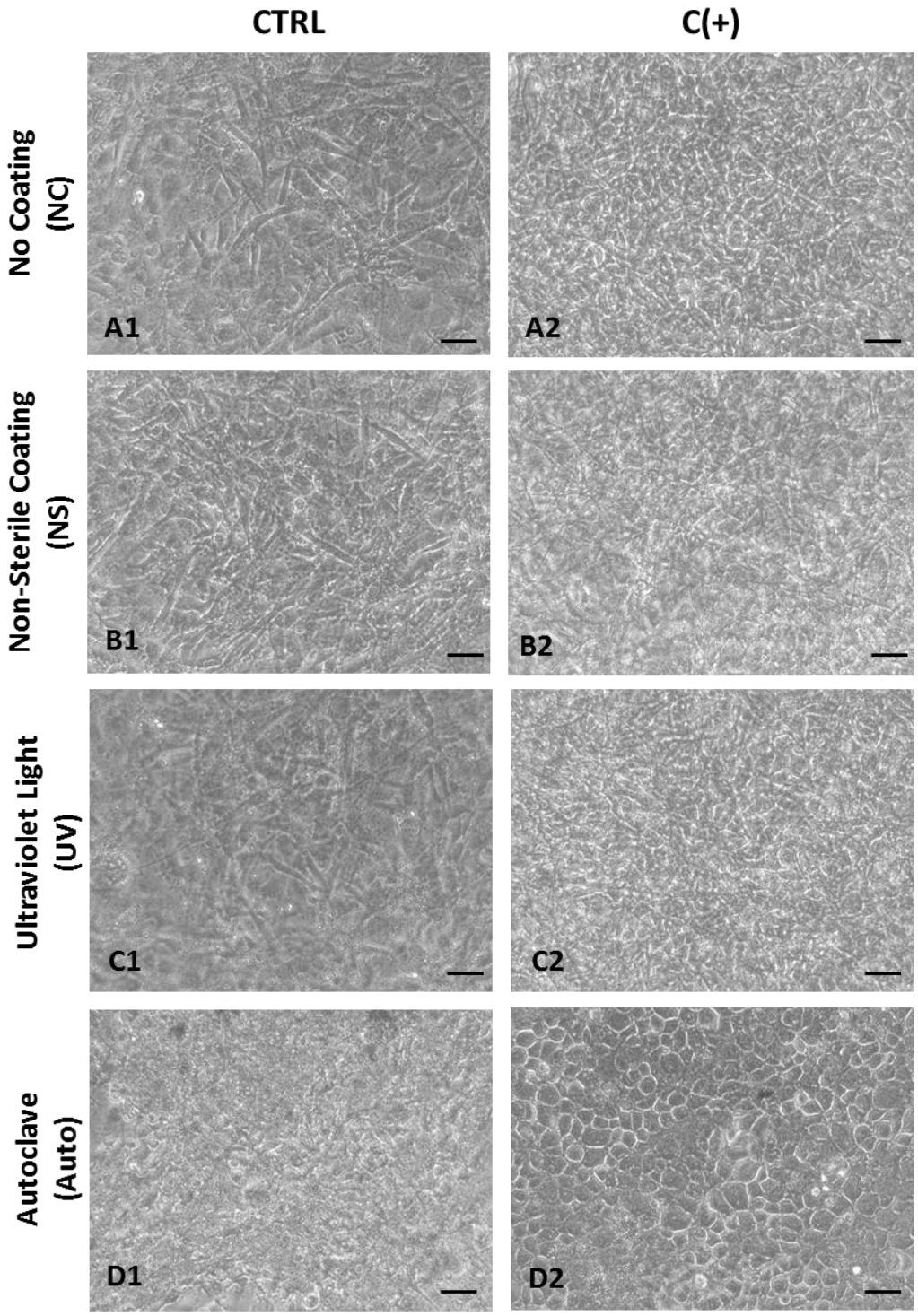

Figure 6.3: Brightfield microscopy images of hPDSC's seeded on dcECM- derived coatings. The coating was either non-sterile (B), UV sterilised (C) or Autoclaved (D). hPDSC's were also seeded in micromass on non-coated tissue culture plastic (A). All samples were seeded in either CTRL (1) or C+(2) conditions. There was a distinct cobblestone pattern observed in hPDSC's seeded onto the autoclaved dcECM coating (D2). (Scale bar = 50μm)

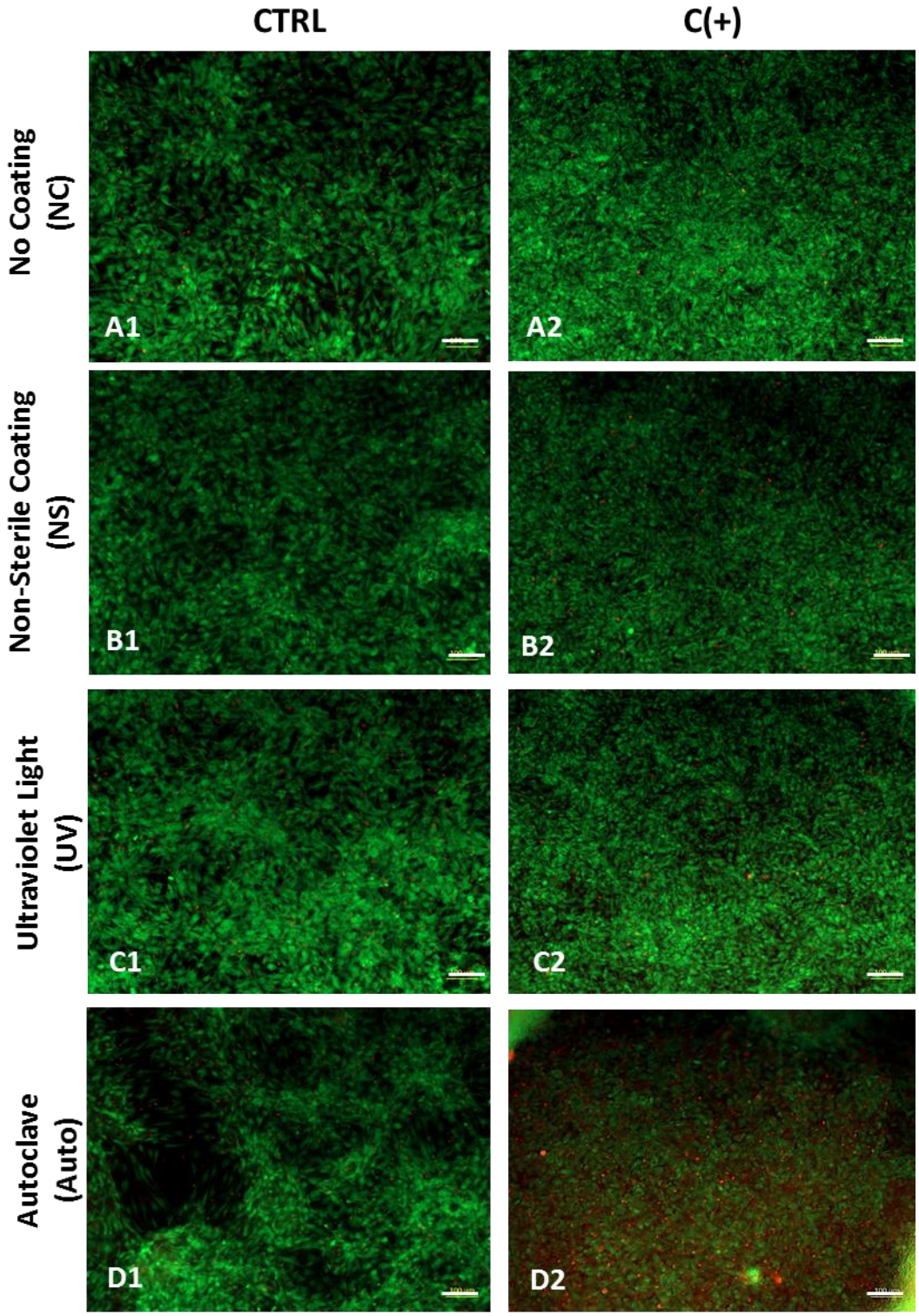

Figure 6.4: Fluorescence images of cells stained using calcein AM (Live) and ethidium homodimer (Dead). hPDSC's were seeded on dcECM- derived coatings that was non-sterile (B), UV sterilised (C) and Autoclaved (D). hPDSC's were also seeded in micromass on non-coated tissue culture plastic (A). All samples were seeded in either CTRL (1) or C+(2) conditions. Cells seeded in Autoclave conditions (D2) demonstrated visibly higher staining for dead cells as compared to the other conditions. (Scale bar = 100µm)

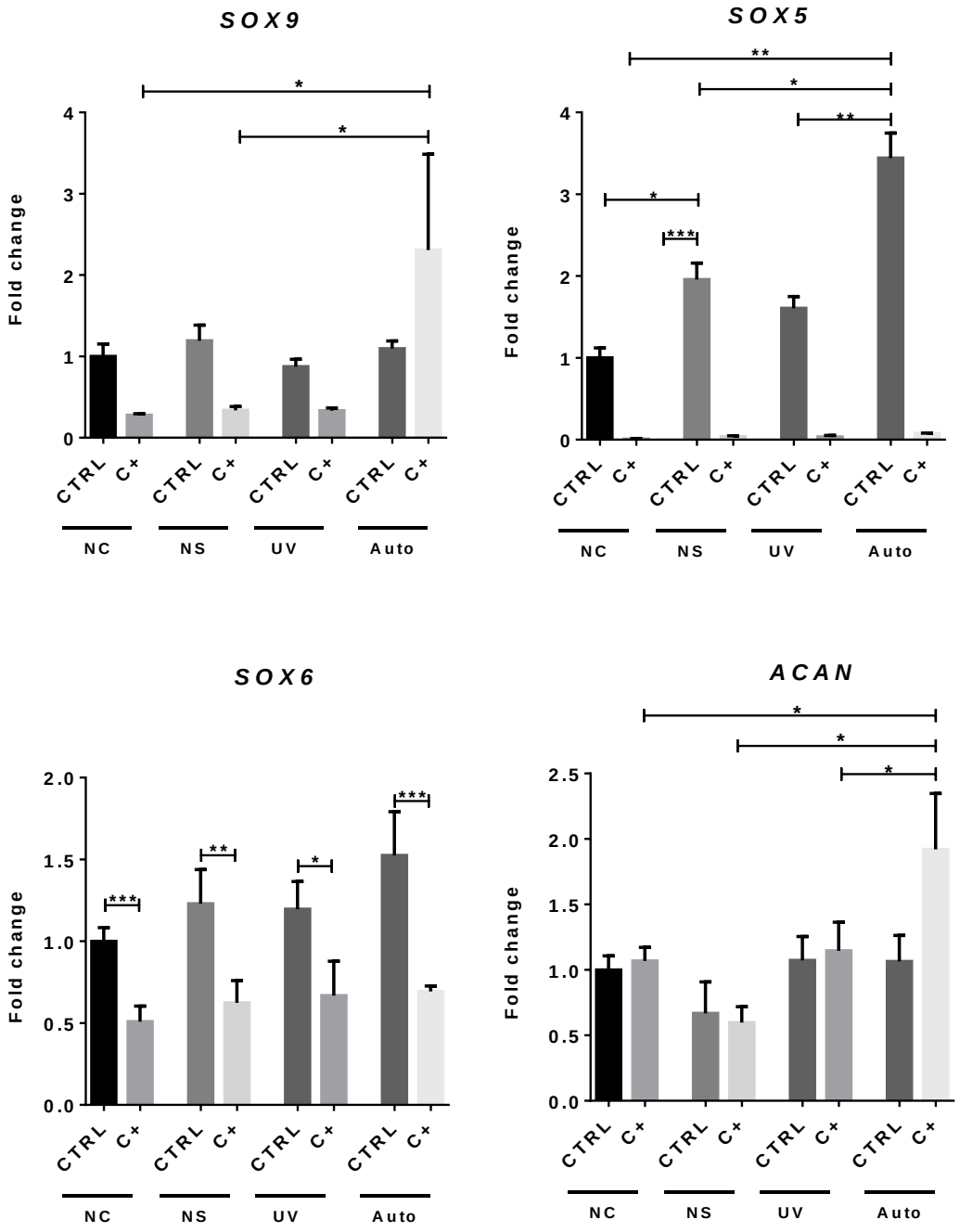

Figure 6.5: Gene expression analysis of hPDSC seeded P-dcECM. Chondrogenic gene expression (*SOX9*, *SOX5*, *SOX6* & *ACAN*) of hPDSCs seeded in MM and dcECM under control conditions (CTRL) and chondrogenic conditions (C+). Micromasses were also seeded on the non-coated surface (NC), Non-sterile coating (NS), Ultraviolet sterilised coating (UV) and Autoclaved coating (Auto). (n=3 *p<0.05, **p<0.01, ***p<0.001). (Fold changes normalised to micromasses in CTRL conditions). Statistical analysis was performed using one-way ANOVA corrected for multiple comparisons using Bonferroni's posthoc analysis.

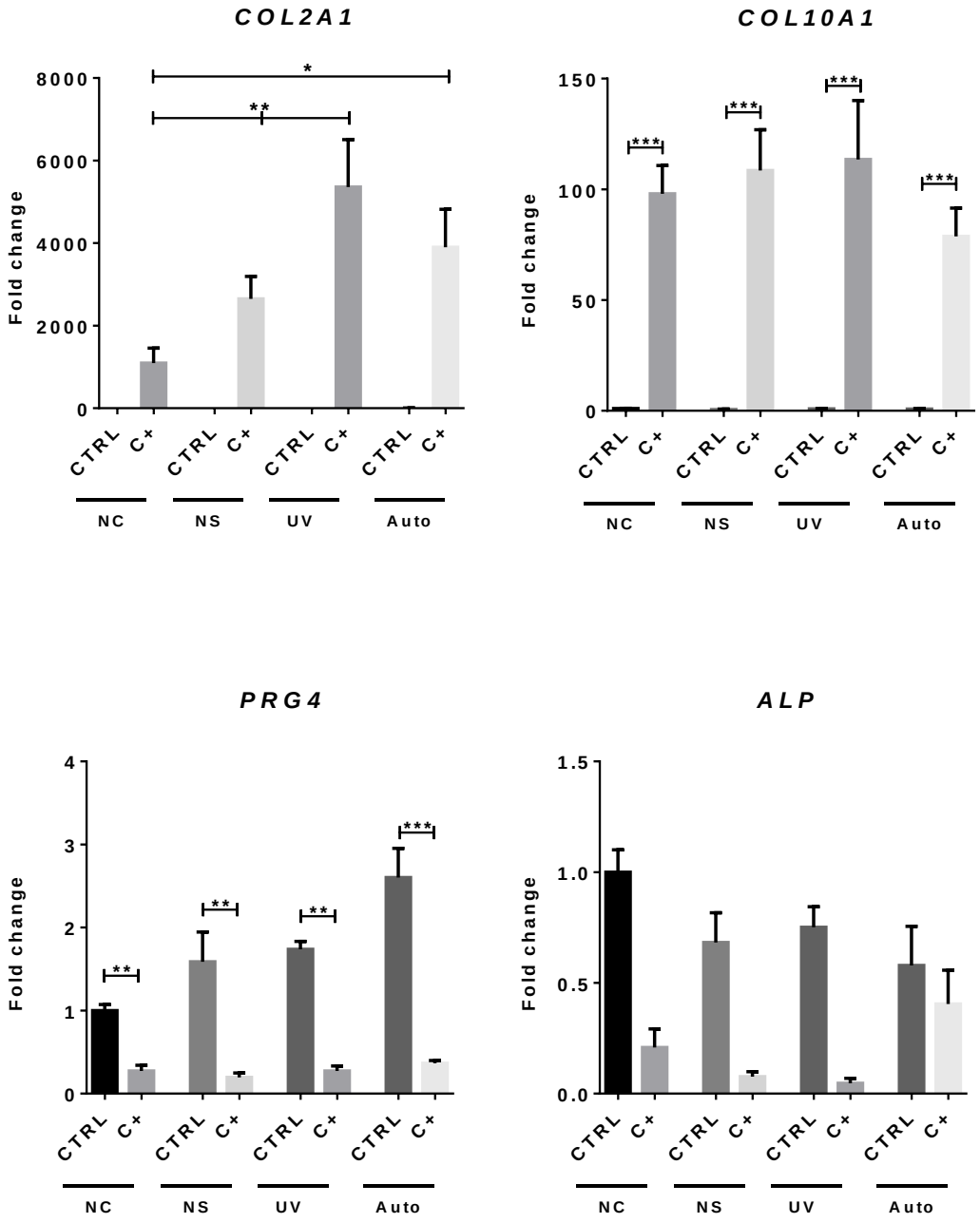

Figure 6.6: **Gene expression analysis of hPDSC seeded P-dcECM.** Chondrogenic and chondrocyte hypertrophy gene expression (*COL2A1*, *COL10A1*, *PRG4* & *ALP*) of hPDSCs seeded in MM and dcECM under control conditions (CTRL) and chondrogenic conditions (C+). Micromasses were also seeded on the non-coated surface (NC), Non-sterile coating (NS), Ultraviolet sterilised coating (UV) and Autoclaved coating (Auto). (n=3 *p<0.05, **p<0.01, ***p<0.001). (Fold changes normalised to micromasses in CTRL conditions). Statistical analysis was performed using one-way ANOVA corrected for multiple comparisons using Bonferroni's posthoc analysis.

6.3.2. Autoclaved dcECM-derived coating requires thorough drying to maintain chondrogenic potential.

The Auto coating was optimised through analysis of insufficient drying and of various seeding densities, defined by its effect on cell morphology and chondrogenic gene expression. Therefore, the Auto coating was dried for either 48 or 72 hours at 37ºC in a dry incubator and seeded with a cellular density of either $1.6x10^6$, $7x10^5$ or $5x10^5$ cells per cm^2 or 100, 70 or 50 thousand cells per 96-werespectively.

Brightfield microscopy images highlighted that after 48 hours of drying there was no significant changes in morphology when comparing hPDSC's in Auto C(+) conditions to its non-coated comparator in C(+) conditions. Moreover at 48 hours, variation in seeding densities also did not have an impact on cellular morphology. However, hPDSC's combined with CTRL conditions demonstrated a distinct rounded morphology, only when seeded at a density of 100,000 cells per 96-well (Figure 6.7). A similar observation was made when the Auto coating was dried for 72 hours, with hPDSC's demonstrating a distinct rounded morphology in CTRL conditions, when at a seeded at a density of 100000 cells. Moreover, drying the Auto coating for 72 hours also resulted in the distinct cobblestone pattern when combined with C(+) conditions. Both seeding densities of 100 and 70 thousand demonstrated the distinct cobblestone pattern, which was not present in the 50 thousand seeding density (Figure 6.8).

Gene expression analysis revealed a higher *COL2A1* expression in samples dried over 72 hours when cultured in C(+) conditions, with a 4000-fold ($p>0.001$) increase when compared to samples dried for just 48 hours. Moreover, samples from the 48-hour group demonstrated a trend towards having lower *SOX9* expression levels. However, this was not observed in the 72-hour group (Figure 42). Interestingly, the 48-hour group in C(+) conditions did not demonstrate a trend towards higher *COL10A1* levels. There were also no significant differences in *RUNX2* or *FABP4* expression. This intimates that a 72 hour drying period is more effective in promoting a chondrogenic phenotype, especially at a cell density of 100 thousand (Figure 6.9, 6.10 &

6.11). These conditions were, therefore, selected for further *in vitro* testing of the ato coating.

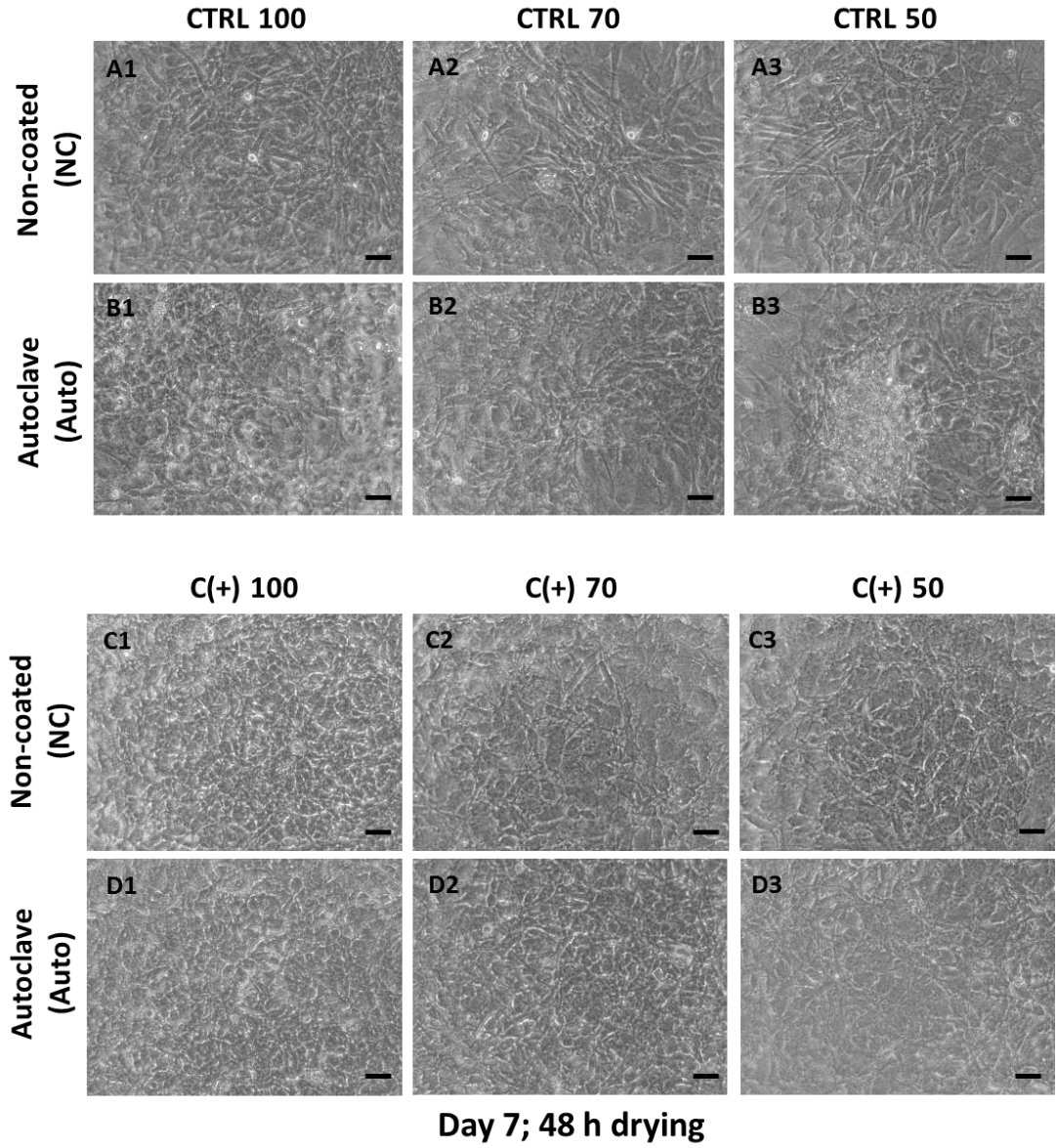

Figure 6.7: Seeding density and digest coating optimisation brightfield images. hPDSC's seeded on the autoclaved dcECM-derived coating and compared to non-coated tissue culture plastic. The dcECM-digest coating was air dried at 37 ºC for 48 hours (h) before seeding. Images were obtained 7 days post-culture. All samples were seeded in either control (CTRL) (A1-B3) or Chondrogenic C(+) conditions (C1-D3). hPDSC's were seeded at a density of $1.6x10^6$(100) $7x10^5$(70) or $5x10^5$(50) cells per cm^2 respectively, into a 96-well plate. Scale bar = 50µm.

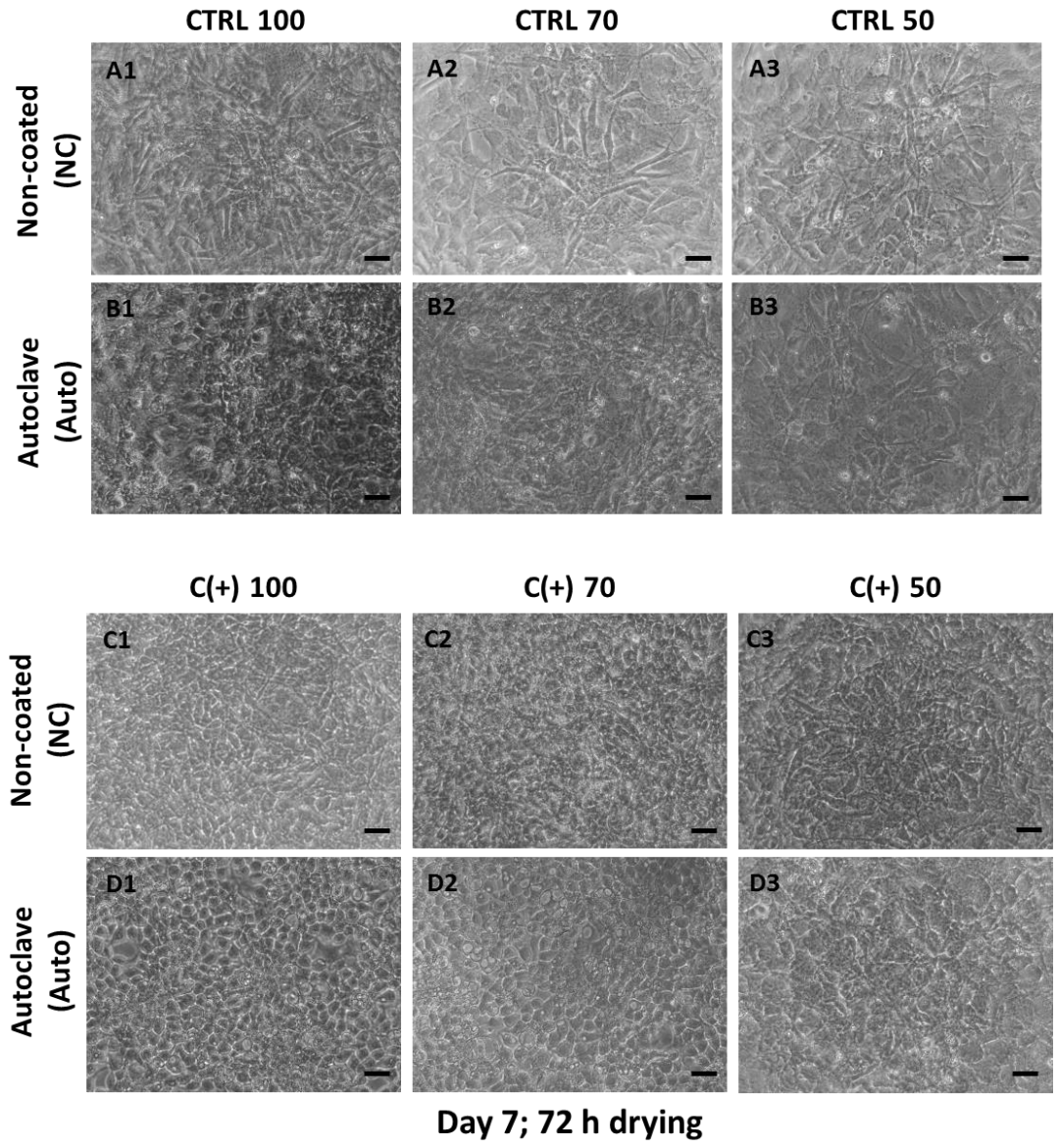

Figure 6.8: Seeding density and digest coating optimisation brightfield images. hPDSC's seeded on autoclaved dcECM-derived coating and compared to non-coated tissue culture plastic. The dcECM-digest coating was air dried at 37 ºC for 72 hours (h) before seeding. Images were obtained 7 days post-culture. All samples were seeded in either control (CTRL) (A1-B3) or Chondrogenic C(+) conditions (C1-D3). hPDSC's were seeded at a density of $1.6x10^6$(100) $7x10^5$(70) or $5x10^5$(50) cells per cm^2, into a 96-well plate. Scale bar = 50µm.

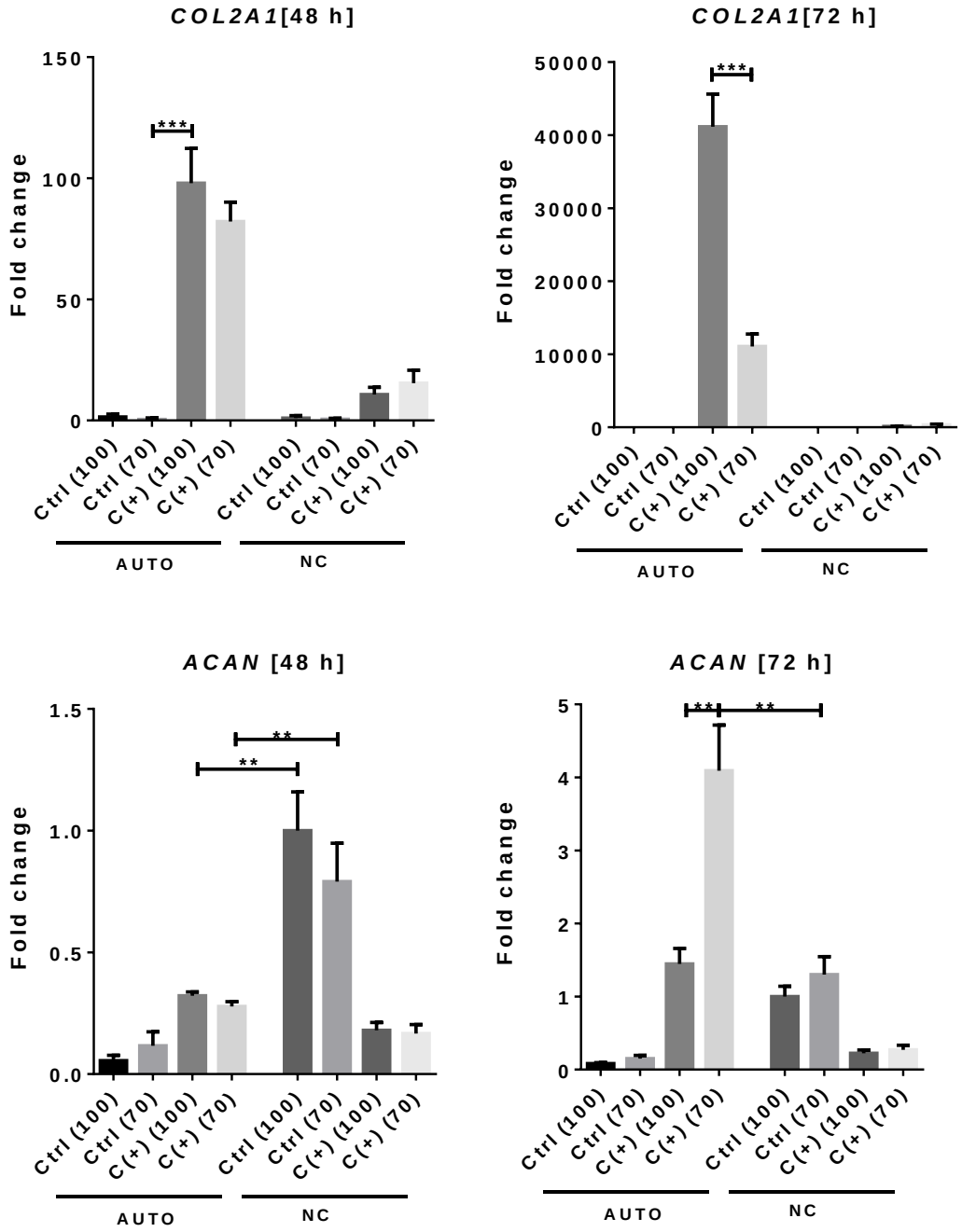

Figure 6.9: Seeding density and digest coating optimisation gene expression analysis. Chondrogenic gene expression (*COL2A1* & *ACAN*) of hPDSCs seeded as micromasses on autoclaved dcECM-derived (Auto) coating and compared to non-coated tissue culture plastic (NC). The coating was air dried at 37 ºC for either 48 or 72 hours [h] before seeding. All samples were seeded in either control (CTRL) or Chondrogenic C(+) conditions. hPDSC's were seeded at a density of $1.6x10^6$(100) $7x10^5$(70) or $5x10^5$(50) cells per cm^2, into a 96-well plate. Gene expression was obtained 7 days post-culture (n=3 *p<0.05, **p<0.01, ***p<0.001). (Fold changes normalised to micromasses in CTRL conditions). Statistical analysis was performed using one-way ANOVA corrected for multiple comparisons using Bonferroni's posthoc analysis.

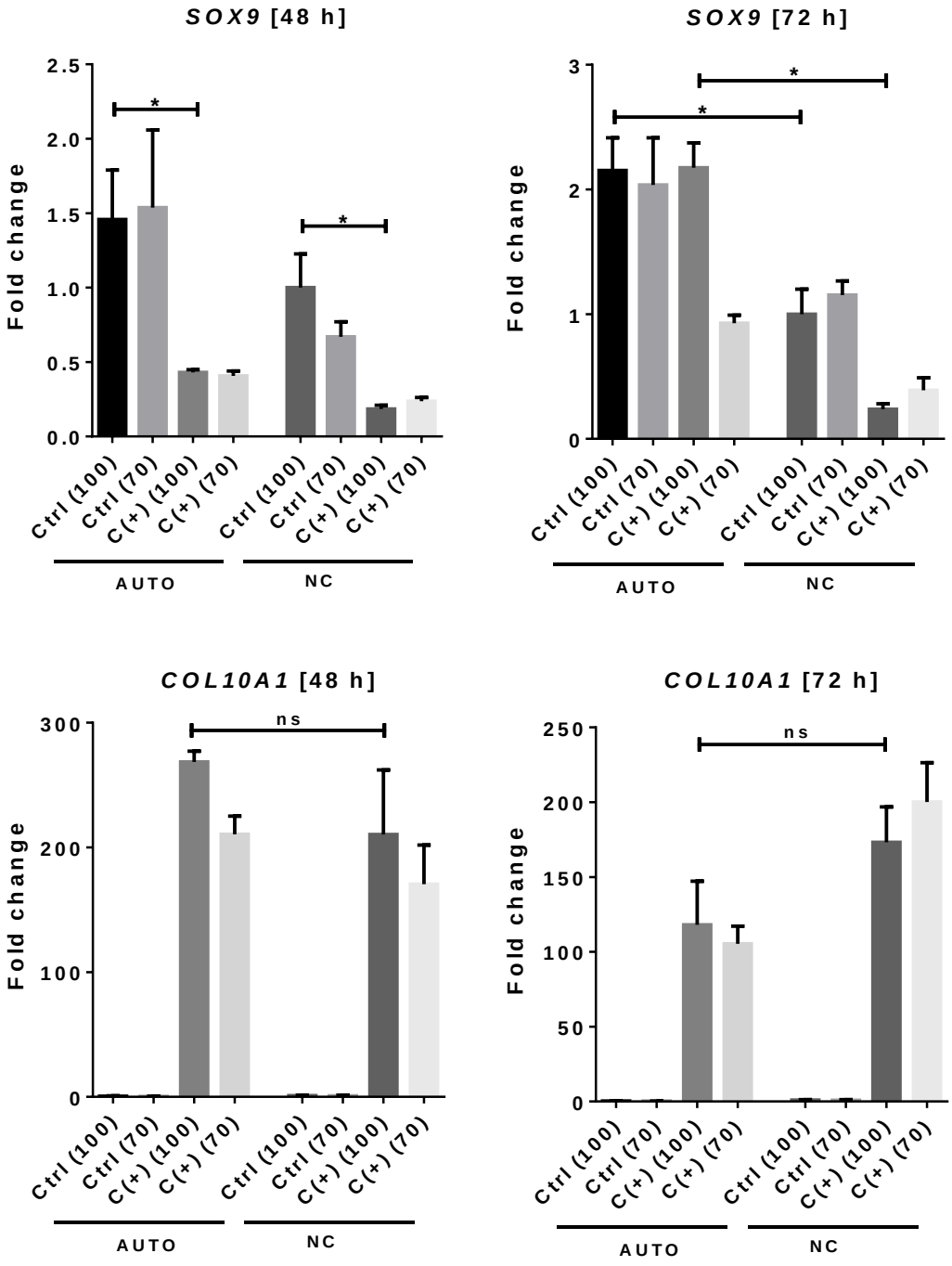

Figure 6.10: Seeding density and digest coating optimisation gene expression analysis. Chondrogenic gene expression (*COL10A1 & SOX9*) of hPDSCs seeded as micromasses on autoclaved dcECM-derived (Auto) coating and compared to non-coated tissue culture plastic (NC). The dcECM-digest coating was air dried at 37 ºC for either 48 or 72 hours [h] before seeding. All samples were seeded in either control (CTRL) or Chondrogenic C(+) conditions. hPDSC's were seeded at a density of $1.6x10^6$(100) and $7x10^5$(70) cells per cm^2 respectively, into a 96-well plate. Gene expression was obtained 7 days post-culture (n=3 *p<0.05, **p<0.01, ***p<0.001). (Fold changes normalised to micromasses in CTRL conditions). Statistical analysis was performed using one-way ANOVA corrected for multiple comparisons using Bonferroni's posthoc analysis.

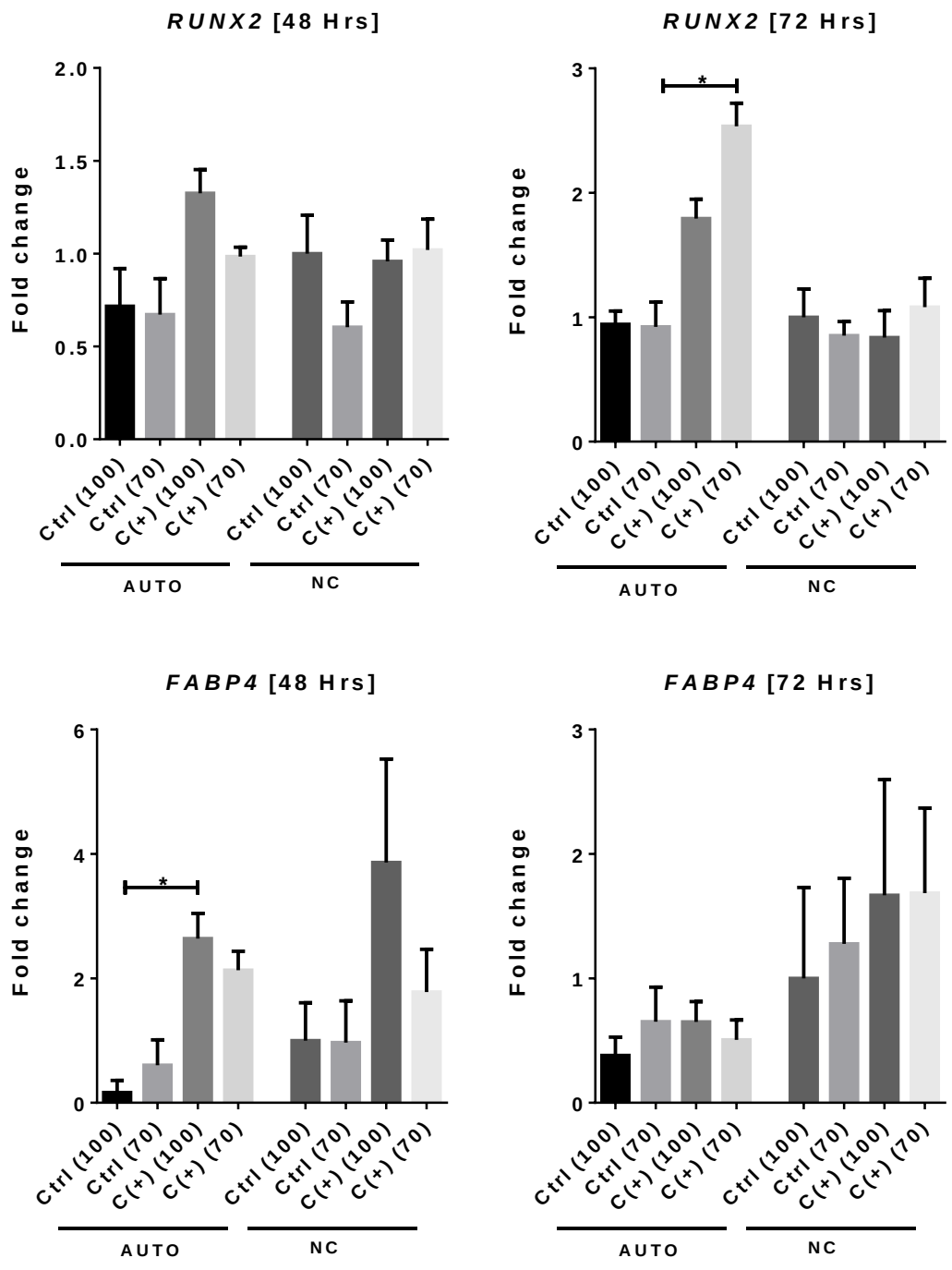

Figure 6.11: **Seeding density and digest coating optimisation gene expression analysis.** Chondrogenic gene expression (*RUNX2* & *FABP4*) of hPDSCs seeded as micromasses on autoclaved dcECM-derived (Auto) coating and compared to non-coated tissue culture plastic (NC). The dcECM-digest coating was air dried at 37 ºC for either 48 or 72 hours [Hrs] before seeding. All samples were seeded in either control (CTRL) or Chondrogenic C(+) conditions. hPDSC's were seeded at a density of $1.6x10^6$(100) $7x10^5$(70) or $5x10^5$(50) cells per cm^2 respectively, into a 96-well plate. Gene expression was obtained 7 days post-culture (n=3 *p<0.05, **p<0.01, ***p<0.001). (Fold changes normalised to micromasses in CTRL conditions). Statistical analysis was performed using one-way ANOVA corrected for multiple comparisons using Bonferroni's posthoc analysis.

To establish a detailed picture of the early changes in gene expression that underlie the enhanced chondrogenesis demonstrated by the Auto coated tissue culture plastic, hPDSC's were seeded onto Auto coated and non-coated plates in either CTRL or C(+) conditions. Samples were monitored for changes in morphology and gene expression over a period of 1,3,5,7 and 21 days.

Brightfield microscopy imaging at day 7, revealed the establishment of a distinct cobblestone phenotype with hPDSC's seeded onto Auto coated samples in C(+) (Figure 6.12), this was accompanied by a significant 2-fold upregulation of the early chondrogenic marker *SOX9* when compared to non-coated conditions. At day 3 (Figure 6.14), the cobblestone morphology was maintained and accompanied by a significant 2.6-fold ($p<0.05$) & 3.3-fold ($p<0.05$) upregulation in *SOX9* and *ACAN expression*, while demonstrating a trend towards an increase in SOX9 expression. At day 5 brightfield images revealed that the cobblestone pattern observed with the auto conditions was not as distinct as Day 1 & 3. However, there was a significant 75-fold increase ($p<0.01$) in *COL2A1* when compared to the Auto coated conditions at Day 3 and a 100-fold ($p<0.01$) upregulation compared to the non-coated condition at Day 5. There was also a significant 5-fold increase in *PRG4* from day 3 and an overall 2.7 fold ($p<0.05$) upregulation when compared to the non-coated controls at day 5. In contrast, however, there was an overall 2.3-fold ($p<0.05$) decrease in *SOX9* compared to the previous Day 3 timepoint, although this was accompanied with a trend towards *SOX9* expression being maintained at a higher level than with the non-coated condition. By day 7 brightfield images revealed a loss of the cobblestone pattern with gaps forming in the micromass culture (Figure 6.12). Moreover, At day 7, both the Auto coated and non-coated conditions revealed a trend towards the increased expression of the hypertrophic marker *COL10A1*. Enhanced chondrogenesis in the Auto coated groups was further highlighted by the increased Alcian blue staining at day 7, indicative of increased sGAG deposition (Figure 6.13). Furthermore, quantification of Alcian blue did indeed reveal a significant upregulation in sGAG deposition in C(+), Auto coated

samples compared to all other conditions. Moreover, in the Auto coated CTRL condition there is a trend towards higher Alcian blue deposition. By day 21 gaps in the monolayer were filled. However, there was no restoration in the cobblestone pattern previously observed with the Auto coated samples.

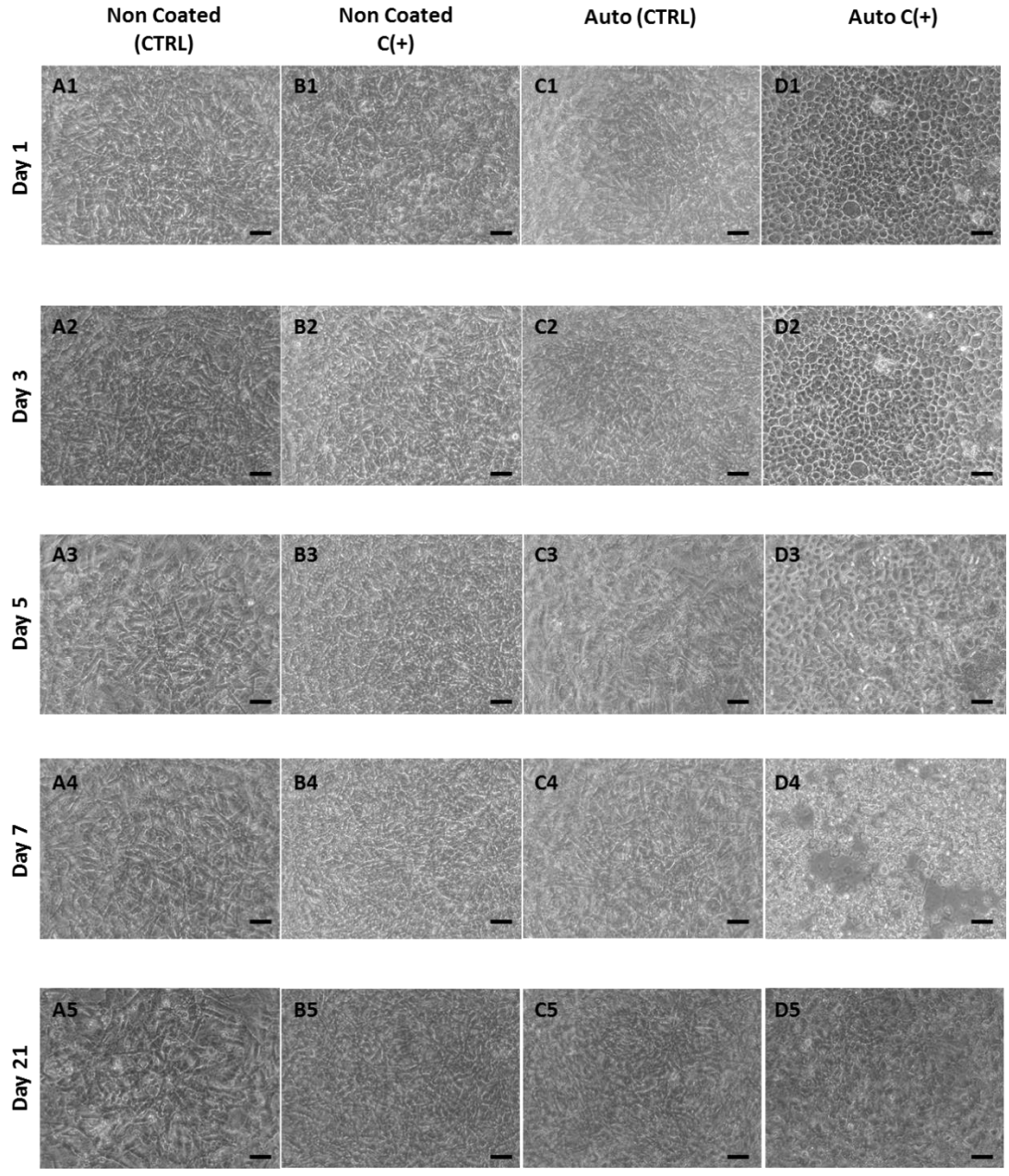

Figure 6.12: Brightfield microscopy images of the Auto coating time course analysis. Brightfield microscopy images of hPDSC's seeded on autoclaved dcECM-derived coating and compared to non-coated tissue culture plastic. Images were obtained at Day 1, 3, 5, 7 and 21. Cells were cultured in both CTRL (A&C) and Chondrogenic C(+) conditions (B&D). Scale bar = 50 µm.

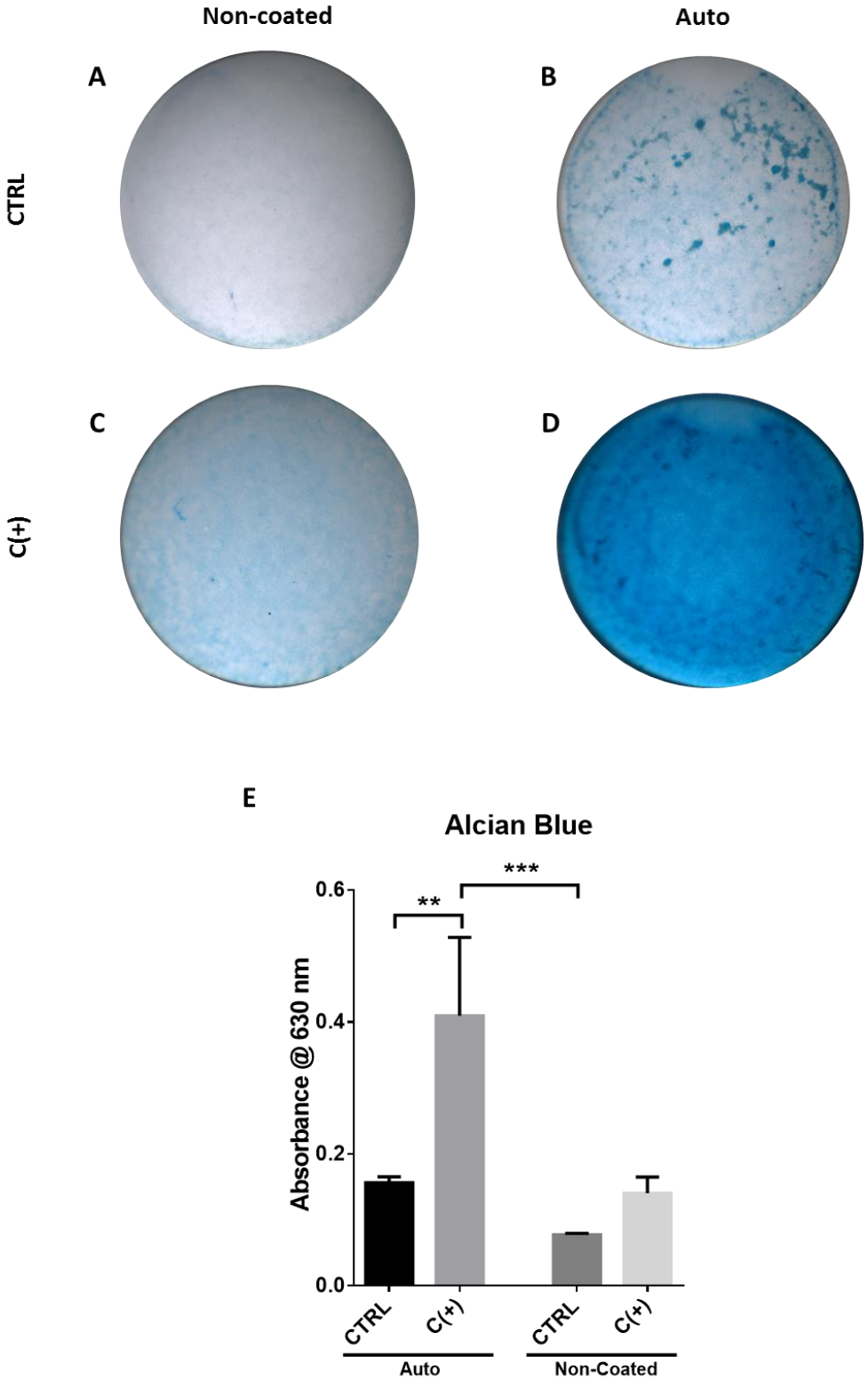

Figure 6.13: Alcian blue analysis of seeded Auto coated surfaces. Brightfield microscopy images of Alcian blue stained samples containing hPDSC's seeded as micromasses onto either tissue culture plastic (NC) or autoclaved dcECM (Auto). Samples were cultured for a period of 7 days in either control (CTRL) (A&B) or Chondrogenic C(+) conditions (C&D). (E) Alcian blue quantification data 7 days post culture. (n=3 *p<0.05, **p<0.01, ***p<0.001)

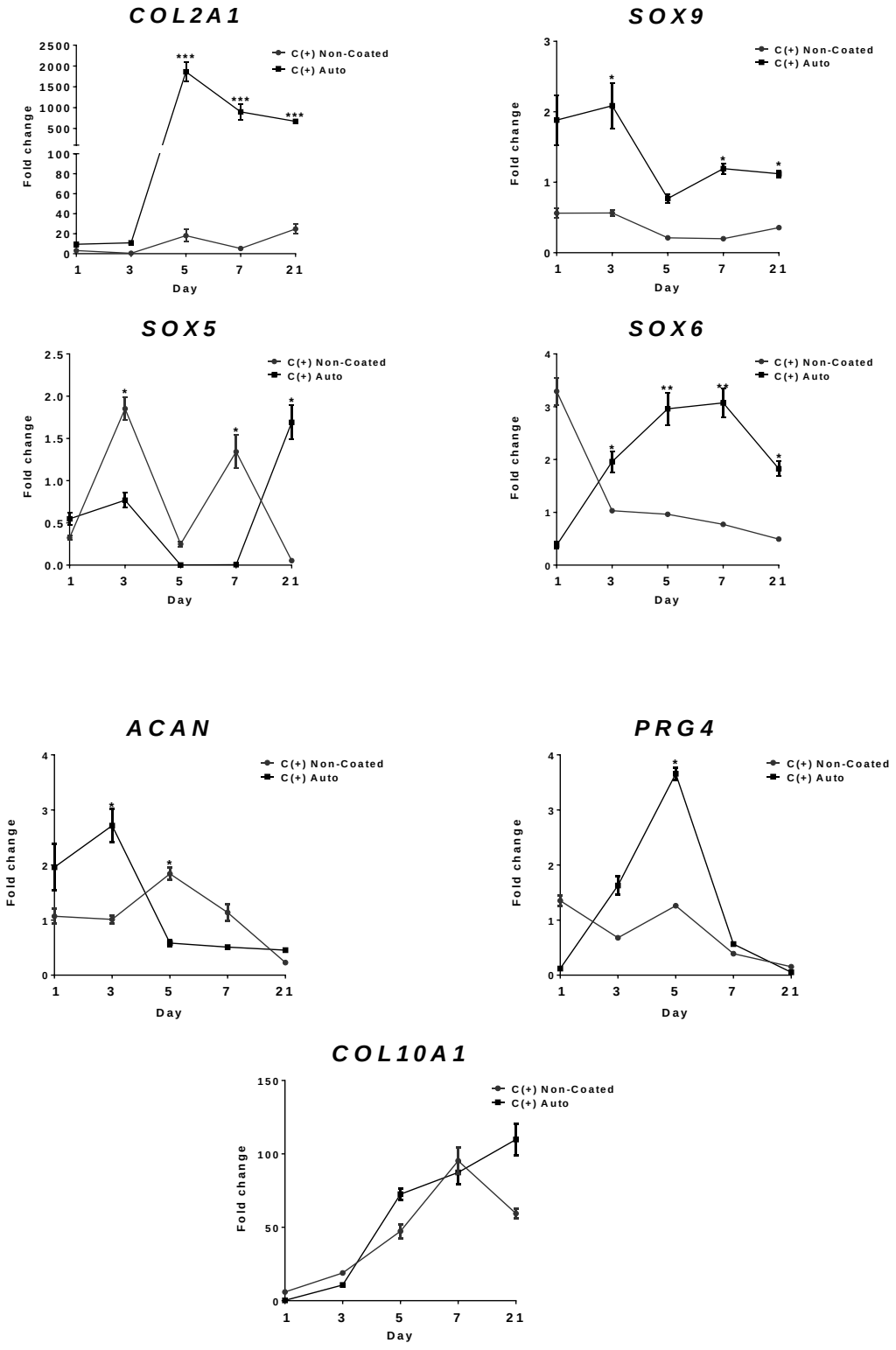

Figure 6.14: Gene expression time course analysis of seeded Auto coated surfaces. Chondrogenic gene expression of hPDSCs seeded as micromasses on autoclaved dcECM-derived (Auto) coating and compared to non-coated tissue culture plastic (NC). Samples were cultured for a period of 1,3,5,7 and 21 days in Chondrogenic C(+) conditions (C&D). (n=3 *p<0.05, **p<0.01, ***p<0.001). (Fold changes normalised to micromasses in CTRL conditions). Statistical analysis was performed using one-way ANOVA corrected for multiple comparisons using Bonferroni's posthoc analysis.

6.4 Discussion

With an ever-increasing demand for more robust stem cell therapies, the ECM and its components have been exploited to generate novel methodologies to enhance cell isolation, survival, proliferation and differentiation[579,580]. This chapter highlights the development of a method for creating dcECM-derived coatings that are capable of enhancing chondrogenesis.

dcECM-derived digests were generated by pepsin digestion of freeze-dried dcECM. The method was adapted from similar approaches to generate ECM-derived hydrogels[577,581,582]. Moreover, these studies suggest that the resultant ECM digest is still capable of inducing chondrogenesis. However,process was not carried out under strictly sterile conditions, thus limiting extended culture. Therefore, the dcECM-derived coating was subject to further sterilisation using either UV or heat mediated autoclave sterilisation. UV sterilisation is capable of inactivating vegetative bacteria and viruses, while also resulting in the crosslinking of collagen components[583]. A study by Rowland and colleagues[584] suggested that cartilage-derived scaolds that were crosslinked by UV exposure drive more robust chondrogenesis and sGAG deposition when seeded with MSC's. However, UV is ineffective at inactivating bacterial spores, mycobacteria and prions and was, therefore, deemed ineffective as a sterilisation methodology, especially considering future clinical applications[585]. There are no known studies that investigate the use of an autoclave for heat-mediated sterilisation of the ECM-derived products, potentially, due to the high temperatures that could result in heat-induced conformational changes in the protein components of the ECM[586,587]. Despite the destructive effect of heat on the ECM, autoclave sterilisation has a proven track record of being able to eliminate all micobiological contaminaton including spores[588]. Other sterilisation techniques such as gamma irridiation and ethylene oxide are also effective alternatives that have been previously employed and compared. Future work should consider these alternative approaches.

Post-sterilisation, the dcECM digest was used to coat tissue culture plastic on 96-well plates by drying 30 µL of the dcECM-digest in each well. Drying was employed instead of creating a gel layer, as the drying process would concentrate the ECM components onto the culture surface. A similar approach

is employed by DeQuach and colleagues who used pepsin digested decellularised cardiac tissue derived coatings and reported efficient ECM deposition onto tissue culture plastic when allowed to dry[572]. This process could be further improved by drying the plates at cooler temperatures under agitation, potentially, slowing down further degradation of the coated ECM components and, moreover, the agitation may generate an even layer. The bioactivity of the coated surfaces was subsequently assessed using hPDSCs.

Brightfield images of the cells seeded onto the autoclaved dcECM-digest coated surface remarkably revealed a cobblestone morphology, as early as Day 1 post culture C+ conditions (Figure 6.12). The rounded cobblestone morphology is a a distinct characteristic of chondrocytes seeded onto tissue culture plastic before dedifferentiation[589]. Moreover, the rounded morphology has also been linked with the upregulation of chondrogenic genes and, subsequently, cartilage-specific matrix deposition[461,575,576]. These findings were confirmed by assessing the associated gene expression data (Figure 6.14). hPDSCs seeded onto Autoclaved samples in C(+) conditions demonstrated significantly higher *SOX9* expression when compared to the non-coated control conditions. The upregulation of *SOX9*, could be a direct result of the synergistic action of ROCKi[461] present in the C(+) conditions and the creation of a chondroinductive topography as a result of the Auto coating process. Previous studies have demonstrated that ROCKi can inhibit the flattening of cultured chondrocytes on tissue culture plastic, thus promoting SOX9 expression[461,590].Similarly, studies have also hilighted the importance of nanotopography on cellular morphology and chhondrogenesis[461,574–576].

Furthermore, the significant upregulation of *SOX9* in C(+) autoclave conditions was accompanied by a significant upregulation in *ACAN*, an early marker of chondrogenesis. In addition to enhanced chondrogenesis, there was observable increase in the number of dead cells present in the C(+) autoclave samples. It is unclear why this occurred only in the C(+) conditions and were not present in auto CTRL conditions or with the other non-coated samples(Figure 6.4). Tsang and colleagues suggest that cells undergoing hypertrophy may eventually result in cell death[591], potentially explaining the observed cell death. Moreover, there is an upregulation in *COL10A1* compared

to control micromass conditions also suggesting chondrocyte hypertrophy(Figure 6.5). Further investigation is required for the assessment of deposited collagen X, as gene expression onlt provides a snapshot and may not be a direct indicator of cumulative protein expression.

Cell-cell interactions mediate chondrogenesis[592]. Therefore, cellular density has a significant impact on chondrogenic differentiation, especially, with regards to mesenchymal stem cell populations[593]. Moreover, the effect of improper drying of coated plastic before seeding remained untested. Therefore, the impact of seeding density and incomplete drying were assessed. Interestingly, the distinct rounded morphology was only present in wells that were sufficiently dried over a for 72 hours (Figure 6.7). This finding suggested that improper drying of the autoclaved digest could prevent sufficient adherence of the matrix proteins to the cell culture surface, facilitating its subsequent removal from the surface when seeded. Cellular density also had an impact on the morphology. The cobblestone pattern observed with auto coated plates in C(+) was the most distinct at a seeding density of 100,000 cells, less distinct at a seeding density of 70,000 cells and not present at 50,000 cells. As previously discussed, the link between seeding density and chondrogenesis has been well established and, therefore, this finding is unremarkable. These results are further supported by the gene expression that reveals a significantly higher expression in the chondrogenic marker *COL2A1* in chondrogenic conditions that contained cells seeded at a density of 100,000 compared to 70,000. To further ensure that the rounded morphology was indicative of chondrogenesis and not adipogenesis, the adipogenic marker *FABP4* was assessed. All autoclave coated conditions expressed *FABP4* at a level that was not significantly different to control non-coated conditions.

Initially, gene expression of the differentiating hPDSC's was assessed at Day 7. However, it was essential to investigate earlier and later time points to monitor changes in gene expression that may have otherwise been missed (Figure 6.14). Therefore, gene expression from the Auto coated group was compared to non-coated controls both cultured in chondrogenic C(+) conditions. The Auto conditions demonstrate a trend towards the early upregulation of SOX9 at Day 1, with a significant upregulation at Day 5. A

significantly higher upregulation of COL2A1 followed this early upregulation of SOX9 at day 5. These findings are in line with literature that suggests the role of SOX9 in promoting the expression of cartilage matrix associated genes[391], further demonstrated by a significantly higher upregulation of the chondrogenic marker *PRG4*[594]. *PRG4* expression may hiilight the increased expression of lubricin, a key component for the lubrication of the articular joint[595]. In a study by Musumeci and colleagues[596] higher lubricin expression was noted in chondrocytes that were cultured from healthy human articular when compared to articular chondrocytes extracted from patients with OA, with overall decline as the cells were cultured *in vitro*. In addition Musumeci and colleagues,[596] also demonstrate that OA chondrocytes encapsulated in Poly (ethylene glycol) based hydrogels restored lubricin protein expression, however there was a significant reduction after 25 days in culture, the Auto coated plates downregulate PRG4 expression after 7 days, however, the protein levels of lubricin were not measured. Due to the ability of the Auto coating to drive the upregultion of *PRG4* the coating may be used as an ideal way to expand chondrocytes for use in ACI. In addition to the gene expression data the potency of the Auto coating was also shown by staining for alcian blue (Figure 46). 7 Days post-seeding, hPDSC's seeded onto the auto coated surface show a significantly higher deposition of sulfated GAG's when compared to non-coated samples in both CTRL and C(+) conditions. Moreover, significantly higher *SOX9* and *COL2A1* expression are maintained through to 21 days. However, an increase in the marker *COL10A1* may suggest the gradual differentiation towards a pre-hypertrophic phenotype[597]. Recently Shi and colleagues published work that indicates the use of a C-type natriuretic peptide (CNP), a peptide expressed in the of long bones could be combined into the culture conditions of MSC-derived chondrocytes to maintain stable chondrocyte phenotype and prevent hypertrophy[598]. Future work may benefit from investigating other factors that could be used in combination with the auto coating to preserve a stable chondrogenic phenotype, potentially.

As demonstrated in chapter 4, hypoxia may further enhance chondrogenesis in micromass 2D micromass cultures, also validated by other studies[599,600601]. Overall, these data highlight the capacity of the auto dc-ECM derived coating

to drive early chondrogenesis but suggests a limited ability to maintain a stable chondrogenic state after long-term culture, likely due to the eventual loss of the attached chondroinductive ECM components after repeated media changes. The autoclave sterilisation used for the generation of the Auto digest coating, may potentially result in the generation of gelatin from the collagenous component of the digested dc-ECM, as high heat is used for the industrial generation of gelatin[602]. A study by brown and colleagues demonstrated that a combination of gelatin and heparin in methacryloyl hydrogels improves chondrogenesis[603]. Similarly, Honarpardaz and colleagues produced gelatin/glycosaminoglycan electrospun nanofibers that enhanced chondrogenesis in MSC's[604]. Therefore, the potential presence of both Gelatin and sGAG's in the digest may synergistically drive chondrogenesis. However, further work is required to compare the dc-ECM derived digest to other gelatin sGAG coatings to determine if it is nesessary to derive the digests from the dcECM.

Within the scope of this chapter, the auto dcECM-derived coating was only tested in the 96-well format. Moreover, as there was no analysis to determine the composition of the dcECM, the mechanisms by which it interacts with hPDSCs remains unexplored. Additionally, although not investigated in this chapter, future work could employ alternative methodologies for sterilisation may prove less damaging to the digested ECM components, while still proving effective for sterilisation. Plasma sterilisation offers a promising alternative that is capable of inactivating viable bacteria and their spores[605]. However, the mechanisms for the inactivation of bacteria and its effect on the extracellular matrix is poorly understood[606]. Alternatively, given the correct resources, the process of digestions could be carried out under sterile conditions. Furthermore, the auto dcECM-derived coating may result in the formation of distinct nano-topographical features present on the coated surface, these features may, subsequently, drive a morphological change in the attached cells, inducing chondrogenesis, as demonstrated by Wu and colleagues[574]. Coating different tissue culture surfaces and sizes may result in a shift in nanotopography. Future work should, therefore, look into the assessment of surface topography using approached such as scanning electron microscopy

or atomic force microscopy[607]. Mendes and colleagues[608], have demonstrated that hPDSC's can be driven towards a chondrogenic phenotype with visibly higher GAG deposition as early as 7 days. The combination of an optimised growth factor cocktail and Auto coated plates can be combined for fututre studies as a potential approach to further enhance the chondrogenesis process. Moreover, factors such as the pH of the digest were not measured, this, in combination with residual pepsin this may influence cell behaviour. Therefore, future work should investigate both factors.

In conclusion the use of auto dcECM-coated plastic is a promising approach for the rapid differentiation of hPDSCs, potentially shortening the time required for their chondrogenic priming. Moreover, the speed of differentiation of vastly faster than traditional methods for the diferentiation of mesenchymal stem cells that can take around 2-3 weeks[609]. Substantial further optimisation and assessment are, however, needed to determine whether the auto coating results in similar findings when combined with various chondroprogenitor cells populations or when combined with various culture surfaces.

7. Final discussion and future work.

Herein we describe the development of an optimised decellularisation methodology, resulting in the production of the dcECM; a non-immunogenic scaffold capable of enhancing chondrogenesis of hPDSC's; a key cellular population involved in fracture healing. Moreover, the dcECM was further processed to give porous scaffolds that retain their chondroinductive potential while being upscalable to meet clinical needs. Moreover, a tissue culture plastic coating was also obtained by processing the dcECM, offering an alternative approach for the expansion and enhanced chondrogenic priming of hPDSC's. In doing so, this thesis aimed to contribute to the growing body of work that aims at addressing some of the challenges faced when addressing bone regeneration, especially, considering the treatment of non-union fractures.

The foundation of current clinical management strategies for non-union fractures is fixation. Therefore, inadequate fixation is a primary underlying cause of delayed or non-union fractures[610]. However, In addition to improper fixation, non-union fractures are also linked with significant bone and soft tissue loss, therefore, requiring further surgical intervention to achieve fracture healing[36–40]. Overall, the treatment of non-unions relies on facilitating favourable biological conditions that allow for bone regeneration. Therefore, the current gold standard treatment for non-unions is autologous bone grafting (ABG). Autologous bone grafts have the three properties that have long been considered to be ideal for bone regeneration; osteoconductivity, osteoinductivity and osteogenecity[41]. Despite these characteristics, good histocompatibility and promising clinical outcomes[51,46,52], complication rates have been reported to be as high as 50% primarily associated with donor site mobility, compounded by the limited availability graft tissue[54–56,58,59]. To address these shortcomings, research has focused on mimicking the desirable properties of ABG's without the associated limitations; these include the development and use of demineralised bone matrix (DBM), obtained from

cadaveric bone tissue. However, processing of these tissues can significantly impact their osteogenic and osteoinductive properties to a varying extent, producing inconsistent clinical outcomes[63]**.** Synthetic biomaterials attempt to overcome the limitations but are unable to mimic the complex native structure and biochemical composition of bone and therefore its osteogenic, osteoinductive and osteoconductive properties[69]. One of the key advantages that should be considered with DMB is, however, the availability of large quantities of non-autologous bone tissue. Advances in bone tissue engineering have, therefore, focused on incorporating both cellular and pharmacological factors into bone regeneration strategies, either in combination with a grafting material or individually[201,611].

Parathyroid hormone (PTH) is produced in response to reduced calcium levels, with the primary function of serum calcium and phosphate homeostasis, achieved via the indirect control of bone resorption[612]. Investigations in both pre-clinical and clinical models have demonstrated that intermittent dosing with PTH can result in increased bone mass[613–615]. Therefore, a modified peptide derived from PTH (teriparatide) has received FDA approval for the treatment of osteoporosis in patients with a high risk of fractures. Moreover, there is also evidence to suggest that teriparatide may enhance fracture healing primarily by accelerating endochondral remodelling of the cartilaginous callus[616,617]. A study by Kim and colleagues suggests that this is facilitated via the differentiation of bone lining cells into osteoblasts[618]. One of the limitations of using PTH alone, however, may be the inability to large segmental bone defects, requiring a grafting material. The P-dcECM was engineered to mimic the cartilage callus phase of fracture repair, therefore, any interventions that promote callus remodelling may be beneficial to enhance the remodelling of the P-dcECM implant, enhancing endochondral bone formation. It would, therefore, be worthwhile investigating the intermittent dosage of PTH alongside the P-dcECM in non-union fracture models.

Interestingly, a recent study by Kiminori and colleagues presents data to suggest that cartilage callus formation was enhanced in mice fracture models when PTH was administered continuously, however, an overall delay in the fracture healing process was also reported[619], since the P-dcECM aims to

mimic the callus phase when implanted delaying the remodelling process may be detrimental to the overall healing times, however, priming the P-dcECM with PTH may be a viable alternative. Moreover, there is currently little evidence to suggest that standard bone-derived ECM would less effective than the P-dcECM at being remodelled into mature bone, therefore, it would have to be included in future investigations as a comparator. Alternatively, fibroblast growth factor-2 (FGF-2) has been shown to enhance cartilaginous callus formation and overall size when tested in small animal models[620,621]. However, there was no improvement in the remodelling of the cartilage callus into osseous tissue and did not enhance the overall healing process; suggesting the need for a supporting matrix, growth factor or cell population that can facilitate osseous remodelling of the fracture callus into mature bone. FGF-2 may be, therefore, be effective during the initial priming of the P-dcECM as there is also evidence to suggest that FGF-2 acts synergistically with TGF-B1 signalling to enhance, chondrogenesis in periosteum-derived cells[622], the cell type chosen in this thesis. Furthermore, FGF signalling is enhanced through its binding with heparan sulfate an s-GAG[623], abundant in the dcECM.

Pharmacological approaches to bone regeneration rely on modulating local cellular populations to enhance bone formation and repair. However, underlying factors such as soft tissue loss, ageing, or diseases can limit the number or functionality of resident cell populations that are essential for bone regeneration and fracture healing[1,28]. Therefore, introducing functional cellular populations into a bone defect is also considered a viable option for the treatment of fractures or bone defects[201]. A recent example of using the cellular approach includes ALLOB®, a population of allogeneic osteoblastic cells derived from healthy donor patients. The latest Phase I/IIA study investigates the efficacy of the approach for the treatment of delayed union. Due to the osteoblastic cell population used in the ALLOB approach, the resulting bone formation would primarily be driven via the intramembranous ossification pathway. This approach may, therefore, be ineffective at participating in early long bone fracture healing, especially, in larger bone defects, where bone healing occurs via the endochondral ossification pathway. Moreover, osteoblasts are not the primary cell source of choice due to their limited self-renewal capacity and heterogeneous cell populations[624]. The P-dcECM aims to mimic the early cartilaginous callus phase

of fracture repair, thus potentially being more effective when treating large bone defects or pathologies such as atrophic non-union fractures, where there is a distinct lack of callus formation. However, the innovative approach used to develop a cell bank of donor cells is worth considering when selecting cell population to be used in combination with the P-dcECM. MSC based therapies have also shown promising results and are, therefore, currently the stem cell of choice. However, articles reviewing cell therapies have suggested that there is still work required to obtain a mainstream cell therapy for the treatment of non-union fractures, and limitations in treating large bone defects still limit an MSC only approach[503]

As highlighted, pharmacological and cell-only approaches do not address the need for a grafting material capable of bridging or filling large bone defects, with some questions also being raised about the localisation or the pharmacological and cellular components of each stratergy[201]. These limitations have resulted in the development of combinational therapies combining pharmacological or cellular approaches with a carrier or grafting material[625]. Quatro and colleagues[626] were the first to report the use of autologous bone marrow-derived MSC's (BM-MSC's) in a pilot study that combined them with Hydroxyapatite blocks to fill bone large bone defects ranging from 4-7 cm. The 3 patients involved were successfully treated for large bone defects in their ulna, humerus and tibia, confirmed in a follow-up screen 6-7 years later[627]. However, there is yet to be any widely applied clinical approach utilising MSC based combinational therapies.

Similar combinational approaches have also been applied for the delivery of pharmacological components. GeneraResearch Ltd has developed Osteogrow, a whole blood coagulum based delivery system for rhBMP-6, aimed at the treatment of non-union fractures[628]. A clinical trial for (EudraCT Number: 2014-005101-21) is currently being undertaken to assess its safety and efficacy when delivered at a fracture site. This is crucial as previously, the use of BMP's, especially BMP-2 has been associated with concerns of adverse effects[495], primarily, due to the non-localised and non-physiological levels of BMP's being used. The Osteogrow system aims to localise rhBMP-6 within the coagulum, with the hope of localising it at the fracture site. Unlike the P-dcECM, this approach is more mimetic of the early inflammatory phase of fracture repair. Moreover, the mechanical properties of the whole blood coagulum have yet to be assessed but could potentially have

insufficient deriable mechanical properties such as compressive strength, compared to a cartilage-based grafting material such as the P-dcECM.

A vast majority of the pharmacological, cellular and scaffold-based therapies still aim to mimic the individual components of the bone microenvironment or signalling to promote bone formation via the intramembranous pathway. However, the fracture healing process, especially, in long bones is driven by endochondral ossification (EO), a process that results in tissue intermediates such as the cartilage callus, before forming bone. Dennis and colleagues reviewed emerging strategies in tissue engineering that harness the intermediate phases of fracture repair, suggesting that mimicking early fracture intermediates such as the cartilage callus may be more effective as they are primed to follow the biological cues present during early fracture repair[8]. The development of the dcECM and P-dcECM described in this thesis is reflective of the paradigm shift towards a more developmental engineering approach to tissue engineering[85,86,629].

Limitations and considerations for translation

Both promise and doubt have always accompanied the concept of xenotransplantation. Early attempts yielded mixed results often leading to death from an acute host response[630], until the later discovery of key immunological barriers to xenotransplantation such as the alpha-gal epitope and donor DNA[222,631]. Initial attempts to overcome these barriers via the use of potent anti-rejection drugs often led to short-lived success and questionable ethics. An article by Annas and colleagues[632] highlights a pivotal case where a baboon heart was transplanted into a heavily immunosuppressed infant, resulting in catastrophic failure and death. Although this was a step back for the concept of xenotransplantation, it later re-emerging when bolstered by the process of decellularisation, with the novel claim of eliminating immunogenic components in non-autologous graft materials rather than suppressing the host immune response to them. A key achievement of this thesis was harnessing previous knowledge on decellularisation and optimising a decellularisation methodology that effectively eliminated Alpha-gal from the xenogeneic cartilage tissue, a key factor in xenogeneic transplant rejection and persistent long-term graft failure if not considered in decellularised

tissues[222,287,288]. Interestingly, this was achieved while maintaining 80% of the native sGAG content, unreported in other studies that investigate decellularisation methodologies for hyaline cartilage. Despite these promising results, there are, however, limiting factors that need to be considered for the successful translation of the concepts discussed in this thesis.

In-depth characterisation of the dcECM and P-dcECM will be a crucial aspect for translation. Although sGAG content was measured, further analysis to elucidate the exact composition of individual sGAG components and associated growth factors may help determine possible mechanisms of action. Moreover, the levels of residual growth factors present within the decellularised tissues is crucial to determine appropriate cell and growth factor priming strategies before implantation. Indeed, factors such as VEG-F, if present in the decellularised tissues, may be advantageous due to the promotion of local vascularisation, a process that is crucial for endochondral fracture healing[1,633].

Findings in the thesis report the complete elimination of alpha-gal and reduction of residual DNA content to levels that are below the *in vivo* immunological threshold. *In vivo* implantation in mice further confirmed the non-inflammatory nature of the dcECM, primarily elucidating a reparative immune response. However, the dcECM was implanted as whole constructs approximately 6 mm in diameter and 1 mm in thickness. Post-explantation, it was observed that there was minimal degradation to the dcECM and native cartilage constructs, this may highlight that cartilage may be naturally immunoprivileged, primarily due to its dense avascular nature, limiting cellular infiltration. The P-dcECM contains smaller fragments of the P-dcECM, provided a relatively larger surface area for interaction with immune cell populations, potentially highlighting a different immune response to whole intact dcECM constructs. Moreover, the processing of the p-dcECM may lead to the generation of more collagen fragments, which may in turn alter its bioactivity at an orthotopic site compared to the dcECM alone. Therefore, future biocompatibility studies with the P-dcECM implantation at an orthotopic site are essential to fully elucidate biocompatibility and the functionality of the constructs, both of which could be limiting factors to translation.

The cell population of choice to be used in combination with the P-dcECM should also be carefully considered. Factors such as ease of isolation, expansion and their functionality are all key factors that will be used to determine the ultimate choice for translation. It is also important to note that grafting materials that contain a cellular component are generally subject to more stringent FDA guidelines to limit variability in the processing of cell populations[634]. In Europe, stem cell-based products are classified as advanced therapeutic medicinal products (ATMP), In general, the more complicated the product or strategy, the tighter the regulations required for approval[635]. It may, therefore be favourable to consider priming the P-dcECM with a chemotactic factor such as SDF-1, proven to facilitate mesenchymal cell chemotaxis to the fracture site and improve fracture healing outcomes in pre-clinical models[636–638]. Additionally, the dc-ECM derived coating developed during this study could be employed during the stem cell chondrogenic priming process, establishing a workflow that will yield not only a usable endochondral grafting material but the rapid generation of a chondrogenically primed cell population that can be used to enhance *in vivo* bioactivity, improving the P-dcECM's potential for translation.

7.1 Future work.

Upscaling the decellularisation process

Much of the Vac-OS decellularisation process is carried out within the vacuum desiccator. Consequently, it would be relatively easy to upscale and automate the process for large-scale production as the constructs remain within the same container. The delivery of each reagent could be automated and controlled by a liquid handling unit linked to a computer (Figure 7.1). The described method is similar to the approach used by Price and colleagues[639].

There are several approaches to evaluate decellularised tissues, and although methodologies can vary depending on the source of native tissue type, the general principle remains the same. Decellularised tissues must fulfil two key criteria; the elimination or reduction of immunogenic components while causing minimal disruption to the collagen integrity. However, as highlighted

by Philips and colleagues in a recent review, there is no standardised method for the evaluation of decellularised tissues[640]. The FDA's minimal manipulation criteria require evidence to demonstrate that processing strategies such as decellularisation and sterilisation inflict minimal disruption to donor tissue[641]. A standardised and automated decellularisation process will further help to reduce variation in Vac-OS decellularised tissues due to minimal human error. Additionally, the FLIM methodology discussed in chapter 3 was effective at monitoring biochemical changes in the costal cartilage ECM, this approach could be further developed and tested as a potential methodology for the rapid assessment of the resultant Vac-OS decellularised tissues and used for batch monitoring and process control. Moreover, collaborative work could be undertaken to incorporate biological assays such as ELISA's into microfluidic lab-on-chip systems that can be automated to provide a rapid point of need analysis, while simultaneously analysing a large number of biological targets such as DNA and alpha-gal[642,643], further speeding up batch analysis and process control.

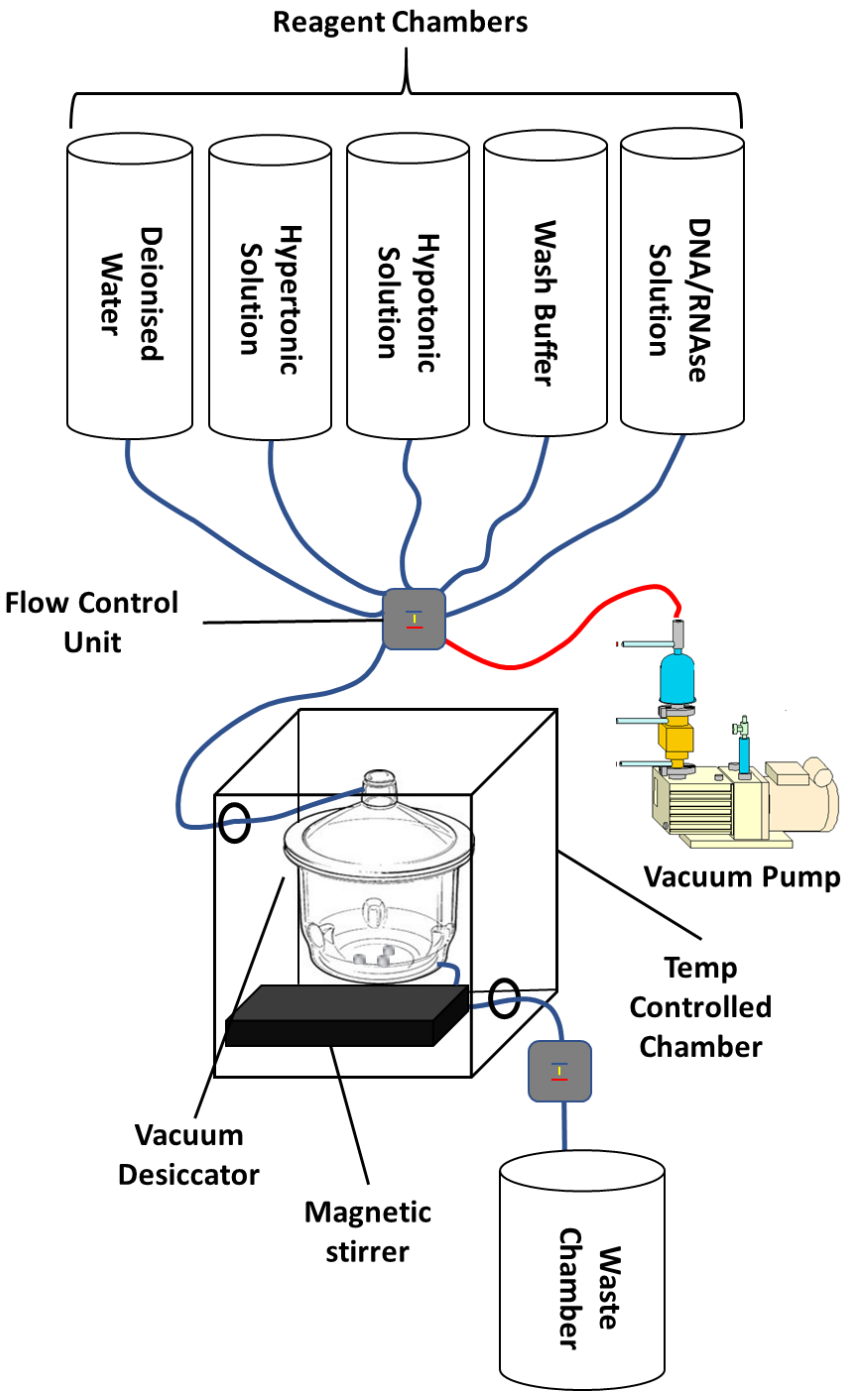

Figure 7.2: Simplified schematic illustrating an automated system for the Vac-OS methodology. Figure generated using the Servier medical art database (http://www.servier.com/Powerpoint-image-bank

In vivo characterisation of the dcECM

Translation of the concepts described in this thesis requires future work to focus on investigating the bone forming capacity of the dcECM or porous dcECM-derived constructs when challenged in an orthotopic non-union fracture model. Moreover, In vivo assessment will also provide crucial information regarding the mechanical kinetic, and presence of toxic degradation products that may result in chronic inflammation.

Large animals were traditionally the ideal choice for fracture models[644,645]. However, there was a gradual shift towards using smaller animal models such as rodents, primarily due to costs associated with their housing and maintenance of large animals[646]. A critical criteria for investigating the P-dcECM would be its ability to facilitate bone regeneration and union when presented with a critical-sized defect (CSD) as the primary aim is the treatment of atrophic non-union fractures. The clinical presentation of non-union fractures is also driven by several additional factors such as age, diabetes, infection, osteoporosis and periosteal damage[4,647]. Therefore, the animal model chosen to investigate the P-dcECM should include one or a combination of these factors. Several non-union fracture models have emerged in both Rats and mice; these have been summarised in supplementary table 2. The options must be carefully considered depending on the clinical requirements being addressed. Moreover, the addition of hPDSC's was also hypothesised to compensate for impaired stem cell availability due to damage caused by surrounding tissues such as the periosteum. Therefore, the ideal fracture model to investigate the efficacy of using the P-dcECM primed with hPDSC's should contain a critical-sized gap that consistently results in non-union fractures without intervention, with further damage to the surrounding periosteum. Other factors such as age and diabetes can eventually be investigated to gauge the regenerative potential of the P-dcECM in various clinical conditions.

In conclusion, there is an extensive range of strategies that target bone regeneration and fracture repair. However, traditional approached to bone tissue engineering did not consider the complex biological processes that

underpin fracture repair, driving a paradigm shift towards the development of bone repair strategies that are biomimetic of the fracture repair process by harnessing repair intermediates such as the cartilage callus, rather than end-stage tissues such as bone. The work carried out in this thesis aims to harness this shift in strategy by developing an efficient decellularisation methodology, resulting in the first reported production of a porcine cartilage-derived decellularised tissue[281]. The resultant dcECM was capable of re-establishing the chondrocytic phenotype in dedifferentiated human articular chondrocytes while enhancing chondrogenic differentiation in human periosteal stem cells. Importantly, the dcECM could be further processed to give upscalable chondroinductive porous scaffolds that supported cellular infiltration, providing a viable approach to the development of cartilage callus mimetic constructs. Overall, bone regeneration remains a key topic for research, with the work in this thesis provided a potential alternative for translation.

References

1. Marsell, R. & Einhorn, T. a. The biology of fracture healing. *Injury* **42**, 551–555 (2011).

2. Einhorn, T. a. The science of fracture healing. *J. Orthop. Trauma* **19**, S4–S6 (2005).

3. Marsell, R. & Einhorn, T. a. Emerging bone healing therapies. *J. Orthop. Trauma* **24 Suppl 1**, S4–S8 (2010).

4. Vas, W. J., Shah, M., Al Hosni, R., Owen, H. C. & Roberts, S. J. Biomimetic strategies for fracture repair: Engineering the cell microenvironment for directed tissue formation. *J. Tissue Eng.* **8**, 204173141770479 (2017).

5. Scotti, C. *et al.* Recapitulation of endochondral bone formation using human adult mesenchymal stem cells as a paradigm for developmental engineering. *Proc. Natl. Acad. Sci. U. S. A.* **107**, 7251–6 (2010).

6. Farrell, E. *et al.* Chondrogenic priming of human bone marrow stromal cells: a better route to bone repair? *Tissue Eng. Part C. Methods* **15**, 285–295 (2009).

7. Tortelli, F., Tasso, R., Loiacono, F. & Cancedda, R. The development of tissue-engineered bone of different origin through endochondral and intramembranous ossification following the implantation of mesenchymal stem cells and osteoblasts in a murine model. *Biomaterials* **31**, 242–9 (2010).

8. Dennis, S. C., Berkland, C. J., Bonewald, L. F. & Detamore, M. S. Endochondral ossification for enhancing bone regeneration: converging native extracellular matrix biomaterials and developmental engineering in vivo. *Tissue Eng. Part B. Rev.* **21**, 247–66 (2015).

9. Lange, J. *et al.* Action of IL-1beta during fracture healing. *J. Orthop. Res.* **28**, 778–84 (2010).

10. Al-Sebaei, M. O. *et al.* Role of Fas and Treg cells in fracture healing as characterized in the fas-deficient (lpr) mouse model of lupus. *J. Bone*

Miner. Res. **29**, 1478–91 (2014).

11. Yang, X. *et al.* Callus mineralization and maturation are delayed during fracture healing in interleukin-6 knockout mice. *Bone* **41**, 928–36 (2007).

12. Wallace, A., Cooney, T. E., Englund, R. & Lubahn, J. D. Effects of interleukin-6 ablation on fracture healing in mice. *J. Orthop. Res.* **29**, 1437–42 (2011).

13. Gerstenfeld, L. C. *et al.* Impaired fracture healing in the absence of TNF-alpha signaling: the role of TNF-alpha in endochondral cartilage resorption. *J. Bone Miner. Res.* **18**, 1584–92 (2003).

14. Glass, G. E. *et al.* TNF-alpha promotes fracture repair by augmenting the recruitment and differentiation of muscle-derived stromal cells. *Proc. Natl. Acad. Sci. U. S. A.* **108**, 1585–90 (2011).

15. Nam, D. *et al.* T-lymphocytes enable osteoblast maturation via IL-17F during the early phase of fracture repair. *PLoS One* **7**, e40044 (2012).

16. Ono, T. *et al.* IL-17-producing γδ T cells enhance bone regeneration. *Nat. Commun.* **7**, 10928 (2016).

17. Han, X. *et al.* Interleukin-17 enhances immunosuppression by mesenchymal stem cells. *Cell Death Differ.* **21**, 1758–68 (2014).

18. Toben, D. *et al.* Fracture healing is accelerated in the absence of the adaptive immune system. *J. Bone Miner. Res.* **26**, 113–124 (2011).

19. Gerstenfeld, L. C., Cullinane, D. M., Barnes, G. L., Graves, D. T. & Einhorn, T. a. Fracture healing as a post-natal developmental process: Molecular, spatial, and temporal aspects of its regulation. *J. Cell. Biochem.* **88**, 873–884 (2003).

20. Colburn, N. T., Zaal, K. J. M., Wang, F. & Tuan, R. S. A role for gamma/delta T cells in a mouse model of fracture healing. *Arthritis Rheum.* **60**, 1694–703 (2009).

21. Maes, C., Carmeliet, G. & Schipani, E. Hypoxia-driven pathways in bone development, regeneration and disease. *Nat. Rev. Rheumatol.* **8**, 358–

66 (2012).

22. Cho, T.-J., Gerstenfeld, L. C. & Einhorn, T. A. Differential temporal expression of members of the transforming growth factor beta superfamily during murine fracture healing. *J. Bone Miner. Res.* **17**, 513–20 (2002).

23. Schmid, G. J., Kobayashi, C., Sandell, L. J. & Ornitz, D. M. Fibroblast growth factor expression during skeletal fracture healing in mice. *Dev. Dyn.* **238**, 766–74 (2009).

24. Yu, Y. Y. *et al.* Immunolocalization of BMPs, BMP antagonists, receptors, and effectors during fracture repair. *Bone* **46**, 841–51 (2010).

25. AI-Aql, Z. S., Alagl, a. S., Graves, D. T., Gerstenfeld, L. C. & Einhorn, T. a. Molecular Mechanisms Controlling Bone Formation during Fracture Healing and Distraction Osteogenesis. *J. Dent. Res.* **87**, 107–118 (2008).

26. Thompson, Z., Miclau, T., Hu, D. & Helms, J. a. A model for intramembranous ossification during fracture healing. *J. Orthop. Res.* **20**, 1091–1098 (2002).

27. Santolini, E., West, R. & Giannoudis, P. V. Risk factors for long bone fracture non-union: a stratification approach based on the level of the existing scientific evidence. *Injury* **46 Suppl 8**, S8–S19 (2015).

28. Graves, D. T., Alblowi, J., Paglia, D. N., O'Connor, J. P. & Lin, S. Impact of Diabetes on Fracture Healing. *J. Exp. Clin. Med.* **3**, 3–8 (2011).

29. Castillo, R. C., Bosse, M. J., MacKenzie, E. J. & Patterson, B. M. Impact of smoking on fracture healing and risk of complications in limb-threatening open tibia fractures. *J. Orthop. Trauma* **19**, 151–157 (2005).

30. Giannoudis, P., Tzioupis, C., Almalki, T. & Buckley, R. Fracture healing in osteoporotic fractures: Is it really different?. A basic science perspective. *Injury* **38**, 0–9 (2007).

31. Panteli, M., Pountos, I., Jones, E. & Giannoudis, P. V. Biological and molecular profile of fracture non-union tissue: current insights. *J. Cell.*

Mol. Med. **19**, 685–713 (2015).

32. Bishop, J. A., Palanca, A. A., Bellino, M. J. & Lowenberg, D. W. Assessment of compromised fracture healing. *J. Am. Acad. Orthop. Surg.* **20**, 273–282 (2012).

33. Mills, L. A. & Simpson, a H. R. W. The relative incidence of fracture non-union in the Scottish population (5.17 million): a 5-year epidemiological study. *BMJ Open* **3**, 1–7 (2013).

34. Bruder, S. P., Fink, D. J. & Caplan, A. I. Mesenchymal stem cells in bone development, bone repair, and skeletal regeneration therapy. *J. Cell. Biochem.* **56**, 283–94 (1994).

35. Roberts, S. J., van Gastel, N., Carmeliet, G. & Luyten, F. P. Uncovering the periosteum for skeletal regeneration: The stem cell that lies beneath. *Bone* **70**, 1–9 (2014).

36. Wood, T. Fracture management in general practice. *Aust. Fam. Physician* **25**, 1385–90 (1996).

37. Srour, M. *et al.* Prospective Evaluation of Treatment of Open Fractures. *JAMA Surg.* **150**, 332 (2015).

38. Hutson, J. J. Chapter 9: Management of the tibia fracture to union. *Tech. Orthop.* **17**, 93–96 (2002).

39. Mckee, G. K. TREATMENT OF COMPOUND FRACTURES OF THE LEG. *Lancet* **236**, 38–40 (1940).

40. Griffin, M., Malahias, M., Hindocha, S. & Khan, W. Update on the management of compound lower limb fractures. *Open Orthop. J.* **6**, 518–24 (2012).

41. Biasibetti, A., Aloj, D., Di Gregorio, G., Masse, A. & Salomone, C. Mechanical and biological treatment of long bone non-unions. *Injury* **36 Suppl 4**, S45-50 (2005).

42. Lewandrowski, K. U., D. Gresser, J., Wise, D. L. & Trantolo, D. J. Bioresorbable bone graft substitutes of different osteoconductivities: A

histologic evaluation of osteointegration of poly(propylene glycol-co-fumaric acid)-based cement implants in rats. *Biomaterials* **21**, 757–764 (2000).

43. Khan, S. N. *et al.* The Biology of Bone Grafting. *J. Am. Acad. Orthop. Surg.* **13**, 77–86 (2005).

44. LeGeros, R. Z. Properties of osteoconductive biomaterials: Calcium phosphates. *Clin. Orthop. Relat. Res.* 81–98 (2002). doi:10.1097/00003086-200202000-00009

45. Giannoudis, P. V, Dinopoulos, H. & Tsiridis, E. Bone substitutes: an update. *Injury* **36 Suppl 3**, S20–S27 (2005).

46. Sen, M. K. & Miclau, T. Autologous iliac crest bone graft: Should it still be the gold standard for treating nonunions? *Injury* **38**, 2–7 (2007).

47. Hadjidakis, D. J. & Androulakis, I. I. Bone remodeling. *Ann. N. Y. Acad. Sci.* **1092**, 385–96 (2006).

48. Matic, I. *et al.* Quiescent Bone Lining Cells Are a Major Source of Osteoblasts During Adulthood. *Stem Cells* **34**, 2930–2942 (2016).

49. Feng, X. Chemical and Biochemical Basis of Cell-Bone Matrix Interaction in Health and Disease. *Curr. Chem. Biol.* **3**, 189–196 (2009).

50. Mansouri, R. *et al.* Osteoblastic heparan sulfate glycosaminoglycans control bone remodeling by regulating Wnt signaling and the crosstalk between bone surface and marrow cells. *Cell Death Dis.* **8**, e2902 (2017).

51. Friedlaender, G. E. *et al.* Osteogenic protein-1 (bone morphogenetic protein-7) in the treatment of tibial nonunions. *J. Bone Joint Surg. Am.* **83**-**A Suppl**, S151-8 (2001).

52. Scaglione, M., Fabbri, L., Dell'omo, D., Gambini, F. & Guido, G. Long bone nonunions treated with autologous concentrated bone marrow-derived cells combined with dried bone allograft. *Musculoskelet. Surg.* **98**, 101–106 (2014).

53. Oakes, D. a & Cabanela, M. E. Impaction bone grafting for revision hip arthroplasty: biology and clinical applications. *J. Am. Acad. Orthop. Surg.* **14**, 620–8 (2006).

54. Perry, C. R. Bone repair techniques, bone graft, and bone graft substitutes. *Clin. Orthop. Relat. Res.* 71–86 (1999).

55. Kanakaris, N. K., Paliobeis, C., Manidakis, N., Giannoudis, P. V. & Nlanidakis, N. Biological enhancement of tibial diaphyseal aseptic non-unions: the efficacy of autologous bone grafting, BMPs and reaming by-products. *Injury* **38**, S65-75 (2007).

56. Fleming, J. E., Cornell, C. N. & Muschler, G. F. Bone cells and matrices in orthopedic tissue engineering. *Orthop. Clin. North Am.* **31**, 357–374 (2000).

57. Dimitriou, R., Mataliotakis, G. I., Angoules, A. G., Kanakaris, N. K. & Giannoudis, P. V. Complications following autologous bone graft harvesting from the iliac crest and using the RIA: A systematic review. *Injury* **42**, S3–S15 (2011).

58. Goulet, J. A., Senunas, L. E., DeSilva, G. L. & Greenfield, M. L. Autogenous iliac crest bone graft. Complications and functional assessment. *Clin. Orthop. Relat. Res.* 76–81 (1997).

59. St John, T. A. *et al.* Physical and monetary costs associated with autogenous bone graft harvesting. *Am. J. Orthop. (Belle Mead. NJ).* **32**, 18–23 (2003).

60. Bostrom, M. P. G. & Seigerman, D. A. The Clinical Use of Allografts, Demineralized Bone Matrices, Synthetic Bone Graft Substitutes and Osteoinductive Growth Factors: A Survey Study. *HSS J.* **1**, 9–18 (2005).

61. Roden, R. D. Principles of Bone Grafting. *Oral and Maxillofacial Surgery Clinics of North America* **22**, 295–300 (2010).

62. Faour, O., Dimitriou, R., Cousins, C. a. & Giannoudis, P. V. The use of bone graft substitutes in large cancellous voids: Any specific needs? *Injury* **42**, S87–S90 (2011).

63. Boyce, T., Edwards, J. & Scarborough, N. Allograft bone: The influence of processing on safety and performance. *Orthop. Clin. North Am.* **30**, 571–581 (1999).

64. Totir, M., Ciuluvica, R., Dinu, I., Careba, I. & Gradinaru, S. Biomaterials for orbital fractures repair. *J. Med. Life* **7 Spec No.**, 62–4 (2014).

65. McKay, W. F., Peckham, S. M. & Badura, J. M. A comprehensive clinical review of recombinant human bone morphogenetic protein-2 (INFUSE?? Bone Graft). *International Orthopaedics* **31**, 729–734 (2007).

66. Fröhlich, M. *et al.* Tissue engineered bone grafts: biological requirements, tissue culture and clinical relevance. *Curr. Stem Cell Res. Ther.* **3**, 254–64 (2008).

67. Laurencin, C., Khan, Y. & El-Amin, S. F. Bone graft substitutes. *Expert Rev. Med. Devices* **3**, 49–57 (2006).

68. Marolt, D., Knezevic, M. & Novakovic, G. V. Bone tissue engineering with human stem cells. *Stem Cell Res. Ther.* **1**, 10 (2010).

69. Bohner, M. Calcium orthophosphates in medicine: From ceramics to calcium phosphate cements. *Injury* **31**, (2000).

70. Elsalanty, M. E. & Genecov, D. G. Bone grafts in craniofacial surgery. *Craniomaxillofac. Trauma Reconstr.* **2**, 125–34 (2009).

71. Rizzo, M. & Moran, S. L. Vascularized bone grafts and their applications in the treatment of carpal pathology. *Semin. Plast. Surg.* **22**, 213–27 (2008).

72. Allman, A. J. *et al.* Xenogeneic extracellular matrix grafts elicit a TH2-restricted immune response. *Transplantation* **71**, 1631–40 (2001).

73. Badylak, S. F. & Gilbert, T. W. Immune response to biologic scaffold materials. *Seminars in Immunology* **20**, 109–116 (2008).

74. Joyce, M. E., Jingushi, S., Scully, S. P. & Bolander, M. E. Role of growth factors in fracture healing. *Prog. Clin. Biol. Res.* **365**, 391–416 (1991).

75. Kanitkar, M., Tailor, H. D. & Khan, W. S. The Use of Growth Factors and Mesenchymal Stem Cells in Orthopaedics. *Open Orthop. J.* **5**, 271–275 (2011).

76. Urist, M. R. *et al.* Bone morphogenesis in implants of insoluble bone gelatin. *Proc. Natl. Acad. Sci. U. S. A.* **70**, 3511–5 (1973).

77. Kanakaris, N. K. *et al.* Application of bone morphogenetic proteins to femoral non-unions: a 4-year multicentre experience. *Injury* **40 Suppl 3**, S54-61 (2009).

78. Rice, I. & Lubahn, J. D. Use of bone morphogenetic protein-2 (rh-BMP-2) in treatment of wrist and hand nonunion with comparison to historical control groups. *J. Surg. Orthop. Adv.* **22**, 256–62 (2013).

79. Garrison, K. *et al.* Bone morphogenetic protein (BMP) for fracture healing in adults. *Cochrane Database of Systematic Reviews* (2008). doi:10.1002/14651858.CD006950

80. Moghaddam, A., Elleser, C., Biglari, B., Wentzensen, A. & Zimmermann, G. Clinical application of BMP 7 in long bone non-unions. *Arch. Orthop. Trauma Surg.* **130**, 71–76 (2010).

81. Crowley, D. J., Kanakaris, N. K. & Giannoudis, P. V. Femoral diaphyseal aseptic non-unions: is there an ideal method of treatment? *Injury* **38 Suppl 2**, S55-63 (2007).

82. Lad, S. P. *et al.* Cancer after spinal fusion: the role of bone morphogenetic protein. *Neurosurgery* **73**, 440–9 (2013).

83. Miron, R. J. & Zhang, Y. F. Osteoinduction: a review of old concepts with new standards. *J. Dent. Res.* **91**, 736–44 (2012).

84. Liu, Y., Lim, J. & Teoh, S.-H. Review: development of clinically relevant scaffolds for vascularised bone tissue engineering. *Biotechnol. Adv.* **31**, 688–705

85. Lenas, P., Moos, M. & Luyten, F. P. Developmental engineering: a new paradigm for the design and manufacturing of cell-based products. Part I: from three-dimensional cell growth to biomimetics of in vivo

development. *Tissue Eng. Part B. Rev.* **15**, 381–94 (2009).

86. Lenas, P., Moos, M. & Luyten, F. P. Developmental engineering: a new paradigm for the design and manufacturing of cell-based products. Part II: from genes to networks: tissue engineering from the viewpoint of systems biology and network science. *Tissue Eng. Part B. Rev.* **15**, 395–422 (2009).

87. Hadjiargyrou, M. & O'Keefe, R. J. The Convergence of Fracture Repair and Stem Cells: Interplay of Genes, Aging, Environmental Factors and Disease. *J. Bone Miner. Res.* **29**, 2307–2322 (2014).

88. Gattazzo, F., Urciuolo, A. & Bonaldo, P. Extracellular matrix: a dynamic microenvironment for stem cell niche. *Biochim. Biophys. Acta* **1840**, 2506–19 (2014).

89. Theocharis, A. D., Skandalis, S. S., Gialeli, C. & Karamanos, N. K. Extracellular matrix structure. *Adv. Drug Deliv. Rev.* **97**, 4–27 (2016).

90. Gentili, C. & Cancedda, R. Cartilage and bone extracellular matrix. *Curr Pharm Des* **15**, 1334–1348 (2009).

91. Kadler, K. E., Hojima, Y. & Prockop, D. J. Assembly of collagen fibrils de novo by cleavage of the type I pC-collagen with procollagen C-proteinase. Assay of critical concentration demonstrates that collagen self-assembly is a classical example of an entropy-driven process. *J. Biol. Chem.* **262**, 15696–701 (1987).

92. Robins, S. P. & Duncan, A. Cross-linking of collagen. Location of pyridinoline in bovine articular cartilage at two sites of the molecule. *Biochem. J.* **215**, 175–82 (1983).

93. Yue, B. Biology of the extracellular matrix: an overview. *J. Glaucoma* **23**, S20-3

94. Kim, S.-H., Turnbull, J. & Guimond, S. Extracellular matrix and cell signalling: the dynamic cooperation of integrin, proteoglycan and growth factor receptor. *J. Endocrinol.* **209**, 139–51 (2011).

95. Pişkin, E. Biodegradable polymers as biomaterials. *J. Biomater. Sci.*

Polym. Ed. **6**, 775–95 (1995).

96. Ji, Y. *et al.* Electrospun three-dimensional hyaluronic acid nanofibrous scaffolds. *Biomaterials* **27**, 3782–92 (2006).

97. Tabata, Y. Biomaterial technology for tissue engineering applications. *J. R. Soc. Interface* **6 Suppl 3**, S311-24 (2009).

98. Alexander, H., Brunski, J. & Cooper, S. Classes of materials used in medicine. *an Introd. to …* (1996).

99. He, C., Xiao, G., Jin, X., Sun, C. & Ma, P. X. Electrodeposition on nanofibrous polymer scaffolds: Rapid mineralization, tunable calcium phosphate composition and topography. *Adv. Funct. Mater.* **20**, 3568–3576 (2010).

100. Wu, C. *et al.* The effect of mesoporous bioactive glass on the physiochemical, biological and drug-release properties of poly(dl-lactide-co-glycolide) films. *Biomaterials* **30**, 2199–2208 (2009).

101. Orefice, R., Clark, A., West, J., Brennan, A. & Hench, L. Processing, properties, and in vitro bioactivity of polysulfone-bioactive glass composites. *J. Biomed. Mater. Res. Part A* **80A**, 565–580 (2007).

102. Zhang, P., Hong, Z., Yu, T., Chen, X. & Jing, X. In vivo mineralization and osteogenesis of nanocomposite scaffold of poly(lactide-co-glycolide) and hydroxyapatite surface-grafted with poly(l-lactide). *Biomaterials* **30**, 58–70 (2009).

103. Ulery, B. D., Nair, L. S. & Laurencin, C. T. Biomedical Applications of Biodegradable Polymers. *J. Polym. Sci. B. Polym. Phys.* **49**, 832–864 (2011).

104. Girones Molera, J., Mendez, J. A. & San Roman, J. Bioresorbable and nonresorbable polymers for bone tissue engineering. *Curr. Pharm. Des.* **18**, 2536–57 (2012).

105. Guo, X. *et al.* Repair of osteochondral defects with autologous chondrocytes seeded onto bioceramic scaffold in sheep. *Tissue Eng.* **10**, 1830–40

106. Zignani, M. *et al.* Improved biocompatibility of a viscous bioerodible poly(ortho ester) by controlling the environmental pH during degradation. *Biomaterials* **21**, 1773–1778 (2000).

107. Nooeaid, P., Salih, V., Beier, J. P. & Boccaccini, A. R. Osteochondral tissue engineering: scaffolds, stem cells and applications. *J. Cell. Mol. Med.* **16**, 2247–70 (2012).

108. Shen, H., Hu, X., Yang, F., Bei, J. & Wang, S. Cell affinity for bFGF immobilized heparin-containing poly(lactide-co-glycolide) scaffolds. *Biomaterials* **32**, 3404–3412 (2011).

109. Kantawong, F. *et al.* Whole proteome analysis of osteoprogenitor differentiation induced by disordered nanotopography and mediated by ERK signalling. *Biomaterials* **30**, 4723–31 (2009).

110. Biggs, M. J. P. *et al.* The use of nanoscale topography to modulate the dynamics of adhesion formation in primary osteoblasts and ERK/MAPK signalling in STRO-1+ enriched skeletal stem cells. *Biomaterials* **30**, 5094–103 (2009).

111. Biggs, M. J. P. *et al.* Interactions with nanoscale topography: adhesion quantification and signal transduction in cells of osteogenic and multipotent lineage. *J. Biomed. Mater. Res. A* **91**, 195–208 (2009).

112. Shafiee, A. *et al.* Enhanced chondrogenesis of human nasal septum derived progenitors on nanofibrous scaffolds. *Mater. Sci. Eng. C* **40**, 445–454 (2014).

113. Wu, Y. *et al.* The Combined Effect of Substrate Stiffness and Surface Topography on Chondrogenic Differentiation of Mesenchymal Stem Cells. *Tissue Eng. Part A* (2016). doi:10.1089/ten.TEA.2016.0123

114. Baker, B. M., Nathan, A. S., Gee, A. O. & Mauck, R. L. The influence of an aligned nanofibrous topography on human mesenchymal stem cell fibrochondrogenesis. *Biomaterials* **31**, 6190–200 (2010).

115. Yin, Z. *et al.* Electrospun scaffolds for multiple tissues regeneration in vivo through topography dependent induction of lineage specific

differentiation. *Biomaterials* **44**, 173–85 (2015).

116. Neves, S. C. *et al.* Additive manufactured polymeric 3D scaffolds with tailored surface topography influence mesenchymal stromal cells activity. *Biofabrication* **8**, 025012 (2016).

117. Balasundaram, G., Storey, D. M. & Webster, T. J. Novel nano-rough polymers for cartilage tissue engineering. *Int. J. Nanomedicine* **9**, 1845–53 (2014).

118. Ranella, A., Barberoglou, M., Bakogianni, S., Fotakis, C. & Stratakis, E. Tuning cell adhesion by controlling the roughness and wettability of 3D micro/nano silicon structures. *Acta Biomater.* **6**, 2711–2720 (2010).

119. Benoit, D. S. W., Schwartz, M. P., Durney, A. R. & Anseth, K. S. Small functional groups for controlled differentiation of hydrogel-encapsulated human mesenchymal stem cells. *Nat. Mater.* **7**, 816–23 (2008).

120. Mei, Y. *et al.* Gradient substrate assembly for quantifying cellular response to biomaterials. *J. Biomed. Mater. Res. A* **79**, 974–88 (2006).

121. Lutolf, M. P., Gilbert, P. M. & Blau, H. M. Designing materials to direct stem-cell fate. *Nature* **462**, 433–41 (2009).

122. Coyle, R., Jia, J. & Mei, Y. Polymer microarray technology for stem cell engineering. *Acta Biomater.* **34**, 60–72 (2016).

123. Anderson, D. G., Levenberg, S. & Langer, R. Nanoliter-scale synthesis of arrayed biomaterials and application to human embryonic stem cells. *Nat. Biotechnol.* **22**, 863–6 (2004).

124. Mei, Y. *et al.* Combinatorial development of biomaterials for clonal growth of human pluripotent stem cells. *Nat. Mater.* **9**, 768–78 (2010).

125. Anderson, D. G., Putnam, D., Lavik, E. B., Mahmood, T. A. & Langer, R. Biomaterial microarrays: rapid, microscale screening of polymer-cell interaction. *Biomaterials* **26**, 4892–7 (2005).

126. Tare, R. S. *et al.* A microarray approach to the identification of polyurethanes for the isolation of human skeletal progenitor cells and

augmentation of skeletal cell growth. *Biomaterials* **30**, 1045–55 (2009).

127. Duffy, C. R. E. *et al.* A high-throughput polymer microarray approach for identifying defined substrates for mesenchymal stem cells. *Biomater. Sci.* **2**, 1683–1692 (2014).

128. Hulsman, M. *et al.* Analysis of high-throughput screening reveals the effect of surface topographies on cellular morphology. *Acta Biomater.* **15**, 29–38 (2015).

129. Unadkat, H. V *et al.* An algorithm-based topographical biomaterials library to instruct cell fate. *Proc. Natl. Acad. Sci. U. S. A.* **108**, 16565–70 (2011).

130. Unadkat, H. V *et al.* A modular versatile chip carrier for high-throughput screening of cell-biomaterial interactions. *J. R. Soc. Interface* **10**, 20120753 (2013).

131. O'Brien, C. M., Holmes, B., Faucett, S. & Zhang, L. G. Three-dimensional printing of nanomaterial scaffolds for complex tissue regeneration. *Tissue Eng. Part B. Rev.* **21**, 103–14 (2015).

132. Bose, S., Vahabzadeh, S. & Bandyopadhyay, A. Bone tissue engineering using 3D printing. *Mater. Today* **16**, 496–504 (2013).

133. Jones, A. C. *et al.* Assessment of bone ingrowth into porous biomaterials using MICRO-CT. *Biomaterials* **28**, 2491–504 (2007).

134. Stoppato, M. *et al.* Influence of scaffold pore size on collagen I development: A new in vitro evaluation perspective. *J. Bioact. Compat. Polym.* **28**, 16–32 (2013).

135. Kucharska, M., Butruk, B., Walenko, K., Brynk, T. & Ciach, T. Fabrication of in-situ foamed chitosan/β-TCP scaffolds for bone tissue engineering application. *Mater. Lett.* **85**, 124–127 (2012).

136. Pavia, F. C., La Carrubba, V., Piccarolo, S. & Brucato, V. Polymeric scaffolds prepared via thermally induced phase separation: tuning of structure and morphology. *J. Biomed. Mater. Res. A* **86**, 459–66 (2008).

137. Inzana, J. A. *et al.* 3D printing of composite calcium phosphate and collagen scaffolds for bone regeneration. *Biomaterials* **35**, 4026–34 (2014).

138. Lee, J.-S. *et al.* 3D printing of composite tissue with complex shape applied to ear regeneration. *Biofabrication* **6**, 024103 (2014).

139. Kundu, J., Shim, J.-H., Jang, J., Kim, S.-W. & Cho, D.-W. An additive manufacturing-based PCL-alginate-chondrocyte bioprinted scaffold for cartilage tissue engineering. *J. Tissue Eng. Regen. Med.* **9**, 1286–97 (2015).

140. Fedorovich, N. E. *et al.* Biofabrication of osteochondral tissue equivalents by printing topologically defined, cell-laden hydrogel scaffolds. *Tissue Eng. Part C. Methods* **18**, 33–44 (2012).

141. Madry, H., Rey-Rico, A., Venkatesan, J. K., Johnstone, B. & Cucchiarini, M. Transforming growth factor Beta-releasing scaffolds for cartilage tissue engineering. *Tissue Eng. Part B. Rev.* **20**, 106–25 (2014).

142. Langer, R. & Vacanti, J. P. Tissue Engineering. *Science (80-.).* **260**, 920–926 (1993).

143. Livesey, S. a, Herndon, D. N., Hollyoak, M. a, Atkinson, Y. H. & Nag, a. Transplanted acellular allograft dermal matrix. Potential as a template for the reconstruction of viable dermis. *Transplantation* **60**, 1–9 (1995).

144. Sutherland, R. S., Baskin, L. S., Hayward, S. W. & Cunha, G. R. Regeneration of bladder urothelium, smooth muscle, blood vessels and nerves into an acellular tissue matrix. *J. Urol.* **156**, 571–577 (1996).

145. Mazza, G. *et al.* Decellularized human liver as a natural 3D-scaffold for liver bioengineering and transplantation. *Sci. Rep.* **5**, 13079 (2015).

146. Guyette, J. P. *et al.* Perfusion decellularization of whole organs. *Nat. Protoc.* **9**, 1451–1468 (2014).

147. Crapo, P. M., Gilbert, T. W. & Badylak, S. F. An overview of tissue and whole organ decellularization processes. *Biomaterials* **32**, 3233–3243 (2011).

148. Gilbert, T. W., Sellaro, T. L. & Badylak, S. F. Decellularization of tissues and organs. *Biomaterials* **27**, 3675–3683 (2006).

149. Cheng, C. W., Solorio, L. D. & Alsberg, E. Decellularized tissue and cell-derived extracellular matrices as scaffolds for orthopaedic tissue engineering. *Biotechnology Advances* **32**, 462–484 (2014).

150. Gawlitta, D. *et al.* Decellularized Cartilage-Derived Matrix as Substrate for Endochondral Bone Regeneration. *Tissue Eng. Part A* **21**, 694–703 (2015).

151. Olsen, B. R., Reginato, A. M. & Wang, W. Bone development. *Annu. Rev. Cell Dev. Biol.* **16**, 191–220 (2000).

152. Klinger, P. *et al.* Chondromodulin 1 stabilizes the chondrocyte phenotype and inhibits endochondral ossification of porcine cartilage repair tissue. *Arthritis Rheum.* **63**, 2721–2731 (2011).

153. Kitahara, H. *et al.* Chondromodulin-I expression in rat articular cartilage. *Arch Histol Cytol* **66**, 221–228 (2003).

154. Hayami, T. *et al.* Expression of the cartilage derived anti-angiogenic factor chondromodulin-I decreases in the early stage of experimental osteoarthritis. *J. Rheumatol.* **30**, 2207–2217 (2003).

155. Bahrami, S. *et al.* Endochondral ossification of costal cartilage is arrested after chondrocytes have reached hypertrophic stage of late differentiation. *Matrix Biol.* **19**, 707–715 (2001).

156. Okihana, H. & Shimomura, Y. Osteogenic activity of growth cartilage examined by implanting decalcified or devitalized ribs and costal cartilage zone, and living growth cartilage cells. *Bone* **13**, 387–393 (1992).

157. Robinson, D. L. *et al.* Mechanical properties of normal and osteoarthritic human articular cartilage. *J. Mech. Behav. Biomed. Mater.* **61**, 96–109 (2016).

158. Peters, A. E., Akhtar, R., Comerford, E. J. & Bates, K. T. The effect of ageing and osteoarthritis on the mechanical properties of cartilage and

bone in the human knee joint. *Sci. Rep.* (2018). doi:10.1038/s41598-018-24258-6

159. Morgan, E. F., Unnikrisnan, G. U. & Hussein, A. I. Bone Mechanical Properties in Healthy and Diseased States. *Annu. Rev. Biomed. Eng.* (2018). doi:10.1146/annurev-bioeng-062117-121139

160. Ifesanya, A. O. & Alonge, T. O. Operative stabilization of open long bone fractures: A tropical tertiary hospital experience. *Niger. Med. J.* **53**, 16–20 (2012).

161. Miclau, T. *et al.* Effects of delayed stabilization on fracture healing. *J. Orthop. Res.* **25**, 1552–8 (2007).

162. McNamara, I. *et al.* Mechanical properties of morcellised bone graft with the addition of hydroxyapatite. *J. Mater. Sci. Mater. Med.* **25**, 321–7 (2014).

163. Xu, Z.-J., Chen, L.-Y., Zhong, C., Tan, Y.-B. & He, R.-X. Mechanical properties of 7-10mm bone grafts and small slurry grafts in impaction bone grafting. *J. Orthop. Res.* **29**, 1491–5 (2011).

164. Roberts, T. T. & Rosenbaum, A. J. Bone grafts, bone substitutes and orthobiologics the bridge between basic science and clinical advancements in fracture healing. *Organogenesis* (2012). doi:10.4161/org.23306

165. Khan, S. N. *et al.* The biology of bone grafting. *The Journal of the American Academy of Orthopaedic Surgeons* (2005). doi:10.5435/00124635-200501000-00010

166. Ogose, A. *et al.* Histological assessment in grafts of highly purified beta-tricalcium phosphate (OSferion®) in human bones. *Biomaterials* (2006). doi:10.1016/j.biomaterials.2005.08.034

167. Liao, J., Joyce, E. M. & Sacks, M. S. Effects of decellularization on the mechanical and structural properties of the porcine aortic valve leaflet. *Biomaterials* **29**, 1065–74 (2008).

168. Zou, Y. & Zhang, Y. Mechanical evaluation of decellularized porcine

thoracic aorta. *J. Surg. Res.* **175**, 359–68 (2012).

169. Evans, M. J. & Kaufman, M. H. Establishment in culture of pluripotential cells from mouse embryos. *Nature* **292**, 154–6 (1981).

170. Thomson, J. A. *et al.* Embryonic stem cell lines derived from human blastocysts. *Science* **282**, 1145–7 (1998).

171. Godfrey, K. J. *et al.* Stem cell-based treatments for Type 1 diabetes mellitus: bone marrow, embryonic, hepatic, pancreatic and induced pluripotent stem cells. *Diabet. Med.* **29**, 14–23 (2012).

172. Shabani, P. *et al.* Exogenous treatment with eicosapentaenoic acid supports maturation of cardiomyocytes derived from embryonic stem cells. *Biochem. Biophys. Res. Commun.* **461**, 281–6 (2015).

173. Sekiguchi, H., Ii, M. & Losordo, D. W. The relative potency and safety of endothelial progenitor cells and unselected mononuclear cells for recovery from myocardial infarction and ischemia. *J. Cell. Physiol.* **219**, 235–42 (2009).

174. Song, Y.-H., Pinkernell, K. & Alt, E. Stem cell induced cardiac regeneration: fusion/mitochondrial exchange and/or transdifferentiation? *Cell Cycle* **10**, 2281–6 (2011).

175. Quattrocelli, M., Cassano, M., Crippa, S., Perini, I. & Sampaolesi, M. Cell therapy strategies and improvements for muscular dystrophy. *Cell Death Differ.* **17**, 1222–9 (2010).

176. Buttery, L. D. *et al.* Differentiation of osteoblasts and in vitro bone formation from murine embryonic stem cells. *Tissue Eng.* **7**, 89–99 (2001).

177. Sottile, V., Thomson, A. & McWhir, J. In vitro osteogenic differentiation of human ES cells. *Cloning Stem Cells* **5**, 149–55 (2003).

178. Jukes, J. M. *et al.* Endochondral bone tissue engineering using embryonic stem cells. *Proc. Natl. Acad. Sci. U. S. A.* **105**, 6840–5 (2008).

179. Bielby, R. C., Boccaccini, A. R., Polak, J. M. & Buttery, L. D. K. In vitro

differentiation and in vivo mineralization of osteogenic cells derived from human embryonic stem cells. *Tissue Eng.* **10**, 1518–25

180. Craft, A. M. *et al.* Generation of articular chondrocytes from human pluripotent stem cells. *Nat. Biotechnol.* **33**, 638–45 (2015).

181. King, N. M. & Perrin, J. Ethical issues in stem cell research and therapy. *Stem Cell Res. Ther.* **5**, 85 (2014).

182. Andrews, P. W. From teratocarcinomas to embryonic stem cells. *Philos. Trans. R. Soc. Lond. B. Biol. Sci.* **357**, 405–17 (2002).

183. Takahashi, K. & Yamanaka, S. Induction of pluripotent stem cells from mouse embryonic and adult fibroblast cultures by defined factors. *Cell* **126**, 663–76 (2006).

184. Takahashi, K. *et al.* Induction of pluripotent stem cells from adult human fibroblasts by defined factors. *Cell* **131**, 861–72 (2007).

185. Villa-Diaz, L. G. *et al.* Derivation of mesenchymal stem cells from human induced pluripotent stem cells cultured on synthetic substrates. *Stem Cells* **30**, 1174–81 (2012).

186. Sheyn, D. *et al.* Human Induced Pluripotent Stem Cells Differentiate Into Functional Mesenchymal Stem Cells and Repair Bone Defects. *Stem Cells Transl. Med.* **5**, 1447–1460 (2016).

187. Ko, J.-Y., Kim, K.-I., Park, S. & Im, G.-I. In vitro chondrogenesis and in vivo repair of osteochondral defect with human induced pluripotent stem cells. *Biomaterials* **35**, 3571–81 (2014).

188. Yamashita, A. *et al.* Generation of scaffoldless hyaline cartilaginous tissue from human iPSCs. *Stem cell reports* **4**, 404–18 (2015).

189. Tam, W. L. *et al.* Sox9 reprogrammed dermal fibroblasts undergo hypertrophic differentiation in vitro and trigger endochondral ossification in vivo. *Cell. Reprogram.* **16**, 29–39 (2014).

190. Amini, A. R., Laurencin, C. T. & Nukavarapu, S. P. Bone tissue engineering: recent advances and challenges. *Crit. Rev. Biomed. Eng.*

40, 363–408 (2012).

191. Bernardo, M. E., Pagliara, D. & Locatelli, F. Mesenchymal stromal cell therapy: a revolution in Regenerative Medicine? *Bone Marrow Transplant.* **47**, 164–71 (2012).

192. Pittenger, M. F. *et al.* Multilineage potential of adult human mesenchymal stem cells. *Science* **284**, 143–7 (1999).

193. Kuhbier, J. W. *et al.* Isolation, characterization, differentiation, and application of adipose-derived stem cells. *Adv. Biochem. Eng. Biotechnol.* **123**, 55–105 (2010).

194. Caplan, A. I. Mesenchymal stem cells. *J. Orthop. Res.* **9**, 641–50 (1991).

195. Tavassoli, M. & Crosby, W. H. Transplantation of marrow to extramedullary sites. *Science* **161**, 54–6 (1968).

196. Friedenstein, A. J. Precursor cells of mechanocytes. *Int. Rev. Cytol.* **47**, 327–59 (1976).

197. Dominici, M. *et al.* Minimal criteria for defining multipotent mesenchymal stromal cells. The International Society for Cellular Therapy position statement. *Cytotherapy* **8**, 315–7 (2006).

198. Arvidson, K. *et al.* Bone regeneration and stem cells. *J. Cell. Mol. Med.* **15**, 718–46 (2011).

199. Yousefi, A.-M. *et al.* Prospect of Stem Cells in Bone Tissue Engineering: A Review. *Stem Cells Int.* **2016**, 6180487 (2016).

200. Breitbart, E. A. *et al.* Mesenchymal stem cells accelerate bone allograft incorporation in the presence of diabetes mellitus. *J. Orthop. Res.* **28**, 942–9 (2010).

201. Gómez-Barrena, E. *et al.* Bone fracture healing: Cell therapy in delayed unions and nonunions. *Bone* **70**, 93–101 (2015).

202. Kawate, K. *et al.* Tissue-engineered approach for the treatment of steroid-induced osteonecrosis of the femoral head: transplantation of autologous mesenchymal stem cells cultured with beta-tricalcium

phosphate ceramics and free vascularized fibula. *Artif. Organs* **30**, 960–2 (2006).

203. Han, D., Han, N., Zhang, P. & Jiang, B. Local transplantation of osteogenic pre-differentiated autologous adipose-derived mesenchymal stem cells may accelerate non-union fracture healing with limited pro-metastatic potency. *Int. J. Clin. Exp. Med.* **8**, 1406–10 (2015).

204. Sesia, S. B. *et al.* Anti-inflammatory/tissue repair macrophages enhance the cartilage-forming capacity of human bone marrow-derived mesenchymal stromal cells. *J. Cell. Physiol.* **230**, 1258–69 (2015).

205. Allen, M. R., Hock, J. M. & Burr, D. B. Periosteum: biology, regulation, and response to osteoporosis therapies. *Bone* **35**, 1003–12 (2004).

206. Colnot, C. Skeletal cell fate decisions within periosteum and bone marrow during bone regeneration. *J. Bone Miner. Res.* **24**, 274–82 (2009).

207. Roberts, S. J. *et al.* The combined bone forming capacity of human periosteal derived cells and calcium phosphates. *Biomaterials* **32**, 4393–405 (2011).

208. Xie, C. *et al.* COX-2 from the injury milieu is critical for the initiation of periosteal progenitor cell mediated bone healing. *Bone* **43**, 1075–83 (2008).

209. Zhang, X. *et al.* Periosteal progenitor cell fate in segmental cortical bone graft transplantations: implications for functional tissue engineering. *J. Bone Miner. Res.* **20**, 2124–37 (2005).

210. Van Gastel, N. *et al.* Expansion of murine periosteal progenitor cells with fibroblast growth factor 2 reveals an intrinsic endochondral ossification program mediated by bone morphogenetic protein 2. *Stem Cells* **32**, 2407–2418 (2014).

211. van Gastel, N. *et al.* Expansion of murine periosteal progenitor cells with fibroblast growth factor 2 reveals an intrinsic endochondral ossification program mediated by bone morphogenetic protein 2. *Stem Cells* **32**,

2407–18 (2014).

212. Scotti, C. *et al.* Recapitulation of endochondral bone formation using human adult mesenchymal stem cells as a paradigm for developmental engineering. *Proc. Natl. Acad. Sci. U. S. A.* **107**, 7251–6 (2010).

213. Frantz, C., Stewart, K. M. & Weaver, V. M. The extracellular matrix at a glance. *J. Cell Sci.* **123**, 4195–200 (2010).

214. Lee, K. C., Joory, K. & Moiemen, N. S. History of burns: The past, present and the future. *Burn. trauma* **2**, 169–80 (2014).

215. Lafferty, K. J. Immunogenicity of foreign tissues. *Transplantation* **29**, 179–82 (1980).

216. Friedlaender, G. E. Immune responses to osteochondral allografts. Current knowledge and future directions. *Clin. Orthop. Relat. Res.* 58–68 (1983).

217. Ozbek, S., Balasubramanian, P. G., Chiquet-Ehrismann, R., Tucker, R. P. & Adams, J. C. The evolution of extracellular matrix. *Mol. Biol. Cell* **21**, 4300–5 (2010).

218. Bernard, M. P. *et al.* Structure of a cDNA for the pro alpha 2 chain of human type I procollagen. Comparison with chick cDNA for pro alpha 2(I) identifies structurally conserved features of the protein and the gene. *Biochemistry* **22**, 1139–45 (1983).

219. Constantinou, C. D. & Jimenez, S. A. Structure of cDNAs Encoding the Triple-Helical Domain of Murine α2 (VI) Collagen Chain and Comparison to Human and Chick Homologues. Use of Polymerase Chain Reaction and Partially Degenerate Oligonucleotides for Generation of Novel cDNA Clones. *Matrix* **11**, 1–9 (1991).

220. Exposito, J. Y., D'Alessio, M., Solursh, M. & Ramirez, F. Sea urchin collagen evolutionarily homologous to vertebrate pro-?2(I) collagen. *J. Biol. Chem.* **267**, 15559–15562 (1992).

221. Keane, T. J., Londono, R., Turner, N. J. & Badylak, S. F. Consequences of ineffective decellularization of biologic scaffolds on the host response.

Biomaterials **33**, 1771–81 (2012).

222. Galili, U. The ??-gal epitope and the anti-Gal antibody in xenotransplantation and in cancer immunotherapy. *Immunology and Cell Biology* **83**, 674–686 (2005).

223. Park, C. S. *et al.* Anti alpha-gal immune response following porcine bioprosthesis implantation in children. *J. Heart Valve Dis.* **19**, 124–30 (2010).

224. Tudorache, I. *et al.* Tissue engineering of heart valves: biomechanical and morphological properties of decellularized heart valves. *J. Heart Valve Dis.* **16**, 567–573; discussion 574 (2007).

225. Schenke-Layland, K. *et al.* Impact of decellularization of xenogeneic tissue on extracellular matrix integrity for tissue engineering of heart valves. *J. Struct. Biol.* **143**, 201–208 (2003).

226. Elder, B. D., Kim, D. H. & Athanasiou, K. A. Developing an articular cartilage decellularization process toward facet joint cartilage replacement. *Neurosurgery* **66**, 722–727 (2010).

227. Cheng, N.-C., Estes, B. T., Awad, H. A. & Guilak, F. Chondrogenic Differentiation of Adipose-Derived Adult Stem Cells by a Porous Scaffold Derived from Native Articular Cartilage Extracellular Matrix. *Tissue Eng. Part A* **15**, 231–241 (2009).

228. Dahl, S. L. M., Koh, J., Prabhakar, V. & Niklason, L. E. Decellularized native and engineered arterial scaffolds for transplantation. *Cell Transplant.* **12**, 659–666 (2003).

229. Reing, J. E. *et al.* The effects of processing methods upon mechanical and biologic properties of porcine dermal extracellular matrix scaffolds. *Biomaterials* **31**, 8626–8633 (2010).

230. Xu, H. *et al.* Host response to human acellular dermal matrix transplantation in a primate model of abdominal wall repair. *Tissue Eng. Part A* **14**, 2009–2019 (2008).

231. Greco, K. V *et al.* Characterisation of porcine dermis scaffolds

decellularised using a novel non-enzymatic method for biomedical applications. *J. Biomater. Appl.* **30**, 239–53 (2015).

232. Kheir, E. *et al.* Development and characterization of an acellular porcine cartilage bone matrix for use in tissue engineering. *J. Biomed. Mater. Res. - Part A* **99 A**, 283–294 (2011).

233. Burk, J. *et al.* Freeze-thaw cycles enhance decellularization of large tendons. *Tissue Eng. Part C. Methods* **20**, 276–84 (2014).

234. Roth, S. P., Erbe, I. & Burk, J. Decellularization of Large Tendon Specimens: Combination of Manually Performed Freeze-Thaw Cycles and Detergent Treatment. *Methods Mol. Biol.* **1283**, 161–9 (2017).

235. Hung, S. H., Su, C. H., Lee, F. P. & Tseng, H. Larynx Decellularization: Combining Freeze-Drying and Sonication as an Effective Method. *J. Voice* **27**, 289–294 (2013).

236. Funamoto, S. *et al.* The use of high-hydrostatic pressure treatment to decellularize blood vessels. *Biomaterials* **31**, 3590–5 (2010).

237. Negishi, J. *et al.* Porcine radial artery decellularization by high hydrostatic pressure. *J. Tissue Eng. Regen. Med.* **9**, E144–E151 (2015).

238. Lange, P. *et al.* Pilot study of a novel vacuum-assisted method for decellularization of tracheae for clinical tissue engineering applications. *J. Tissue Eng. Regen. Med.* (2015). doi:10.1002/term.1979

239. Cartmell, J. S. & Dunn, M. G. Effect of chemical treatments on tendon cellularity and mechanical properties. *J. Biomed. Mater. Res.* **49**, 134–140 (2000).

240. Woods, T. & Gratzer, P. F. Effectiveness of three extraction techniques in the development of a decellularized bone-anterior cruciate ligament-bone graft. *Biomaterials* **26**, 7339–7349 (2005).

241. Vavken, P., Joshi, S. & Murray, M. M. TRITON-X is most effective among three decellularization agents for ACL tissue engineering. *J. Orthop. Res.* **27**, 1612–8 (2009).

242. O'Neill, J. D. *et al.* Decellularization of human and porcine lung tissues for pulmonary tissue engineering. *Ann. Thorac. Surg.* **96**, 1046–55; discussion 1055-6 (2013).

243. Youngstrom, D. W., Barrett, J. G., Jose, R. R. & Kaplan, D. L. Functional characterization of detergent-decellularized equine tendon extracellular matrix for tissue engineering applications. *PLoS One* **8**, e64151 (2013).

244. Rieder, E. *et al.* Decellularization protocols of porcine heart valves differ importantly in efficiency of cell removal and susceptibility of the matrix to recellularization with human vascular cells. *J. Thorac. Cardiovasc. Surg.* **127**, 399–405 (2004).

245. Chen, R.-N., Ho, H.-O., Tsai, Y.-T. & Sheu, M.-T. Process development of an acellular dermal matrix (ADM) for biomedical applications. *Biomaterials* **25**, 2679–2686 (2004).

246. Elder, B. D., Eleswarapu, S. V. & Athanasiou, K. A. Extraction techniques for the decellularization of tissue engineered articular cartilage constructs. *Biomaterials* **30**, 3749–3756 (2009).

247. Yu, B.-T., Li, W.-T., Song, B.-Q. & Wu, Y.-L. Comparative study of the Triton X-100-sodium deoxycholate method and detergent-enzymatic digestion method for decellularization of porcine aortic valves. *Eur. Rev. Med. Pharmacol. Sci.* **17**, 2179–84 (2013).

248. Gajera, H., Patel, S. & Golakiya, B. . *Fundamentals of Biochemistry: A textbook*. *A Text Book* (2008). doi:10.1038/137559c0

249. Rahman, S., Griffin, M., Naik, A., Szarko, M. & Butler, P. E. M. Optimising the decellularization of human elastic cartilage with trypsin for future use in ear reconstruction. *Sci. Rep.* **8**, 3097 (2018).

250. Perea-Gil, I. *et al.* In vitro comparative study of two decellularization protocols in search of an optimal myocardial scaffold for recellularization. *Am. J. Transl. Res.* **7**, 558–73 (2015).

251. Xu, K. *et al.* Efficient decellularization for tissue engineering of the tendon-bone interface with preservation of biomechanics. *PLoS One* **12**,

e0171577 (2017).

252. Xu, H. *et al.* Comparison of decellularization protocols for preparing a decellularized porcine annulus fibrosus scaffold. *PLoS One* **9**, e86723 (2014).

253. Lu, Y., Parker, K. H. & Wang, W. Effects of osmotic pressure in the extracellular matrix on tissue deformation. *Philos. Trans. A. Math. Phys. Eng. Sci.* **364**, 1407–22 (2006).

254. Beck, E. C. *et al.* Chondroinduction from Naturally Derived Cartilage Matrix: A Comparison Between Devitalized and Decellularized Cartilage Encapsulated in Hydrogel Pastes. *Tissue Eng. Part A* **22**, 665–79 (2016).

255. Sutherland, A. J. *et al.* Decellularized cartilage may be a chondroinductive material for osteochondral tissue engineering. *PLoS One* **10**, e0121966 (2015).

256. Gilpin, A. & Yang, Y. Decellularization Strategies for Regenerative Medicine: From Processing Techniques to Applications. *BioMed Research International* **2017**, (2017).

257. Dejardin, L. M., Arnoczky, S. P., Ewers, B. J., Haut, R. C. & Clarke, R. B. Tissue-engineered rotator cuff tendon using porcine small intestine submucosa. Histologic and mechanical evaluation in dogs. *Am. J. Sports Med.* **29**, 175–184 (2001).

258. Badylak, S. F. *et al.* The use of xenogeneic small intestinal submucosa as a biomaterial for Achille's tendon repair in a dog model. *J. Biomed. Mater. Res.* **29**, 977–985 (1995).

259. Sellaro, T. L., Ravindra, A. K., Stolz, D. B. & Badylak, S. F. Maintenance of hepatic sinusoidal endothelial cell phenotype in vitro using organ-specific extracellular matrix scaffolds. *Tissue Eng.* **13**, 2301–2310 (2007).

260. Cheng, C. W., Solorio, L. D. & Alsberg, E. Decellularized tissue and cell-derived extracellular matrices as scaffolds for orthopaedic tissue

engineering. *Biotechnol. Adv.* **32**, 462–484 (2014).

261. Faldini, C. *et al.* Use of homologous bone graft in the treatment of aseptic forearm nonunion. *Musculoskelet. Surg.* **95**, 31–5 (2011).

262. Bansal, M. R., Bhagat, S. B. & Shukla, D. D. Bovine cancellous xenograft in the treatment of tibial plateau fractures in elderly patients. *Int. Orthop.* **33**, 779–84 (2009).

263. Schook, L. B. *et al.* Unraveling the swine genome: implications for human health. *Annu. Rev. Anim. Biosci.* **3**, 219–44 (2015).

264. Lau, A., Oyen, M. L., Kent, R. W., Murakami, D. & Torigaki, T. Indentation stiffness of aging human costal cartilage. *Acta Biomater.* (2008). doi:10.1016/j.actbio.2007.06.008

265. Millington, P. F. Cartilage-bone interface. *Eng. Med.* (1984). doi:10.1243/EMED_JOUR_1984_013_034_02

266. Frisbie, D. D., Cross, M. W. & McIlwraith, C. W. A comparative study of articular cartilage thickness in the stifle of animal species used in human pre-clinical studies compared to articular cartilage thickness in the human knee. *Vet. Comp. Orthop. Traumatol.* **19**, 142–6 (2006).

267. Sophia Fox, A. J., Bedi, A. & Rodeo, S. A. The basic science of articular cartilage: structure, composition, and function. *Sports Health* **1**, 461–8 (2009).

268. Schwarz, S. *et al.* Decellularized Cartilage Matrix as a Novel Biomatrix for Cartilage Tissue-Engineering Applications. *Tissue Eng. Part A* **18**, 120720085805006 (2012).

269. Utomo, L. *et al.* Preparation and characterization of a decellularized cartilage scaffold for ear cartilage reconstruction. *Biomed. Mater.* **10**, 015010 (2015).

270. Rider, C. C. Heparin/heparan sulphate binding in the TGF-beta cytokine superfamily. *Biochem. Soc. Trans.* **34**, 458–60 (2006).

271. Turnbull, J., Powell, A. & Guimond, S. Heparan sulfate: Decoding a

dynamic multifunctional cell regulator. *Trends in Cell Biology* **11**, 75–82 (2001).

272. French, M. M. *et al.* Chondrogenic activity of the heparan sulfate proteoglycan perlecan maps to the N-terminal domain I. *J. Bone Miner. Res.* **17**, 48–55 (2002).

273. Ingavle, G. C., Frei, A. W., Gehrke, S. H. & Detamore, M. S. Incorporation of aggrecan in interpenetrating network hydrogels to improve cellular performance for cartilage tissue engineering. *Tissue Eng. Part A* **19**, 1349–59 (2013).

274. Mohan, N., Gupta, V., Sridharan, B., Sutherland, A. & Detamore, M. S. The potential of encapsulating 'raw materials' in 3D osteochondral gradient scaffolds. *Biotechnol. Bioeng.* **111**, 829–41 (2014).

275. Jochmann, K., Bachvarova, V. & Vortkamp, A. Reprint of: Heparan sulfate as a regulator of endochondral ossification and osteochondroma development. *Matrix Biology* **35**, 239–247 (2014).

276. Drouzas, A. E. & Schubert, H. Microwave application in vacuum drying of fruits. *J. Food Eng.* **28**, 203–209 (1996).

277. Macchiarini, P. *et al.* Clinical transplantation of a tissue-engineered airway. *Lancet (London, England)* **372**, 2023–30 (2008).

278. Conconi, M. T. *et al.* Tracheal matrices, obtained by a detergent-enzymatic method, support in vitro the adhesion of chondrocytes and tracheal epithelial cells. *Transpl. Int.* **18**, 727–34 (2005).

279. Butler, C. R. *et al.* Vacuum-assisted decellularization: an accelerated protocol to generate tissue-engineered human tracheal scaffolds. *Biomaterials* **124**, 95–105 (2017).

280. Lu, X. L. & Mow, V. C. Biomechanics of articular cartilage and determination of material properties. *Medicine and Science in Sports and Exercise* (2008). doi:10.1249/mss.0b013e31815cb1fc

281. Vas, W. J. *et al.* Decellularized Cartilage Directs Chondrogenic Differentiation: Creation of a Fracture Callus Mimetic. *Tissue Eng. Part*

A (2018). doi:10.1089/ten.TEA.2017.0450

282. Benders, K. E. M. *et al.* Multipotent Stromal Cells Outperform Chondrocytes on Cartilage-Derived Matrix Scaffolds. *Cartilage* **5**, 221–30 (2014).

283. White, L. J. *et al.* The impact of detergents on the tissue decellularization process: A ToF-SIMS study. *Acta Biomater.* **50**, 207–219 (2017).

284. Lin, Y., Lin, H., Liu, Z., Wang, K. & Yan, Y. Improvement of a sample preparation method assisted by sodium deoxycholate for mass-spectrometry-based shotgun membrane proteomics. *J. Sep. Sci.* **37**, 3321–9 (2014).

285. Horton, W. A. & Machado, M. M. Extracellular matrix alterations during endochondral ossification in humans. *J. Orthop. Res.* **6**, 793–803 (1988).

286. Ortega, N., Behonick, D. J. & Werb, Z. Matrix remodeling during endochondral ossification. *Trends Cell Biol.* **14**, 86–93 (2004).

287. Konakci, K. Z. *et al.* Alpha-Gal on bioprostheses: xenograft immune response in cardiac surgery. *Eur. J. Clin. Invest.* **35**, 17–23 (2005).

288. Mangold, A. *et al.* Alpha-Gal specific IgG immune response after implantation of bioprostheses. *Thorac. Cardiovasc. Surg.* **57**, 191–5 (2009).

289. Kim, Y.-G., Gil, G.-C., Harvey, D. J. & Kim, B.-G. Structural analysis of alpha-Gal and new non-Gal carbohydrate epitopes from specific pathogen-free miniature pig kidney. *Proteomics* **8**, 2596–610 (2008).

290. Rozario, T. & DeSimone, D. W. The extracellular matrix in development and morphogenesis: a dynamic view. *Dev. Biol.* **341**, 126–40 (2010).

291. Järveläinen, H., Sainio, A., Koulu, M., Wight, T. N. & Penttinen, R. Extracellular matrix molecules: potential targets in pharmacotherapy. *Pharmacol. Rev.* **61**, 198–223 (2009).

292. Bateman, J. F., Boot-Handford, R. P. & Lamandé, S. R. Genetic diseases of connective tissues: Cellular and extracellular effects of ECM

mutations. *Nature Reviews Genetics* **10**, 173–183 (2009).

293. Dzamba, B. J., Jakab, K. R., Marsden, M., Schwartz, M. A. & DeSimone, D. W. Cadherin adhesion, tissue tension, and noncanonical Wnt signaling regulate fibronectin matrix organization. *Dev. Cell* **16**, 421–32 (2009).

294. Page-McCaw, A., Ewald, A. J. & Werb, Z. Matrix metalloproteinases and the regulation of tissue remodelling. *Nature Reviews Molecular Cell Biology* **8**, 221–233 (2007).

295. Lu, P., Takai, K., Weaver, V. M. & Werb, Z. Extracellular matrix degradation and remodeling in development and disease. *Cold Spring Harb Perspect Biol* **3**, 1–24 (2011).

296. Midwood, K. S., Williams, L. V. & Schwarzbauer, J. E. Tissue repair and the dynamics of the extracellular matrix. *International Journal of Biochemistry and Cell Biology* **36**, 1031–1037 (2004).

297. Ahmed, M. & Ffrench-Constant, C. Extracellular Matrix Regulation of Stem Cell Behavior. *Curr. stem cell reports* **2**, 197–206

298. Lu, P., Weaver, V. M. & Werb, Z. The extracellular matrix: A dynamic niche in cancer progression. *Journal of Cell Biology* **196**, 395–406 (2012).

299. Legate, K. R., Wickström, S. A. & Fässler, R. Genetic and cell biological analysis of integrin outside-in signaling. *Genes and Development* **23**, 397–418 (2009).

300. Buitenhuis, M. The role of PI3K/protein kinase B (PKB/c-akt) in migration and homing of hematopoietic stem and progenitor cells. *Curr. Opin. Hematol.* **18**, 226–30 (2011).

301. Hynes, R. O. The extracellular matrix: Not just pretty fibrils. *Science* **326**, 1216–1219 (2009).

302. Klagsbrun, M. The affinity of fibroblast growth factors (FGFs) for heparin; FGF-heparan sulfate interactions in cells and extracellular matrix. *Curr. Opin. Cell Biol.* **2**, 857–863 (1990).

303. Bonnans, C., Chou, J. & Werb, Z. Remodelling the extracellular matrix in development and disease. *Nature Reviews Molecular Cell Biology* **15**, 786–801 (2014).

304. Miller, E. J., Van Der Korst, J. K. & Sokoloff, L. Collagen of human articular and costal cartilage. *Arthritis Rheum.* **12**, 21–29 (1969).

305. Lai, W. M., Hou, J. S. & Mow, V. C. A triphasic theory for the swelling and deformation behaviors of articular cartilage. *J. Biomech. Eng.* **113**, 245–58 (1991).

306. LINN, F. C. & SOKOLOFF, L. MOVEMENT AND COMPOSITION OF INTERSTITIAL FLUID OF CARTILAGE. *Arthritis Rheum.* **8**, 481–94 (1965).

307. Mow, V. C., Kuei, S. C., Lai, W. M. & Armstrong, C. G. Biphasic creep and stress relaxation of articular cartilage in compression? Theory and experiments. *J. Biomech. Eng.* **102**, 73–84 (1980).

308. Mow, V. C., Zhu, W. & Ratcliffe, A. Structure and function of articular cartilage and meniscus. *Basic Orthop. Biomech. Raven Press. New York.* 143–1998 (1991).

309. Wu, J. J., Woods, P. E. & Eyre, D. R. Identification of cross-linking sites in bovine cartilage type IX collagen reveals an antiparallel type II-type IX molecular relationship and type IX to type IX bonding. *J. Biol. Chem.* **267**, 23007–23014 (1992).

310. Ichimura, S., Wu, J. J. & Eyre, D. R. Two-dimensional peptide mapping of cross-linked type IX collagen in human cartilage. *Arch. Biochem. Biophys.* **378**, 33–39 (2000).

311. Diab, M., Wu, J. J. & Eyre, D. R. Collagen type IX from human cartilage: a structural profile of intermolecular cross-linking sites. *Biochem. J.* **314**, 327–332 (1996).

312. Eyre, D. R., Mcdevitt, C. A., Billinghamii, M. E. J. & Muiri, H. Biosynthesis of Collagen and other Matrix Proteins by Articular Cartilage in Experimental Osteoarthrosis. *Biochem. J* **188**, 823–837 (1980).

313. Kiani, C., Chen, L., Wu, Y. J., Yee, A. J. & Yang, B. B. Structure and function of aggrecan. *Cell Res.* **12**, 19–32 (2002).

314. Esko, J. D., Kimata, K. & Lindahl, U. *Proteoglycans and Sulfated Glycosaminoglycans*. *Essentials of Glycobiology* (2009).

315. Nolting, D., Hansen, B. F., Keeling, J. W. & Kjaer, I. Histological examinations of bone and cartilage in the axial skeleton of human triploidy fetuses. *APMIS* **110**, 186–92 (2002).

316. Hoemann, C. D., Sun, J., Chrzanowski, V. & Buschmann, M. D. A multivalent assay to detect glycosaminoglycan, protein, collagen, RNA, and DNA content in milligram samples of cartilage or hydrogel-based repair cartilage. *Anal. Biochem.* **300**, 1–10 (2002).

317. Hoemann, C. D. Molecular and biochemical assays of cartilage components. *Methods Mol. Med.* **101**, 127–56 (2004).

318. Videman, T., Eronen, I. & Candolin, T. [3H]proline incorporation and hydroxyproline concentration in articular cartilage during the development of osteoarthritis caused by immobilization. A study in vivo with rabbits. *Biochem. J.* **200**, 435–40 (1981).

319. Palmer, A. W., Guldberg, R. E. & Levenston, M. E. Analysis of cartilage matrix fixed charge density and three-dimensional morphology via contrast-enhanced microcomputed tomography. *Proc. Natl. Acad. Sci. U. S. A.* **103**, 19255–60 (2006).

320. Xie, L., Lin, A. S. P., Guldberg, R. E. & Levenston, M. E. Nondestructive assessment of sGAG content and distribution in normal and degraded rat articular cartilage via EPIC-microCT. *Osteoarthr. Cartil.* **18**, 65–72 (2010).

321. Gessner, R. C. *et al.* Functional ultrasound imaging for assessment of extracellular matrix scaffolds used for liver organoid formation. *Biomaterials* **34**, 9341–9351 (2013).

322. Kaleva, E. *et al.* Arthroscopic Ultrasound Assessment of Articular Cartilage in the Human Knee Joint: A Potential Diagnostic Method.

Cartilage **2**, 246–53 (2011).

323. Ozaki, Y. & Šašić, S. Introduction to Raman Spectroscopy. *Pharmaceutical Applications of Raman Spectroscopy* 1–28 (2007). doi:10.1002/9780470225882.ch1

324. Bumbrah, G. S. & Sharma, R. M. Raman spectroscopy – Basic principle, instrumentation and selected applications for the characterization of drugs of abuse. *Egyptian Journal of Forensic Sciences* **6**, 209–215 (2016).

325. De Oliveira Penido, C. A. F., Pacheco, M. T. T., Lednev, I. K. & Silveira, L. Raman spectroscopy in forensic analysis: Identification of cocaine and other illegal drugs of abuse. *Journal of Raman Spectroscopy* **47**, 28–38 (2016).

326. Morris, M. D. & Mandair, G. S. Raman assessment of bone quality. in *Clinical Orthopaedics and Related Research* **469**, 2160–2169 (2011).

327. Lim, N. S. J., Hamed, Z., Yeow, C. H., Chan, C. & Huang, Z. Early detection of biomolecular changes in disrupted porcine cartilage using polarized Raman spectroscopy. *J. Biomed. Opt.* **16**, 017003 (2011).

328. Bauer, N. J., Hendrikse, F. & March, W. F. In vivo confocal Raman spectroscopy of the human cornea. *Cornea* **18**, 483–8 (1999).

329. Lui, H., Zhao, J., McLean, D. & Zeng, H. Real-time raman spectroscopy for in vivo skin cancer diagnosis. *Cancer Res.* **72**, 2491–2500 (2012).

330. Matousek, P. & Stone, N. Recent advances in the development of Raman spectroscopy for deep non-invasive medical diagnosis. *Journal of Biophotonics* **6**, 7–19 (2013).

331. Mazza, G. *et al.* Rapid production of human liver scaffolds for functional tissue engineering by high shear stress oscillation-decellularization. *Sci. Rep.* **7**, (2017).

332. Biela, E. *et al.* Col-F, a fluorescent probe for ex vivo confocal imaging of collagen and elastin in animal tissues. *Cytometry. A* **83**, 533–9 (2013).

333. Baldivia, S. *et al.* A Novel Organ Culture Model to Quantify Collagen Remodeling in Tree Shrew Sclera. *PLoS One* **11**, e0166644 (2016).

334. Sanderson, M. J., Smith, I., Parker, I. & Bootman, M. D. Fluorescence microscopy. *Cold Spring Harb. Protoc.* **2014**, pdb.top071795 (2014).

335. Paddock, S. W. & Eliceiri, K. W. Laser scanning confocal microscopy: history, applications, and related optical sectioning techniques. *Methods Mol. Biol.* **1075**, 9–47 (2014).

336. Becker, W. Fluorescence lifetime imaging - techniques and applications. *J. Microsc.* **247**, 119–136 (2012).

337. Bhosale, A. M. & Richardson, J. B. Articular cartilage: Structure, injuries and review of management. *British Medical Bulletin* **87**, 77–95 (2008).

338. Ranjit, S. *et al.* Imaging Fibrosis and Separating Collagens using Second Harmonic Generation and Phasor Approach to Fluorescence Lifetime Imaging. *Sci. Rep.* **5**, 13378 (2015).

339. Chen, X., Nadiarynkh, O., Plotnikov, S. & Campagnola, P. J. Second harmonic generation microscopy for quantitative analysis of collagen fibrillar structure. *Nat. Protoc.* **7**, 654–669 (2012).

340. Lutz, V. *et al.* Impact of collagen crosslinking on the second harmonic generation signal and the fluorescence lifetime of collagen autofluorescence. *Skin Res. Technol.* **18**, 168–79 (2012).

341. Deveney, M. J., Walton, A. G. & Koenig, J. L. Raman spectra of imino acids and poly-L-hydroxyproline. *Biopolymers* **10**, 615–30 (1971).

342. Bansil, R., Yannas, I. V & Stanley, H. E. Raman spectroscopy: a structural probe of glycosaminoglycans. *Biochim. Biophys. Acta* **541**, 535–42 (1978).

343. Dehring, K. A. *et al.* Identifying chemical changes in subchondral bone taken from murine knee joints using Raman spectroscopy. *Appl. Spectrosc.* **60**, 1134–41 (2006).

344. Bergholt, M. S. *et al.* Raman Spectroscopy Reveals New Insights into

the Zonal Organization of Native and Tissue-Engineered Articular Cartilage. *ACS Cent. Sci.* **2**, 885–895 (2016).

345. Samouillan, V. *et al.* The use of thermal techniques for the characterization and selection of natural biomaterials. *J. Funct. Biomater.* **2**, 230–48 (2011).

346. Than, P. & Kereskai, L. Thermal analysis of the osteoarthritic human hyaline cartilage. in *Journal of Thermal Analysis and Calorimetry* **82**, 213–216 (2005).

347. Butler, H. J. *et al.* Using Raman spectroscopy to characterize biological materials. *Nat. Protoc.* **11**, 664–687 (2016).

348. Eggleston, G., Trask-Morrell, B. J. & Vercellotti, J. R. Use of Differential Scanning Calorimetry and Thermogravimetric Analysis to Characterize the Thermal Degradation of Crystalline Sucrose and Dried Sucrose-Salt Residues. *J. Agric. Food Chem.* **44**, 3319–3325 (1996).

349. Williams, R. M., Zipfel, W. R. & Webb, W. W. Interpreting second-harmonic generation images of collagen I fibrils. *Biophys. J.* **88**, 1377–86 (2005).

350. Menter, J. M. Temperature dependence of collagen fluorescence. *Photochem. Photobiol. Sci.* **5**, 403–10 (2006).

351. Suhling, K. *et al.* Fluorescence lifetime imaging (FLIM): Basic concepts and some recent developments. *Med. Photonics* **27**, 3–40 (2015).

352. Talbot, C. B. *et al.* Fluorescence lifetime imaging of articular cartilage. *Int. J. Exp. Pathol.* **85**, A31–A32 (2008).

353. Hashimoto, Y. *et al.* Ultrastructural analysis of the decellularized cornea after interlamellar keratoplasty and microkeratome-assisted anterior lamellar keratoplasty in a rabbit model. *Sci. Rep.* **6**, (2016).

354. Wang, S. *et al.* Protein stability in stored decellularized heart valve scaffolds and diffusion kinetics of protective molecules. *Biochim. Biophys. Acta* **1844**, 430–8 (2014).

355. Rutgers, M. *et al.* Effect of collagen type I or type II on chondrogenesis by cultured human articular chondrocytes. *Tissue Eng. Part A* **19**, 59–65 (2013).

356. Hyllested, J. L., Veje, K. & Ostergaard, K. Histochemical studies of the extracellular matrix of human articular cartilage - A review. *Osteoarthr. Cartil.* **10**, 333–343 (2002).

357. Schmitz, N., Laverty, S., Kraus, V. B. & Aigner, T. Basic methods in histopathology of joint tissues. *Osteoarthr. Cartil.* **18**, (2010).

358. Esmonde-White, K. Raman spectroscopy of soft musculoskeletal tissues. *Appl. Spectrosc.* **68**, 1203–18 (2014).

359. Shoulders, M. D. & Raines, R. T. Collagen structure and stability. *Annu. Rev. Biochem.* **78**, 929–58 (2009).

360. Han, L., Grodzinsky, A. J. & Ortiz, C. Nanomechanics of the Cartilage Extracellular Matrix. *Annu. Rev. Mater. Res.* **41**, 133–168 (2011).

361. Ember, K. J. I. *et al.* Raman spectroscopy and regenerative medicine: a review. *npj Regen. Med.* **2**, 12 (2017).

362. Rojkind, M., Blumenfeld, O. O. & Gallop, P. M. Localization and partial characterization of an aldehydic component in tropocollagen. *J. Biol. Chem.* **241**, 1530–6 (1966).

363. Bornstein, P., Kang, A. H. & Piez, K. A. The nature and location of intramolecular cross-links in collagen. *Proc. Natl. Acad. Sci. U. S. A.* **55**, 417–24 (1966).

364. Bailey, A. J. & Peach, C. M. Isolation and structural identification of a labile intermolecular crosslink in collagen. *Biochem. Biophys. Res. Commun.* **33**, 812–9 (1968).

365. Robins, S. P., Shimokomaki, M. & Bailey, A. J. The chemistry of the collagen cross-links. Age-related changes in the reducible components of intact bovine collagen fibres. *Biochem. J.* **131**, 771–80 (1973).

366. Fujimoto, D. Isolation and characterization of a fluorescent material in

bovine achilles tendon collagen. *Biochem. Biophys. Res. Commun.* **76**, 1124–9 (1977).

367. Masahiko, T. *et al.* Temporal changes in collagen cross-links in spontaneous articular cartilage repair. *Cartilage* **3**, 278–287 (2012).

368. Eyre, D. R., Dickson, I. R. & Van Ness, K. Collagen cross-linking in human bone and articular cartilage. Age-related changes in the content of mature hydroxypyridinium residues. *Biochem. J.* **252**, 495–500 (1988).

369. Chiu, M. H. & Prenner, E. J. Differential scanning calorimetry: An invaluable tool for a detailed thermodynamic characterization of macromolecules and their interactions. *J. Pharm. Bioallied Sci.* **3**, 39–59 (2011).

370. Privalov, P. L. & Dragan, A. I. Microcalorimetry of biological macromolecules. *Biophys. Chem.* **126**, 16–24 (2007).

371. Lorch, M., Mason, J. M., Sessions, R. B. & Clarke, A. R. Effects of mutations on the thermodynamics of a protein folding reaction: implications for the mechanism of formation of the intermediate and transition states. *Biochemistry* **39**, 3480–5 (2000).

372. Weber, P. C. & Salemme, F. R. Applications of calorimetric methods to drug discovery and the study of protein interactions. *Curr. Opin. Struct. Biol.* **13**, 115–21 (2003).

373. Mabrey, S. & Sturtevant, J. M. Investigation of phase transitions of lipids and lipid mixtures by sensitivity differential scanning calorimetry. *Proc. Natl. Acad. Sci. U. S. A.* **73**, 3862–3866 (1976).

374. Than, P. Differential scanning calorimetric examination of the osteoarthritic hyaline cartilage in rabbits. *Thermochim. Acta* **404**, 149–153 (2003).

375. Miles, C. A., Avery, N. C., Rodin, V. V & Bailey, A. J. The increase in denaturation temperature following cross-linking of collagen is caused by dehydration of the fibres. *J. Mol. Biol.* **346**, 551–6 (2005).

376. Khankari, R. K., Law, D. & Grant, D. J. W. Determination of water content in pharmaceutical hydrates by differential scanning calorimetry. *Int. J. Pharm.* **82**, 117–127 (1992).

377. Deangelis, N. J. & Papariello, G. J. Differential Scanning Calorimetry. *J. Pharm. Sci.* **57**, 1868–1873 (1968).

378. Talbot, C. B. *et al.* Fluorescence lifetime imaging of articular cartilage. *Int. J. Exp. Pathol.* **85**, A31–A32 (2008).

379. Sanders, R., Draaijer, A., Gerritsen, H. C., Houpt, P. M. & Levine, Y. K. Quantitative pH Imaging in Cells Using Confocal Fluorescence Lifetime Imaging Microscopy. *Anal. Biochem.* **227**, 302–308 (1995).

380. Piston, D. W., Kirby, M. S., Cheng, H., Lederer, W. J. & Webb, W. W. Two-photon-excitation fluorescence imaging of three-dimensional calcium-ion activity. *Appl. Opt.* **33**, 662 (1994).

381. French, T. *et al.* Two-photon fluorescence lifetime imaging microscopy of macrophage-mediated antigen processing. *J. Microsc.* **185**, 339–353 (1997).

382. Phipps, J. E., Sun, Y., Fishbein, M. C. & Marcu, L. A fluorescence lifetime imaging classification method to investigate the collagen to lipid ratio in fibrous caps of atherosclerotic plaque. *Lasers Surg. Med.* **44**, 564–71 (2012).

383. Kon, T. *et al.* Expression of osteoprotegerin, receptor activator of NF-kappaB ligand (osteoprotegerin ligand) and related proinflammatory cytokines during fracture healing. *J. Bone Miner. Res.* **16**, 1004–14 (2001).

384. Roberts, S. J., van Gastel, N., Carmeliet, G. & Luyten, F. P. Uncovering the periosteum for skeletal regeneration: The stem cell that lies beneath. *Bone* **70**, 10–18 (2015).

385. Bolander, J. *et al.* Early BMP, Wnt and Ca(2+)/PKC pathway activation predicts the bone forming capacity of periosteal cells in combination with calcium phosphates. *Biomaterials* **86**, 106–18 (2016).

386. Lodish, H. *et al. Molecular Cell Biology. 4th edition*. *New York: W. H. Freeman* (2000). doi:10.1017/CBO9781107415324.004

387. Yoo, H. J. *et al.* Gene expression profile during chondrogenesis in human bone marrow derived mesenchymal stem cells using a cDNA microarray. *J. Korean Med. Sci.* **26**, 851–8 (2011).

388. Boeuf, S. *et al.* A chondrogenic gene expression signature in mesenchymal stem cells is a classifier of conventional central chondrosarcoma. *J. Pathol.* **216**, 158–66 (2008).

389. Saha, A., Rolfe, R., Carroll, S., Kelly, D. J. & Murphy, P. Chondrogenesis of embryonic limb bud cells in micromass culture progresses rapidly to hypertrophy and is modulated by hydrostatic pressure. *Cell Tissue Res.* **368**, 47–59 (2017).

390. Barham, G. & Clarke, N. M. P. Genetic regulation of embryological limb development with relation to congenital limb deformity in humans. *J. Child. Orthop.* **2**, 1–9 (2008).

391. Hino, K. *et al.* Master regulator for chondrogenesis, Sox9, regulates transcriptional activation of the endoplasmic reticulum stress transducer BBF2H7/CREB3L2 in chondrocytes. *J. Biol. Chem.* **289**, 13810–20 (2014).

392. Akiyama, H. Control of chondrogenesis by the transcription factor Sox9. *Modern Rheumatology* (2008). doi:10.1007/s10165-008-0048-x

393. Murakami, S., Kan, M., McKeehan, W. L. & de Crombrugghe, B. Up-regulation of the chondrogenic Sox9 gene by fibroblast growth factors is mediated by the mitogen-activated protein kinase pathway. *Proc. Natl. Acad. Sci. U. S. A.* **97**, 1113–8 (2000).

394. Leung, V. Y. L. *et al.* SOX9 governs differentiation stage-specific gene expression in growth plate chondrocytes via direct concomitant transactivation and repression. *PLoS Genet.* (2011). doi:10.1371/journal.pgen.1002356

395. Hardingham, T. E., Oldershaw, R. A. & Tew, S. R. Cartilage, SOX9 and

Notch signals in chondrogenesis. *J. Anat.* **209**, 469–80 (2006).

396. Zhao, Q., Eberspaecher, H., Lefebvre, V. & De Crombrugghe, B. Parallel expression of Sox9 and Col2a1 in cells undergoing chondrogenesis. *Dev. Dyn.* **209**, 377–86 (1997).

397. Bell, D. M. *et al.* SOX9 directly regulates the type-II collagen gene. *Nat. Genet.* (1997). doi:10.1038/ng0697-174

398. Aspberg, A. Cartilage proteoglycans. in *Cartilage: Volume 1: Physiology and Development* (2016). doi:10.1007/978-3-319-29568-8_1

399. Mwale, F., Stachura, D., Roughley, P. & Antoniou, J. Limitations of using aggrecan and type X collagen as markers of chondrogenesis in mesenchymal stem cell differentiation. *J. Orthop. Res.* **24**, 1791–8 (2006).

400. Liu, C.-F. & Lefebvre, V. The transcription factors SOX9 and SOX5/SOX6 cooperate genome-wide through super-enhancers to drive chondrogenesis. *Nucleic Acids Res.* **43**, 8183–203 (2015).

401. Hirao, M., Tamai, N., Tsumaki, N., Yoshikawa, H. & Myoui, A. Oxygen tension regulates chondrocyte differentiation and function during endochondral ossification. *J. Biol. Chem.* (2006). doi:10.1074/jbc.M602296200

402. Leijten, J. C. H., Moreira Teixeira, L. S., Landman, E. B. M., van Blitterswijk, C. A. & Karperien, M. Hypoxia inhibits hypertrophic differentiation and endochondral ossification in explanted tibiae. *PLoS One* **7**, e49896 (2012).

403. Dickson, K., Katzman, S., Delgado, E. & Contreras, D. Delayed unions and nonunions of open tibial fractures. Correlation with arteriography results. *Clin. Orthop. Relat. Res.* 189–93 (1994).

404. Brownlow, H. C., Reed, A. & Simpson, A. H. R. W. The vascularity of atrophic non-unions. *Injury* **33**, 145–50 (2002).

405. Giannoudis, P. V *et al.* The synergistic effect of autograft and BMP-7 in the treatment of atrophic nonunions. *Clin. Orthop. Relat. Res.* **467**,

3239–48 (2009).

406. Asahara, T. *et al.* VEGF contributes to postnatal neovascularization by mobilizing bone marrow-derived endothelial progenitor cells. *EMBO J.* **18**, 3964–72 (1999).

407. Ramakrishnan, S., Anand, V. & Roy, S. Vascular endothelial growth factor signaling in hypoxia and inflammation. *J. Neuroimmune Pharmacol.* **9**, 142–60 (2014).

408. Hankenson, K. D., Dishowitz, M., Gray, C. & Schenker, M. Angiogenesis in bone regeneration. *Injury* **42**, 556–61 (2011).

409. Yue, J. & Mulder, K. M. Transforming growth factor-beta signal transduction in epithelial cells. *Pharmacol. Ther.* **91**, 1–34 (2001).

410. Kawakami, Y., Rodriguez-León, J. & Izpisúa Belmonte, J. C. The role of TGFbetas and Sox9 during limb chondrogenesis. *Curr. Opin. Cell Biol.* **18**, 723–9 (2006).

411. Freitas Mendes, L. F. *et al.* Combinatorial analysis of growth factors reveals the contribution of bone morphogenetic proteins to chondrogenic differentiation of human periosteal cells. *Tissue Eng. Part C. Methods* (2016). doi:10.1089/ten.TEC.2015.0436

412. Vinatier, C. *et al.* Cartilage tissue engineering: towards a biomaterial-assisted mesenchymal stem cell therapy. *Curr. Stem Cell Res. Ther.* **4**, 318–29 (2009).

413. van der Kraan, P. M., Blaney Davidson, E. N. & van den Berg, W. B. Bone Morphogenetic Proteins and articular cartilage. To serve and protect or a wolf in sheep clothing's? *Osteoarthritis and Cartilage* (2010). doi:10.1016/j.joca.2010.03.001

414. Wozney, J. M. The bone morphogenetic protein family and osteogenesis. *Mol. Reprod. Dev.* **32**, 160–7 (1992).

415. Chen, D., Zhao, M. & Mundy, G. R. Bone morphogenetic proteins. *Growth Factors* **22**, 233–41 (2004).

416. Schmitt, B. *et al.* BMP2 initiates chondrogenic lineage development of adult human mesenchymal stem cells in high-density culture. *Differentiation.* **71**, 567–77 (2003).

417. Liao, J. *et al.* Sox9 potentiates BMP2-induced chondrogenic differentiation and inhibits BMP2-induced osteogenic differentiation. *PLoS One* (2014). doi:10.1371/journal.pone.0089025

418. Wang, Q., Huang, C., Xue, M. & Zhang, X. Expression of endogenous BMP-2 in periosteal progenitor cells is essential for bone healing. *Bone* **48**, 524–32 (2011).

419. Platt, J., DiSesa, V., Gail, D., Massicot-Fisher, J. & National Heart, Lung, and B. I. H. and L. X. W. G. Recommendations of the National Heart, Lung, and Blood Institute Heart and Lung Xenotransplantation Working Group. *Circulation* **106**, 1043–7 (2002).

420. Franz, S., Rammelt, S., Scharnweber, D. & Simon, J. C. Immune responses to implants - A review of the implications for the design of immunomodulatory biomaterials. *Biomaterials* (2011). doi:10.1016/j.biomaterials.2011.05.078

421. Chung, L., Maestas, D. R., Housseau, F. & Elisseeff, J. H. Key players in the immune response to biomaterial scaffolds for regenerative medicine. *Advanced Drug Delivery Reviews* (2017). doi:10.1016/j.addr.2017.07.006

422. Moskalewski, S., Hyc, A. & Osiecka-Iwan, A. Immune response by host after allogeneic chondrocyte transplant to the cartilage. *Microsc. Res. Tech.* **58**, 3–13 (2002).

423. Schlundt, C. *et al.* Macrophages in bone fracture healing: Their essential role in endochondral ossification. *Bone* (2018). doi:10.1016/j.bone.2015.10.019

424. Wu, A. C., Raggatt, L. J., Alexander, K. A. & Pettit, A. R. Unraveling macrophage contributions to bone repair. *Bonekey Rep.* **2**, 373 (2013).

425. Sridharan, R., Cameron, A. R., Kelly, D. J., Kearney, C. J. & O'Brien, F.

J. Biomaterial based modulation of macrophage polarization: A review and suggested design principles. *Materials Today* (2015). doi:10.1016/j.mattod.2015.01.019

426. Mantovani, A., Biswas, S. K., Galdiero, M. R., Sica, A. & Locati, M. Macrophage plasticity and polarization in tissue repair and remodelling. *J. Pathol.* **229**, 176–85 (2013).

427. Mantovani, A. *et al.* The chemokine system in diverse forms of macrophage activation and polarization. *Trends Immunol.* **25**, 677–86 (2004).

428. Gordon, S. & Martinez, F. O. Alternative activation of macrophages: mechanism and functions. *Immunity* **32**, 593–604 (2010).

429. Casellas, J. Inbred mouse strains and genetic stability: a review. *Animal* **5**, 1–7 (2011).

430. Sellers, R. S., Clifford, C. B., Treuting, P. M. & Brayton, C. Immunological Variation Between Inbred Laboratory Mouse Strains: Points to Consider in Phenotyping Genetically Immunomodified Mice. *Vet. Pathol.* **49**, 32–43 (2012).

431. Cunniffe, G. M. *et al.* Porous decellularized tissue engineered hypertrophic cartilage as a scaffold for large bone defect healing. *Acta Biomater.* **23**, 82–90 (2015).

432. Seyednejad, H. *et al.* In vivo biocompatibility and biodegradation of 3D-printed porous scaffolds based on a hydroxyl-functionalized poly(ε-caprolactone). *Biomaterials* **33**, 4309–18 (2012).

433. Roberts, S. J., Chen, Y., Moesen, M., Schrooten, J. & Luyten, F. P. Enhancement of osteogenic gene expression for the differentiation of human periosteal derived cells. *Stem Cell Res.* **7**, 137–144 (2011).

434. Bolander, J. *et al.* Early BMP, Wnt and Ca2+/PKC pathway activation predicts the bone forming capacity of periosteal cells in combination with calcium phosphates. *Biomaterials* **86**, 106–118 (2016).

435. Akkiraju, H. & Nohe, A. Role of Chondrocytes in Cartilage Formation,

Progression of Osteoarthritis and Cartilage Regeneration. *J. Dev. Biol.* **3**, 177–192 (2015).

436. Ahrens, P. B., Solursh, M. & Reiter, R. S. Stage-related capacity for limb chondrogenesis in cell culture. *Dev. Biol.* **60**, 69–82 (1977).

437. Livak, K. J. & Schmittgen, T. D. Analysis of relative gene expression data using real-time quantitative PCR and. *Methods* **25**, 402–408 (2001).

438. Schmitt, B. *et al.* BMP2 initiates chondrogenic lineage development of adult human mesenchymal stem cells in high-density culture. *Differentiation* **71**, 567–577 (2003).

439. Caron, M. M. J. *et al.* Hypertrophic differentiation during chondrogenic differentiation of progenitor cells is stimulated by BMP-2 but suppressed by BMP-7. *Osteoarthr. Cartil.* **21**, 604–613 (2013).

440. Kugimiya, F. *et al.* Involvement of endogenous bone morphogenetic protein (BMP) 2 and BMP6 in bone formation. *J. Biol. Chem.* **280**, 35704–35712 (2005).

441. Loi, F. *et al.* Inflammation, fracture and bone repair. *Bone* **86**, 119–30 (2016).

442. Nobes, C. D. & Hall, A. Rho, Rac, and Cdc42 GTPases regulate the assembly of multimolecular focal complexes associated with actin stress fibers, lamellipodia, and filopodia. *Cell* (1995). doi:10.1016/0092-8674(95)90370-4

443. Aspenström, P. Effectors for the Rho GTPases. *Curr. Opin. Cell Biol.* (1999). doi:10.1016/S0955-0674(99)80011-8

444. Lu, C. *et al.* The role of oxygen during fracture healing. *Bone* **52**, 220–9 (2013).

445. Mahla, R. S. Stem Cells Applications in Regenerative Medicine and Disease Therapeutics. *Int. J. Cell Biol.* **2016**, 6940283 (2016).

446. Caron, M. M. J. *et al.* Redifferentiation of dedifferentiated human articular chondrocytes: comparison of 2D and 3D cultures. *Osteoarthr.*

Cartil. **20**, 1170–8 (2012).

447. Tew, S. R., Pothacharoen, P., Katopodi, T. & Hardingham, T. E. SOX9 transduction increases chondroitin sulfate synthesis in cultured human articular chondrocytes without altering glycosyltransferase and sulfotransferase transcription. *Biochem. J.* **414**, 231–6 (2008).

448. Chen, J. *et al.* Exogenous Heparan Sulfate Enhances the TGF-β3-Induced Chondrogenesis in Human Mesenchymal Stem Cells by Activating TGF-β/Smad Signaling. *Stem Cells Int.* **2016**, 1520136 (2016).

449. Van der Kraan, P. M., Buma, P., Van Kuppevelt, T. & Van Den Berg, W. B. Interaction of chondrocytes, extracellular matrix and growth factors: Relevance for articular cartilage tissue engineering. *Osteoarthr. Cartil.* **10**, 631–637 (2002).

450. Oka, K. *et al.* The role of TGF-beta signaling in regulating chondrogenesis and osteogenesis during mandibular development. *Dev. Biol.* **303**, 391–404 (2007).

451. Murphy, M. K., Huey, D. J., Hu, J. C. & Athanasiou, K. A. TGF-β1, GDF-5, and BMP-2 stimulation induces chondrogenesis in expanded human articular chondrocytes and marrow-derived stromal cells. *Stem Cells* **33**, 762–73 (2015).

452. Ellman, M. B., An, H. S., Muddasani, P. & Im, H.-J. Biological impact of the fibroblast growth factor family on articular cartilage and intervertebral disc homeostasis. *Gene* **420**, 82–9 (2008).

453. Bornes, T. D., Jomha, N. M., Mulet-Sierra, A. & Adesida, A. B. Optimal Seeding Densities for In Vitro Chondrogenesis of Two- and Three-Dimensional-Isolated and -Expanded Bone Marrow-Derived Mesenchymal Stromal Stem Cells Within a Porous Collagen Scaffold. *Tissue Eng. Part C. Methods* **22**, 208–20 (2016).

454. Colnot, C. Skeletal cell fate decisions within periosteum and bone marrow during bone regeneration. *J. Bone Miner. Res.* **24**, 274–82 (2009).

455. Lin, Z., Fateh, A., Salem, D. M. & Intini, G. Periosteum: biology and applications in craniofacial bone regeneration. *J. Dent. Res.* **93**, 109–16 (2014).

456. Ikeda, T. *et al.* Distinct roles of Sox5, Sox6, and Sox9 in different stages of chondrogenic differentiation. *J. Bone Miner. Metab.* **23**, 337–40 (2005).

457. Gu, J. *et al.* Identification and characterization of the novel Col10a1 regulatory mechanism during chondrocyte hypertrophic differentiation. *Cell Death Dis.* **5**, e1469 (2014).

458. Pelttari, K. *et al.* Premature induction of hypertrophy during in vitro chondrogenesis of human mesenchymal stem cells correlates with calcification and vascular invasion after ectopic transplantation in SCID mice. *Arthritis Rheum.* (2006). doi:10.1002/art.22136

459. Zelzer, E. *et al.* VEGFA is necessary for chondrocyte survival during bone development. *Development* **131**, 2161–71 (2004).

460. Kumar, D. & Lassar, A. B. The transcriptional activity of Sox9 in chondrocytes is regulated by RhoA signaling and actin polymerization. *Mol. Cell. Biol.* **29**, 4262–73 (2009).

461. Woods, A., Wang, G. & Beier, F. RhoA/ROCK signaling regulates Sox9 expression and actin organization during chondrogenesis. *J. Biol. Chem.* **280**, 11626–34 (2005).

462. Woods, A. & Beier, F. RhoA/ROCK Signaling Regulates Chondrogenesis in a Context-dependent Manner. *J. Biol. Chem.* **281**, 13134–13140 (2006).

463. Eyckmans, J., Lin, G. L. & Chen, C. S. Adhesive and mechanical regulation of mesenchymal stem cell differentiation in human bone marrow and periosteum-derived progenitor cells. *Biol. Open* **1**, 1058–68 (2012).

464. Matsumoto, E., Furumatsu, T., Kanazawa, T., Tamura, M. & Ozaki, T. ROCK inhibitor prevents the dedifferentiation of human articular

chondrocytes. *Biochem. Biophys. Res. Commun.* (2012). doi:10.1016/j.bbrc.2012.02.127

465. Xu, T., Wu, M., Feng, J., Lin, X. & Gu, Z. RhoA/Rho kinase signaling regulates transforming growth factor-β1-induced chondrogenesis and actin organization of synovium-derived mesenchymal stem cells through interaction with the Smad pathway. *Int. J. Mol. Med.* **30**, 1119–25 (2012).

466. Kim, M. J., Kim, S., Kim, Y., Jin, E. J. & Sonn, J. K. Inhibition of RhoA but not ROCK induces chondrogenesis of chick limb mesenchymal cells. *Biochem. Biophys. Res. Commun.* (2012). doi:10.1016/j.bbrc.2012.01.053

467. Schmandke, A., Schmandke, A. & Strittmatter, S. M. ROCK and Rho: biochemistry and neuronal functions of Rho-associated protein kinases. *Neuroscientist* **13**, 454–69 (2007).

468. Lee, H.-H. *et al.* Hypoxia enhances chondrogenesis and prevents terminal differentiation through PI3K/Akt/FoxO dependent anti-apoptotic effect. *Sci. Rep.* **3**, 2683 (2013).

469. Tsai, C.-C., Yew, T.-L., Yang, D.-C., Huang, W.-H. & Hung, S.-C. Benefits of hypoxic culture on bone marrow multipotent stromal cells. *Am. J. Blood Res.* **2**, 148–59 (2012).

470. Danišovič, L., Varga, I. & Polák, S. Growth factors and chondrogenic differentiation of mesenchymal stem cells. *Tissue Cell* **44**, 69–73 (2012).

471. Puetzer, J. L., Petitte, J. N. & Loboa, E. G. Comparative review of growth factors for induction of three-dimensional in vitro chondrogenesis in human mesenchymal stem cells isolated from bone marrow and adipose tissue. *Tissue Eng. Part B. Rev.* **16**, 435–44 (2010).

472. Coleman, C. M. *et al.* Growth differentiation factor-5 enhances in vitro mesenchymal stromal cell chondrogenesis and hypertrophy. *Stem Cells Dev.* **22**, 1968–76 (2013).

473. Ayerst, B. I. *et al.* Growth Differentiation Factor 5-Mediated Enhancement of Chondrocyte Phenotype Is Inhibited by Heparin:

Implications for the Use of Heparin in the Clinic and in Tissue Engineering Applications. *Tissue Eng. Part A* **23**, 275–292 (2017).

474. Tuli, R. *et al.* Transforming growth factor-beta-mediated chondrogenesis of human mesenchymal progenitor cells involves N-cadherin and mitogen-activated protein kinase and Wnt signaling cross-talk. *J. Biol. Chem.* **278**, 41227–36 (2003).

475. Wang, W., Rigueur, D. & Lyons, K. M. TGFβ signaling in cartilage development and maintenance. *Birth Defects Res. C. Embryo Today* **102**, 37–51 (2014).

476. Joyce, M. E., Roberts, A. B., Sporn, M. B. & Bolander, M. E. Transforming growth factor-beta and the initiation of chondrogenesis and osteogenesis in the rat femur. *J. Cell Biol.* **110**, 2195–207 (1990).

477. Shen, B., Wei, A., Tao, H., Diwan, A. D. & Ma, D. D. F. BMP-2 enhances TGF-beta3-mediated chondrogenic differentiation of human bone marrow multipotent mesenchymal stromal cells in alginate bead culture. *Tissue Eng. Part A* **15**, 1311–20 (2009).

478. Keller, B. *et al.* Interaction of TGFβ and bmp signaling pathways during chondrogenesis. *PLoS One* (2011). doi:10.1371/journal.pone.0016421

479. Guo, Y. *et al.* How is mRNA expression predictive for protein expression? A correlation study on human circulating monocytes. *Acta Biochim. Biophys. Sin. (Shanghai).* **40**, 426–36 (2008).

480. Liu, Y., Beyer, A. & Aebersold, R. On the Dependency of Cellular Protein Levels on mRNA Abundance. *Cell* (2016). doi:10.1016/j.cell.2016.03.014

481. Einhorn, T. A. & Gerstenfeld, L. C. Fracture healing: mechanisms and interventions. *Nat. Rev. Rheumatol.* **11**, 45–54 (2014).

482. Lertkiatmongkol, P., Liao, D., Mei, H., Hu, Y. & Newman, P. J. Endothelial functions of platelet/endothelial cell adhesion molecule-1 (CD31). *Curr. Opin. Hematol.* **23**, 253–9 (2016).

483. Dohle, D. S. *et al.* Chick ex ovo culture and ex ovo CAM assay: how it

really works. *J. Vis. Exp.* (2009). doi:10.3791/1620

484. Arzi, B. *et al.* Cartilage immunoprivilege depends on donor source and lesion location. *Acta Biomater.* **23**, 72–81 (2015).

485. Brown, B. N., Valentin, J. E., Stewart-Akers, A. M., McCabe, G. P. & Badylak, S. F. Macrophage phenotype and remodeling outcomes in response to biologic scaffolds with and without a cellular component. *Biomaterials* **30**, 1482–91 (2009).

486. Almeida, C. R. *et al.* Impact of 3-D printed PLA- and chitosan-based scaffolds on human monocyte/macrophage responses: unraveling the effect of 3-D structures on inflammation. *Acta Biomater.* **10**, 613–22 (2014).

487. Evers, M. *et al.* Enhanced quantification of metabolic activity for individual adipocytes by label-free FLIM. *Sci. Rep.* (2018). doi:10.1038/s41598-018-27093-x

488. Muhamed, J., Revi, D., Rajan, A., Geetha, S. & Anilkumar, T. V. Biocompatibility and Immunophenotypic Characterization of a Porcine Cholecyst–derived Scaffold Implanted in Rats. *Toxicol. Pathol.* (2015). doi:10.1177/0192623314550722

489. Cross, W. W. & Swiontkowski, M. F. Treatment principles in the management of open fractures. *Indian J. Orthop.* **42**, 377–86 (2008).

490. Hoff, W. S., Bonadies, J. A., Cachecho, R. & Dorlac, W. C. East Practice Management Guidelines Work Group: update to practice management guidelines for prophylactic antibiotic use in open fractures. *J. Trauma* **70**, 751–4 (2011).

491. Court-Brown, C. M. & Caesar, B. Epidemiology of adult fractures: A review. *Injury* (2006). doi:10.1016/j.injury.2006.04.130

492. White, A. P. *et al.* Clinical applications of BMP-7/OP-1 in fractures, nonunions and spinal fusion. *Int. Orthop.* **31**, 735–41 (2007).

493. McKay, W. F., Peckham, S. M. & Badura, J. M. A comprehensive clinical review of recombinant human bone morphogenetic protein-2 (INFUSE

Bone Graft). *Int. Orthop.* **31**, 729–34 (2007).

494. Aro, H. T. *et al.* Recombinant human bone morphogenetic protein-2: a randomized trial in open tibial fractures treated with reamed nail fixation. *J. Bone Joint Surg. Am.* **93**, 801–8 (2011).

495. James, A. W. *et al.* A Review of the Clinical Side Effects of Bone Morphogenetic Protein-2. *Tissue Eng. Part B. Rev.* **22**, 284–97 (2016).

496. Chrastil, J., Low, J. B., Whang, P. G. & Patel, A. A. Complications associated with the use of the recombinant human bone morphogenetic proteins for posterior interbody fusions of the lumbar spine. *Spine (Phila. Pa. 1976).* **38**, E1020-7 (2013).

497. Wang, M.-H. *et al.* BMP2 promotes proliferation and invasion of nasopharyngeal carcinoma cells via mTORC1 pathway. *Aging (Albany. NY).* **9**, 1326–1340 (2017).

498. Bach, D.-H., Park, H. J. & Lee, S. K. The Dual Role of Bone Morphogenetic Proteins in Cancer. *Mol. Ther. oncolytics* **8**, 1–13 (2018).

499. Yamada, T. *et al.* Hybrid grafting using bone marrow aspirate combined with porous β-tricalcium phosphate and trephine bone for lumbar posterolateral spinal fusion: a prospective, comparative study versus local bone grafting. *Spine (Phila. Pa. 1976).* **37**, E174-9 (2012).

500. Fischer, C. R. *et al.* A systematic review of comparative studies on bone graft alternatives for common spine fusion procedures. *Eur. Spine J.* **22**, 1423–35 (2013).

501. Damron, T. A. *et al.* Ultraporous β-tricalcium phosphate alone or combined with bone marrow aspirate for benign cavitary lesions: comparison in a prospective randomized clinical trial. *J. Bone Joint Surg. Am.* **95**, 158–66 (2013).

502. Mousaei Ghasroldasht, M. *et al.* Application of Mesenchymal Stem Cells to Enhance Non-Union Bone Fracture Healing. *J. Biomed. Mater. Res. A* (2018). doi:10.1002/jbm.a.36441

503. Killington, K., Mafi, R., Mafi, P. & Khan, W. S. A Systematic Review of

Clinical Studies Investigating Mesenchymal Stem Cells for Fracture Non-Union and Bone Defects. *Curr. Stem Cell Res. Ther.* **13**, 284–291 (2018).

504. Huey, D. J., Hu, J. C. & Athanasiou, K. A. Unlike bone, cartilage regeneration remains elusive. *Science* **338**, 917–21 (2012).

505. Kosher, R. A., Kulyk, W. M. & Gay, S. W. Collagen gene expression during limb cartilage differentiation. *J. Cell Biol.* **102**, 1151–6 (1986).

506. Lyashenko, N. *et al.* Differential requirement for the dual functions of β-catenin in embryonic stem cell self-renewal and germ layer formation. *Nat. Cell Biol.* **13**, 753–61 (2011).

507. Solorio, L. D., Fu, A. S., Hernández-Irizarry, R. & Alsberg, E. Chondrogenic differentiation of human mesenchymal stem cell aggregates via controlled release of TGF-beta1 from incorporated polymer microspheres. *J. Biomed. Mater. Res. A* **92**, 1139–44 (2010).

508. Mackay, A. M. *et al.* Chondrogenic differentiation of cultured human mesenchymal stem cells from marrow. *Tissue Eng.* **4**, 415–28 (1998).

509. Welter, J. F., Solchaga, L. A. & Penick, K. J. Simplification of aggregate culture of human mesenchymal stem cells as a chondrogenic screening assay. *Biotechniques* (2007). doi:10.2144/000112451

510. Detzel, C. J. & Van Wie, B. J. Use of a centrifugal bioreactor for cartilaginous tissue formation from isolated chondrocytes. *Biotechnol. Prog.* **27**, 451–9

511. Erickson, I. E. *et al.* Differential maturation and structure-function relationships in mesenchymal stem cell- and chondrocyte-seeded hydrogels. *Tissue Eng. Part A* **15**, 1041–52 (2009).

512. Mauck, R. L., Byers, B. A., Yuan, X. & Tuan, R. S. Regulation of cartilaginous ECM gene transcription by chondrocytes and MSCs in 3D culture in response to dynamic loading. *Biomech. Model. Mechanobiol.* **6**, 113–25 (2007).

513. Thorpe, S. D. *et al.* The response of bone marrow-derived mesenchymal

stem cells to dynamic compression following TGF-beta3 induced chondrogenic differentiation. *Ann. Biomed. Eng.* **38**, 2896–909 (2010).

514. Nasiri, B. & Mashayekhan, S. Fabrication of porous scaffolds with decellularized cartilage matrix for tissue engineering application. *Biologicals* **48**, 39–46 (2017).

515. Amadori, S. *et al.* Highly Porous Gelatin Reinforced 3D Scaffolds for Articular Cartilage Regeneration. *Macromol. Biosci.* **15**, 941–52 (2015).

516. Yang, Q. *et al.* A cartilage ECM-derived 3-D porous acellular matrix scaffold for in vivo cartilage tissue engineering with PKH26-labeled chondrogenic bone marrow-derived mesenchymal stem cells. *Biomaterials* **29**, 2378–87 (2008).

517. Chen, J. *et al.* Improvement of In Vitro Three-Dimensional Cartilage Regeneration by a Novel Hydrostatic Pressure Bioreactor. *Stem Cells Transl. Med.* **6**, 982–991 (2017).

518. Rowland, C. R., Colucci, L. A. & Guilak, F. Fabrication of anatomically-shaped cartilage constructs using decellularized cartilage-derived matrix scaffolds. *Biomaterials* **91**, 57–72 (2016).

519. Kock, L., van Donkelaar, C. C. & Ito, K. Tissue engineering of functional articular cartilage: the current status. *Cell Tissue Res.* **347**, 613–27 (2012).

520. Griffon, D. J., Sedighi, M. R., Schaeffer, D. V, Eurell, J. A. & Johnson, A. L. Chitosan scaffolds: interconnective pore size and cartilage engineering. *Acta Biomater.* **2**, 313–20 (2006).

521. Xu, Y. *et al.* Multiple binding sites in collagen type I for the integrins alpha1beta1 and alpha2beta1. *J. Biol. Chem.* **275**, 38981–9 (2000).

522. Wang, S. *et al.* Freeze-Dried Heart Valve Scaffolds. *Tissue Eng. Part C Methods* (2012). doi:10.1089/ten.tec.2011.0398

523. VeDepo, M. C., Detamore, M. S., Hopkins, R. A. & Converse, G. L. Recellularization of decellularized heart valves: Progress toward the tissue-engineered heart valve. *J. Tissue Eng.* **8**, 2041731417726327

524. Draenert, Y. & Draenert, K. Ice crystal damage in freeze-dried articular cartilage studied by scanning electron microscopy. *Scan. Electron Microsc.* 1799–804 (1982).

525. Bruker. Analysis of bone by micro-CT General information. *BRUKER MicroCT Acad.* (2017).

526. Campbell, G. M. & Sophocleous, A. Quantitative analysis of bone and soft tissue by micro-computed tomography: applications to ex vivo and in vivo studies. *Bonekey Rep.* (2014). doi:10.1038/bonekey.2014.59

527. Liao, J. F., Qu, Y., Chu, B., Zhang, X. & Qian, Z. Biodegradable CSMA/PECA/graphene porous hybrid scaffold for cartilage tissue engineering. *Sci. Rep.* (2015). doi:10.1038/srep09879

528. Leijten, J. *et al.* Bioinspired seeding of biomaterials using three dimensional microtissues induces chondrogenic stem cell differentiation and cartilage formation under growth factor free conditions. *Sci. Rep.* **6**, 36011 (2016).

529. Watanabe, Y., Matsushita, T., Bhandari, M., Zdero, R. & Schemitsch, E. H. Ultrasound for fracture healing: current evidence. *J. Orthop. Trauma* **24 Suppl 1**, S56-61 (2010).

530. Shafaei, H. *et al.* Optimizing a novel method for low intensity ultrasound in chondrogenesis induction. *Adv. Biomed. Res.* **2**, 79 (2013).

531. Kwon, H. J., Lee, G. S. & Chun, H. Electrical stimulation drives chondrogenesis of mesenchymal stem cells in the absence of exogenous growth factors. *Sci. Rep.* (2016). doi:10.1038/srep39302

532. Merlin Rajesh Lal, L. P., Suraishkumar, G. K. & Nair, P. D. Chitosan-agarose scaffolds supports chondrogenesis of Human Wharton's Jelly mesenchymal stem cells. *J. Biomed. Mater. Res. A* **105**, 1845–1855 (2017).

533. Ragetly, G. R. *et al.* Effect of chitosan scaffold microstructure on mesenchymal stem cell chondrogenesis. *Acta Biomater.* **6**, 1430–6 (2010).

534. Lu, T.-J., Chiu, F.-Y., Chiu, H.-Y., Chang, M.-C. & Hung, S.-C. Chondrogenic Differentiation of Mesenchymal Stem Cells in Three-Dimensional Chitosan Film Culture. *Cell Transplant.* **26**, 417–427 (2017).

535. Esko, J. D., Kimata, K. & Lindahl, U. Proteoglycans and Sulfated Glycosaminoglycans. in *Essentials of Glycobiology* 784 (2009). doi:10:0-87969-559-5

536. Ravi, M., Paramesh, V., Kaviya, S. R., Anuradha, E. & Solomon, F. D. P. 3D cell culture systems: advantages and applications. *J. Cell. Physiol.* **230**, 16–26 (2015).

537. Zhou, Y. Understanding the cancer/tumor biology from 2D to 3D. *J. Thorac. Dis.* **8**, E1484–E1486 (2016).

538. Shamir, E. R. & Ewald, A. J. Three-dimensional organotypic culture: Experimental models of mammalian biology and disease. *Nature Reviews Molecular Cell Biology* (2014). doi:10.1038/nrm3873

539. Lee, K. S. *et al.* Sequential sub-passage decreases the differentiation potential of canine adipose-derived mesenchymal stem cells. *Res. Vet. Sci.* **96**, 267–75 (2014).

540. Zhang, F.-B. *et al.* Passage-restricted differentiation potential of mesenchymal stem cells into cardiomyocyte-like cells. *Biochem. Biophys. Res. Commun.* **336**, 784–92 (2005).

541. Hoshi, K. *et al.* Implant-type Tissue-engineered Cartilage for Secondary Correction of Cleft Lip-nose Patients: An Exploratory First-in-human Trial. *J. Clin. Trials* **07**, (2017).

542. Phull, A.-R., Eo, S.-H., Abbas, Q., Ahmed, M. & Kim, S. J. Applications of Chondrocyte-Based Cartilage Engineering: An Overview. *Biomed Res. Int.* **2016**, 1879837 (2016).

543. Harris, J. D., Siston, R. A., Pan, X. & Flanigan, D. C. Autologous chondrocyte implantation: a systematic review. *J. Bone Joint Surg. Am.* **92**, 2220–33 (2010).

544. Jayasuriya, C. T. & Chen, Q. Potential benefits and limitations of utilizing chondroprogenitors in cell-based cartilage therapy. *Connect. Tissue Res.* **56**, 265–71 (2015).

545. Kessler, M. W. & Grande, D. A. Tissue engineering and cartilage. *Organogenesis* **4**, 28–32 (2008).

546. Mobasheri, A., Kalamegam, G., Musumeci, G. & Batt, M. E. Chondrocyte and mesenchymal stem cell-based therapies for cartilage repair in osteoarthritis and related orthopaedic conditions. *Maturitas* (2014). doi:10.1016/j.maturitas.2014.04.017

547. Koochekpour, S., Merzak, A. & Pilkington, G. J. Extracellular matrix proteins inhibit proliferation, upregulate migration and induce morphological changes in human glioma cell lines. *Eur. J. Cancer* **31A**, 375–80 (1995).

548. Williams, C. M., Engler, A. J., Slone, R. D., Galante, L. L. & Schwarzbauer, J. E. Fibronectin expression modulates mammary epithelial cell proliferation during acinar differentiation. *Cancer Res.* **68**, 3185–92 (2008).

549. Bosnakovski, D. *et al.* Chondrogenic differentiation of bovine bone marrow mesenchymal stem cells (MSCs) in different hydrogels: influence of collagen type II extracellular matrix on MSC chondrogenesis. *Biotechnol. Bioeng.* **93**, 1152–63 (2006).

550. Chastain, S. R., Kundu, A. K., Dhar, S., Calvert, J. W. & Putnam, A. J. Adhesion of mesenchymal stem cells to polymer scaffolds occurs via distinct ECM ligands and controls their osteogenic differentiation. *J. Biomed. Mater. Res. A* **78**, 73–85 (2006).

551. Everitt, E. A., Malik, A. B. & Hendey, B. Fibronectin enhances the migration rate of human neutrophils in vitro. *J. Leukoc. Biol.* **60**, 199–206 (1996).

552. Liberio, M. S., Sadowski, M. C., Soekmadji, C., Davis, R. A. & Nelson, C. C. Differential effects of tissue culture coating substrates on prostate cancer cell adherence, morphology and behavior. *PLoS One* **9**, e112122

(2014).

553. Brafman, D. A., Shah, K. D., Fellner, T., Chien, S. & Willert, K. Defining long-term maintenance conditions of human embryonic stem cells with arrayed cellular microenvironment technology. *Stem Cells Dev.* **18**, 1141–54 (2009).

554. Flaim, C. J., Teng, D., Chien, S. & Bhatia, S. N. Combinatorial signaling microenvironments for studying stem cell fate. *Stem Cells Dev.* **17**, 29–39 (2008).

555. Steele, J. G., Dalton, B. A., Johnson, G. & Underwood, P. A. Adsorption of fibronectin and vitronectin onto Primaria and tissue culture polystyrene and relationship to the mechanism of initial attachment of human vein endothelial cells and BHK-21 fibroblasts. *Biomaterials* **16**, 1057–67 (1995).

556. Koller, M. R., Palsson, M. A., Manchel, I., Maher, R. J. & Palsson, B. O. Tissue culture surface characteristics influence the expansion of human bone marrow cells. *Biomaterials* **19**, 1963–72 (1998).

557. Ng, J. *et al.* Extracellular matrix components and culture regimen selectively regulate cartilage formation by self-assembling human mesenchymal stem cells in vitro and in vivo. *Stem Cell Res. Ther.* **7**, 183 (2016).

558. Li, A., Wei, Y., Hung, C. & Vunjak-Novakovic, G. Chondrogenic properties of collagen type XI, a component of cartilage extracellular matrix. *Biomaterials* **173**, 47–57 (2018).

559. Cheng, A. *et al.* Recombinant Extracellular Matrix Protein Fragments Support Human Embryonic Stem Cell Chondrogenesis. *Tissue Eng. Part A* **24**, 968–978 (2018).

560. Tiruvannamalai Annamalai, R., Mertz, D. R., Daley, E. L. H. & Stegemann, J. P. Collagen Type II enhances chondrogenic differentiation in agarose-based modular microtissues. *Cytotherapy* **18**, 263–77 (2016).

561. Lu, Z., Doulabi, B. Z., Huang, C., Bank, R. A. & Helder, M. N. Collagen type II enhances chondrogenesis in adipose tissue-derived stem cells by affecting cell shape. *Tissue Eng. Part A* **16**, 81–90 (2010).

562. Lei, J., Trevino, E. & Temenoff, J. Cell number and chondrogenesis in human mesenchymal stem cell aggregates is affected by the sulfation level of heparin used as a cell coating. *J. Biomed. Mater. Res. A* **104**, 1817–29 (2016).

563. Cooper, S. T. *et al.* C2C12 co-culture on a fibroblast substratum enables sustained survival of contractile, highly differentiated myotubes with peripheral nuclei and adult fast myosin expression. *Cell Motil. Cytoskeleton* **58**, 200–11 (2004).

564. Luo, Y., Kobler, J. B., Zeitels, S. M. & Langer, R. Effects of growth factors on extracellular matrix production by vocal fold fibroblasts in 3-dimensional culture. *Tissue Eng.* **12**, 3365–74 (2006).

565. Radisic, M. *et al.* Pre-treatment of synthetic elastomeric scaffolds by cardiac fibroblasts improves engineered heart tissue. *J. Biomed. Mater. Res. A* **86**, 713–24 (2008).

566. Kleinman, H. K. & Martin, G. R. Matrigel: basement membrane matrix with biological activity. *Semin. Cancer Biol.* **15**, 378–86 (2005).

567. Hughes, C. S., Postovit, L. M. & Lajoie, G. A. Matrigel: a complex protein mixture required for optimal growth of cell culture. *Proteomics* **10**, 1886–90 (2010).

568. Dickhut, A., Gottwald, E., Steck, E., Heisel, C. & Richter, W. Chondrogenesis of mesenchymal stem cells in gel-like biomaterials in vitro and in vivo. *Front. Biosci.* **13**, 4517–28 (2008).

569. Ramos-Hryb, A. B., Da-Costa, M. C., Trentin, A. G. & Calloni, G. W. Matrigel supports neural, melanocytic and chondrogenic differentiation of trunk neural crest cells. *Int. J. Dev. Biol.* **57**, 885–90 (2013).

570. Dashtdar, H. *et al.* Ultra-structural changes and expression of chondrogenic and hypertrophic genes during chondrogenic

differentiation of mesenchymal stromal cells in alginate beads. *PeerJ* **4**, e1650 (2016).

571. VanWinkle, W. B., Snuggs, M. B. & Buja, L. M. Cardiogel: a biosynthetic extracellular matrix for cardiomyocyte culture. *In Vitro Cell. Dev. Biol. Anim.* **32**, 478–85 (1996).

572. DeQuach, J. A. *et al.* Simple and high yielding method for preparing tissue specific extracellular matrix coatings for cell culture. *PLoS One* **5**, e13039 (2010).

573. Grogan, S. P. *et al.* Influence of cartilage extracellular matrix molecules on cell phenotype and neocartilage formation. *Tissue Eng. Part A* **20**, 264–74 (2014).

574. Wu, Y.-N. *et al.* Substrate topography determines the fate of chondrogenesis from human mesenchymal stem cells resulting in specific cartilage phenotype formation. *Nanomedicine* **10**, 1507–16 (2014).

575. McBride, S. H. & Knothe Tate, M. L. Modulation of stem cell shape and fate A: the role of density and seeding protocol on nucleus shape and gene expression. *Tissue Eng. Part A* **14**, 1561–72 (2008).

576. Gao, L., McBeath, R. & Chen, C. S. Stem cell shape regulates a chondrogenic versus myogenic fate through Rac1 and N-cadherin. *Stem Cells* **28**, 564–72 (2010).

577. Sawkins, M. J. *et al.* Hydrogels derived from demineralized and decellularized bone extracellular matrix. *Acta Biomater.* **9**, 7865–73 (2013).

578. Wang, J. *et al.* Osteogenic differentiation of mesenchymal stem cells promoted by overexpression of connective tissue growth factor. *J. Zhejiang Univ. Sci. B* **10**, 355–67 (2009).

579. Zhang, Y. *et al.* Tissue-specific extracellular matrix coatings for the promotion of cell proliferation and maintenance of cell phenotype. *Biomaterials* **30**, 4021–8 (2009).

580. McClelland, R., Wauthier, E., Uronis, J. & Reid, L. Gradients in the liver's extracellular matrix chemistry from periportal to pericentral zones: influence on human hepatic progenitors. *Tissue Eng. Part A* **14**, 59–70 (2008).

581. Saldin, L. T., Cramer, M. C., Velankar, S. S., White, L. J. & Badylak, S. F. Extracellular matrix hydrogels from decellularized tissues: Structure and function. *Acta Biomater.* **49**, 1–15 (2017).

582. Rothrauff, B. B., Yang, G. & Tuan, R. S. Tissue-specific bioactivity of soluble tendon-derived and cartilage-derived extracellular matrices on adult mesenchymal stem cells. *Stem Cell Res. Ther.* **8**, 133 (2017).

583. Weadock, K. S., Miller, E. J., Keuffel, E. L. & Dunn, M. G. Effect of physical crosslinking methods on collagen-fiber durability in proteolytic solutions. *J. Biomed. Mater. Res.* (1996). doi:10.1002/(SICI)1097-4636(199610)32:2<221::AID-JBM11>3.0.CO;2-M

584. Rowland, C. R., Lennon, D. P., Caplan, A. I. & Guilak, F. The effects of crosslinking of scaffolds engineered from cartilage ECM on the chondrogenic differentiation of MSCs. *Biomaterials* **34**, 5802–12 (2013).

585. Dai, Z., Ronholm, J., Tian, Y., Sethi, B. & Cao, X. Sterilization techniques for biodegradable scaffolds in tissue engineering applications. *J. Tissue Eng.* **7**, 2041731416648810

586. Sun, W. Q., Xu, H., Sandor, M. & Lombardi, J. Process-induced extracellular matrix alterations affect the mechanisms of soft tissue repair and regeneration. *J. Tissue Eng.* **4**, 2041731413505305 (2013).

587. Ozcelikkale, A. & Han, B. Thermal Destabilization of Collagen Matrix Hierarchical Structure by Freeze/Thaw. *PLoS One* **11**, e0146660 (2016).

588. Huesca-Espitia, L. C. *et al.* Effects of steam autoclave treatment on Geobacillus stearothermophilus spores. *J. Appl. Microbiol.* **121**, 1300–1311 (2016).

589. Costa Martínez, E. *et al.* Human chondrocyte morphology, its dedifferentiation, and fibronectin conformation on different PLLA

microtopographies. *Tissue Eng. Part A* **14**, 1751–62 (2008).

590. Haudenschild, D. R., Chen, J., Pang, N., Lotz, M. K. & D'Lima, D. D. Rho kinase-dependent activation of SOX9 in chondrocytes. *Arthritis Rheum.* **62**, 191–200 (2010).

591. Tsang, K. Y., Chan, D. & Cheah, K. S. E. Fate of growth plate hypertrophic chondrocytes: death or lineage extension? *Dev. Growth Differ.* **57**, 179–92 (2015).

592. Solchaga, L. A., Penick, K. J. & Welter, J. F. Chondrogenic differentiation of bone marrow-derived mesenchymal stem cells: tips and tricks. *Methods Mol. Biol.* **698**, 253–278 (2011).

593. DeLise, A. M., Fischer, L. & Tuan, R. S. Cellular interactions and signaling in cartilage development. *Osteoarthr. Cartil.* (2000). doi:10.1053/joca.1999.0306

594. Lee, S. Y., Nakagawa, T. & Reddi, A. H. Induction of chondrogenesis and expression of superficial zone protein (SZP)/lubricin by mesenchymal progenitors in the infrapatellar fat pad of the knee joint treated with TGF-beta1 and BMP-7. *Biochem. Biophys. Res. Commun.* **376**, 148–53 (2008).

595. Lee, Y., Choi, J. & Hwang, N. S. Regulation of lubricin for functional cartilage tissue regeneration: a review. *Biomater. Res.* **22**, 9 (2018).

596. Musumeci, G. *et al.* Lubricin is expressed in chondrocytes derived from osteoarthritic cartilage encapsulated in poly (ethylene glycol) diacrylate scaffold. *Eur. J. Histochem.* **55**, e31 (2011).

597. Dy, P. *et al.* Sox9 directs hypertrophic maturation and blocks osteoblast differentiation of growth plate chondrocytes. *Dev. Cell* **22**, 597–609 (2012).

598. Shi, Q. *et al.* Maintaining the Phenotype Stability of Chondrocytes Derived from MSCs by C-Type Natriuretic Peptide. *Front. Physiol.* **8**, 143 (2017).

599. Gómez-Leduc, T. *et al.* Hypoxia Is a Critical Parameter for Chondrogenic

Differentiation of Human Umbilical Cord Blood Mesenchymal Stem Cells in Type I/III Collagen Sponges. *Int. J. Mol. Sci.* **18**, (2017).

600. Shang, J., Liu, H., Li, J. & Zhou, Y. Roles of hypoxia during the chondrogenic differentiation of mesenchymal stem cells. *Curr. Stem Cell Res. Ther.* **9**, 141–7 (2014).

601. Meretoja, V. V, Dahlin, R. L., Wright, S., Kasper, F. K. & Mikos, A. G. The effect of hypoxia on the chondrogenic differentiation of co-cultured articular chondrocytes and mesenchymal stem cells in scaffolds. *Biomaterials* **34**, 4266–73 (2013).

602. Mad-Ali, S., Benjakul, S., Prodpran, T. & Maqsood, S. Characteristics and Gel Properties of Gelatin from Goat Skin as Influenced by Alkaline-pretreatment Conditions. *Asian-Australasian J. Anim. Sci.* **29**, 845–54 (2016).

603. Brown, G. C. J., Lim, K. S., Farrugia, B. L., Hooper, G. J. & Woodfield, T. B. F. Covalent Incorporation of Heparin Improves Chondrogenesis in Photocurable Gelatin-Methacryloyl Hydrogels. *Macromol. Biosci.* **17**, (2017).

604. Honarpardaz, A., Irani, S., Pezeshki-Modaress, M., Zandi, M. & Sadeghi, A. Enhanced chondrogenic differentiation of bone marrow mesenchymal stem cells on gelatin/glycosaminoglycan electrospun nanofibers with different amount of glycosaminoglycan. *J. Biomed. Mater. Res. A* **107**, 38–48 (2019).

605. Lerouge, S., Wertheimer, M. R. & Yahia, L. Plasma sterilization: A review of parameters, mechanisms, and limitations. *Plasmas Polym.* (2001). doi:10.1023/A:1013196629791

606. Shintani, H., Sakudo, A., Burke, P. & McDonnell, G. Gas plasma sterilization of microorganisms and mechanisms of action. *Exp. Ther. Med.* **1**, 731–738 (2010).

607. Chen, W. *et al.* Nanotopography influences adhesion, spreading, and self-renewal of human embryonic stem cells. *ACS Nano* **6**, 4094–103 (2012).

608. Mendes, L. F. *et al.* Combinatorial Analysis of Growth Factors Reveals the Contribution of Bone Morphogenetic Proteins to Chondrogenic Differentiation of Human Periosteal Cells. *Tissue Eng. Part C. Methods* **22**, 473–86 (2016).

609. Solchaga, L. A., Penick, K. J. & Welter, J. F. Chondrogenic differentiation of bone marrow-derived mesenchymal stem cells: tips and tricks. *Methods Mol. Biol.* **698**, 253–78 (2011).

610. Taljanovic, M. S. *et al.* Fracture fixation. *Radiographics* **23**, 1569–90

611. Roberts, S. J. & Ke, H. Z. Anabolic Strategies to Augment Bone Fracture Healing. *Curr. Osteoporos. Rep.* **16**, 289–298 (2018).

612. Lombardi, G. *et al.* The roles of parathyroid hormone in bone remodeling: prospects for novel therapeutics. *J. Endocrinol. Invest.* **34**, 18–22 (2011).

613. Potts, J. T. *et al.* Synthesis of a biologically active N-terminal tetratriacontapeptide of parathyroid hormone. *Proc. Natl. Acad. Sci. U. S. A.* **68**, 63–7 (1971).

614. Neer, R. M. *et al.* Effect of parathyroid hormone (1-34) on fractures and bone mineral density in postmenopausal women with osteoporosis. *N. Engl. J. Med.* **344**, 1434–41 (2001).

615. Dobnig, H. & Turner, R. T. The effects of programmed administration of human parathyroid hormone fragment (1-34) on bone histomorphometry and serum chemistry in rats. *Endocrinology* **138**, 4607–12 (1997).

616. Bukata, S. V & Puzas, J. E. Orthopedic uses of teriparatide. *Curr. Osteoporos. Rep.* **8**, 28–33 (2010).

617. Chintamaneni, S., Finzel, K. & Gruber, B. L. Successful treatment of sternal fracture nonunion with teriparatide. *Osteoporos. Int.* **21**, 1059–63 (2010).

618. Kim, S. W. *et al.* Intermittent parathyroid hormone administration converts quiescent lining cells to active osteoblasts. *J. Bone Miner. Res.* **27**, 2075–84 (2012).

619. Yukata, K. *et al.* Continuous infusion of PTH1-34 delayed fracture healing in mice. *Sci. Rep.* **8**, 13175 (2018).

620. Nakajima, F. *et al.* Spatial and temporal gene expression in chondrogenesis during fracture healing and the effects of basic fibroblast growth factor. *J. Orthop. Res.* **19**, 935–44 (2001).

621. Nakajima, F., Nakajima, A., Ogasawara, A., Moriya, H. & Yamazaki, M. Effects of a single percutaneous injection of basic fibroblast growth factor on the healing of a closed femoral shaft fracture in the rat. *Calcif. Tissue Int.* **81**, 132–8 (2007).

622. Stevens, M. M., Marini, R. P., Martin, I., Langer, R. & Prasad Shastri, V. FGF-2 enhances TGF-beta1-induced periosteal chondrogenesis. *J. Orthop. Res.* **22**, 1114–9 (2004).

623. Forsten-Williams, K., Chua, C. C. & Nugent, M. A. The kinetics of FGF-2 binding to heparan sulfate proteoglycans and MAP kinase signaling. *J. Theor. Biol.* **233**, 483–99 (2005).

624. Martínez, M. E. *et al.* Influence of skeletal site of origin and donor age on osteoblastic cell growth and differentiation. *Calcif. Tissue Int.* **64**, 280–6 (1999).

625. Ho-Shui-Ling, A. *et al.* Bone regeneration strategies: Engineered scaffolds, bioactive molecules and stem cells current stage and future perspectives. *Biomaterials* **180**, 143–162 (2018).

626. Quarto, R. *et al.* Repair of large bone defects with the use of autologous bone marrow stromal cells. *N. Engl. J. Med.* **344**, 385–6 (2001).

627. Marcacci, M. *et al.* Stem cells associated with macroporous bioceramics for long bone repair: 6- to 7-year outcome of a pilot clinical study. *Tissue Eng.* **13**, 947–55 (2007).

628. Vukicevic, S. *et al.* The clinical use of bone morphogenetic proteins revisited: a novel biocompatible carrier device OSTEOGROW for bone healing. *Int. Orthop.* **38**, 635–47 (2014).

629. Ingber, D. E. *et al.* Tissue engineering and developmental biology: going

biomimetic. *Tissue Eng.* **12**, 3265–83 (2006).

630. Cooper, D. K. C., Ekser, B. & Tector, A. J. A brief history of clinical xenotransplantation. *Int. J. Surg.* **23**, 205–210 (2015).

631. Wong, M. L. & Griffiths, L. G. Immunogenicity in xenogeneic scaffold generation: antigen removal vs. decellularization. *Acta Biomater.* **10**, 1806–16 (2014).

632. Annas, G. J. Baby Fae: the 'anything goes' school of human experimentation. *Hastings Cent. Rep.* **15**, 15–7 (1985).

633. Dai, J. & Rabie, a B. M. VEGF: an essential mediator of both angiogenesis and endochondral ossification. *J. Dent. Res.* **86**, 937–950 (2007).

634. Knoepfler, P. S. & Turner, L. G. The FDA and the US direct-to-consumer marketplace for stem cell interventions: a temporal analysis. *Regen. Med.* **13**, 19–27 (2018).

635. Hanna, E., Rémuzat, C., Auquier, P. & Toumi, M. Advanced therapy medicinal products: current and future perspectives. *J. Mark. access Heal. policy* **4**, (2016).

636. Ferretti, C. & Mattioli-Belmonte, M. Periosteum derived stem cells for regenerative medicine proposals: Boosting current knowledge. *World J. Stem Cells* **6**, 266–77 (2014).

637. Liu, X. *et al.* SDF-1 promotes endochondral bone repair during fracture healing at the traumatic brain injury condition. *PLoS One* **8**, e54077 (2013).

638. The role of SDF-1 in fracture repair. *Bonekey Rep.* **1**, 158 (2012).

639. Price, A. P. *et al.* Automated decellularization of intact, human-sized lungs for tissue engineering. *Tissue Eng. Part C. Methods* **21**, 94–103 (2015).

640. Philips, C., Cornelissen, M. & Carriel, V. Evaluation methods as quality control in the generation of decellularized peripheral nerve allografts. *J.*

Neural Eng. **15**, 021003 (2018).

641. Center for Biologics Evaluation and Research. Regulatory Considerations for Human Cells, Tissues, and Cellular and Tissue-Based Products: Minimal Manipulation and Homologous Use. *Food Drug Adm.* (2017).

642. Costantini, F. *et al.* Lab-on-chip system combining a microfluidic-ELISA with an array of amorphous silicon photosensors for the detection of celiac disease epitopes. *Sens. Bio-Sensing Res.* (2015). doi:10.1016/j.sbsr.2015.11.003

643. Conde, J. P. *et al.* Lab-on-chip systems for integrated bioanalyses. *Essays Biochem.* **60**, 121–31 (2016).

644. Reifenrath, J., Angrisani, N., Lalk, M. & Besdo, S. Replacement, refinement, and reduction: Necessity of standardization and computational models for long bone fracture repair in animals. *Journal of Biomedical Materials Research - Part A* (2014). doi:10.1002/jbm.a.34920

645. Nagel, D. A., Kramers, P. C., Rahn, B. A., Cordey, J. & Perren, S. M. A paradigm of delayed union and nonunion in the lumbosacral joint. A study of motion and bone grafting of the lumbosacral spine in sheep. *Spine (Phila. Pa. 1976).* **16**, 553–9 (1991).

646. Garcia, P. *et al.* Rodent animal models of delayed bone healing and non-union formation: A comprehensive review. *Eur. Cells Mater.* (2013). doi:10.22203/eCM.v026a01

647. Zura, R., Mehta, S., Della Rocca, G. J. & Steen, R. G. Biological Risk Factors for Nonunion of Bone Fracture. *JBJS Rev.* **4**, (2016).

648. Yin, Y., Si, X., Gao, Y., Gao, L. & Wang, J. The nuclear factor-κB correlates with increased expression of interleukin-6 and promotes progression of gastric carcinoma. *Oncol. Rep.* **29**, 34–8 (2013).

649. Boos, A. M. *et al.* Autologous serum improves bone formation in a primary stable silica-embedded nanohydroxyapatite bone substitute in

combination with mesenchymal stem cells and rhBMP-2 in the sheep model. *Int. J. Nanomedicine* **9**, 5317–39 (2014).

650. Jensen, K. P. *et al.* FKBP5 variation is associated with the acute and chronic effects of nicotine. *Pharmacogenomics J.* **15**, 340–6 (2015).

651. Senger, S. *et al.* Intranasal administration of a recombinant alpha-gliadin down-regulates the immune response to wheat gliadin in DQ8 transgenic mice. *Immunol. Lett.* **88**, 127–34 (2003).

652. Lisignoli, G. *et al.* Osteogenesis of large segmental radius defects enhanced by basic fibroblast growth factor activated bone marrow stromal cells grown on non-woven hyaluronic acid-based polymer scaffold. *Biomaterials* (2002). doi:10.1016/S0142-9612(01)00216-2

653. Hsu, W. K. *et al.* Lentiviral-mediated BMP-2 gene transfer enhances healing of segmental femoral defects in rats. *Bone* (2007). doi:10.1016/j.bone.2006.10.030

654. Zhang, Z. Y. *et al.* Neo-vascularization and bone formation mediated by fetal mesenchymal stem cell tissue-engineered bone grafts in critical-size femoral defects. *Biomaterials* (2010). doi:10.1016/j.biomaterials.2009.09.078

655. Kokubu, T., Hak, D. J., Hazelwood, S. J. & Reddi, A. H. Development of an atrophic nonunion model and comparison to a closed healing fracture in rat femur. *J. Orthop. Res.* (2003). doi:10.1016/S0736-0266(02)00209-7

656. Dickson, G. R., Geddis, C., Fazzalari, N., Marsh, D. & Parkinson, I. Microcomputed tomography imaging in a rat model of delayed union/non-union fracture. *J. Orthop. Res.* **26**, 729–36 (2008).

657. Schoen, M. *et al.* Introduction of a new interlocked intramedullary nailing device for stabilization of critically sized femoral defects in the rat: A combined biomechanical and animal experimental study. *J. Orthop. Res.* (2008). doi:10.1002/jor.20501

658. Kaspar, K. *et al.* A new animal model for bone atrophic nonunion:

Fixation by external fixator. *J. Orthop. Res.* (2008). doi:10.1002/jor.20651

659. Chen, X. *et al.* Characterization of a chronic infection in an internally-stabilized segmental defect in the rat femur. *J. Orthop. Res.* (2005). doi:10.1016/j.orthres.2005.01.009

660. Azad, V. *et al.* rhBMP-2 enhances the bone healing response in a diabetic rat segmental defect model. *J. Orthop. Trauma* **23**, 267–76 (2009).

661. Choi, P., Ogilvie, C., Thompson, Z., Miclau, T. & Helms, J. A. Cellular and molecular characterization of a murine non-union model. *J. Orthop. Res.* **22**, 1100–7 (2004).

662. Garcia, P. *et al.* The LockingMouseNail--a new implant for standardized stable osteosynthesis in mice. *J. Surg. Res.* **169**, 220–6 (2011).

663. Garcia, P. *et al.* Rodent animal models of delayed bone healing and non-union formation: a comprehensive review. *Eur. Cell. Mater.* **26**, 1–12; discussion 12-4 (2013).

Appendix

Gene ID/Ref	NCBI accession number/ Species		Sequence 5'-3'
COL2A1[528]	NM_001844.4	Forward	GGCTTCCATTTCAGCTATGG
	Human	Reverse	AGCTGCTTCGTCCAGATAGG
SOX9[528]	NM_000346.3	Forward	TGGAGACTTCTGAACGAGAGC
	Human	Reverse	CGTTCTTCACCGACTTCCTC
SOX5	NM_001261414.2	Forward	TGCTTACTGACCCTGATTTACC
	Human	Reverse	CACTCTCCTCTTCTTCCACTTTC
SOX6	NM_001145811.1	Forward	AACAACGGCAGCAAATGGAC
	Human	Reverse	CATGTGACCCTGAACCTGGA
VEGF-A[648]	NM_001025366.2	Forward	AGTCCAACATCACCATGCAG
	Human	Reverse	TTCCCTTTCCTCGAACTGATTT
RUNX2[649]	NM_001015051.3	Forward	CGCATTCCTCATCCCAGTAT
	Human	Reverse	GCCTGGGGTCTGTAATCTGA
COL10A1[528]	NM_000493.3	Forward	ACGATACCAAATGCCCACAG
	Human	Reverse	GTGGACCAGGAGTACCTTGC
ACAN	NM_001135.3	Forward	TGTGGGACTGAAGTTCTTGG
	Human	Reverse	AGCGAGTTGTCATGGTCTG
HPRT1[650]	NM_000194.2	Forward	TGAGGATTTGGAAAGGGTGT
	Human	Reverse	GAGCACACAGAGGGCTACAA
hprt1	NM_204848.1	Forward	GATGAACAAGGTTACGACCTGGA
	Chicken	Reverse	TATAGCCACCCTTGAGTACACAGAG
cd31	XM_004946203.2	Forward	GGCAGAACATAGCTCAGCACAA
	Chicken	Reverse	GCACAGGGAGTTCAGCACAA
hprt1	NM_013556.2	Forward	GTTGGGCTTACCTCACTGCT
	Mouse	Reverse	TCATCGCTAATCACGACGCT
cd163	NM_001170395.1	Forward	CCAGTGCCTCCCAAAAATGAC
	Mouse	Reverse	AGTCGCTGAATCTGTCGTCG
cd31	NM_001032378.2	Forward	CACCAAGAGAACGGAAGGCT

	Mouse	Reverse	TGGGGACAGGCTCATAAATACG
cxcl9	NM_008599.4	Forward	TCGGACTTCACTCCAACACAG
	Mouse	Reverse	AGGGTTCCTCGAACTCCACA
il-6	NM_001314054.1	Forward	GGAGCCCACCAAGAACGATA
	Mouse	Reverse	GTCACCAGCATCAGTCCCAA
cd86	NM_001291058.1	Forward	GCAAAGGGGATTGGATTGAGG
	Mouse	Reverse	TCCTCTGTTCCTTGGGCTAT
il-2r	NM_008367.3	Forward	CTGGCAACACAGATGGAGGA
	Mouse	Reverse	CGTTAGGTGAATGCTTGGCG
tnf-a	NM_001278601.1	Forward	CCCTCACACTCACAAACCAC
	Mouse	Reverse	ACAAGGTACAACCCATCGGC
inf-g[651]	NM_008337.4	Forward	GAACTGGCAAAAGGATGGTGAC
	Mouse	Reverse	TTGCTGATGGCCTGATTGTC

Supp Table 1: qPCR primer sequences. Primers were exon spanning, designed using Primer3 Plus, NCBI or obtained from published sources.

Author	Bone	Fixation	Fracture model	Observation time	Non-union Rate
RAT					
Lisignoli et al. 2002[652]	radius	no fixation	5 mm osteotomy	28 weeks	100%
Hsu et al. 2007[653]	femur	polyethylene plate with screws & cerclage	6 mm osteotomy & periosteum elevated	8 weeks	100 %
Zhang et al. 2010[654]	femur	radioluscent plate	7 mm osteotomy	12 weeks	100 %
Kokubu et al. 2003[655]	femur	metallic pin intramedullar	closed fracture & periosteum cauterised	8 weeks	100%
Dickson et al. 2008[656]	femur	external fixator	0 mm osteotomy & periosteum cauterised & endosteum reamed	14 weeks	87.5 %

Schoen et al. 2008[657]	femur	intramedullar pin and diaphysal screws	5 mm osteotomy	12 weeks	100 %
Kaspar et al. 2008[658]	femur	external fixator	~0.5 mm osteotomy & bone marrow removal & periosteum cauterised	8 weeks	100%
Chen et al. 2005[659]	femur	polyethylene plate with threaded K-wire	6 mm osteotomy & infection Staph. aureus	12 weeks	100 %
Azad et al. 2009[660]	femur	polyethylene plate with screws and cerclage	3 mm osteotomy & collagen sponge & diabetic rat	9 weeks	100%
MICE					
Choi et al. 2004[661]	tibia	external fixator	osteotomy + distraction	4 weeks	60 % atrophic
Garcia et al. 2009[662]	femur	Locking Mouse Nail interlocked	2.0 mm osteotomy	10 weeks	100 % atrophic

Supp Table 2: Non-union rodent fracture models. Adapted from Garcia et al, 2013[663]